USGS
science for a changing world

U.S. Geological Survey Subsidence Interest Group Conference, Proceedings of the Technical Meeting, Galveston, Texas, November 27–29, 2001

Open-File Report 03–308

U.S. Department of the Interior
U.S. Geological Survey

U.S. Geological Survey Subsidence Interest Group Conference, Proceedings of the Technical Meeting, Galveston, Texas, November 27–29, 2001

Keith R. Prince and Devin L. Galloway, Editors

U.S. GEOLOGICAL SURVEY
Open-File Report 03–308

Austin, Texas
2003

U.S. DEPARTMENT OF THE INTERIOR

Gale A. Norton, Secretary

U.S. GEOLOGICAL SURVEY

Charles G. Groat, Director

For additional information write to

District Chief
U.S. Geological Survey
8027 Exchange Dr.
Austin, TX 78754–4733
E-mail: dc_tx@usgs.gov

Copies of this report can be purchased from

U.S. Geological Survey
Information Services
Box 25286
Denver, CO 80225–0286
E-mail: infoservices@usgs.gov

Preface

The fourth conference of the Aquifer Mechanics and Subsidence Interest Group (referred to herein as the Subsidence Interest Group) was held in Galveston, Tex., November 27–29, 2001. The conference consisted of 2 days of technical presentations, including a poster session, followed by a field trip to view and discuss subsidence features in the Houston-Galveston area. The conference was jointly hosted by the Harris-Galveston Coastal Subsidence District and the Water Discipline Office, Texas District, U.S. Geological Survey (USGS). The focus of the conference was on water-related causes of land subsidence, for example aquifer-system compaction, drainage and subsequent oxidation of organic soils, and sinkholes in carbonate and evaporite rocks. Most of the presentations addressed the detection, measurement, monitoring, analysis, and (or) simulation of processes associated with the compaction of susceptible aquifer systems that typically accompanies the exploitation of ground-water resources. The goal in convening the conference was to broaden the understanding and knowledge, on behalf of scientists and non-scientists alike, with regard to subsidence-related science and societal issues.

The oral technical presentations were arranged in seven moderated sessions organized loosely around geographic and technical themes. For example, most of the presentations pertaining to subsidence in the Houston-Galveston area were delivered in the first three sessions. Other sessions included two presentations on subsidence in the Las Vegas, Nev., area. One other session and grouping of talks focused on the application of Interferometric Synthetic Aperture Radar (InSAR) to detect and map subsidence in high spatial detail and measurement resolution, and to constrain conceptual and numerical simulations of ground-water flow and aquifer-system compaction. The application of satellite-borne SAR data, using InSAR, to subsidence detection has emerged since the third USGS Subsidence Interest Group Conference held in Las Vegas, February 14–16, 1995. Consequently, this fourth conference consisted of a number of oral and poster presentations demonstrating the applications of this powerful new technique—InSAR.

Each of the presenters was encouraged to submit short papers for these proceedings. Not all oral and poster presentations are documented in this report but many are. Some of the contributed papers have titles that differ from the title of the presentation and expand upon the content of the presentation. The information presented at the conference and in these proceedings should expand the knowledge and technical basis for characterizing and managing land subsidence.

The Subsidence Interest Group was formed in 1989 to facilitate technology transfer and to provide a forum for the exchange of information and ideas among USGS scientists actively working in subsidence and aquifer-mechanics-related projects. The decision was made to open attendance to the fourth conference of the Subsidence Interest Group to anyone actively working on issues related to land subsidence. Nearly one-half of the conference attendees and presenters were from outside the USGS, greatly expanding the scope of the conference and resulting in a broader range of topics and technical issues than was presented at any of the previous conferences. Having recognized the benefits to the Subsidence Interest Group of broadening the exposure of the group to scientific research and activities beyond the USGS, membership in the group has been opened to include anyone working on subsidence-related issues. Membership is free and can be obtained by contacting Keith R. Prince, U.S. Geological Survey, 345 Middlefield Road, MS 470, Menlo Park, CA 94025, or by e-mail to krprince@usgs.gov.

Acknowledgments

The USGS Subsidence Interest Group gratefully acknowledges the support of the Harris-Galveston Coastal Subsidence District for co-hosting this conference and accompanying field trip. We are especially grateful to Ron Neighbors, General Manager, Tom Michel, Assistant to the General Manager, and Carole Baker, Director of Intergovernmental Relations, for their role in planning and coordinating the conference. The hospitality extended to the meeting attendees by the Harris-Galveston Coastal Subsidence District was outstanding, and the excellent hotel accommodations and meeting facilities resulted in a very fruitful and productive meeting. We are grateful to all those who attended the conference, presented talks and posters, and submitted papers for these proceedings. Finally, we would also like to thank the USGS Texas District Water Discipline Office for co-hosting the conference and providing support for the publication of these proceedings. We are grateful to Joe Broadus, Houston Subdistrict Chief, for advocating and facilitating the convening of this conference in the Houston-Galveston area and assisting in the conduct of the meeting; and to the Texas District Publications Section, for editing, formatting, and publishing this document.

SUBSIDENCE INTEREST GROUP CONFERENCE AGENDA

Galveston, Texas
November 27–29, 2001

Tuesday, November 27

7:00–8:00 AM Registration: sign-in, distribution of agenda, nametags, local maps, sign-up for group dinner, sign-up for field trip.

Session I

Moderator: Keith Prince, U.S. Geological Survey, Menlo Park, Calif.

8:00–8:15 Welcoming Remarks/Meeting Announcements:
Keith Prince, U.S. Geological Survey, Menlo Park, Calif.;
Ron Neighbors, Harris-Galveston Coastal Subsidence District, Friendswood, Tex.;
Joe Broadus, U.S. Geological Survey, Houston, Tex.

8:15–9:00 Keynote Address: Aquifer Mechanics—Where Do We Go From Here?:
Francis S. Riley, U.S. Geological Survey (*Emeritus*), Menlo Park, Calif.

9:00–9:30 Measuring and Monitoring Subsidence in Houston:
Ron Neighbors, Harris-Galveston Coastal Subsidence District, Friendswood, Tex.

9:30–10:00 Break

Session II

Moderator: Marti Ikehara, National Geodetic Survey, Sacramento, Calif.

10:00–10:30 An Automated GPS Subsidence Monitoring Project in the Houston-Galveston Region:
Dave Zilkoski, National Geodetic Survey, Silver Springs, Md.

10:30–11:00 Hydrogeology and Simulation of Ground-Water Flow and Land-Surface Subsidence in the Chicot and Evangeline Aquifers, Houston, Area, Texas:
Mark Kasmarek, U.S. Geological Survey, Houston, Tex.

11:00–11:30 Optimal Management of Elastic Storage in the Houston Area:
Wes Danskin, U.S. Geological Survey, San Diego, Calif.

11:30–1:00 PM Lunch

Session III

Moderator: Eric Strom, U.S. Geological Survey, Austin, Tex.

1:00–1:30 PM Regulatory Plan Development in Houston:
Tom Michel, Harris-Galveston Coastal Subsidence District, Friendswood, Tex.

1:30–2:00 International Land Subsidence Data Base:
Keith Prince, U.S. Geological Survey, Menlo Park, Calif.

2:00–2:30 Break

Session IV

Moderator: Chuck Heywood, U.S. Geological Survey, Albuquerque, N. Mex.

2:30–3:00 Land Subsidence in Las Vegas, Nevada, Synthesis of the Evolution, Spatial Patterns, and Rates through 2000:
John Bell, Nevada Bureau of Mines and Geology, Reno, Nev.

3:00–3:30	Estimating Subsidence-Controlling Parameters Using Nonlinear Regression Methods With a 1-D Model of the Lorenzi Extensometer, Las Vegas, Nevada: Michael Pavelko, U.S. Geological Survey, Las Vegas, Nev.
3:30–4:00	Aquifer-System Characterization Using Interferometric Synthetic Aperture Radar: Michelle Sneed, U.S. Geological Survey, Sacramento, Calif.
4:00	Adjourn
4:30–7:00	Poster Session

Wednesday, November 28

Session V

Moderator: Devin Galloway, U.S. Geological Survey, Sacramento, Calif.

8:00–8:30 AM	Operational Use of Radar InterferometrySubsidence Measurements for Infrastructure and Water Resource Management: Sean Buckley, University of Texas, Austin, Tex.
8:30–9:00	Using Radar Interferometry to Elucidate Aquifer Mechanics: Jörn Hoffmann, Stanford University, Stanford, Calif.
9:00–9:30	Ground-Water Pumping Masks Tectonic Deformation in Metropolitan Los Angeles, California: Gerald Bawden, U.S. Geological Survey, Menlo Park, Calif.
9:30–10:00	Break

Session VI

Moderator: Stan Leake, U.S. Geological Survey, Tucson, Ariz.

10:00–10:30	Sea-Level Rise and Subsidence: Implications for New Orleans and Vicinity: Virginia Burkett, U.S. Geological Survey, Lafayette, La.
10:30–11:00	Characterization and Modeling of Land Subsidence due to Ground-Water Withdrawals From the Confined Aquifers of the Virginia Coastal Plain: Jason Pope, U.S. Geological Survey, Richmond, Va.
11:00–11:30	Simulation of Land Subsidence in a Glacial Aquifer System Above a Salt Mine Collapse in New York, USA: Richard Yager, U.S. Geological Survey, Ithaca, N.Y.
11:30–1:00 PM	Lunch

Session VII

Moderator: Keith Prince, U.S. Geological Survey, Menlo Park, Calif.

1:00–1:30 PM	Land and Water-Resource Development Activities Increase Sinkhole Frequency in the Mantled Karst Region of Florida, USA: Ann Tihansky, U.S. Geological Survey, Tampa, Fla.
1:30–3:30	Subsidence Interest Group Business Meeting (USGS only)
6:30–8:00	Group Dinner

Thursday, November 29

8:00 AM–5:00 PM Field trip to view land-subsidence features, instrumentation, and monitoring installations.

List of Poster Presentations

Aquifer-System Characterization Using Interferometric Synthetic Aperture Radar,
By Sylvia V. Stork and Michelle Sneed

Characterization and Modeling of Land Subsidence due to Ground-Water Withdrawals From the Confined Aquifers of the Virginia Coastal Plain,
By Jason P. Pope and Thomas J. Burbey

Ground-Water Pumping Masks Tectonic Deformation in Metropolitan Los Angeles, California,
By Gerald W. Bawden

Ground Displacements Caused by Aquifer-System Water-Level Variations Near Albuquerque, New Mexico,
By Charles E. Heywood, Devin L. Galloway, and Sylvia V. Stork

InSAR Detection of Post-Seismic and Coseismic Ground-Surface Deformation Associated With Underground Weapons Testing, Yucca Flat, Nevada Test Site,
By Randell J. Laczniak, Devin L. Galloway, and Michelle Sneed

International Land Subsidence Data Base,
By Keith R. Prince

The Role of Aquitard Drainage in Land-Subsidence Predictions at Edwards Air Force Base, Antelope Valley, California,
By Michelle Sneed

Use of InSAR to Identify Land-Surface Displacement and Aquifer-System Compaction, Paso Robles Area, California,
By Jill N. Densmore, Devin L. Galloway, and David W. Valentine

CONTENTS

CONVERSION FACTORS, ABBREVIATIONS, AND VERTICAL DATUM

Multiply	By	To obtain
acre-foot per square mile (acre-ft/mi^2)	476.1	cubic meter per square kilometer
foot (ft)	0.3048	meter
inch (in.)	25.4	millimeter
million gallons per day (Mgal/d)	0.04381	cubic meter per second
square mile (mi^2)	2.590	square kilometer
centimeter (cm)	0.3937	inch
centimeter per year (cm/yr)	0.3937	inch per year
cubic meter per day (m^3/d)	35.31	cubic foot per day
cubic kilometer per year (km^3/yr)	0.2399	cubic mile per year
gram per cubic centimeter (g/cm^3)	0.5781	ounce per cubic inch
kilometer (km)	0.6214	mile
liter per second (L/s)	0.2642	gallon per second
meter (m)	3.281	foot
meter per day (m/d)	3.281	foot per day
millimeter (mm)	0.03937	inch
millimeter per year (mm/yr)	0.03937	inch per year
square kilometer (km^2)	0.3861	square mile
square millimeter (mm^2)	0.00155	square inch

Abbreviations:
Ah, amp-hour (ampere-hour)
MB, megabyte
m/Pa, meter per Pascal
V, volt

Unless otherwise stated, vertical coordinate information is referenced to the National Geodetic Vertical Datum of 1929 (NGVD 29).

Keynote Address

On Aquifer Mechanics: How Did We Get Here and Where Might We Go?

By Francis S. Riley[1]

Good morning, ladies and gentlemen. Today we are meeting just across the bay from the Goose Creek oilfield, which is recognized as the first locale in which land subsidence was attributed to the compaction of clays interbedded with sand lenses from which fluid was being extracted. In the words of Pratt and Johnson, published in 1926:

> "The pore spaces [in the sands] are * * * occupied by water draining in more slowly from the adjacent clays; and it is a well-known fact that the draining of clays causes them to become more compact. This, in turn, would permit subsidence of the overlying surface."

Thus was born what has come to be known as the aquitard-drainage concept of land subsidence due to fluid withdrawal.

In related and very fundamental developments just a year earlier Karl Terzaghi had formulated the hydrodynamic theory of time-dependent soil consolidation, and Oscar Meinzer had concluded that the large quantities of water produced from the Dakota Sandstone required that the aquifer undergo elastic compression due to the reduction of internal pore pressures. Both of these pioneers in their respective disciplines recognized the principle of effective stress, which states that a reduction in internal pore pressure transfers an equivalent portion of the overburden load to the skeletal matrix of the sediment, which must then deform in accordance with its modulus of compressibility. However, Terzaghi focused on the slow consolidation of fine-grained soils in response to the application of an external load, a process greatly delayed by the low permeability of clays, whereas Meinzer addressed the rapid production of water from the concurrent reduction in the pore volume of a sandstone.

[1] U.S. Geological Survey (*Emeritus*), Menlo Park, Calif.

In the late 1930s, C.F. Tolman (known as "Chief") and his graduate student and assistant instructor at Stanford University, Joseph F. Poland, were investigating the geology and water resources of the Santa Clara Valley, at the south end of San Francisco Bay. In a seminal paper and follow-up discussion, published in 1940, they analyzed the land subsidence that had become evident as a result of repeat leveling surveys and attributed it to:

> "* * * a reduction in pressure in all aquifers tapped by wells. This reduction in pressure permits escape of water from the clay into the adjacent aquifers, and compaction of clay under the load of overlying material, throughout the zone penetrated by wells."

In the same era, C.V. Theis, working from a different perspective, translated Meinzer's concept of aquifer elasticity into a quantitative "coefficient of storage" that included both the compressibility of the aquifer skeleton and the compressibility of the pore water, as well as the thickness of the aquifer. These parameters, together with the hydraulic conductivity, were incorporated in an analogy between heat flow and ground-water flow. Addition of the storage parameter to the well established concept of steady-state Darcian flow enabled a theoretical prediction of the transient, or non-equilibrium, response of water levels in and near a well that starts to extract the water stored in an elastic aquifer confined between theoretically impervious confining units.

By 1940, C.E. Jacob had demonstrated a rigorous derivation of Theis' non-equilibrium formula from basic physical principles of ground-water flow. However, in a remarkably prescient caveat, he noted that:

> "* * * the chief source of water derived from storage 'within' an artesian aquifer is probably the contiguous and interbedded clay beds (or shale beds, in a sandstone aquifer)

and that because of the low permeability of the clays (or shales) there is a time lag between the lowering of pressure in the aquifer and the appearance of that part of the water which is derived from storage in those clays (or shales)."

This prediction constituted an important departure from Theis' assumption that the full potential yield of water from storage would occur as an instantaneous response to decline in aquifer head. Its reality proved to be particularly troublesome in pumping-test analysis, in which time-drawdown data were used to derive the coefficients of storage and transmissivity of the aquifer, using a trial-and-error graphical procedure to fit the data plot to a dimensionless "type curve" representing the predictive model. The problem was addressed over the next two decades in a series of papers by Jacob, Mahdi Hantush, and others. At first, these authors added to pumping-test theory only the low but finite permeability of the leaky confining beds. Subsequently, and much more realistically, Hantush also incorporated their relatively large elastic specific storage, which is dominated by skeletal compressibility, although it also includes the compressibility and volume of the pore water. These enhancements enabled a distinction between the roles of aquifer and aquitard properties in defining the development and shape of the cone of depression as measured in observation wells. They also demonstrated the sometimes subtle but always significant ability of these parameters to displace or distort Theis' classic "type curve" of transient drawdown in ways that could lead an unwary analyst to unreliable or physically unreasonable results, or cause a more cautious one to give up on the interpretation. In addition, they laid the foundations for subsequent expansion on these concepts by Shlomo Neuman and Paul Witherspoon, who quantified the vertical propagation of aquifer drawdowns into the adjacent aquitards and unpumped aquifers. In an important practical corollary, Neuman and Witherspoon also demonstrated the possibility of using the delayed drawdown measured in an aquitard piezometer to determine the vertical hydraulic diffusivity of the aquitard.

In 1955 Joe Poland, then California's District Geologist for the Ground Water Branch of the Water Resources Division, U.S. Geological Survey, undertook an investigation of the subsidence problems coming to the attention of Federal and State surface-water managers in the San Joaquin Valley. In 1956, Poland's Mechanics of Aquifer Systems program became the first federally funded project under the newly instituted National Research Program. It continued for almost 30 years under the successive direction of Poland, Ben Lofgren, and me. Among its many products, perhaps the most enduring achievement, in terms of technology transfer, was the practical melding of theoretical soil mechanics, aquifer hydraulics, and subsurface geology into a new discipline, aquifer mechanics, which stands as the legacy of Joe Poland's early insights and decades of leadership.

The key tools developed in this process proved to be the borehole extensometer and Don Helm's numerical model of one-dimensional aquitard deformation. The early extensometers consisted simply of a tensioned cable anchored at the bottom of a deep well and connected at land surface to a converted water-level chart recorder. In the mid-1950s these so-called compaction recorders promptly confirmed, for the first time, that the observed surface subsidence was attributable to compaction of the pumped aquifer system, and that changes in the rates of compaction reflected seasonal variations in pumpage and the accompanying changes in head in the aquifers. Multiple-depth extensometer installations permitted assignment of the overall compaction to specific depth intervals and demonstrated that compaction was concentrated in the deeper, heavily pumped zones of the confined aquifer systems. A few of the extensometers were completed at the base of the pumped interval and demonstrated total compaction essentially equivalent to the observed subsidence of nearby benchmarks.

As a footnote, I should mention that in some areas of aquifer-system compaction the surface subsidence problem was compounded by the superposition of near-surface hydrocompaction. This phenomenon reflected the partial collapse of low-density soils above the water table, caused by weakening of intergranular clay bonds as a result of anthropogenic rewetting for the first time since the desiccation that followed deposition.

At numerous sites in the San Joaquin and Santa Clara Valleys the first and second generation extensometers produced long-term time-series data of aquifer-system compaction and expansion, which could be coupled with aquifer water-level histories to display continuous drawdown-compaction, or stress-strain relations. Given a favorable loading history incorporating repeated annual cycles of drawdown and recovery through roughly the same range, the slopes and points of change in slope in the stress-strain graph

could be interpreted, within the theoretical structure of Terzaghi's model, in terms of the bulk elastic and inelastic storage coefficients of the aquifer system. In addition, they displayed the gradual annual increase of preconsolidation stress, expressed as the values of pore pressure at which the effective stress became equal to the maximum past stress. At this point, aquitard deformation began to change from elastic to inelastic during drawdown and back to elastic during recovery.

When interpreted in conjunction with a detailed log of the number and thicknesses of clay beds, the stress-strain graphs allowed estimation of the essential constitutive properties of a "characteristic aquitard" of weighted average thickness. These derived parameters, which represent average properties at each site, included the vertical hydraulic conductivity, as well as the elastic and inelastic compressibilities. The compressibilities, together with aggregate thickness, defined the ultimate elastic and inelastic deformation, and hence the potential ultimate changes in storage, in response to a given change in head in the bounding aquifers. When combined with hydraulic conductivity, these parameters also defined the elastic and inelastic time constants that determine the time lag inherent in the depletion and, in the elastic case, also the replenishment of aquitard storage.

The time constant represents the time required to complete about 90 percent of the ultimate aquitard drainage (or recharge) and accompanying deformation in response to an initial stepwise change in stress (drawdown or recovery) on the aquitard-aquifer boundary. As you would expect, it varies inversely with the hydraulic conductivity and directly with the specific storage of the fine-grained material. For clays and silts undergoing inelastic compression, the specific storage is essentially equivalent to the sediment compressibility, that is, the reduction in pore volume per unit decrease in pore pressure. Under elastic deformation, the compressibility of the pore water itself constitutes a modest but significant component of the specific storage. The time constants also vary directly as the square of the bed thickness. Bed thickness occurs twice, in the second power, in the time-constant definition, because it is a measure of the total quantity of water that must eventually be expelled for a given change in pore pressure, and also of the length of the flow lines along which the drainage occurs. It therefore exerts a powerful influence on the duration of the transient response of aquifer systems to changes in discharge and recharge. An awareness of the idealized nature of the time constant may be gained by recalling that all three of the parameters involved in its definition are assumed to be constants when, in fact, they all vary to some degree as a function of stress. In general, vertical hydraulic conductivity probably is the parameter most sensitive to stress changes.

For typical aquitards, as recognized in well logs, the time constants are likely to range from days to a decade for elastic processes and from several years to millennia for irreversible compaction. The time required for essentially complete expulsion of the potential water of compaction and decay of residual excess pore pressures is about two time constants. The strongly nonlinear nature of the transient process is further illustrated by the fact that one-half of the ultimate compaction occurs in only 20 percent of the time constant.

Helm's numerical model was initially developed to test the ability of the graphically derived parameters to reproduce the extensometer record when incorporated in a physical model based on the same admittedly simplistic concepts and driven by the related water-level history. Its striking success in so doing was quickly followed by its inverse application to the derivation of these parameters, in a manner more rigorous and less constrained than the graphical method. This was achieved by applying trial-and-error modeling to water-level and extensometer or benchmark histories at numerous locations in California, Arizona, and elsewhere. The relatively limited variability of the average constitutive properties determined at many sites came as something of a surprise but provides potentially powerful criteria for assessing the physical reasonableness of parameters derived from or embodied in other interpretive and predictive endeavors. With aquitard properties experimentally defined *in situ*, or reasonably postulated, it became possible to apply the model to the prediction of aquifer-system deformation in response to projected head changes resulting from proposed strategies of future resource management.

More than two decades ago, the accumulated advances in the theory and practice of aquifer mechanics and hydraulics (two inextricably linked subjects) reportedly led one of the Nation's most distinguished hydrologists to proclaim, "We don't need to spend any more money on aquifer mechanics. You guys have solved that problem." At the time, the remark seemed gratifying in some ways and frustrating in others, for reasons that need no amplification for this audience. The attendance here today and the range of topics on

the program suggest that his pronouncement may also have been a bit premature.

Within the USGS, in the interim, we have seen Stan Leake's development and refinement of the Interbed Storage Package for the MODFLOW ground-water flow model. Michelle Sneed and Devin Galloway have also demonstrated an ingenious 90-degree flip of MODFLOW that sets the areal model on edge and allows it to be applied to the one-dimensional vertical flows embodied in the drainage of a sequence of aquitards of various thicknesses and differing properties, interbedded with aquifers exhibiting different heads. It thus serves as a convenient alternative to the classic Helm model.

Galloway also pioneered recognition of the potential of satellite-based InSAR to delineate in unprecedented spatial detail the areal distribution of changes in confined aquifer-system storage, both elastic and inelastic, as reflected in subtle changes in land-surface elevation over periods of months or years.

Accumulated experience and continued evolution of extensometer design are embodied in recent single and dual installations built by Charles Heywood, Devin Galloway, and me. These instruments use pipes rather than cables as the extensometer element, or length standard, and are referenced to a nominal land-surface datum that is based below the surficial zone of soil shrink/swell caused by moisture and temperature change and other sources of disturbance. In addition, they employ highly sensitive electronic transducers that resolve movements of the datum on the order of 1.0×10^{-5} ft. These state-of-the-art extensometers can record elastic compression and expansion in response to water-level changes of as little as a few hundredths of a foot. In so doing they can delineate short-lived and subtle changes in the stress-strain relation that may allow distinction between the properties of the more and less permeable layers in the system.

Tom Holzer and Mike Carpenter, among others, have conducted comprehensive field studies of surface fissuring associated with subsidence. Their applications of tectonic fault-dislocation models to fissures would appear to have potential application in other areas where buried faults constitute barriers to ground-water flow or separate sedimentary sequences having markedly different characteristics. Carpenter's continuous monitoring of the Picacho fault/fissure in central Arizona, using a buried horizontal extensometer, demonstrated conclusively that small-scale opening and closing of the fissure were correlated with drawdown and recovery of water levels in nearby wells.

In the next days you will learn about advances in the application of GPS technology to the precise determination of benchmark elevations and locations; you will see new demonstrations of the remarkable power of radar interferometry, known as InSAR; and you will be introduced to a number of interesting case histories.

This morning I have been generously accorded the opportunity to indulge in some unbridled speculation as to where we might go from here. I will leave further discussion of two of the most exciting technologies, GPS and InSAR, to those who have been working with them, and will focus on a few problem areas and some more-or-less untried approaches that may shed light on them.

In many localities, the relentlessly increasing demand for water is stressing the readily available supplies and can be expected to require carefully engineered strategies of conjunctive use of surface-water flows and the storage and recharge capacities of the ground-water systems. If adjacent water bodies, low-gradient flood plains, and highly sensitive infrastructure are not limiting factors, then intermittent and broadly distributed ground-water mining, with modest magnitudes of attendant subsidence, may be considered an acceptable interim measure. This process of exploiting the nonrenewable resource embodied in the water of inelastic compaction has the additional attraction of preconsolidating the aquifer system to strain equilibrium with drawdowns larger than could be accommodated elastically under the initial conditions. Subsequent intermediate and longer-term cycles of depletion and recharge can then take advantage of the resulting increase in strictly elastic storage capacity under the probable future constraint of progressively diminishing tolerance for ongoing nonrecoverable subsidence. However, any such proposal clearly must be based on adequate aquifer-system characterization and an effective monitoring plan. In areas of higher vulnerability, even minor subsidence identified as nonrecoverable may be deemed unacceptable.

In any case, wherever areas of potentially high demand are underlain by thick unconsolidated aquifer systems, ground-water development that is poorly considered and inadequately monitored can be expected to increase the probability of an unanticipated and initially unrecognized transition from elastic to nonrecoverable compaction, with the attendant risks of flooding, damage to engineered infrastructure, and perhaps the

sudden appearance and rapid erosional enlargement of destructive earth fissures. Historical precedent suggests that such fissuring may be the first recognized symptom of an already well-established subsidence process, if local releveling has not been done previously or has not been referenced to a stable benchmark. Thus, a critical planning requirement is the ability to predict the threshold drawdown, or preconsolidation stress, at which a transition from elastic to inelastic compaction can be expected. Under many circumstances, this may turn out to be a challenging undertaking.

Some areas of large historical drawdowns and known or presumed subsidence have recently experienced major recovery, in some cases to near virgin water levels, as the result of reduced agricultural demand or the importation of surface water, or both. With population growth and increasing industrial development, water-resource managers are again faced with a foreseeable need to draw heavily on groundwater storage during seasonal intervals of high demand and during possibly prolonged periods of diminished supply. If the historical cycle of subsidence and elastic rebound were recorded by extensometers and water-level measurements, it should be possible to identify on the recovery curve the approximate value of aquifer head equivalent to the highest residual pore pressures that remained in the middle of thick aquitards at the end of the first drawdown cycle. This is the point at which inelastic compaction can be expected to resume, perhaps at very modest rates initially, on a cycle of renewed large-scale drawdown. If these data were not recorded, there may be little basis for predicting what the preconsolidation legacy will turn out to be. For the typical accumulation of Quaternary alluvium, normally consolidated during a period of continuous deposition and unaffected by anomalous stress increases prior to development, the upper limit of possible preconsolidation stress is, of course, the minimum sustained historical water level. In minimally developed areas with little historical drawdown, natural processes of desiccation and incipient diagenesis are likely to have imposed a modest preconsolidation stress, equivalent to perhaps 40 to 80 ft of aquifer drawdown.

If the aquitards are generally thin and relatively permeable, it might be possible to reimpose drawdowns that closely approach the maximum sustained historical values without causing a significant resumption of nonrecoverable compaction. This proposition is seductively simple, sounds plausible, and may be cited in support of a proposed development but perhaps without recognition of the all-important "if." Its validity would require that virtually all the potential water of compaction had been expressed during the first drawdown cycle. For this to be true, the calculated inelastic time constants would typically need to be less than one-half the number of years involved in a prior history of ongoing drawdown below the virgin preconsolidation stress. It must also be noted that under these optimal and probably uncommon circumstances, the volume of water available from elastic storage on the second and subsequent drawdown cycles would be limited to a very small fraction, perhaps 1 to 5 percent, of that produced during the initial episode of ground-water mining.

To evaluate these constraints it is instructive to consider the inelastic time constants derived by Helm for the San Joaquin and Santa Clara Valley extensometer sites. These range from 5 to 1,350 years and average 159 years. Eliminating the two extreme values produces a range of 13 to 215 years and reduces the average to 79 years. Very few of the sites would likely fit the time-constant criterion for nearly complete expression of the potential water of compaction during the several decades of historical drawdown.

Even with the safeguard of monitoring extensometers, the design and successful realization of sophisticated management strategies will be dependent on reliable characterization and simulation of both the hydraulic conductivity and the intermediate and long-term *elastic* storative properties of complex aquifer-aquitard systems. By highlighting the time dependency of *system* storative properties, I have automatically injected the role of aquitard properties into the challenge of achieving a balance between supply and demand across a wide range of timescales. As succinctly stated by Freeze and Cherry, "In many aquifer-aquitard systems, the *aquitards provide* the water, and the *aquifers transmit* it to the wells." In the central-valley and distal alluvial-fan areas of a typical intermountain ground-water basin the aquitards are likely to make up 50 to 80 percent of the sedimentary sequence, and to have total elastic compressibilities (skeletal plus water, in other words, specific storage values) about five times larger than those of the interbedded aquifers. Thus, their aggregate storage potential may constitute roughly 90 percent of the confined storage capacity of the basin. However, the inherent delay in aquitard drainage, even under elastic conditions, imposes serious limitations on how rapidly this volume can be accessed, for either extraction or replenishment. If the total aquitard thickness is concentrated in a few

relatively massive layers, ranging, perhaps, between 35 and 125 ft in thickness, the volume actually available during semiannual drawdown and recovery cycles probably will not exceed 50 percent of the potential and may be less than 10 percent. Thus, the rate at which aquitard storage can be accessed becomes the critical parameter and this, in turn, is profoundly influenced not only by the constitutive properties of the aquitards but also, very strongly, by the number of aquifer-aquitard interfaces through which drainage can occur.

Let us briefly explore a couple of hypothetical examples at the ends of what might be considered a typical range of stratigraphic distribution, one that reflects considerable differences in depositional history and environment: Consider two aquifer systems, each 1,000-ft thick and containing aggregate thicknesses of clay up to 750 ft. In one, the clay is concentrated in five layers each 150-ft thick; in the other, clays having the same constitutive properties are distributed among 50 layers each 15-ft thick. Assuming a typical elastic specific storage of 5×10^{-6} ft^{-1}, a sustained decline in confined head of 150 ft would eventually produce 0.56 ft of recoverable subsidence and a yield from storage of about 430 acre-ft/mi^2 from each of these systems. With clays of typical permeability, a 6-month pumping season could be longer than the elastic time constant of the thinly bedded system and could thus allow it to produce most of its stored water and potential elastic compression, although the actual percentage could be considerably less, depending on the permeability and on the time distribution of the seasonal drawdown, that is, the shape of the drawdown curve. However, given the same properties and conditions, the massively bedded system would produce only one-tenth of the long-term potential. The same set of assumed properties, considered from a different perspective, leads to the conclusion that the 6-month yield of any beds more than about 30-ft thick will be essentially the same, regardless of their actual thickness, because the storage capacity of their inner regions remains inaccessible during a short-term pumping season. The bed thickness to which such a statement applies obviously increases for longer time periods, but only as the square root of the time. Thus, after 5 years the lower limit of thickness is still only about 100 ft. Grossly simplified generalizations of this kind obviously must be viewed with caution because of the number and ranges of the variables involved and the assumptions that must be evaluated. Nevertheless, they serve to emphasize the need for careful evaluation of the best possible well logs, including geophysical logs such as the microresistivity and guard logs that reveal the presence of thin sand drains or thinly interbedded sands and clays. It is my impression that a heightened awareness of the significance of the real number of draining interfaces could be instructive to anyone who might attempt to calibrate or apply an areal flow model that lumps a number of aquitards into a single layer or incorporates only Theis' classical concept of a time-independent storage coefficient.

The issues I have raised suggest several areas in which we might try to improve our tools and techniques. One of the most important and challenging is the determination of preconsolidation stresses in an aquifer system in which current heads have recovered to levels substantially higher than their historic lows. A closely related issue would be the same determination for a previously undeveloped aquifer system, which might be an older, possibly preconsolidated formation underlying the developed one. The obvious brute-force (and expensive) approach would be to pump several closely spaced, high-capacity wells hard enough to quickly recreate local drawdown that might approach the maximum historic values, which may have taken decades to attain and may or may not be known with any degree of reliability. The concurrent task would be to monitor the system to detect the initial transition from elastic to inelastic deformation. Presumably, a carefully designed extensometer/piezometer installation could achieve this, but a somewhat lengthy monitoring period might be required. Both experience and theory as Paul Hsieh has demonstrated indicate that the extensometer should not be too close to the production wells, because of the complex three-dimensional strains that develop in response to concentrated centripetal seepage stresses near the wells. As a rule of thumb, a separation equal to the thickness of the producing interval is suggested. Therefore, the actual drawdowns in and close to the production wells would need to be substantially greater than the target value at the extensometer site.

The data from a single or even dual extensometer probably would not be able to identify a limited depth interval or major aquitard with the lowest preconsolidation stress and earliest vulnerability to future compaction. Such identification might be a significant factor in the design of new facilities for increased production. Assuming uniform historical drawdowns throughout the developed depth interval, we could reasonably surmise that the thickest aquitards would be

the likely candidates. Such layers might be expected to have the largest time constants and therefore to have experienced the least pore-pressure declines in their medial regions during the period of historical drawdown. However, differences in hydraulic conductivity might readily override the thickness (squared) factor and cause a thinner but less permeable layer to have the largest time constant. In any event, ongoing drawdown could be expected to trigger inelastic compaction expanding vertically from the medial regions of successively thinner or more permeable aquitards, or both, until the entire section was involved. A pumping regime programmed to generate a series of small stepwise stress increases and subsequent decreases over a period of weeks or longer might be expected to facilitate the least ambiguous interpretation. Whether such a program would be considered feasible would likely depend on economic and political factors, as well as the obvious technical elements. Given the capital investment and operating costs of a long-term aquifer storage and recovery (ASR) program, the resources required for the development of reliable design and performance criteria might be considered a worthwhile alternative to *ad hoc* management.

A highly experimental but intriguing alternative for identifying preconsolidation levels may be found in the detection of acoustic emissions (AE). The technique is based on the observation that many materials, including metals, rock, and soils, emit very small acoustical or microseismic signals when subjected to stresses greater than those to which they are equilibrated. These noises are believed to be caused by microscopic dislocations in the crystalline or particulate structure of the materials, as they deform. Lord and his coauthors, reporting on triaxial shear tests of soil samples, note that:

> "Under constant load, the strain and acoustic emission behavior is identical. Stress/strain and stress/acoustic emission behavior always results in similarly shaped curves at all confining pressure levels."

Metals characteristically exhibit a great increase in the emission of acoustical energy when they are stressed beyond the maximum stress imposed on them in the past. This phenomenon, termed the "Kaiser effect," is usefully applied in the testing of pressure vessels. It is hardly surprising that a similar effect has been noted by Hardy and Leighton in the cyclical loading and reloading of soils. These observations strongly suggest that an appropriate detector, a piezoelectric transducer, placed against the wellbore wall in the middle of an interbedded aquitard would detect the transition from elastic to inelastic behavior even before it was well defined by a change in the trend of the stress/strain relation.

At the relatively high frequencies observed for soil emissions, the signals are attenuated within short distances in transmission through the sediment. Therefore, a vertical array of several detectors distributed through a relatively thick aquitard might be able to track the propagation of a drawdown cycle into the interior of the layer, and thereby define its hydraulic diffusivity. Further slow progression of aquifer drawdown toward its historical low could be expected to trigger the Kaiser effect, first in the middle of an interbed and progressively toward its boundaries, thus defining the approximate shape of the minimum past pore-pressure curve. If the drawdown occurred very rapidly—attaining the historic low in less than 5 percent of the elastic time constant of the aquitard—the Kaiser effect would propagate inward from the aquifer interface. What I have just suggested is, of course, largely speculative, but seems promising enough to warrant serious investigation.

Exploration of the potential of AE probably should begin in the soils laboratory, where practical instrumentation issues could be addressed under controlled conditions. Triaxial loading experiments conducted at a constant, slow strain rate on cores from deep aquitards could be instrumented with AE detectors. These might be expected to identify, through the Kaiser effect, the elusive preconsolidation stress, which is not usefully resolved by the conventional graphical interpretation of stepwise-loaded consolidation tests that span the requisite high in-situ stresses. That, in itself, would be a very significant achievement, although the representativeness of aquitard properties measured in a few cores is always open to challenge. Despite my admitted bias in favor of *in-situ* testing, I would surmise that preconsolidation stress, if determinable in the laboratory by AE, would be the property least likely to be deflected from a representative value by the textural variability typical of an alluvial sequence. A convincing demonstration of the reliability of the technique could add a great deal of value to the laboratory tests that are often incorporated in exploratory programs, perhaps with inadequate regard for their inherent limitations.

In the field environment, AE could also be applied in conjunction with some unconventional loading techniques that might be used instead of pumping high-capacity, fully penetrating production wells. Perhaps the most readily tested procedure would involve creating large drawdowns in limited depth intervals or individual aquitards by extracting water at small to moderate flow rates from a short borehole interval isolated between straddle packers. Similarly, if a piezometer fitted with an AE detector were screened only in the medial portion of an aquitard, it might be possible to create large, highly localized pore-pressure drops simply by bailing. This procedure, or pumping with a small diameter sampling pump, should generate a slowly expanding quasi-spherical volume in which the increase in effective stress would be great enough to trigger the Kaiser effect.

This last suggestion raises the broader issue of reliable pore-pressure measurement in aquitards. A variety of techniques and equipment have been tested and reported, primarily in the geotechnical literature, but the technology remains somewhat challenging and is apparently intimidating to many hydrologists. For whatever reasons, it is all too rarely incorporated in the multiple piezometer installations that are increasingly recognized as valuable tools in aquifer-system characterization. We need to accumulate a body of widely shared experience in the construction, instrumentation, and performance evaluation of aquitard piezometers in order to develop a more comprehensive documentation of the transient hydraulic and coupled mechanical processes that occur within an aquitard undergoing changing stresses on its boundaries. This coupling may be somewhat less straightforward than we commonly assume.

Behind the success of compaction simulators based on Terzaghi's simplified and linearized model of consolidation, there lurks an element of uncertainty about the physical significance of the values of hydraulic conductivity so derived. These values are dependent on the assumption that the time delay of compaction is entirely determined by the hydraulic impedance to the escape of the required volume of the water of compaction. In making this assumption we are discounting the possible role of the clay properties that manifest themselves in the non-hydrodynamic, or secondary, consolidation that is routinely observed in laboratory consolidation tests, in which diminishing rates of compaction continue long after excess pore pressures in the sample have essentially dissipated. Don Helm has addressed the mathematical complexities involved in reconciling the hydrodynamic and non-hydrodynamic phases of the laboratory observations within a unifying physical model of transient response to increased stress. He concludes:

> "The premise that the skeletal structure of saturated sediments behaves more nearly like a nonlinear viscous fluid than a linearly elastic solid has been corroborated by analysis of a series of standard one-dimensional consolidation tests. * * * Subsidence prediction can be significantly improved by the application of the new theory to the transient removal of subsurface fluids from sedimentary basins."

Extrapolating Helm's concepts and the laboratory experience to the field environment, admittedly a large step, raises a question as to whether pore-pressure measurements in the middle of an aquitard might reveal a nearly complete decay of residual excess pore pressures while mechanical measurement of deformation showed continuing compaction. Such an observation would imply that our mechanically defined values of hydraulic conductivity incorporate a component attributable to the viscoelastic properties of the aquitard skeleton and are therefore too low. This component would impose an additional delay that would masquerade as hydrodynamic lag in the consolidation process. Presumably, a combination of relatively high permeability (for an aquitard) and high skeletal viscosity would exacerbate the problem, whereas the converse might cause it to disappear. While these concerns might seem academic in terms of our ability to evaluate and predict subsidence and the concomitant yield from storage, they are fundamental to our understanding of essential aquitard properties and aquifer-system mechanics. In addition, they gain practical significance in the context of quantifying the hydraulic responses of leaky confined aquifers. If drawdowns observed in aquitard piezometers yield larger values of diffusivity than stress-strain analysis, then we have some explaining to do, as well as a need for some of the basic data needed to do it. A practical consequence of such a discrepancy would be the propagation of drawdown through upper and lower confining beds, and the extraction of water from the bounding unpumped aquifers, more rapidly than predicted from deformation analysis.

Rigorous exploration of these possibilities would likely require more vertically detailed resolution of

deformation than is provided by a single or dual extensometer. Incremental borehole-extensometry techniques that employ repeated logging of the changes in depth of targets, such as magnets, inductive bands, or radioactive bullets, imbedded in the borehole wall could provide this information. Significant refinement of existing equipment probably would be required to achieve the desired resolution over limited depth intervals. Such techniques would also shed light on the variability of sediment properties as a function of lithologic differences among the targeted depth intervals.

Multiple nested piezometer installations constructed with axially compliant PVC pipe also afford opportunities to test low-cost methods for acquiring increased detail in vertical deformation. The feasibility of installing at least six 2-in. piezometers at various depths in a single borehole has been demonstrated, and the installation of a pipe or rod extensometer in each one of these should be readily achievable. Automatic compensation for the changing buoyant support of the extensometer with fluctuating piezometer water levels could be incorporated in the data-logging or reduction programs.

In areas of fairly rapid subsidence, periodic measurement of the total depths of PVC piezometers with dimensionally stable steel tapes or sounding wires could provide useful data at minimal cost. Potential difficulties due to silt accumulation in the casing sumps could be prevented by incorporating a steel measurement stop in the casing string just above the screen. Use of a substantial permanent magnet as the sounding weight would facilitate the application of a precisely repeatable tension on the tape during measurement. Other features of conventional tape extensometer design could be incorporated, probably resulting in repeatability of 0.001 ft, or better.

Many of the points I have raised take on additional significance when considered in the context of comprehensive pumping tests designed to characterize both the short-term hydraulic and longer term hydromechanical properties of an entire aquifer system. The design and interpretation of such tests has been rendered vastly more efficient and effective by the development of computer programs, such as AQTESOLV (HydroSOLVE, 2003), that facilitate analysis of complex, multivariable systems. The mutually reinforcing combination of pore-pressure and deformation data obtainable with readily available technology promises to minimize ambiguities inherent in either dataset alone. I anticipate that the requirements of carefully engineered conjunctive-use programs will result in a steady increase in the incorporation of multiple piezometer/extensometer installations in aquifer-test design. When used in conjunction with borehole flowmeter logs in the pumped well, these installations should facilitate the determination of the conductive and storative properties of all major elements in the aquifer system.

Before closing, I would like to address briefly the issue of subsidence-related surface fissures. These have sometimes been the first recognized indicator of subsidence and may be its most obvious and alarming manifestation, particularly after their rapid and often spectacular enlargement by erosion. It is apparent that they represent tensile failures in the unsaturated zone and presumably localized extensional strain to some depth below the depths of actual failure, yet the specific mechanisms involved in their formation are not well documented and have been a subject of considerable speculation and controversy. I will not delve into the theoretical aspects of the problem, but will focus on observational techniques that may help to constrain the mechanisms. The data obtained thus far are limited to measurements of horizontal and vertical displacements of the land surface. I have referred to Carpenter's analysis of the time series generated by a 98-ft-long horizontal extensometer spanning a major, long-established fissure. His Professional Paper 497–H also reports on repeated horizontal and vertical control surveys along a profile 4,730 ft in length that spans the same fissure, as well as several others. Vertical control was established using precise differential leveling; horizontal control was established using tape extensometry over distances less than 100 ft close to the fissure and by electronic distance measurement over longer distances. These techniques were very effective in defining the displacements at land surface and could be employed to good advantage in any investigations of fissuring, unless they were severely restricted by natural or manmade obstacles. However, they provided no direct measurement of the stresses or strains at the depths where the phenomena had their origins.

Future investigations of fissuring would benefit from efforts to compare surface deformations with movements occurring at depth. A straightforward way of comparing horizontal movements is by means of a borehole inclinometer. This instrument is a highly sensitive, two-axis tiltmeter built into a logging probe equipped with wheels that run in grooved tracks cut into the inner surface of a plastic well casing. A

semi-continuous three-dimensional plot of borehole alignment can be generated by taking readings of the departure from plumb at closely spaced depth intervals. Repeated logging referenced to known surface displacements of the well head would define the vertical distribution of relative horizontal strain over time in a well bore adjacent to a known fissure or in an unfissured zone believed to be at risk. This information would help to define the shape and origin of the strain field that manifests itself as tensile failure near the land surface. Numerous surface observations and trenching studies have made it clear that fissures typically are open to moderate depths for some time before they break through to the surface, often during a period of heavy rain. However, it is not known whether the maximum extensional strain occurs near the surface and diminishes steadily with depth, as would be expected in the case of simple convex-upward flexure of sediments overlying a zone of localized differential compaction in the aquifer system. Alternatively, the maximum strain might originate and be maintained at depth by localized differences in the rate of horizontal translation of the aquifer system toward the center of pumping. In a zone of active fissure movement, this key question probably could be resolved by repeated logging of a borehole inclinometer casing that penetrated to the base of the aquifer system.

A supplement or possible alternative to the borehole inclinometer may be found in the inverted pendulum. This device comprises a light wire anchored at the bottom of a borehole and suspended at the land surface from a doughnut-shaped buoy that is submerged in a liquid-filled toroidal chamber large enough to accommodate the anticipated range of movement. The buoyancy of the buoy, or float, seemingly acts to invert gravity and thus maintain the wire under constant tension and in a rigorously plumb alignment. Horizontal movement of the float chamber relative to the float, and thus to the bottom-hole anchor, is monitored in two orthogonal directions with a high level of precision and may be continuously recorded, if desired. If vertical deformation in the spanned depth interval were considered likely, that could also be recorded, thus incorporating vertical extensometry and converting the instrument into a three-dimensional deformation monitor. The principal limitation of the device is the depth to which its borehole can be drilled sufficiently straight and plumb to ensure that the wire does not contact the well casing. Among its attractive features are simplicity, relatively low cost, and most especially, the potential for continuous recording. This last feature could prove particularly instructive when the instrument is used in conjunction with a continuously recording horizontal extensometer. If acceptable boreholes can be drilled to sufficient depth, perhaps 150 ft or more, the inverted pendulum might provide the first clear-cut answer to the question of the locus of maximum strain and direction of vertical propagation of failure, up or down, in an enlarging fissure.

In addition to monitoring existing active fissures in an effort to elucidate the principles of their origin, it is of great practical importance to attempt to detect incipient or potential fissures before they break the surface and inflict major damage. Several investigators have demonstrated that small-scale seismic profiling using a sledgehammer energy source can locate subsurface failure planes or incipient fissures. These techniques are particularly useful for mapping the anticipated future extension of an existing fissure.

If InSAR imagery or repeat GPS or conventional surveys delineate bands of concentrated differential subsidence or horizontal extension, these zones must be considered potentially vulnerable to fissuring and worthy of focused exploratory and monitoring efforts. Unfortunately, the total historical accumulation of surface strain will seldom have been recorded, and, in any case, the tensile strain at failure of shallow soils *in situ* is not well known. If the extent and rate of progress toward failure are to be evaluated, it should be of great interest to determine the magnitude and pattern of the horizontal component of geostatic stress at depth. In normally consolidated, undeformed alluvial sediments, the ratio of the horizontal to the vertical compressive stresses due to the overburden typically varies from about 0.4 to 0.7. In sediments undergoing horizontal extension, this so-called lateral stress ratio would be expected to become strongly anisotropic, with minimum values parallel to the direction of extension. Presumably, the ratio controlled by this least principal stress, if individually identified, would have to drop through zero and become some negative number, indicative of tensile stress, before tensional failure could occur. The increase with depth of both the horizontal and vertical components of geostatic stress indicates that the actual value of least principal stress would remain positive at depth even after comparable strain had produced tensile stresses and failure in the relatively shallow subsurface. This relation implies that the field evidence of fissure initiation well below the surface may be due more to a reduction in tensile

strength with depth than to an increase in strain with depth. Confirmation at depth of anomalously low values of the average lateral stress ratio or anisotropy in its orthogonal components, or both, would be at least a qualitative indicator of potential fissuring.

Identification of the magnitude and orientation of the least principal stress at depth has long been practiced in low-permeability oil and gas fields by means of hydraulic fracturing experiments. An isolated depth interval in an open borehole is pressurized hydraulically until a fracture is pried open normal to the least principal stress. The pressure required to hold it open is determined by the magnitude of the stress, and the increment of higher pressure required to initiate the fracture is a measure of the tensile strength of the rock. Direct transfer of this technology to alluvial sediments would seem problematic because of their high permeability. Nevertheless, it may be possible to find ways to circumvent this limitation. One approach would be to use a high-solids bentonite abandonment gel as the pressurizing fluid, instead of water. Once jelled, this pressure medium would essentially eliminate fluid loss to the formation and pore-pressure buildup around the borehole, and should allow measurement of the breakdown pressure and least principal stress. Subsequent logging with an acoustic velocity televiewer might be reasonably expected to provide an oriented image of the resulting fracture.

Another possible approach would be based on the principles embodied in the Menard pressuremeter. This device, widely used in Europe for *in-situ* geotechnical testing, may be envisaged as a highly compliant inflatable rubber packer, or membrane, as it is called, in which both pressure and simultaneous volume increases are recorded as the packer is pressurized and expanded against the borehole wall. The resulting stress-radial strain relation defines, among other things, a pressuremeter modulus that has been very successfully applied, on a largely *ad hoc* empirical basis, to foundation design. It would seem intuitively evident, and was initially believed, that the early part of the stress-strain curve should include an identifiable point representing the undisturbed lateral pressure in the formation. However, according to Baguelin and his coauthors, experience has shown that this value—our desired result—is not reliably defined in the conventional pressuremeter test. The problem apparently is attributable to disturbance of the borehole wall and the adjacent stress field during drilling. Newer, more complex versions of the pressuremeter incorporate a self-drilling capability that emplaces the packer in a gauged-to-fit borehole that has no opportunity to deform inward before the instrument is in place. This development may make the pressure required to initiate borehole expansion a useful indicator of the average lateral stress at rest. Denby and Hughes have described their experiments using a self-boring pressuremeter to measure horizontal stress and also provided useful annotated references to the work of others.

It occurs to me that one might experiment with a pressuremeter that incorporated four expansion chambers occupying divided quadrants of the supporting mandrel. The pressure-volume relation in the two pairs of opposed chambers would be observed independently and would thus provide a means of detecting and gauging orthogonal components of the stress anisotropy that is present in sediments undergoing unidirectional horizontal strain. An additional enhancement could be the incorporation of an AE detector, which might be expected to record a pattern of changing AE that would reflect the initial equilibration between instrument and formation pressures and perhaps, as the test progressed, the virgin lateral stress before anthropogenic distortion of the stress field.

I threatened you with some unbridled speculation, and I seem to be getting close to delivering on that. If I have also stimulated your imaginations in ways that will urge you down new investigative paths, then I will consider the exercise a personal success. To all of you, I wish success in expanding the circle of those who recognize that land subsidence remains an important and rewarding field of study.

The Harris-Galveston Coastal Subsidence District/ National Geodetic Survey Automated GPS Subsidence Monitoring Project

By David B. Zilkoski[1], Lucy W. Hall[1], Gilbert J. Mitchell[1], Vasanthi Kammula[1], Ajit Singh[1], William M. Chrismer[2], *and* Ronald J. Neighbors[2]

Abstract

Subsidence can severely damage property and infrastructure in a developed area. Typically when subsidence is human-induced, its mitigation can be very costly. For example, when the subsidence is caused by the compaction of susceptible aquifer systems related to ground-water pumping and the accompanying ground-water-level declines, water-resource managers might choose to reduce use of the ground-water resource, which often entails some effort to convert from ground-water to surface-water supplies. Accurate monitoring of subsidence over time is vital to providing calibration data for modeling and prediction purposes. The method of geodetic differential leveling used previously to measure subsidence was satisfactory but very costly. A cooperative study by the Harris-Galveston Coastal Subsidence District (HGCSD) and the National Geodetic Survey (NGS) is using GPS methods to measure subsidence at a fraction of the cost of the previous leveling method. Because of the broad extent of subsidence in the Houston-Galveston region, no stable benchmarks are in the area. Therefore, relatively stable borehole extensometers were equipped with GPS antennas to provide a reference frame to measure subsidence at other stations in the area. These stations are known as local GPS Continuously Operating Reference Stations (CORS). In support of the project, it was also necessary to design and construct portable GPS measuring stations called Port-A-Measure (PAM) units.

The project uses dual-frequency, full-wavelength GPS instruments with geodetic antennas. Data are collected at 30-second intervals and averaged over 24 hours. The goal is to yield differential accuracy of less than 1 centimeter vertically in an automated mode operated by HGCSD personnel. Data have now been collected from three CORS and four PAM units for more than 4 years in the Houston-Galveston region. Results between CORS and PAM units indicate that some monuments are subsiding at rates of 7 centimeters per year and correlate well with extensometer data.

In addition to the GPS CORS and PAM units, NGS and HGCSD also performed two GPS network surveys to estimate subsidence in the area—one survey in 1995 and another in 2000. This report presents a brief summary of the CORS and PAM units results and discusses the use of GPS for estimating subsidence in the Houston-Galveston region of Texas.

INTRODUCTION

For several decades, parts of the upper Gulf Coast region of Texas have subsided. Land subsidence is the lowering (sinking) of the land surface in response to the removal of subsurface support. Compaction of subsurface clay layers owing to withdrawal of ground water is the primary cause of subsidence in the Houston-Galveston region. Subsidence can lead to costly damage in coastal regions because of the relative rise of sea level, the associated landward shift of the shoreline, and the increased risk of flooding from storm surges. In inland regions subsidence causes several problems, including modifying stream gradients and

[1] National Geodetic Survey, National Ocean Service, National Oceanic and Atmospherice Administration, Silver Springs, Md.

[2] Harris-Galveston Coastal Subsidence District, Friendswood, Tex.

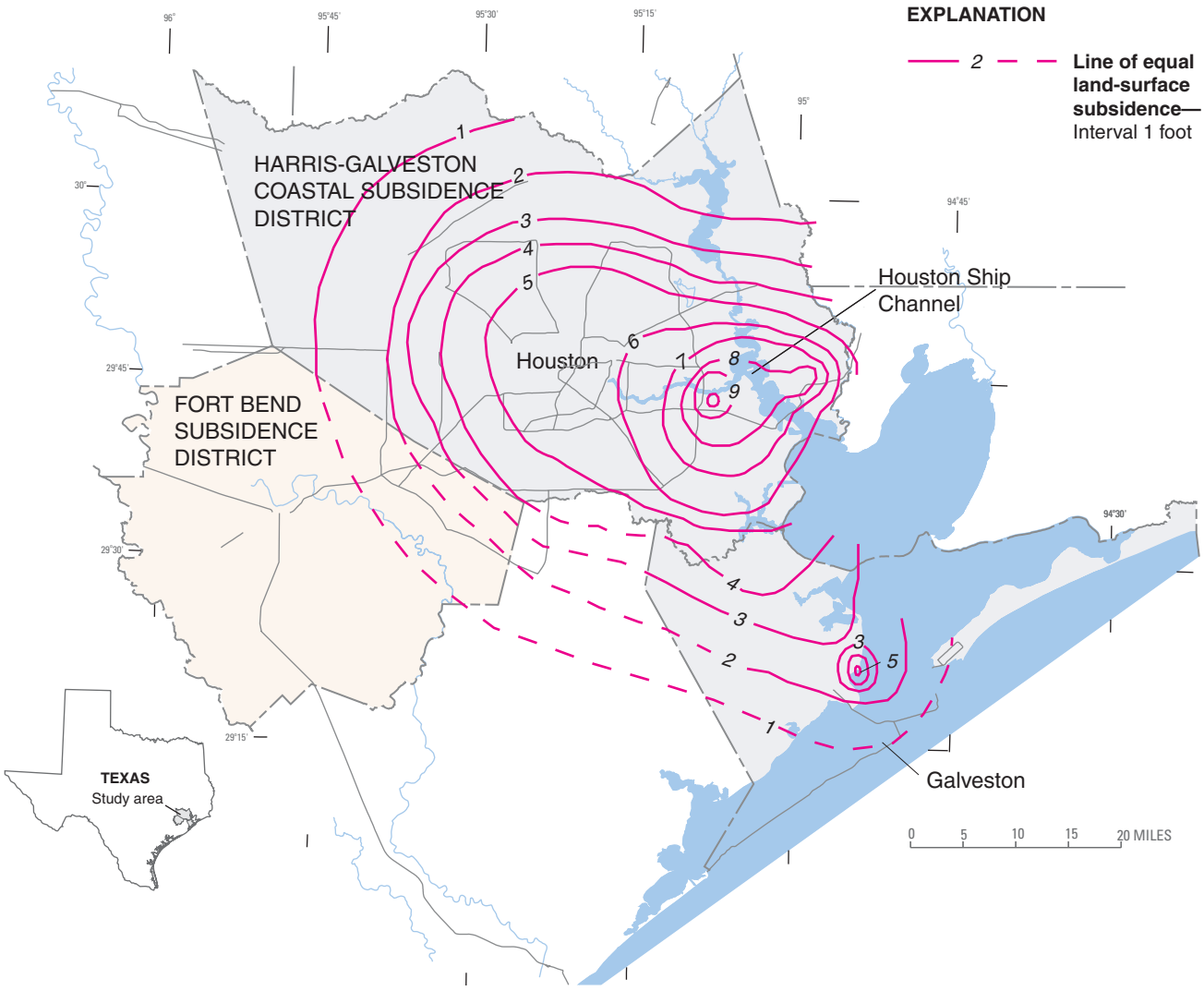

Figure 1. Subsidence occurring between 1906 and 1987 in the Houston-Galveston region, Texas.

changing the geomorphology of flood plains. In 1975 the Texas Legislature created the Harris-Galveston Coastal Subsidence District (HGCSD) to mitigate the subsidence problem in Harris and Galveston Counties through regulation and management of the groundwater resource. In 1989, the Texas Legislature created the Fort Bend Subsidence District (FBSD) to manage subsidence in Fort Bend County. FBSD, a separate district with its own Board of Directors, has adopted an inter-local agreement with HGCSD to provide staff for its operation. FBSD is a partner in the GPS project. Figure 1 is a map of HGCSD and FBSD showing subsidence occurring between 1906 and 1987. Subsidence has occurred throughout most of the two districts, with the greatest amount of subsidence occurring near the Houston Ship Channel.

In the past, the National Geodetic Survey (NGS), a program office of the National Ocean Service, National Oceanic and Atmospheric Administration (NOAA), and HGCSD have used two methods to measure subsidence. The first method, releveling, used conventional differential leveling. More than 2,500 benchmarks are in the area. Some of these were established as early as 1906. Simple algebraic subtraction along level lines yielded the subsidence that occurred between any two releveling epochs. This method gives excellent spatial subsidence data. The cost of the releveling procedure, about $1,170,000 (2001 dollars) for a

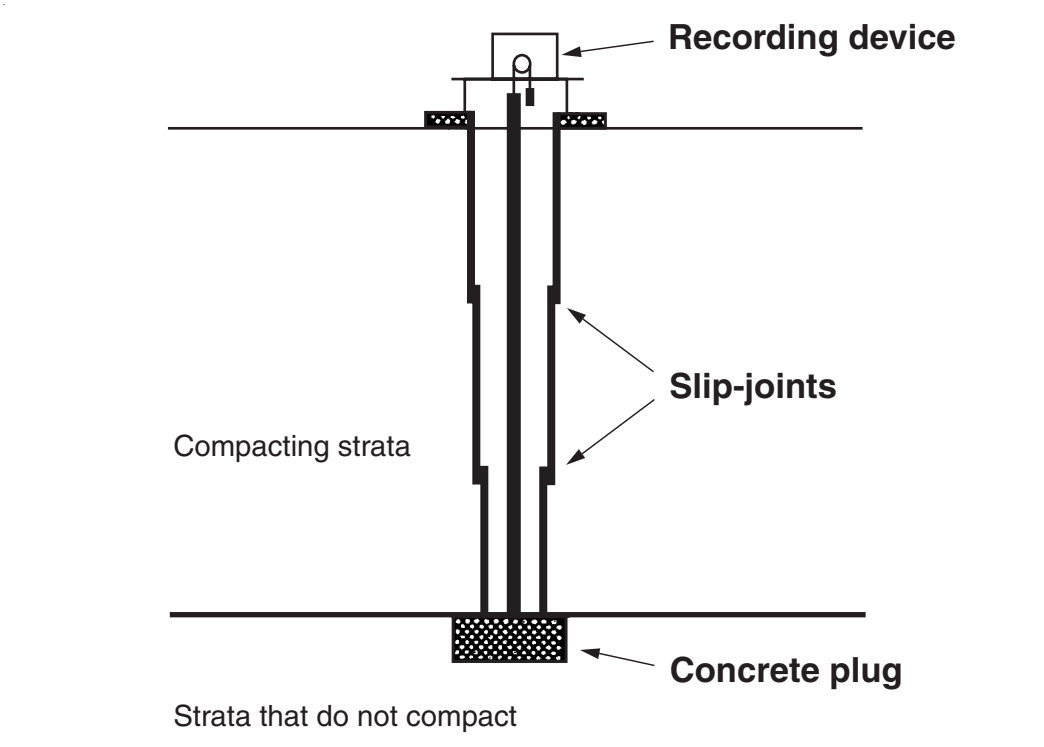

Figure 2. Extensometer used by HGCSD.

single epoch of leveling, prohibits frequent releveling. The development of the GPS in the late 1980s resulted in an affordable alternate method to accurately measure land-surface datums.

The second method of measuring subsidence used deep borehole extensometers, established as deeply-anchored benchmarks. The U.S. Geological Survey (USGS) designed and installed the first of these extensometers in the early 1960s. Figure 2 shows the typical construction of such a benchmark. To construct an extensometer, a hole is drilled to a depth at which the strata are relatively stable. Then, the hole is lined with a steel casing with slip-joints to prevent crumpling as subsidence occurs. An inner pipe rests on a concrete plug at the bottom of the borehole and extends to the top. This inner pipe then transfers the stable elevation below to the surface. A measurement of the distance from the inner pipe to the surrounding land surface gives the amount of subsidence that has occurred. Since many of these extensometers were constructed, the design of borehole extensometers was improved (Riley, 1986) by counter-weighting the inner pipe to reduce frictional forces between the inner and outer pipes and by establishing a more stable surface datum using shallow (15- to 20-ft deep) piers bored in the subsurface. A chart recorder provides a continuous record of subsidence over time. Figure 3 is a typical plot generated from extensometer data for the Addicks extensometer. The six project borehole extensometers in the Houston-Galveston region represent an estimated investment of $800,000 each (in 2001 dollars). Borehole extensometers provide excellent subsidence data, but their cost prohibits their use in sufficient numbers to provide adequate information for the entire area of HGCSD and FBSD.

THE PROPOSED GPS SOLUTION

In late 1993, HGCSD and NGS signed a cooperative agreement to jointly pursue improved, less expensive methods of monitoring land subsidence in the Houston metropolitan area. The agreement between HGCSD and NGS resulted in an experimental study to use GPS to measure subsidence. The project used dual-frequency, full-wavelength GPS instruments and geodetic antennas. Data were collected at 30-second intervals and averaged over 24 hours. The goal was to yield a differential vertical accuracy of less than 1 cm in an automated mode. The collection, processing,

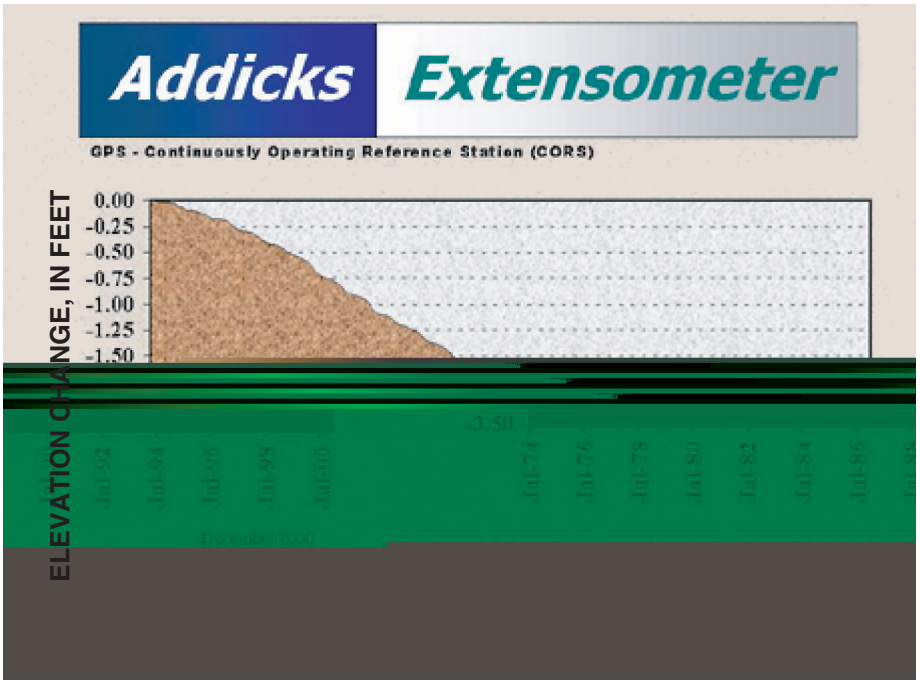

Figure 3. Addicks extensometer data, July 1974–July 2000.

and analysis of the observed GPS data are accomplished automatically using computer software. This report describes the results of the data collection and processing.

No stable benchmarks except for a few extensometers are in the Houston-Galveston region. Therefore, only the extensometers would be available as a reference to measure other stations. The borehole extensometers, which are not typical benchmarks, are relatively stable and provide the location for the project's three GPS Continuously Operating Reference Stations (CORS) (fig. 4). The CORS are Lake Houston, Northeast, and Addicks. Figure 5 is a photograph of the Northeast station, which also is part of the NOAA national CORS system.

It was recognized that any additional GPS receivers used to expand the network would need to be portable. Portability provides flexibility in long-term relocation or, as planned for this project, short-term relocation. Trailers provide the ability to move the equipment from point to point and also provide adequate housing and protection. Port-A-Measure (PAM) units are required to stay in one location for a sufficient time to provide a statistically valid difference in height relative to the three stable CORS.

Design of CORS and PAM Units

The three CORS are colocated on borehole extensometers. These three CORS are considered fixed locations relative to one another. Shelters housing the CORS measure about 6 by 7 ft (fig. 5). These shelters house the borehole extensometers, GPS receivers, and related monitoring equipment. The pipe extending through the roof of the shelter holds the GPS antenna and is an extension of the inner pipe of the borehole extensometer. AC power and a conventional telephone line serve each CORS. A personal computer (PC) receives and stores the data from the GPS receiver. A modem is used to download data from the PC at any time. The capacity of the hard disk on the PC is 300 MB, which is sufficient to store several months of data. An uninterruptable power supply manages the electricity to the GPS receiver, PC, and modem.

Each of the PAM trailers would occupy one reference site for 1 week and then rotate among three other PAM sites, thereby providing measurements of land-surface height changes from the four sites on a monthly basis. A small trailer was selected to house each PAM unit (fig. 6). Each PAM trailer is truly portable with its own power supply and cellular phone. Each site has its own benchmark that the GPS antenna is

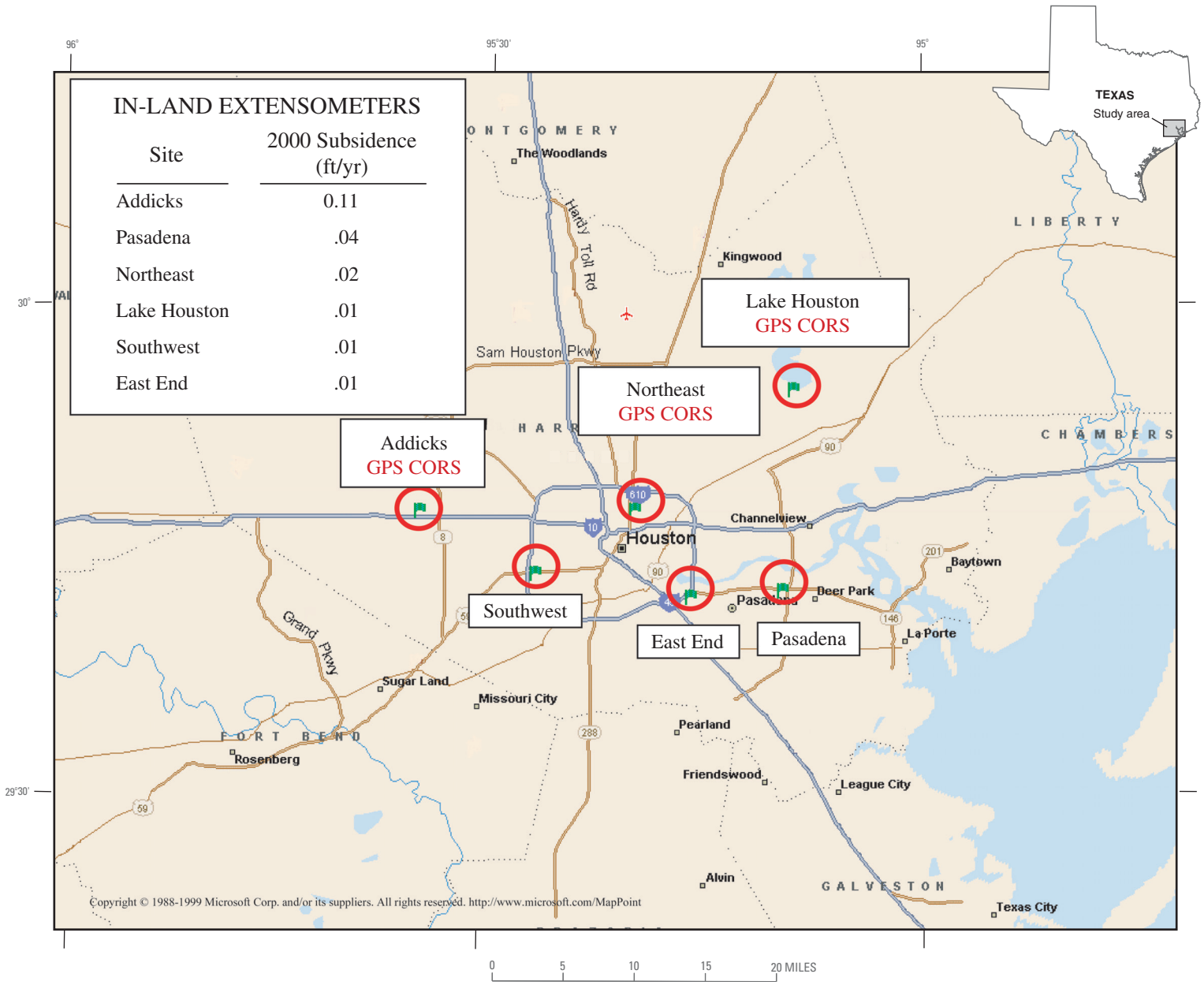

Figure 4. Locations of the three GPS CORS colocated with borehole extensometers, locations of other project borehole extensometers, and rates of subsidence in six extensometers in the Houston-Galveston region, Texas.

Figure 5. Northeast GPS CORS.

Figure 6. Trailer at PAM site.

mounted upon. The PAM trailer is connected to the antenna and relies on its own power and communication devices to transmit data to the office. The cellular antenna and other equipment also can be stored inside. Three 50-watt solar panels routed through a charge controller to four 80-Ah gel cell batteries provide the power supply. A 12-V DC power bus supplies current to the remainder of the equipment. The receiver is powered continuously and draws directly from the 12-V power bus. In the beginning of the project, a timer turned on the power for the modem and cellular phone for 1 hour each day to transmit data to the office, but this proved unreliable. Owing to problems with transmitting data via cellular telephone and modem, the data were subsequently downloaded from the receivers on a weekly basis when the PAM trailers were moved to a new site.

Monumentation of PAM Sites

Clay-rich soils with a high shrink-swell potential (vertisols) are widespread in the HGCSD area. The soil-moisture active zone, the depth at which large variations in soil moisture cause shrink-swell behavior, can extend 4 to 6 m (15 to 20 ft) below the surface. Measurements show that as much as 6 to 9 cm (0.2 to 0.3 ft) of vertical movement can occur in a few days, as expansive clay soils respond to seasonal variations in rainfall and temperature. The reference mark devised for the PAM sites (fig. 7) minimizes this movement.

During 2001, five PAM trailers and 20 PAM sites were operated cooperatively by the City of Houston, Harris County, Fort Bend County, Texas Gas Co., Houston Pipeline, and West Houston Airport. The first of the three CORS (fig. 4) started collecting data in 1993, and all three have been operational since 1996. The first of the five PAM units began collecting data in January 1994, and the fifth PAM trailer was deployed on January 15, 1999. The locations of the 20 sites that the five PAM trailers are moved to on a weekly basis are shown in figure 8.

Stability of Local CORS

The Lake Houston GPS CORS is part of the NOAA National CORS, and its coordinates are monitored daily by the NGS CORS project team. Plots of Lake Houston CORS data are available on the NGS Web site at http://www.ngs.noaa.gov/CORS/Texas/texas_lkhu.html.

Coordinates for the Lake Houston CORS are held fixed when the other two CORS coordinates, tropospheric delays, and phase bias values are determined. The daily coordinates at the other two CORS, Addicks and Northeast, determined using 24-hour datasets, were compared for 1996–2001 to ensure that the system was working properly. These stations are on relatively stable platforms, deep borehole extensometers, and should not be moving provided the anchored depths of the extensometers are below the zones in

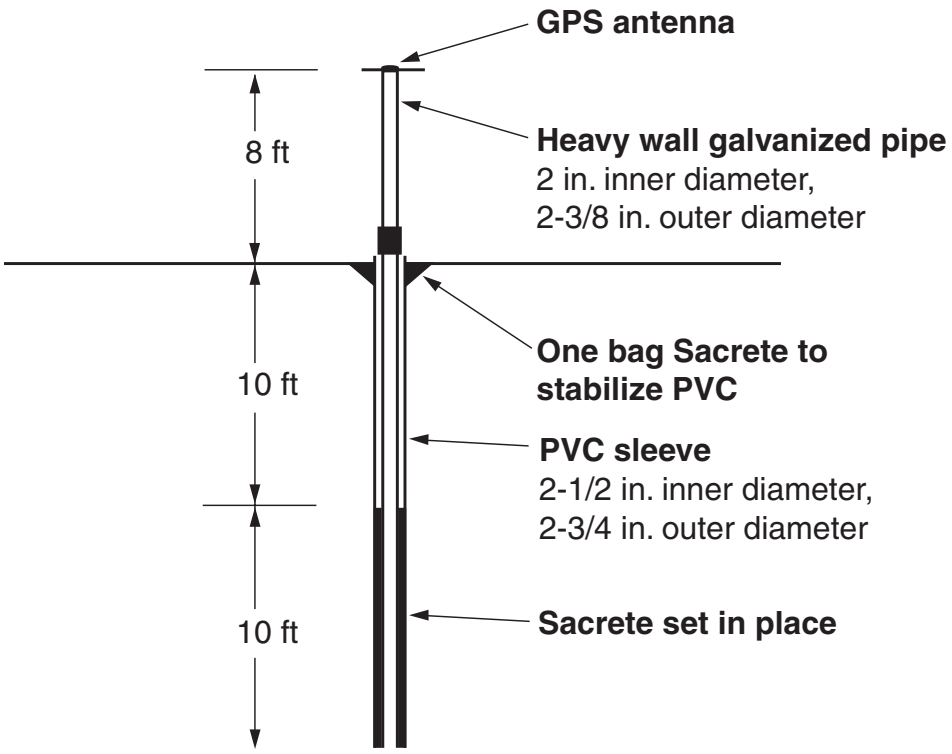

Figure 7. Design of PAM monuments.

the aquifer system affected by aquifer-system compaction. Figures 9 and 10 depict the difference in estimates of ellipsoid heights for 5 years (1996–2001) between the other two CORS and the Lake Houston CORS. The GPS solutions were computed using NGS automated data editing and reduction software, PAGES (Schenewerk and others, 1999). The vertical components computed by PAGES were plotted and all outliers were removed manually.

The slope of the line between Northeast GPS CORS and Lake Houston GPS CORS is 0.06 cm/yr, well within the noise of the measurement techniques. This was expected because on the basis of other hydrogeologic and geodetic information, these two stations should not be moving. The slope of the line between Addicks GPS CORS and Lake Houston GPS CORS is 0.13 cm/yr. A slope of 0.13 cm/yr is small, but the fact that the slope between the two control stations is greater than 0.1 cm/yr is notable. Other hydrogeologic and geodetic data indicate that the Addicks site is not subsiding, but it is located near a region, centered on Jersey Village, that is subsiding (Stork and Sneed, 2002). The PAM 07 site is located in Jersey Village (fig. 8). The GPS data from 2001 currently are being investigated.

A major goal of the HGCSD project is to determine GPS-derived ellipsoid height differences at the 1-centimeter accuracy level at designated PAM sites using an automated approach. Some of the results indicated that a few of the residuals were larger than 1 cm but typically less than 3 cm. NGS is analyzing the GPS data to reduce the noise level of the results. Future studies include correlating ellipsoid height differences with atmospheric conditions and changes in temperature. Preliminary analyses indicate that larger differences in ellipsoid heights occur during the summer months when the Houston region weather is hot, humid, and stormy.

Estimation of Height Changes at PAM Sites

Coordinates of the CORS are held fixed when coordinates, tropospheric delays, and carrier-phase ambiguities of the four PAM sites are determined. Therefore, each PAM site has three vectors associated with it every day it is occupied—one relative to Addicks CORS, one to Northeast CORS, and one to

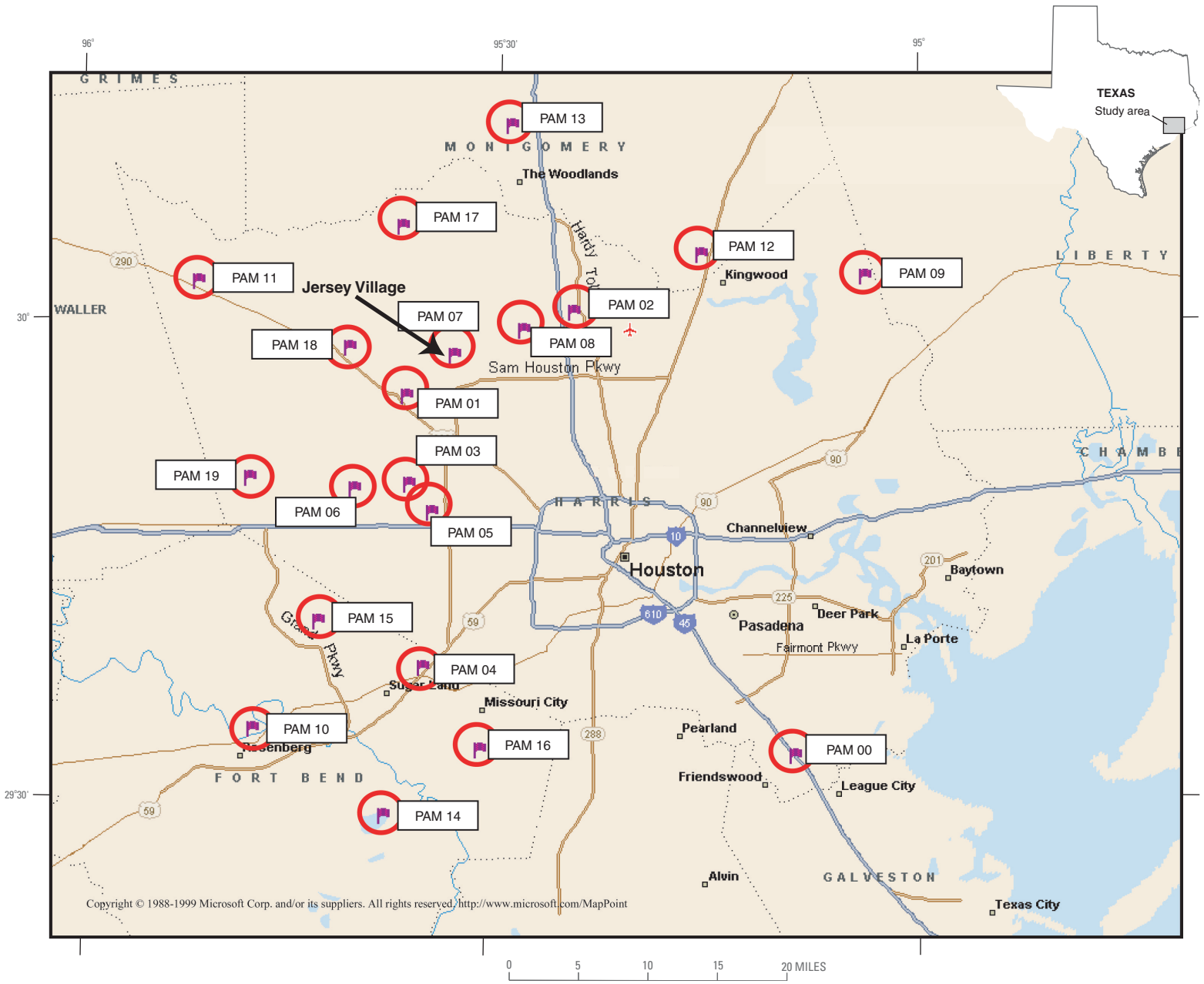

Figure 8. Locations of 20 PAM sites in the Houston-Galveston region, Texas.

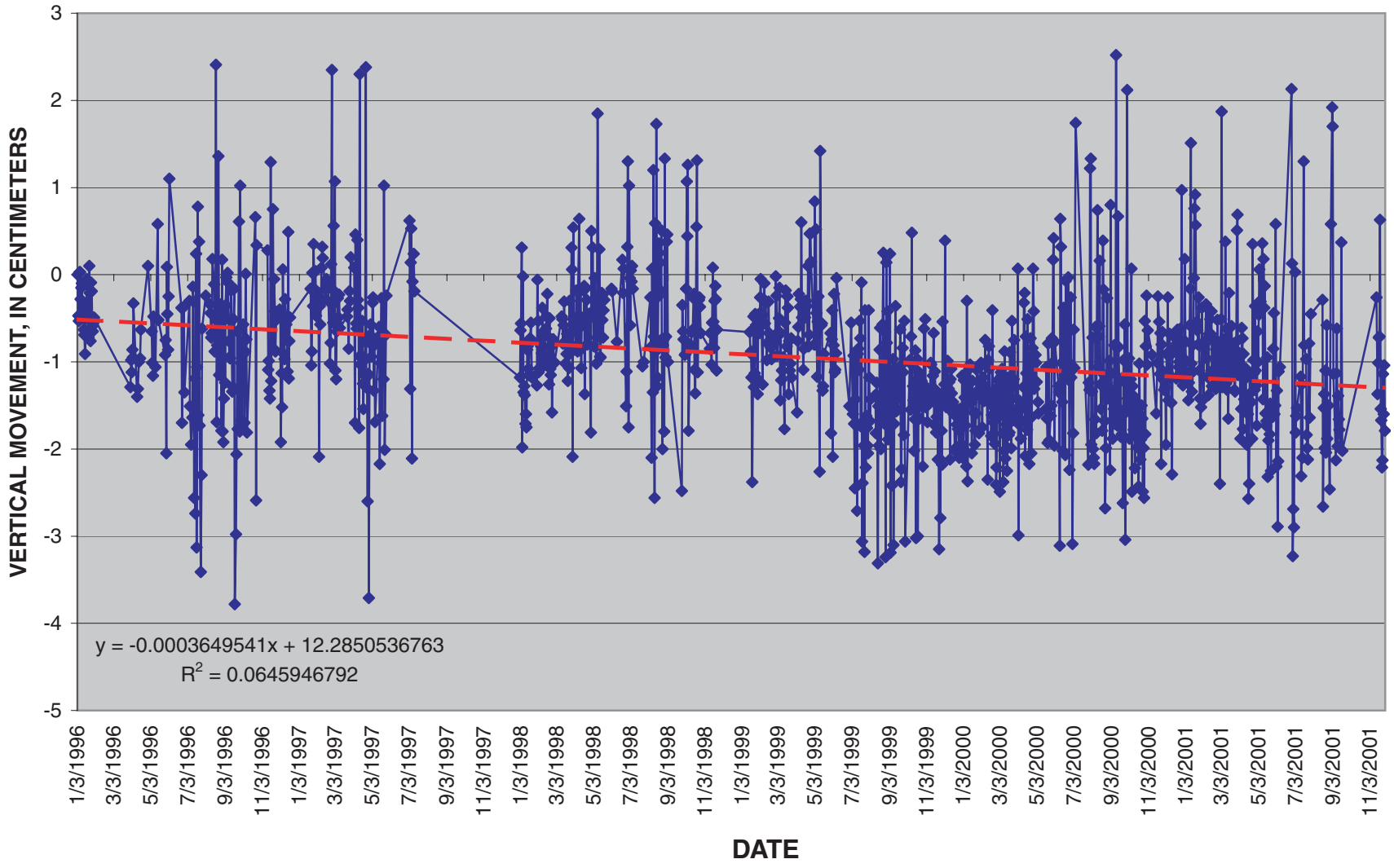

Figure 9. Ellipsoid height differences between Lake Houston CORS and Addicks CORS.

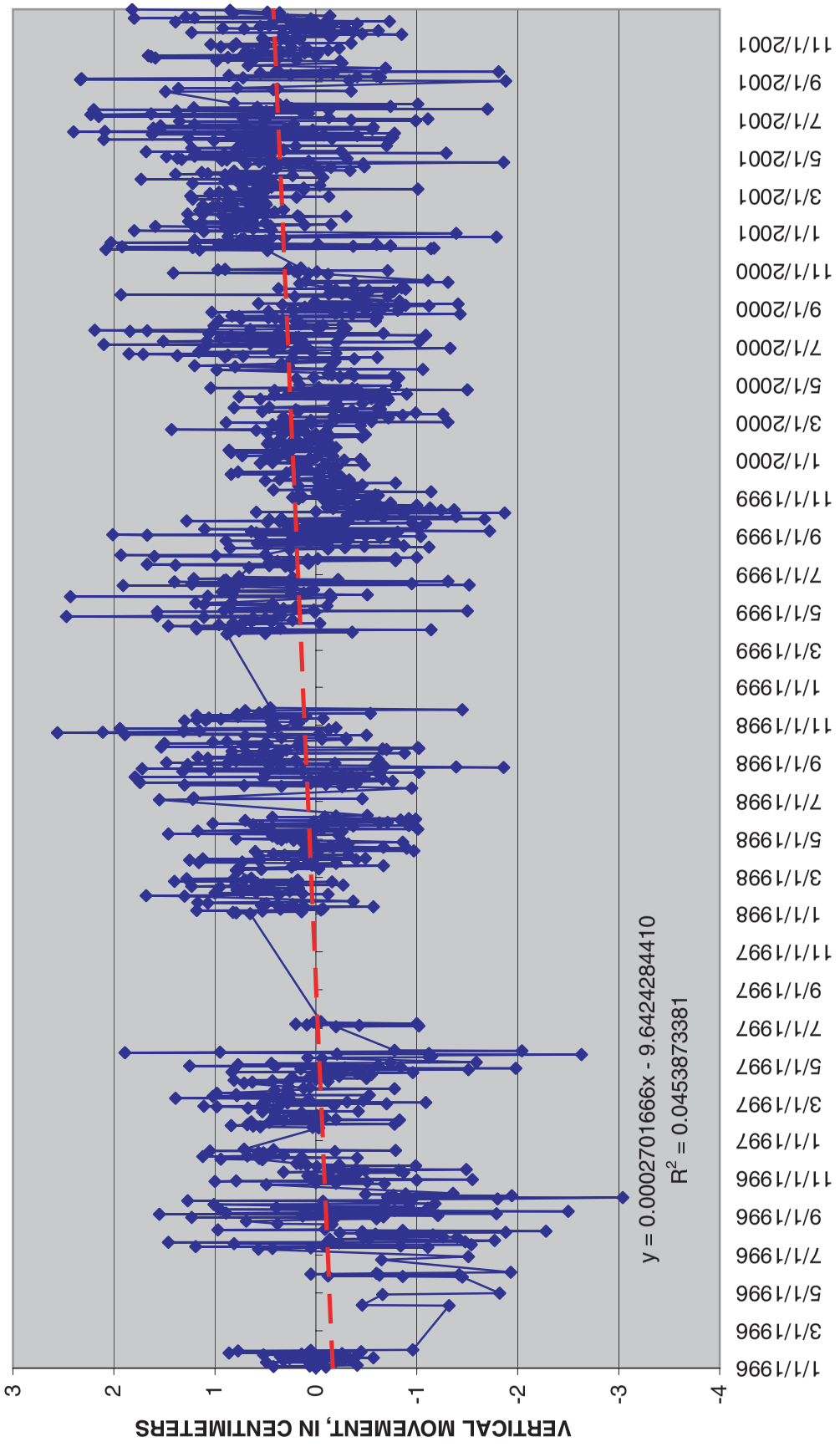

Figure 10. Ellipsoid height differences between Lake Houston CORS and Northeast CORS.

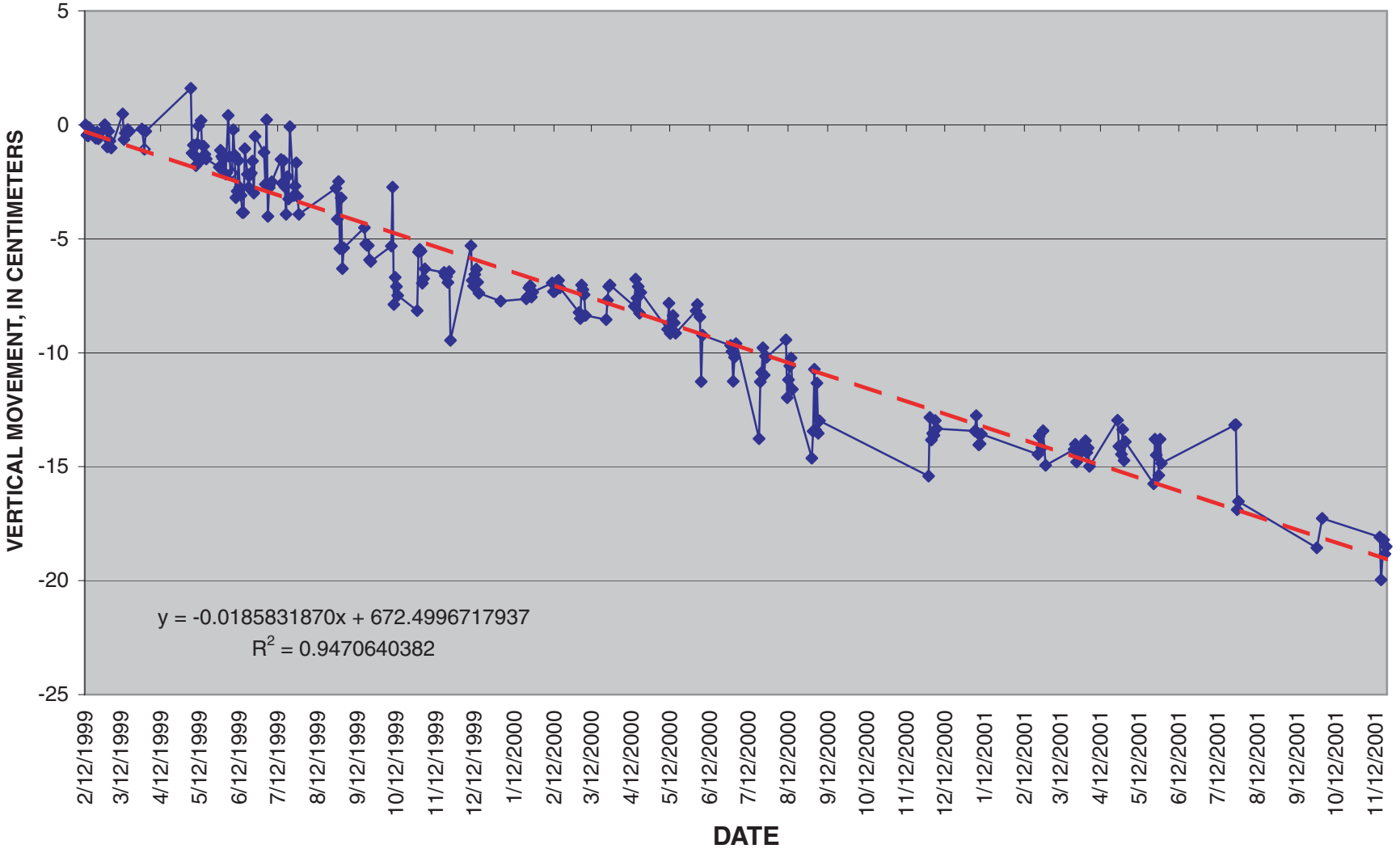

Figure 11. Ellipsoid height differences between Lake Houston CORS and PAM 07 site.

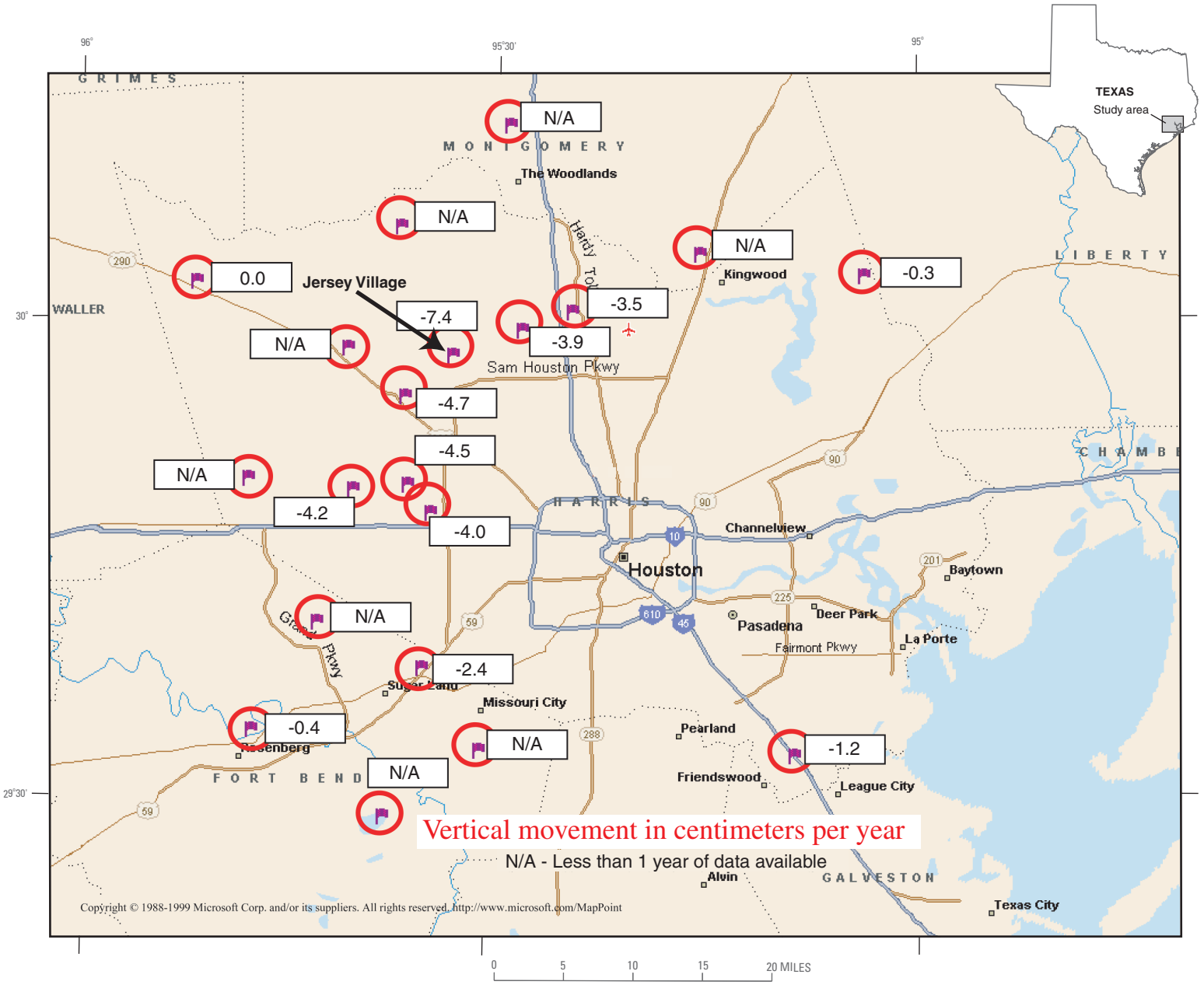

Figure 12. Weighted mean subsidence rates for PAM sites in the Houston-Galveston region, Texas.

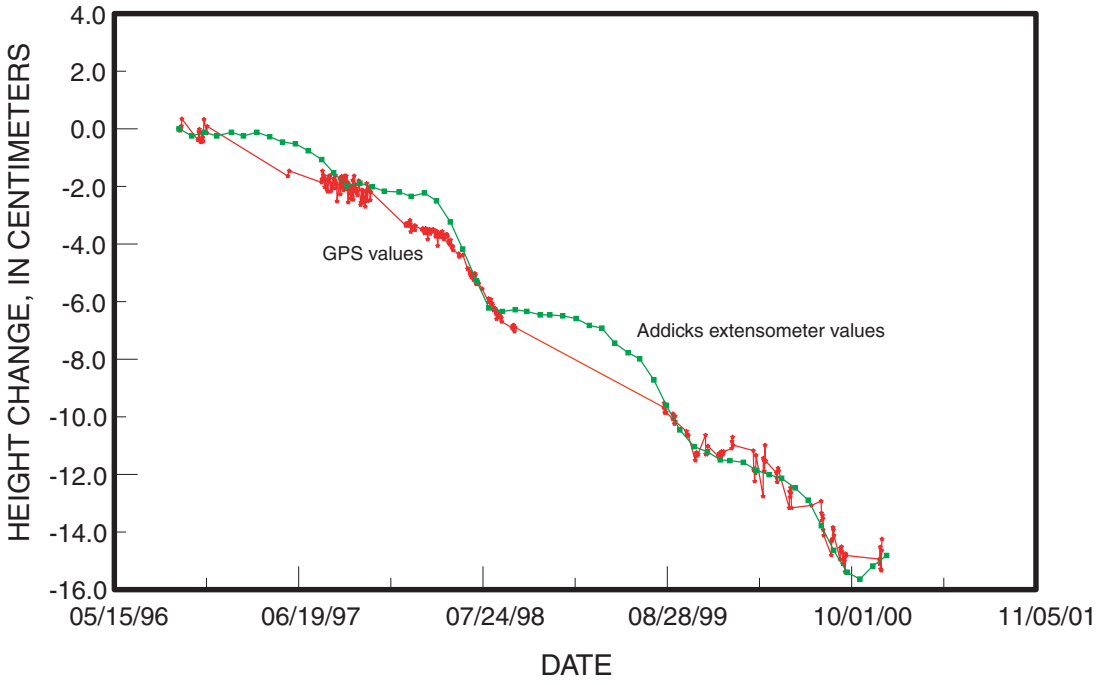

Figure 13. Comparison of techniques to estimate subsidence—Addicks extensometer values versus PAM 05 GPS ellipsoid height values.

Lake Houston CORS. Each month, a PAM trailer collects data at a site for 1 week so the site has 21 vectors associated with it each week. Once a week for 4 weeks, each PAM trailer is moved to another site for a week, returning to the original site every fifth week of the rotation. Thus, every site is occupied 12 different times a year and 7 days of GPS data are collected during each occupation. Some weeks data are missing because of equipment malfunction and alternate use of PAM units during special GPS surveys.

GPS data from the PAM sites are compiled and processed weekly, the height differences are plotted monthly, and individual and weighted average subsidence rates are computed and analyzed quarterly. NGS then provides the results to HGCSD for their review and dissemination. In the near future, the results will be placed on the NGS Web site for others to use.

Figure 11 depicts the estimates of ellipsoid heights for the PAM 07 site relative to the Lake Houston CORS. This is the largest subsidence rate reported by the PAM units, nearly 7 cm/yr as of December 2001. PAM sites are located in areas of known subsidence, as well as in areas where subsidence rates are not known, to assess subsidence in the area.

As previously mentioned, each day that a PAM site is occupied, it has three vectors associated with it, one relative to each GPS CORS. Each vector is computed using 24 hours of GPS data, sampled at 30-second intervals. The vector is used to compute an ellipsoid height value. Therefore, three ellipsoid height values are estimated for each day that a PAM site is occupied. An initial ellipsoid height was determined for each PAM site from an average of seven 24-hour solutions; this is considered the reference ellipsoid height for the PAM site. Subsequently, each ellipsoid height determined at the PAM site is subtracted from the reference ellipsoid height to obtain a change in ellipsoid height. These ellipsoid height changes are tabulated and plotted weekly. Subsidence rates are estimated using a least-squares straight-line fit to the height differences. A standard error of the rate is computed using the statistics from the results of the least-square straight-line fit. The final subsidence rate is computed using a weighted mean of the three rates. The subsidence rates for all PAM sites that have been collecting data for at least 1 year are listed in table 1. The data indicate that the HGCSD/NGS GPS network can accurately measure a 1-cm/yr subsidence rate with

2 to 3 years of data and can potentially detect a smaller rate (for example, 0.5 cm/yr) over the same period.

Figure 12 shows the weighted mean subsidence rates for each PAM site. Sites that have been collecting data for less than 1 year are labeled N/A.

Validation of the PAM Monitoring System

To support the validation of the system, a PAM site was installed near one of the GPS CORS. Addicks CORS was selected because the subsidence rate around this site is known to be about 4 cm/yr. This will provide a large enough signal-to-noise ratio to detect movement over a few years.

Figure 13 depicts subsidence estimates at the Addicks extensometer and PAM 05 site. Because the two stations are only 50 m apart, the subsidence estimates should be approximately equivalent. The subsidence trends are step-like, not linear, and very similar. During fall and winter, subsidence is less than during spring and summer. This cyclic pattern probably is related to seasonal variations in ground-water pumping for irrigation and municipal/industrial water supply. As indicated in figure 13, this pattern also is evident in the GPS data. This site provides HGCSD and NGS with assurance that the automated system is functioning properly.

SUMMARY AND CONCLUSIONS

The joint HGCSD/NGS automated GPS subsidence cooperative project was initiated in late 1993. Since 1996, data have been routinely collected from three CORS in the Houston-Galveston region. Five portable GPS measuring stations, called PAM units, have been built and are successfully providing data for estimating subsidence at 20 additional sites in the Houston-Galveston region. Data have currently (2003) been collected from PAMs for more than 6 years in the Houston-Galveston region. Results indicate that some monuments northwest of downtown Houston are subsiding at rates of 7 cm/yr and correlate well with extensometer and PAM unit data.

The data collected by the GPS stations should prove useful to the commercial sector. Several meetings with local surveyors using GPS equipment in the area have indicated that there is a need for data from stable base stations in the Houston-Galveston region. An Internet connection allows local surveyors to download data from stations applicable to their particular needs and time periods. This system provides a common vertical and horizontal reference upon which all future GPS surveying can be referenced.

ACKNOWLEDGMENTS

Several people contributed to the progress of this cooperative project. Most helpful were Miranda Chin, Ross Mackay, Gerald Mader, and Neil Weston (NGS Geosciences Division), and Mark Schenewerk (formerly of NGS) who developed the multi-baseline processing production and CORS data-retrieval software. Without their assistance this project would not have been possible.

The first PAM trailer was designed and equipped by Leo Gittings, retired chief of NGS Instrumentation and Methodologies Branch (IMB). IMB personnel also designed and provided the antenna mounting hardware. Mark Kasmarek, USGS, provided the benchmark data. J.C. “Bud” Holzschuh, formerly of HGCSD, assisted in the engineering and construction of the PAM hardware, including the equipment to make it completely portable. Mr. Holzschuh also developed the data-retrieval software.

Table 1. Subsidence rates for all PAM sites

[m, meters; cm, centimeters; Std. err, standard error; cm/yr, centimeters per year; ADKS, Addicks; LKHD, Lake Houston; NETP, Northeast]

HGCSD: Analysis of data to Dec. 26, 2001								
Site	Years observed	Reference site	Distance (m)	No. observations	Yearly vertical movement (cm)	Std. err (± cm)	Weighted mean (cm/yr)	Model
00	1999–2001	ADKS	50,488	147	-1.5501	0.1234		
		LKHU	41,555	180	-1.2422	.0858	-1.44	Linear
		NETP	33,075	166	-1.5799	.0906		
							±.06	Std. err
01	1996–2001	ADKS	13,717	392	-4.8492	.0405		
		LKHU	45,472	438	-4.9327	.0402	-4.96	Linear
		NETP	30,393	416	-5.0911	.0386		
							±.02	Std. err
02	1996–2001	ADKS	23,489	351	-3.5153	.0316		
		LKHU	27,807	381	-3.5577	.0249	-3.59	Linear
		NETP	24,525	340	-3.7262	.0297		
							±.02	Std. err
03	1999–2001	ADKS	4,212	170	-4.6767	.0969		
		LKHU	46,332	212	-4.7585	.0814	-4.79	Linear
		NETP	27,187	212	-4.9925	.0804		
							±.06	Std. err
04	1996–2001	ADKS	17,828	444	-2.2713	.0454		
		LKHU	53,737	513	-2.3611	.0474	-2.39	Linear
		NETP	31,040	481	-2.5498	.044		
							±.03	Std. err
05	1996–2001	ADKS	55	421	-3.8303	.0296		
		LKHU	44,638	495	-3.8965	.0434	-3.89	Linear
		NETP	24,335	501	-4.0376	.0429		
							±.02	Std. err
06	1997, 1999–2001	ADKS	9,272	248	-4.3257	.0448		
		LKHU	52,517	274	-4.2899	.0364	-4.32	Linear
		NETP	33,332	277	-4.3497	.0441		
							±.02	Std. err
07	1999–2001	ADKS	16,137	203	-6.6237	.1018		
		LKHU	41,684	246	-6.7831	.1027	-6.73	Linear
		NETP	28,416	219	-6.798	.1008		
							±.06	Std. err
08	1999–2001	ADKS	23,468	153	-3.6944	.0998		
		LKHU	32,741	187	-3.7939	.0769	-3.83	Linear
		NETP	25,000	175	-4.1072	.1042		
							±.05	Std. err
09	1999–2001	ADKS	56,775	182	-.2071	.092		
		LKHU	15,568	239	-.0646	.0743	-.24	Linear
		NETP	37,327	220	-.6675	.103		
							±.05	Std. err

Table 1. Subsidence rates for all PAM sites—Continued

HGCSD: Analysis of data to Dec. 26, 2001								
Site	**Years observed**	**Reference site**	**Distance (m)**	**No. observations**	**Yearly vertical movement (cm)**	**Std. err (± cm)**	**Weighted mean (cm/yr)**	**Model**
10	1999–2001	ADKS	32,309	433	-0.316	0.0684		
		LKHU	73,997	481	-.4434	.0622	-0.48	Linear
		NETP	51,442	436	-.721	.081		
							±.04	Std. err
11	1999–2001	ADKS	37,945	178	-.0726	.0821		
		LKHU	70,673	230	.0656	.0717	-.03	Linear[1]
		NETP	57,822	218	-.1062	.0818		
							±.05	Std. err
12	2000–2001	ADKS	43,152	49	-1.268	.7554		
		LKHU	61,081	69	-1.0794	.6682	-1.1	Linear
		NETP	39,168	71	-.9303	.6081		
							±.4	Std. err
13	2000–2001	ADKS	45,722	65	-2.2161	.3022		
		LKHU	45,548	74	-2.3861	.3413	-2.2	Linear
		NETP	47,202	71	-2.0955	.3464		
							±.19	Std. err
14	2000–2001	ADKS	35,614	44	.8048	.3788		
		LKHU	68,577	55	.3248	.3202	.64	Linear
		NETP	46,250	45	.7055	.6926		
							±.26	Std. err
15	2000–2001	ADKS	17,578	54	-.3239	.3541		
		LKHU	61,081	91	-1.5778	.2759	-.95	Linear
		NETP	39,168	102	-1.6318	.2629		
							±.2	Std. err
16	2000–2001	ADKS	27,918	60	.4504	.3251		
		LKHU	55,092	79	-.3298	.2894	-.08	Linear[1]
		NETP	33,119	61	-.4499	.226		
							±.17	Std. err
17	2000–2001	ADKS	33,393	33	.2757	.3702		
		LKHU	49,400	37	-.7859	.3868	-.29	Linear[1]
		NETP	42,922	31	-.5878	.3264		
							±.21	Std. err
18	2000–2001	ADKS	21,226	41	-.0545	.5321		
		LKHU	51,723	44	-.5467	.448	-.43	Linear[1]
		NETP	38,411	47	-.984	.4338		
							±.29	Std. err
19	2000–2001	ADKS	21,881	53	.1319	.3804		
		LKHU	64,221	81	-1.2981	.2262	-.64	Linear
		NETP	45,875	63	-.8781	.191		
							±.16	Std. err
ADKS	1996–2001	LKHU	44,692	1,278	-.1332	.0143	-.13	Linear
NETP	1996–2001	LKHU	22,704	1,311	.0986	.0125	.1	Linear

[1] Rate highly uncertain.

Hydrogeology and Simulation of Ground-Water Flow and Aquifer-System Compaction in the Chicot and Evangeline Aquifers, and Land Subsidence in the Houston Area, Texas

By Mark C. Kasmarek[1] *and* Eric W. Strom[2]

Abstract

The U.S. Geological Survey, in cooperation with the City of Houston Utilities Planning Section and the City of Houston Department of Public Works & Engineering has developed a numerical finite-difference model to better understand the hydrology, flow, and aquifer-system compaction in the Chicot and Evangeline aquifers, and the resulting land subsidence.

The model successfully simulates the release of water from storage in clay layers and the concomitant aquifer-system compaction and land subsidence resulting from ground-water withdrawal. The study area covers 18,100 square miles. The model was vertically discretized into three 103-row by 109-column layers resulting in a total of 33,681 grid cells. Layer 1 represents the water table using a specified head, layer 2 represents the Chicot aquifer, and layer 3 represents the Evangeline aquifer.

The transient model was calibrated using available ground-water-level data for the years 1977 and 1996. The simulated and measured potentiometric surfaces of the Chicot and Evangeline aquifers for these years match closely.

Simulation of water released from storage in the more compressible, fine-grained interbeds in the aquifer system, aquifer-system compaction, and land subsidence was accomplished using the Interbed-Storage Package for the MODFLOW ground-water model. In addition to calibrating to hydraulic head variations over time, the model also was calibrated by trial-and-error by comparing simulated long-term subsidence (1891–1995) to measured long-term subsidence (1906–95) and by comparing simulated short-term subsidence (1978–95) to measured short-term subsidence (1978–95) until acceptable matches were achieved.

Simulated 1996 volumetric budgets indicate that a net flow of 562.6 cubic feet per second recharges the Chicot aquifer in the outcrop area. Water released from storage from the interbedded fine-grained deposits in the Chicot aquifer is about 19 percent of the total water withdrawn. Simulated 1996 Evangeline aquifer flow rates indicate that a net flow of 14.8 cubic feet per second recharges the Evangeline aquifer in the outcrop area, and a net flow of 459.5 cubic feet per second passes through the Chicot aquifer into the Evangeline aquifer. The water released from storage from the interbedded fine-grained deposits in the Evangeline aquifer is about 10 percent of the total water withdrawn from the aquifer.

HYDROGEOLOGY OF THE CHICOT AND EVANGELINE AQUIFERS

Ground water in the Chicot and Evangeline aquifers generally flows from northwest to southeast. Precipitation infiltrating the outcrop areas flows downward and laterally through the aquifers toward the coast. Near the coastline and at depth, denser saline water is present in the sediments and forms an effective boundary to continued downdip flow.

Hydrogeologic Units and Geologic Setting

The Chicot and Evangeline aquifers, and the underlying Burkeville confining unit are the uppermost hydrogeologic units of the Gulf Coast aquifer system.The lateral extent of the Gulf Coast aquifer system

[1] U.S. Geological Survey, Houston, Tex.
[2] U.S. Geological Survey, Austin, Tex.

extends from the western panhandle of Florida westward parallel to the Texas Gulf Coast into Mexico. In the study area, the northwestern updip limit of the Chicot aquifer is an undulating surface approximately parallel to the coastline extending as far northwest as Austin, Colorado, Montgomery, Polk, San Jacinto, and Waller Counties (fig. 1). To the southeast, the freshwater part of the aquifer extends into the Gulf of Mexico.

In the study area, the northwestern updip limit of the Evangeline aquifer is an undulating surface approximately parallel to the coastline extending as far northwest as Austin, Fayette, Grimes, Montgomery, Polk, San Jacinto, Walker, and Washington Counties (fig. 1). To the southeast, the freshwater part of the aquifer is approximately coincident with the coastline.

In the updip area of the Chicot aquifer and the outcrop area of the Evangeline aquifer, water-table conditions generally exist. The water table generally is a subdued replica of the topography (Williams and Williamson, 1989) and ranges from about 10 to 30 ft below land surface on the basis of seismic refraction work by Noble and others (1996). Hydrographs indicate that the water table remains fairly stable where not directly influenced by a nearby pumping well. This is attributed to the relatively high annual precipitation and infiltration that normally occur in the Houston area.

The Burkeville confining unit lies stratigraphically below the Evangeline aquifer. This unit is considered a no-flow basal unit in the Houston area that restricts the upward movement of more dense saline water from depth.

The paleo-depositional environment is a fluvial deltaic and a shallow-marine environment that produced interlayered, discontinuous sequences of sand, silt, clay, and gravel. Changes in land-surface altitudes related to naturally occurring land subsidence of the depositional basin and sea-level transgressions and regressions created cyclical sedimentation facies. During periods when the sea level declined, fluvial-deltaic processes deposited continental sediments; but as the sea level rose, the deposited continental sediments were reworked and marine sediments were deposited.

Recharge and Discharge

The primary mechanism of recharge to the Chicot and Evangeline aquifers deep flow system is infiltration of precipitation into the northern updip outcrop areas of the aquifers. Beneath much of the greater Houston area and southern areas of the aquifers, the deeper layers of the aquifers act as a confined system.

Naturally occurring discharge from the aquifer system occurs in several ways. These include evapotranspiration, discharge through seeps and springs in areas of low topographic relief that flows into the many streams and rivers, and discharge from the aquifers along the coast.

SIMULATION OF GROUND-WATER FLOW AND LAND SUBSIDENCE IN THE CHICOT AND EVANGELINE AQUIFERS

A numerical model of ground-water flow, aquifer-system compaction, and land subsidence was developed to simulate potentiometric surfaces from 1891 to 1996 in the Chicot and Evangeline aquifers and land subsidence resulting from potentiometric-surface declines in the aquifers in Harris, Galveston, and surrounding counties.

Numerical Model

The U.S. Geological Survey (USGS) modular finite-difference ground-water model program—MODFLOW (McDonald and Harbaugh, 1988; Harbaugh and McDonald, 1996) and the Interbed-Storage Package for MODFLOW (Leake and Prudic, 1991) were used to simulate ground-water flow and aquifer-system compaction in the Chicot and Evangeline aquifers.

Model Grid

The finite-difference grid used in the numerical model (fig. 1) covers 18,100 mi^2 and encompasses all of Brazoria, Chambers, Fort Bend, Galveston, Harris, Liberty, and Waller Counties and parts of Austin, Colorado, Fayette, Grimes, Hardin, Jefferson, Matagorda, Montgomery, Polk, San Jacinto, Walker, Washington, and Wharton Counties. The model grid was oriented approximately north-south column-wise assuming the aquifer system was horizontally isotropic; the grid consists of 103 rows and 109 columns. The grid cells are variably sized. The smallest cells are 0.95 mi^2 in the primary area of interest, and the largest cells at the model boundaries are 4.54 mi^2. Vertically the model was discretized into three layers. Layer 1 represents the water table using a specified head, layer 2 represents the Chicot aquifer, and layer 3 represents the Evangeline aquifer.

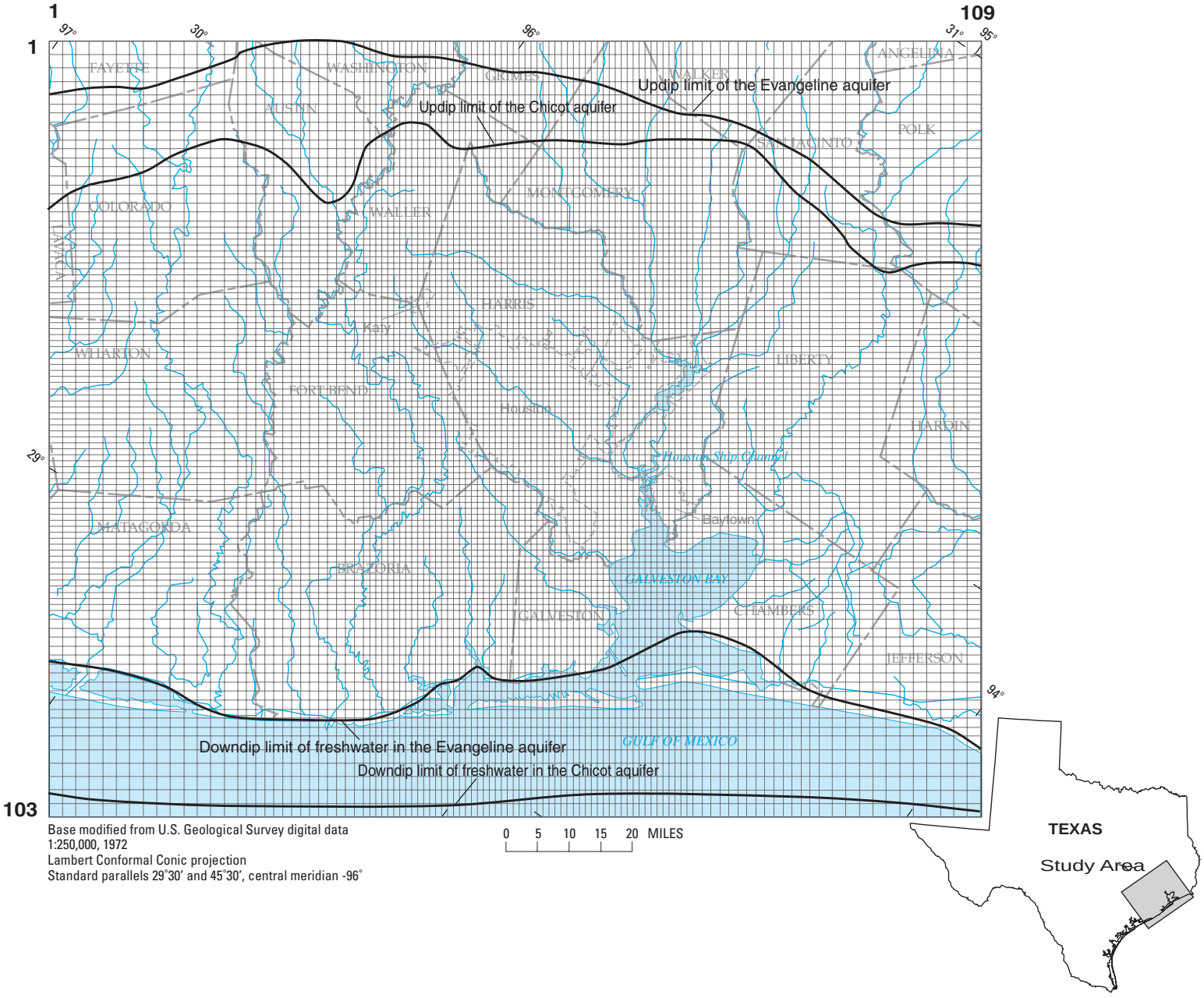

Base modified from U.S. Geological Survey digital data
1:250,000, 1972
Lambert Conformal Conic projection
Standard parallels 29°30′ and 45°30′, central meridian -96°

Figure 1. Location of study area with finite-difference grid used in the numerical model of the Chicot and Evangeline aquifer system.

Model Calibration

Using the results of previous models, the initial model calibration strategy was to modify, by trial-and-error, the best-known hydraulic properties as little as possible and to vary the least-known hydraulic properties to achieve the best overall agreement between simulated and measured values. Two years, 1977 and 1996, were chosen to match simulated heads and land subsidence to measured values for transient model calibration.

Potentiometric Surfaces

The years 1977 and 1996 were chosen as potentiometric-surface calibration periods for the model. The year 1977 was chosen because, during the mid-1970s, the potentiometric surfaces in both aquifers had declined to record low levels in Harris and Galveston Counties. In addition, the first water-level-altitude maps of both aquifers were published for 1977 by the USGS (Gabrysch, 1979). The year 1996 was chosen because 1996 was the most recent year that water-level data from wells were available; current land-surface altitudes were determined in late 1995. The geographic area having land-surface subsidence during 1978–95 coincides with the potentiometric-surface declines in the underlying aquifers during 1977–96; the magnitude and distribution of ground-water withdrawals were very different from that in 1977. Water-level data from wells and land-surface-altitude data for 1996 indicated a broad range of stresses, both spatially and temporally, and served to better constrain model calibration.

Land Subsidence and Interbed Storage

Simulation of land subsidence and water released from storage by the compaction of compressible interbeds interspersed within the Chicot and Evangeline aquifers was accomplished using the Interbed-Storage Package for MODFLOW developed by Leake and Prudic (1991). The simulated compaction is based on Terzaghi's principle of effective stress, which relates total stress, effective stress and pore-fluid pressure. For the case when only the vertical component of stress is considered, as is the case in the model used here, Terzaghi's one-dimensional (vertical) effective stress law can be expressed as,

$$\sigma_T = \sigma_e + h, \quad (1)$$

where the stresses are expressed in units of equivalent hydraulic head, and

σ_T is the total (geostatic) stress [L],
σ_e is the effective (intergranular) stress [L], and
h is hydraulic head [L].

For a constant total stress any change in effective stress is equal and opposite to the change in hydraulic head. The lowering of hydraulic head in the aquifers results in increased effective stress. Previous investigations (Riley, 1969; Helm, 1975) show that for sediments in confined aquifer systems where the geostatic stress remains constant, compaction (or expansion) of the interbeds is proportional to the change in hydraulic head and is governed by the skeletal specific storage and thickness of the interbeds, or

$$\Delta b = - S_{sk}\, b_o \Delta h, \quad (2)$$

where

Δb is the amount of compaction or expansion [L] where compaction is a positive value,
S_{sk} is the skeletal component of specific storage [L^{-1}] where it can have two values, one for the elastic range of stress and one for the inelastic range of stress; whether the elastic or inelastic component is used is determined by the previous effective stress history of the material,
b_o is the aggregate thickness of the compacting interbeds [L], and
Δh is the change in hydraulic head [L].

For changes in hydraulic head that remain above a given preconsolidation head, an elastic response is calculated, but for changes in hydraulic head that are below a given preconsolidation head, an inelastic response is calculated, and the resultant minimum head becomes the new preconsolidation stress threshold. An initial preconsolidation head of 70 ft below the water table was used in the models of Meyer and Carr (1979) and Carr and others (1985).

Values for the elastic and inelastic skeletal specific storages were adjusted during model calibration. The mean values of simulated inelastic skeletal specific storage for the Chicot and Evangeline aquifers were 7.34×10^{-5} ft^{-1} and 1.42×10^{-5} ft^{-1}, respectively, and consistent with simulated inelastic skeletal specific storage determined by Meyer and Carr (1979).

Simulated subsidence was computed as the sum of aquifer-system compaction in the individual aquifers, and land subsidence was calibrated by comparing simulated long-term subsidence (1891–1995) (fig. 2) to measured long-term subsidence (1906–95) (fig. 3)

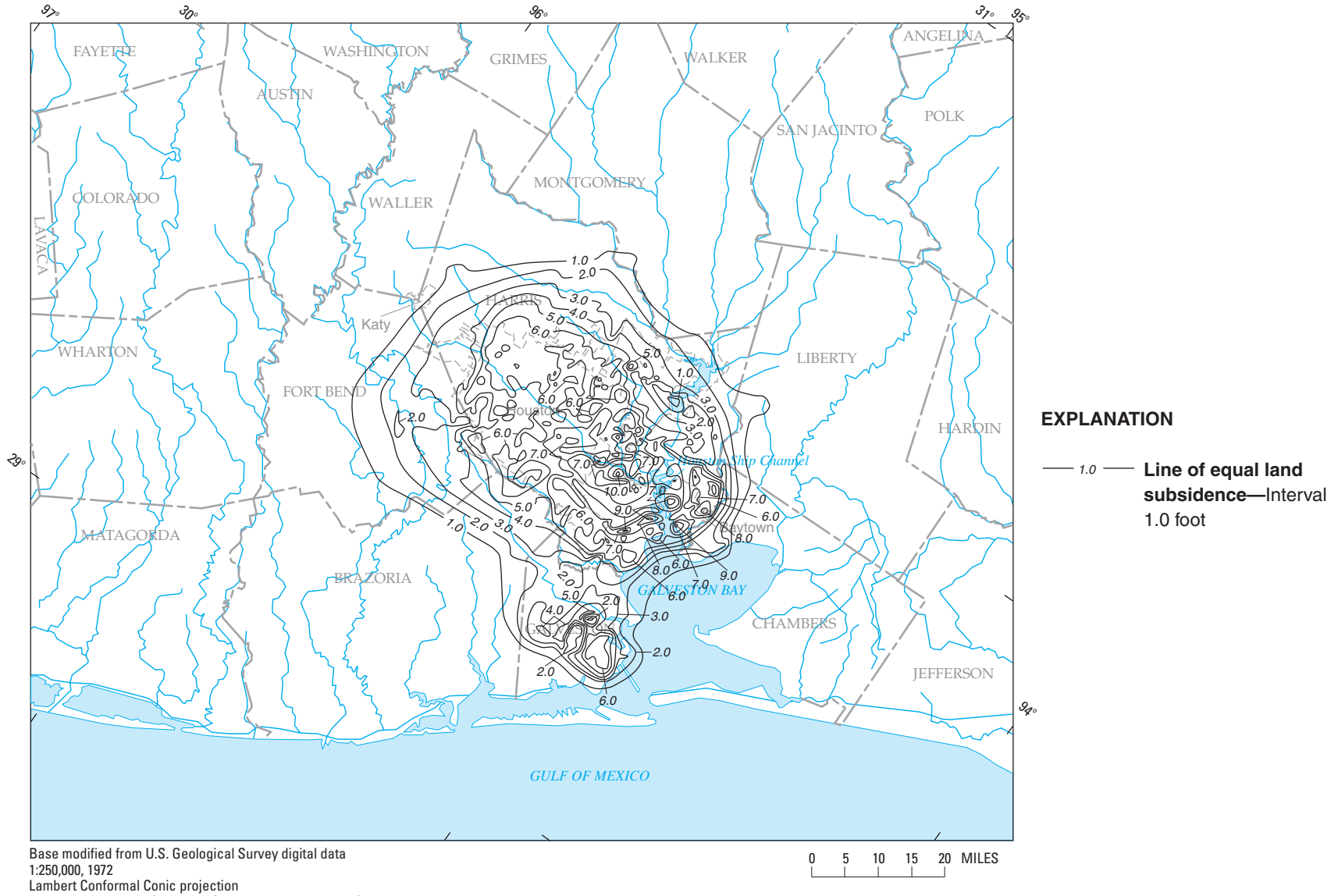

Figure 2. Simulated land subsidence, Houston area, Texas, 1891–1995.

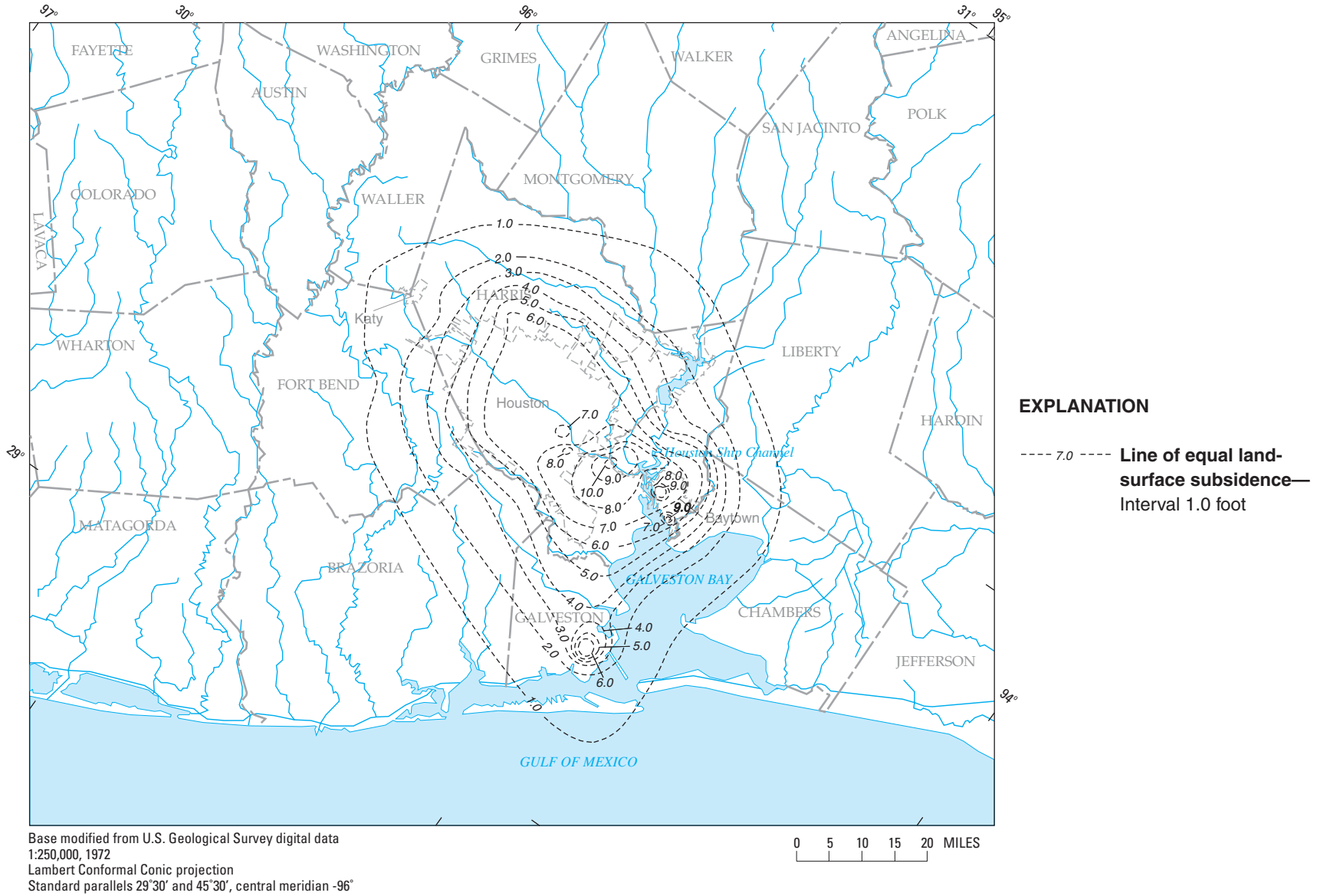

Figure 3. Measured land subsidence, Houston area, Texas, 1906–95 (modified from Harris-Galveston Coastal Subsidence District, 1998).

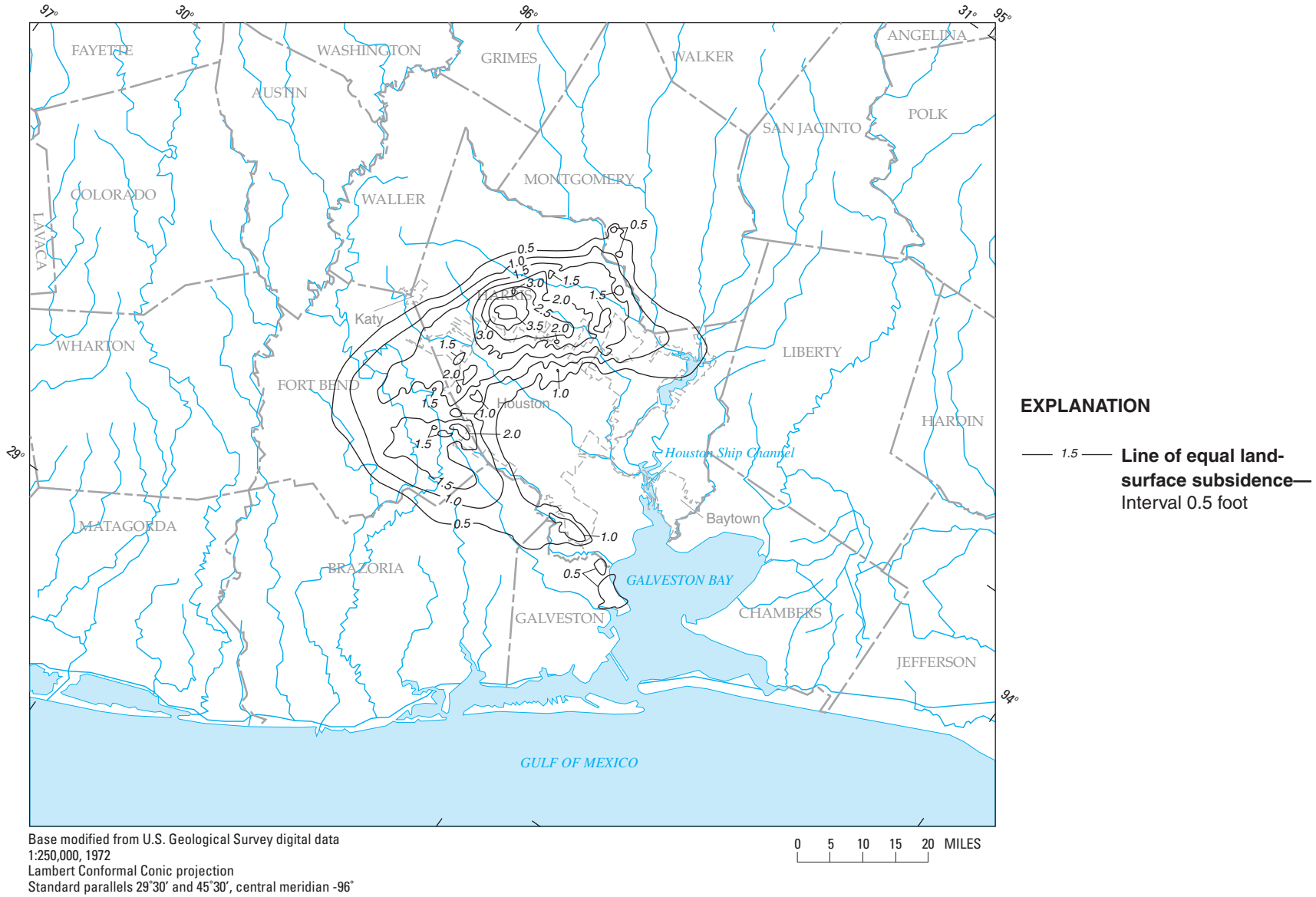

Figure 4. Simulated land subsidence, Houston area, Texas, 1978–95.

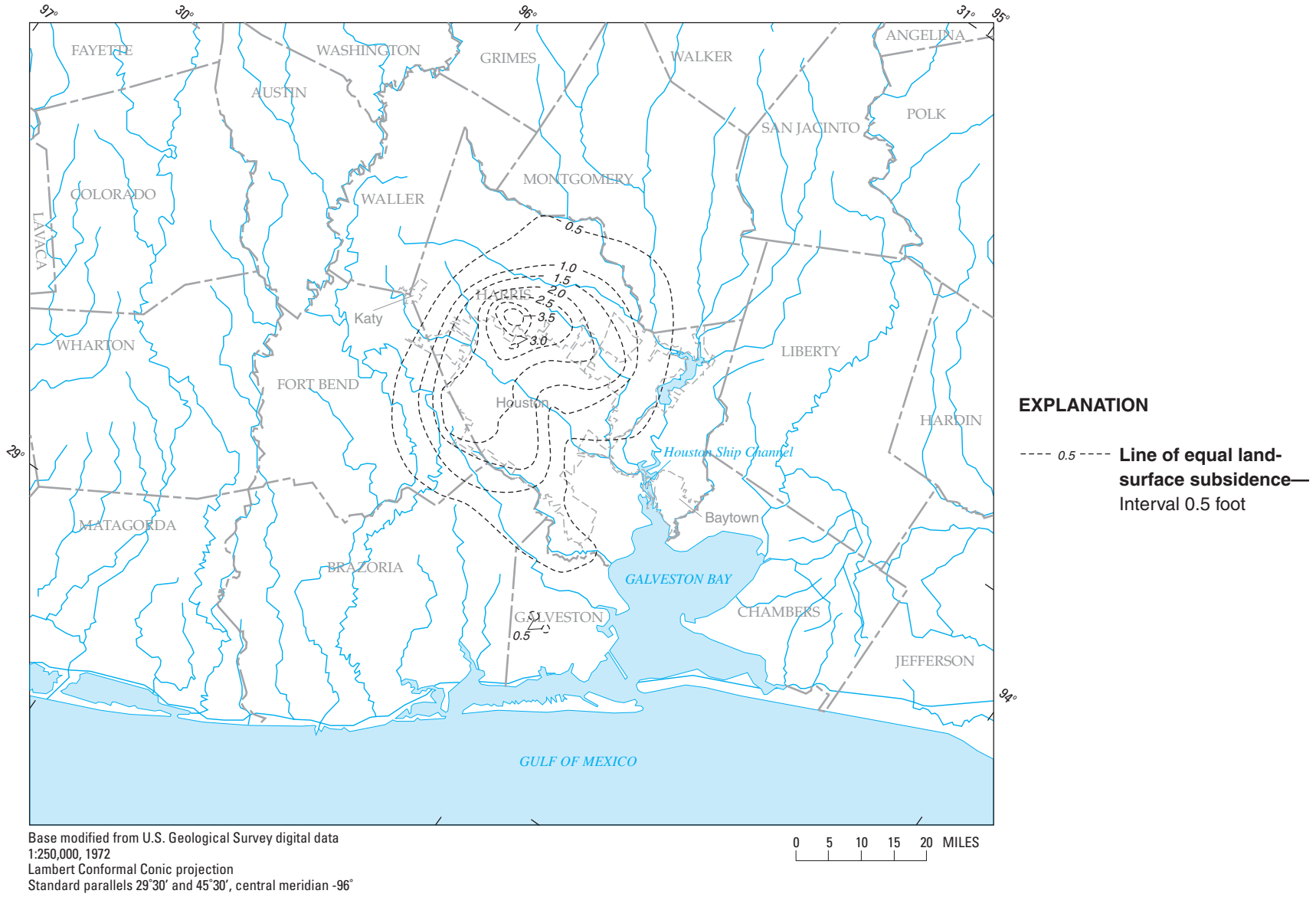

Figure 5. Measured land subsidence, Houston area, Texas, 1978–95 (modified from Harris-Galveston Coastal Subsidence District, 1998).

and by comparing simulated short-term subsidence (1978–95) (fig. 4) to measured short-term subsidence (1978–95) (fig. 5) until acceptable matches were achieved. In the equation controlling land subsidence used in the model, all aquifer properties that affect the potentiometric surfaces also affect land subsidence.

Measured land subsidence during 1906–95 (fig. 3) indicates that as much as 9 to 10 ft occurred in the southeastern Houston area. A larger geographic area encompassing the maximum land-surface-subsidence areas and much of the immediate Houston area has subsided at least 6 ft. The configurations of measured land subsidence for 1906–95 (fig. 3) and simulated land subsidence for 1891–1995 (fig. 2) are quite similar. Additionally, the configuration, similarity, and magnitude can be seen for measured land subsidence for 1978–95 (fig. 5) and simulated land subsidence for 1978–95 (fig. 4). Model simulations reflect more spatial detail in land subsidence because the resolution of the model grid is considerably finer than the spacing of the benchmarks where subsidence is measured.

The simulated 1996 volumetric budgets for the aquifers indicate that about 19 percent of the total water withdrawn from the Chicot aquifer is supplied from water released from storage in interbeds, but only about 10 percent of the total water withdrawn from the Evangeline aquifer is supplied from water derived from interbed storage (Kasmarek and Strom, 2002).

Optimal Withdrawal of Elastically Stored Ground Water in the Chicot Aquifer, Houston Area, Texas

By Wesley R. Danskin[1], Mark C. Kasmarek[2], *and* Eric W. Strom[3]

Abstract

By the mid-1970s, withdrawal of ground water from the Chicot and Evangeline aquifers in the Houston area, Texas, had caused as much as 10 feet of land-surface subsidence. After 1976, decreasing ground-water withdrawals in Harris and Galveston Counties resulted in a water-level rise in the Chicot aquifer that was more than 180 feet by 1996. This rise suggests that the aquifer now has elastically stored water that theoretically could be withdrawn without causing additional nonrecoverable subsidence. A constrained optimization model was used with a ground-water-flow model to identify the maximum quantity of ground water that could be withdrawn from the Chicot aquifer in southeastern Harris County near Baytown without inducing additional permanent aquifer-system compaction and land subsidence. Constraints included keeping hydraulic head in the aquifer above the preconsolidation head, the lowest previous ground-water level. Our technique used response functions, linear programming, and spreadsheet software. Optimal results indicate that 1,200,000 cubic feet per day could be produced from five well sites for 10 years. This elastically derived quantity of ground water from storage is renewable, but it is less than 2 percent of the historical extraction, much of which was obtained from inelastic, permanent compaction and nonrenewable storage from the aquifer.

INTRODUCTION

Large amounts of ground water have been withdrawn from the Chicot and Evangeline aquifers in the Houston area of Texas (fig. 1). Withdrawals for municipal and agricultural uses began in the late 1800s. Withdrawals for industrial use began after the opening of the Houston Ship Channel in 1914. The rate of ground-water withdrawal grew slowly until the late 1930s and then increased rapidly in the early 1940s. Withdrawals caused declines in the potentiometric surface of as much as 300 ft in the Chicot aquifer and as much as 350 ft in the underlying Evangeline aquifer between 1943 and 1977. These water-level declines in turn caused as much as 10 ft of subsidence in southeastern Harris County.

The Harris-Galveston Coastal Subsidence District was created by the State of Texas in 1975 for the purpose of "ending subsidence, which contributes to or precipitates flooding, inundation, or overflow of the district, including without limitation rising water resulting from storms or hurricanes" (Harris-Galveston Coastal Subsidence District, 1999). Water from Lake Livingston became available to coastal areas in late 1976 and was used to augment existing ground-water withdrawals. After 1976, withdrawals decreased in both Galveston County and southeastern Harris County. By 1996, potentiometric surfaces of the Chicot and Evangeline aquifers had risen about 180 and 200 ft, respectively, in southeastern Harris County.

The substantial rise in potentiometric surface, particularly southeast of Houston near Baytown, might offer the opportunity to extract from storage, elastically available ground water from the area. To prevent further subsidence, any extractions would need to be adjusted to ensure that the potentiometric surface stays above the preconsolidation head, the lowest previous ground-water level. The quantity of elastically available ground water that could be withdrawn is not known and is the subject of this study. Because the Baytown area has not relied on ground water for many years, it is likely that the necessary wells and pipelines are no longer usable. Identifying the infrastructure necessary to obtain and use any elastically available water from ground-water storage was not a part of this study.

The Chicot and Evangeline aquifers can be viewed as an aquifer system with low permeability, fine-grained sediments (clays and silts) interspersed with

[1] U.S. Geological Survey, San Diego, Calif.
[2] U.S. Geological Survey, Houston, Tex.
[3] U.S. Geological Survey, Austin, Tex.

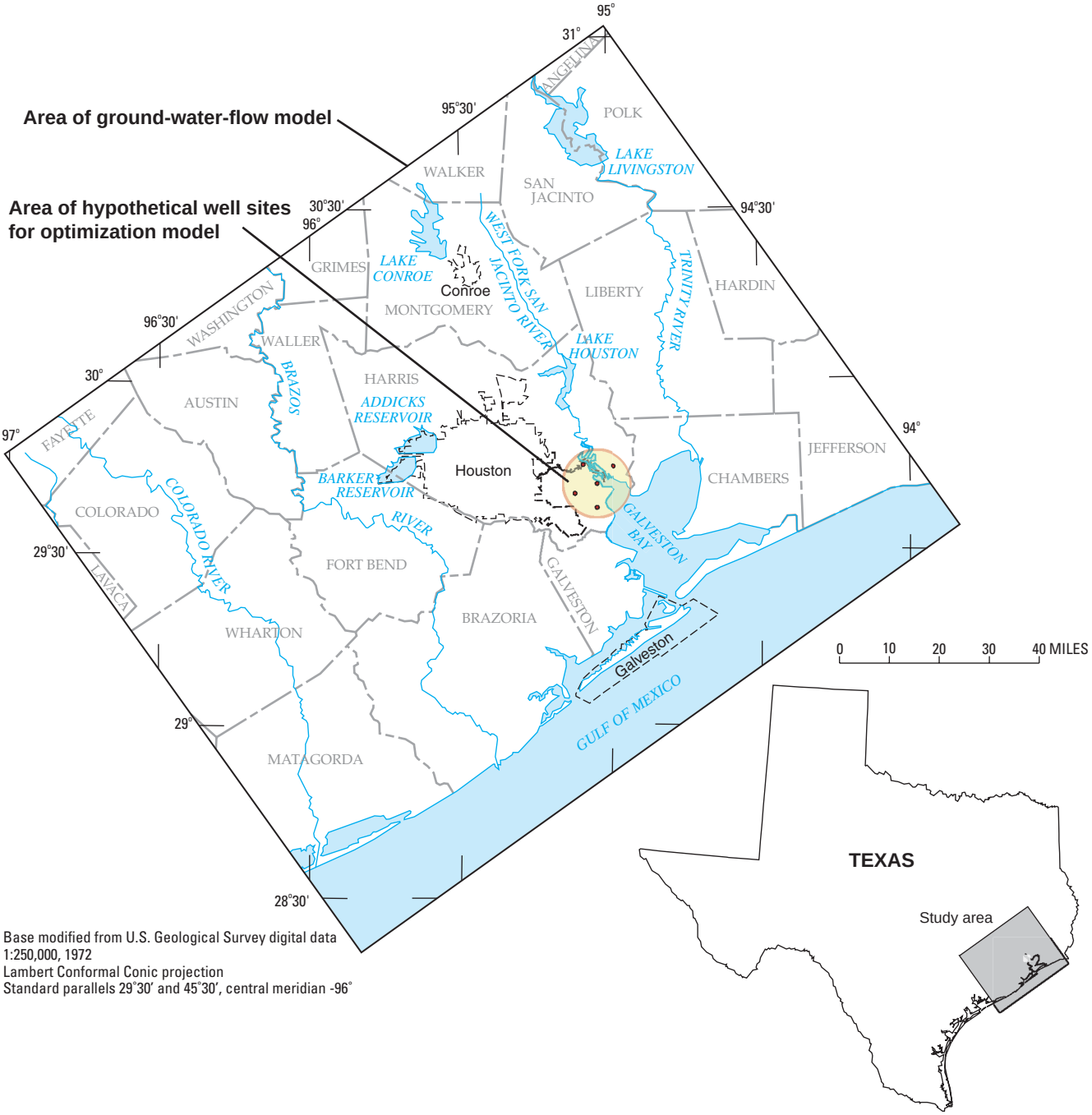

Figure 1. Location of the study area near Houston, Texas.

high permeability, coarse-grained sediments (sands and gravels). Almost all of the subsidence related to ground-water extraction is the result of aquifer-system compaction occurring in the more compressible fine-grained sediments as they equilibrate with lowered hydraulic heads caused by ground-water pumping in the surrounding coarse-grained sediments. Vertical ground-water flow from the fine-grained sediments to the coarse-grained sediments and the accompanying hydraulic-head declines in the fine-grained sediments create increases in the intergranular (effective) stresses in the fine-grained sediments causing them to compact.

The changes in hydraulic head and effective stresses in the fine-grained units are reversible; when

heads in the coarse-grained sediment increase, the heads and effective stresses in the fine-grained units undergo a time-dependent re-equilibration that chiefly depends on the vertical hydraulic diffusivity and the thickness of the fine-grained unit. However, the changes in compaction might not be reversible depending on the state of effective stresses in the fine-grained units. A critical effective-stress threshold, which can be expressed as a critical hydraulic head, defines the stress or head at which the fine-grained units compact elastically (reversible) or inelastically (permanent). This stress threshold is equivalent to the previous maximum stress or minimum hydraulic head occurring in the fine-grained sediments and is termed the preconsolidation stress or preconsolidation head. Lowering of heads in the fine-grained sediments beyond the preconsolidation head results in permanent inelastic compaction of the aquifer system and land-surface subsidence. If hydraulic heads remain above these critical stress thresholds, the aquifer system deforms elastically in response to changes in hydraulic heads, and any subsidence or uplift of land surface that occurs is fully recoverable.

The two modes of compaction, elastic and inelastic, are further differentiated by the large differences in the compressibilities of the fine-grained sediments depending on the state of effective stress. In the range of stress that creates inelastic compaction, the fine-grained sediments are 50 to 100 times more compressible than they are when stresses are maintained above the preconsolidation stresses—the elastic range of stress. Thus the magnitude of aquifer-system compaction and land-surface subsidence is much greater for inelastic compaction than for elastic compaction.

As unconsolidated confined aquifers such as the Chicot and Evangeline deform, water is released from or taken into storage by the fine-grained sediments. The amount of water released from or taken into storage in the fine-grained sediments is defined by a storage coefficient that is a function (summation) of the compressibility of saturated sediments (matrix compressibility) and the product of the porosity of the sediments and compressibility of water. Because of the two modes of compressibility of the sediments, elastic and inelastic, the storage coefficient takes on two values, one for elastic and one for inelastic storage. Owing to the larger inelastic compressibilities, the inelastic storage coefficient, and thus the amount of water released from storage when heads decline below the preconsolidation heads, is significantly greater than the elastic storage coefficient that governs the release from and uptake to storage in the elastic range of stress. For example when hydraulic heads in a confined aquifer system decline but remain above the preconsolidation heads, the water expands slightly, the aquifer-system matrix compresses slightly, and water is released from storage in the aquifer system. This produces an elastic contribution of water to a well. If water is added back to the aquifer, such as by natural recharge, hydraulic heads rise, the water compresses slightly, the aquifer-system matrix expands slightly, and water is taken into storage in the aquifer system. For each of these cases the aquifer system responds elastically, and any associated deformation of the aquifer system or land-surface subsidence is small and reversible. A comparable amount of water can be recharged into the aquifer and withdrawn from the aquifer repeatedly without causing further land-surface subsidence.

Because inelastic compressibilities of fine-grained sediments are much larger than elastic compressibilities, the volume of water released from storage that accompanies inelastic compaction of the aquifer system is as much as 50 to 100 times greater than is released when the aquifer system compacts elastically, for the same magnitude of change (decline) in hydraulic head. The water released from storage as a result of inelastic compaction is a one-time release and cannot be restored to the permanently compacted fine-grained sediments. In the Baytown area, therefore, the quantity of any elastically available ground water will be much less than the quantity of water that was historically withdrawn from the aquifer by inelastic compaction of either the Chicot or Evangeline aquifer.

Additional information about elastic and inelastic response of an aquifer is presented in Gabrysch and Bonnet (1975), Helm (1975), Leake and Prudic (1991), and Galloway and others (1999).

Purpose and Scope

The purpose of this study is to identify the approximate quantity of ground water that theoretically could be withdrawn from the Chicot aquifer in southeastern Harris County near Houston, Tex., without causing additional land-surface subsidence. The scope of this study includes use of a pre-existing ground-water-flow model to simulate aquifer response to ground-water withdrawal from five hypothetical well sites. The simulation period is 10 years and uses average hydrologic conditions based on ground-water levels and withdrawals in 1996. A constrained optimization model

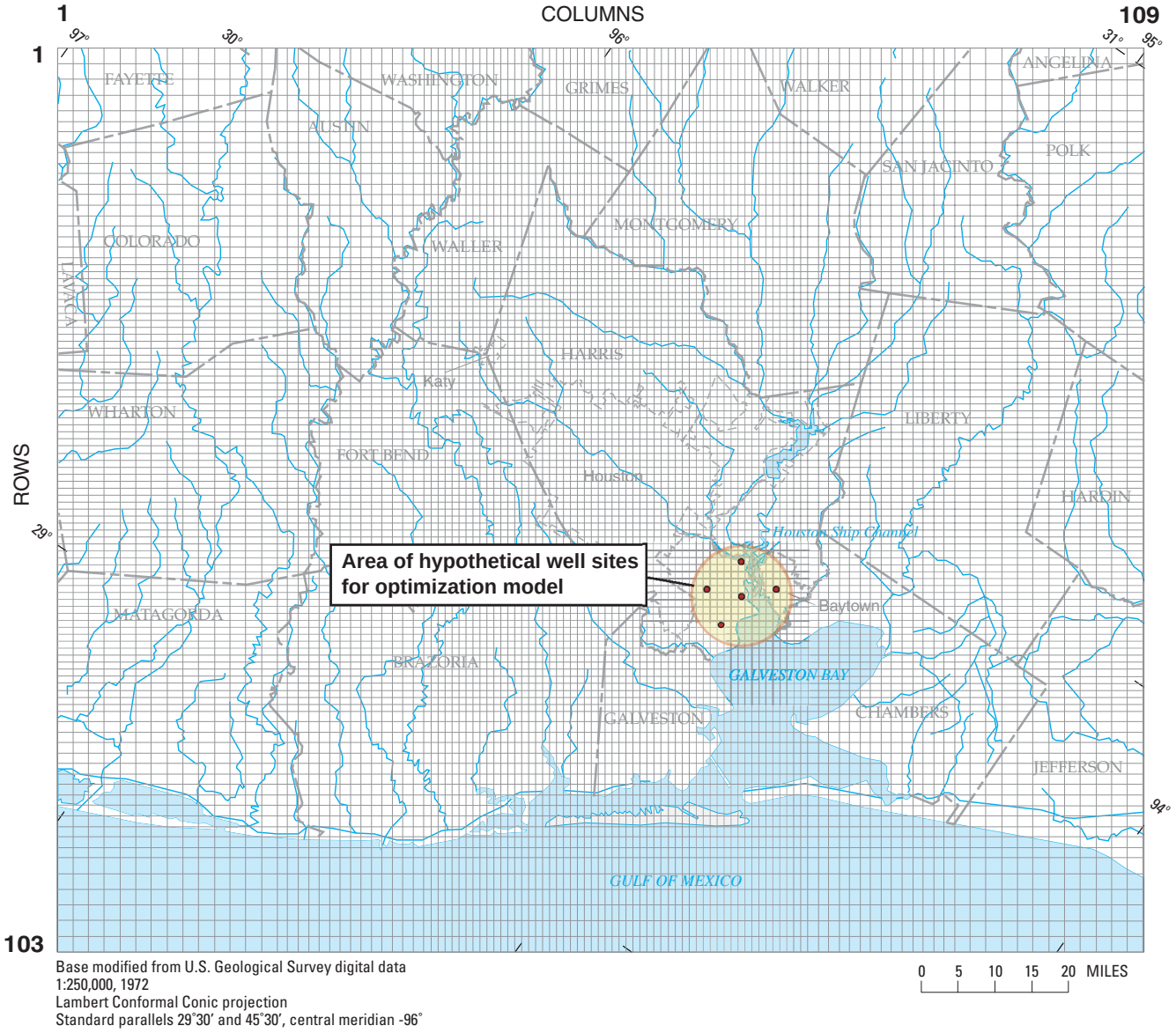

Figure 2. Ground-water-flow model grid and location of hypothetical well sites used in the optimization model of the Houston area, Texas.

uses results from the ground-water-flow model to identify a maximum quantity of withdrawal. Relative withdrawal from the five sites is fixed, but total withdrawal is allowed to vary annually. Results of this study can be used to determine if a more comprehensive analysis is warranted.

METHODS

Ground-Water-Flow Model

A ground-water-flow model of the greater Houston area was previously developed to simulate historical changes in ground-water levels and land-surface subsidence, thereby creating a management tool that can be used to aid in planning future ground-water use (Kasmarek and Strom, 2002). The total modeled area covers 18,100 mi^2, and focuses on ground-water levels and land-surface subsidence in Harris and Galveston Counties (fig. 2). The model is vertically discretized into three layers, each having 103 rows and 109 columns, for a total of 33,681 grid cells. Layer 1 represents the water table using a specified-head layer, layer 2 represents the Chicot aquifer, and layer 3 represents the Evangeline aquifer. The model

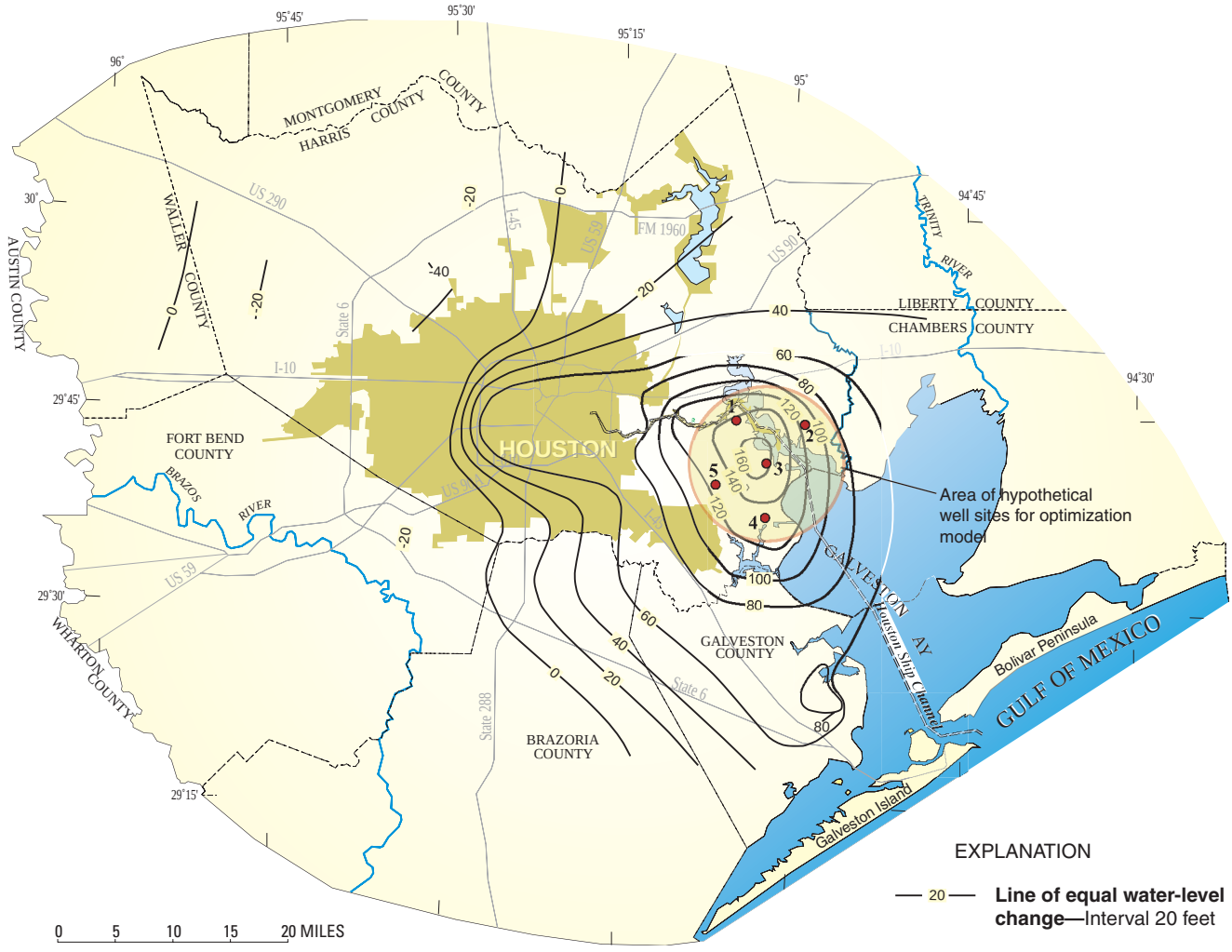

Figure 3. Approximate water-level changes in the Chicot aquifer, Houston-Galveston area, Texas, 1977–96 (modified from Kasmarek and others, 1996).

uses the MODFLOW computer code (Harbaugh and McDonald, 1996; McDonald and Harbaugh, 1988) and was calibrated for hydrologic and land-surface-subsidence conditions from 1891 to 1996.

Simulation of land-surface subsidence and water released from storage in clay layers was accomplished using the Interbed-Storage Package (Leake and Prudic, 1991). The elastic and inelastic skeletal specific storage coefficients were calibrated interactively using potentiometric surfaces of the aquifers. Land-surface subsidence was calibrated by trial and error by comparing simulated long-term (1891–1995) and short-term (1978–95) land-surface subsidence with published maps of land-surface subsidence for about the same periods until an acceptable match was achieved.

The calibration of potentiometric surfaces was based on water levels measured in wells in 1977 and 1996. Simulated and measured potentiometric surfaces of the Chicot and Evangeline aquifers for the two periods show a good correlation. Water-level measurements indicate that by 1977, large volumes of ground water withdrawn in the east-central and southeastern areas of Harris County had caused the potentiometric surfaces to decline as much as 300 ft below sea level in the Chicot aquifer and as much as 350 ft below sea level in the Evangeline aquifer. In the southeastern Houston area, the large potentiometric-surface declines observed in 1977 show significant recovery by 1996 (fig. 3).

Constrained Optimization Model

Many methods are available to identify possible improvements in water management. Probably the most common method is a simple evaluation of historical operations and the use of engineering judgment to make minor adjustments to improve efficiency or to increase flexibility. A more comprehensive, but often more time-consuming and expensive method involves trial-and-error use of a simulation model, such as the ground-water-flow model of the Houston area. This approach involves an integrated, rigorous analysis of the interrelated parts of a complex physical system. Simulated model results commonly are used to confirm engineering judgments about possible future ground-water management within the range of historical operations. Simulated model results also can be used to investigate possible future operations that are different from historical operations.

Less commonly used methods involve the use of operations research, a broad field with many mathematical approaches, to answer the central question of how to improve management of a particular operation, such as scheduling airplanes, routing telephone calls, or withdrawing ground water at a well field (Wagner, 1975; Winston, 1987; Ahlfeld and Mulligan, 2000). Part of the operations-research field involves the use of constrained optimization techniques. The most basic of these is linear programming, which is simple, but much more powerful than trial-and-error use of a simulation model. Though developed several decades ago, linear programming is just now becoming widespread, partly because it has been incorporated as part of commonly available spreadsheet software such as Microsoft® Excel. Linear programming is referred to as "Solver" in Excel and is part of the standard software package, although it must be installed separately as part of "add-ins."

Linear programming uses linear algebraic equations. The main equation is referred to as the objective function and is composed of decision variables, those variables whose values are determined through the optimization procedure. The rest of the equations are constraints that restrict the values of the decision variables. The purpose of the linear program is to identify the maximum or minimum value of the objective equation (Z) while satisfying all the constraint equations. Linear programming, as well as all other constrained optimization problems, can be expressed as:

$$\text{Maximize or minimize } Z \tag{1a}$$

subject to

$$\text{all constraint equations.} \tag{1b}$$

In linear programming, the optimization problem takes the form,

$$\text{Maximize or minimize } Z = cx \tag{2a}$$

subject to

$$ax \geq b, \tag{2b}$$

where

Z is the objective function;

c is a vector of coefficients;

x is a row vector of decision variables;

a is a matrix of coefficients; and

b is a vector of constants, which is referred to as the right-hand side (RHS of equation 2b).

FORMULATION

In this study, linear programming is used to maximize the amount of ground water that can be withdrawn without re-initiating land-surface subsidence. This is accomplished by keeping the simulated ground-water levels above the preconsolidation head. For this initial study, five hypothetical well sites were chosen to cover the general area of potentiometric rise (fig. 3). A management period of 10 years was chosen to ensure that the effects of ground-water withdrawal in a single year would become apparent in subsequent years. The number of wells and years determines the dimensions of the linear-programming problem and the maximum size of problem that can be solved. In this case using Excel 5.0 spreadsheet software, a larger, more complex problem than what is presented here was not possible.

The five wells were assumed to withdraw water only from the Chicot aquifer because it yields more water elastically per unit decline in head than the Evangeline aquifer. The total capacity of ground-water withdrawal from all wells is 1,500,000 ft^3/d, or about 1,500 gal/min per well, which is typical for municipal wells that had formerly operated in the area. Although each well has a relatively large capacity, the total capacity of the five wells is only about 0.5 percent of the total current (2001) withdrawal in the Houston area.

Response Functions

The key to using linear programming with a ground-water-flow model is the response function. This relation defines the response of ground-water levels to a

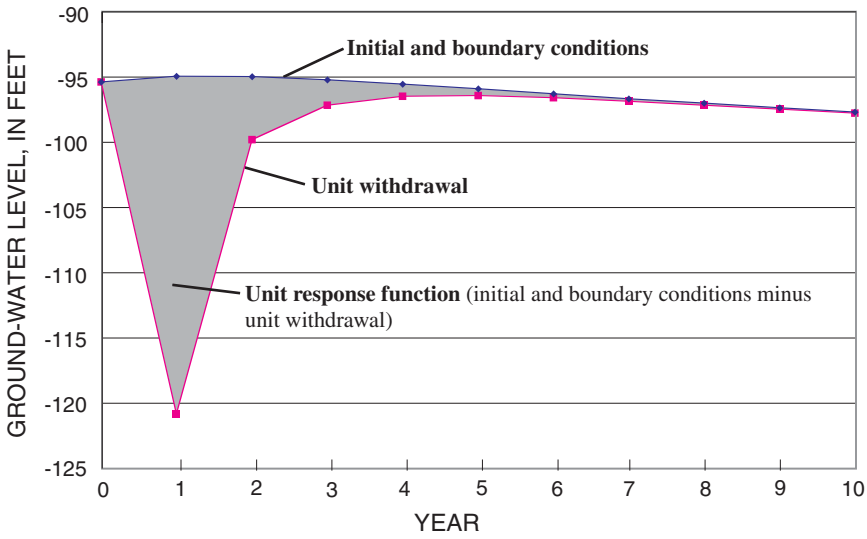

Figure 4. Response of the Chicot aquifer at well site 2 to initial and boundary conditions and to a unit withdrawal of 1,500,000 cubic feet per day for 1 year.

given stress. In the simplest aquifer, the response of ground-water levels is linearly related to the amount of ground-water withdrawal: Twice the withdrawal will produce twice the drawdown. This linear relation allows the response function to become part of the linear equations used for a linear-programming problem; and this is somewhat of a limitation, as the actual response is best defined as an exponential function.

In this study, response functions were calculated using the ground-water-flow model. An "initial and boundary condition" simulation was made for the 10-year management period. Recharge and discharge conditions in 1996 were assumed to continue for the next 10 years. The resulting heads at the end of each year of the model simulation were saved. These heads represent aquifer conditions with no additional withdrawal. As expected, ground-water levels remain nearly constant for the 10-year period (fig. 4).

To create a response function for the hypothetical wells, a response simulation was prepared. Maximum withdrawal at all five well sites for the first year (unit withdrawal) was added to the model dataset for the initial and boundary condition simulation. Withdrawal at the five well sites was set to zero in all subsequent years. The heads from this response simulation were saved and then subtracted from the initial and boundary condition heads. This difference is a (unit) response function for the five wells observed at a single location (fig. 4). The unit response, observed at all locations in the model at the end of each of the 10 years, is shown in figure 5.

Using the principle of superposition, the unit response function can be scaled to represent any withdrawal rate, and it can be shifted in time to simulate withdrawal in another year. Then, all response functions

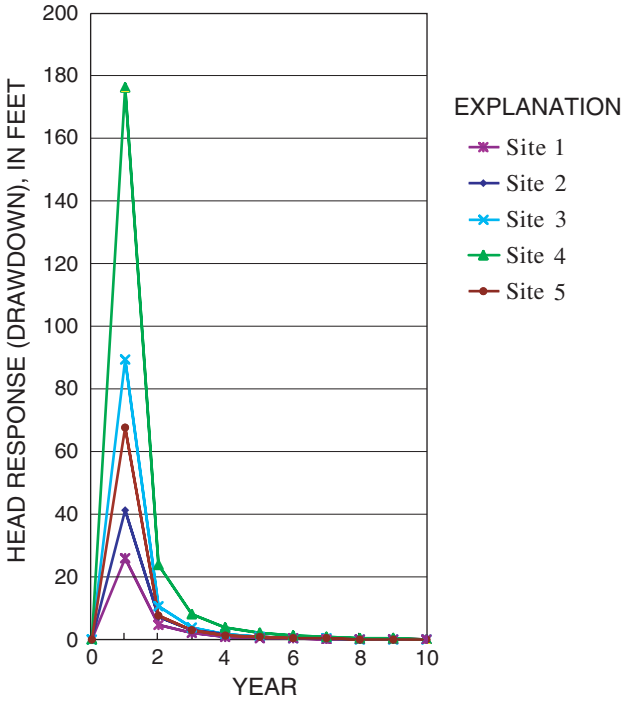

Figure 5. Unit response functions at five hypothetical well sites (shown in fig. 3) resulting from 1 year of unit withdrawal (1,500,000 cubic feet per day).

can be added together with the initial and boundary condition heads to compute the total head resulting from the addition of withdrawal from the hypothetical wells to the basic initial and boundary condition run. The only caveat is that the ground-water-flow model has hydraulic nonlinearities, whereas the principle of superposition strictly applies only to a purely linear system. Therefore, the effect of any nonlinearity in the ground-water-flow model, such as the use of dual storage coefficients (elastic and inelastic), needs to be quantified as part of interpreting the results of the optimization model.

Optimization Model

The objective of the optimization model is to maximize withdrawal from the five hypothetical well sites over a period of 10 years. To reduce the size of the problem, the five well sites were lumped together to calculate the response functions; therefore, the five sites are treated as a single variable (q) with 10 annual values ($q_1, q_2, \ldots q_{10}$). The objective of the optimization model then becomes simply,

$$\text{Maximize } Z = \text{sum } (q_k). \tag{3}$$

The constraints of the optimization model are to keep managed heads above the preconsolidation head at each location of interest during each of the 10 years. This approach ignores residual compaction that typically occurs in thick, compressible, low-permeability, fine-grained sediments that might not have hydraulically equilibrated with heads in the surrounding aquifers. The five hypothetical well sites were chosen to constrain the head, assuming that those locations would be the sites of the greatest drawdown. The first step in formulating the constraint is to compute the total managed head (h^{man}), which is the sum of the head produced by the initial and boundary condition (h^{ibc}) run plus the response caused by the managed well withdrawal (r*q). The unit response at a specific location and time is defined as $r_{j,k}$. For example, at location j = 3 for time period k = 1, the constraint is

$$h^{man}_{3,1} = h^{ibc}_{3,1} + (r_{3,1} * q_1). \tag{4a}$$

For period 2, the managed head is the sum of the initial and boundary conditions for that period plus the residual response (drawdown) created by managed withdrawal in period 1, plus the response caused by managed withdrawal in period 2. That is,

$$h^{man}_{3,2} = h^{ibc}_{3,2} + (r_{3,2} * q_1) + (r_{3,1} * q_2). \tag{4b}$$

The trick is offsetting each unit response function shown in figure 5 in time so that it corresponds to the time when the stress (withdrawal) is applied, and then keeping track of residual drawdown resulting from previous withdrawal.

In matrix form, these calculations become

$$H^{man}_{j,k} = H^{ibc}_{j,k} + R_{j,k}Q_k, \tag{4c}$$

where

H^{man} is a matrix of head values at j locations for k time periods,

H^{ibc} is a matrix of heads obtained from the initial and boundary condition simulation,

R is a matrix of responses obtained from use of the ground-water-flow model, and

Q is a vector of withdrawal values obtained from the optimization program.

The constraint then becomes

$$H^{man}_{j,k} \le H^{pc}_{j}, \tag{5}$$

where

H^{pc} is a vector of preconsolidation heads at the five hypothetical well sites.

The value of preconsolidation head was obtained from simulation of historical conditions using the ground-water-flow model.

Additional constraints, referred to as bounds, are required to restrict the values of withdrawal to reasonable values. In this case, the withdrawal must be greater than zero and less than the maximum value of 1,500,000 ft^3/d:

$$0 \le Q_k \le 1{,}500{,}000. \tag{6}$$

RESULTS

Results from the optimization model indicate that about 80 percent of the maximum value, or about 1,200,000 ft^3/d, theoretically could be produced continuously for 10 years without causing additional land-surface subsidence from the five sites near Baytown. Optimal annual values of withdrawal, shown in figure 6, decreased from 100 percent of the maximum available withdrawal in the first year, to about 84 percent in the third year, to slightly more than 80 percent in the tenth year. This decline in optimal withdrawal is related to an expanding drawdown cone caused by the additional

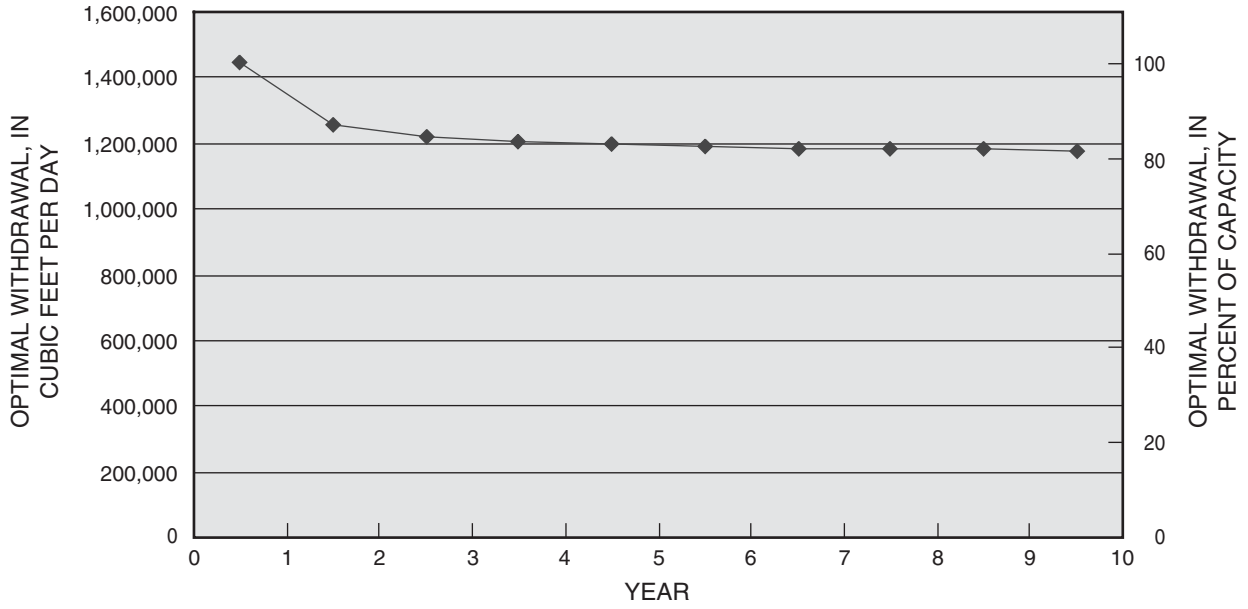

Figure 6. Optimal withdrawal from five hypothetical well sites near Baytown, Texas.

withdrawal and to declining ground-water levels as illustrated in the initial and boundary condition simulation (fig. 4).

In addition to providing the value of the objective function, the optimal solution provides useful information about the overall problem and possible implementation. The binding constraint on all solutions was head at site 4, which is not surprising because site 4 had the largest response function (fig. 5). Withdrawing less water from site 4 and more from the other sites likely would increase the total withdrawal that is possible.

Testing the management alternative of allowing withdrawal to vary at each site would require reformulating the optimization problem so that q has dimensions of both sites and time ($q_{i,k}$) and the response matrix includes functions for each site affecting each other site. These changes are straightforward but do increase the dimension of the problem by a factor of 5^2, from 10 by 50 to 50 by 250, and might require use of other linear-programming software.

Greater flexibility in an optimization problem typically improves the optimal value, as indicated by allowing withdrawal to vary at each site. Similarly, adding more withdrawal sites to the optimization problem likely would increase the optimal value of withdrawal. Conversely, adding more constraints or more restrictive constraints, such as limiting withdrawal at each site to different amounts, tends to decrease the optimal value. These minor modifications to the optimization problem or more major modifications, such as incorporating surface-water supply or demand, can be analyzed using essentially the same optimization techniques as those described above.

Sensitivity of the objective function (optimal withdrawal) in the initial problem is shown in figure 7 for different minimum constraint values (distance above the preconsolidation head). For a safety factor of 20 ft, maximum average withdrawal declines about 10 percent; for a safety factor of 100 ft, maximum average withdrawal declines more than 50 percent. The linear sensitivity of the objective function is caused by the inherent linearity of the optimization problem.

Limitations of this analysis include the hydraulic nonlinearity of the system that involves the question of whether residual compaction of thick material is occurring. Although this was an initial concern, comparing heads from the optimization model with heads from the mildly nonlinear ground-water model showed that they were within about 0.2 ft of being the same at the end of the 10-year management period. Of greater concern is whether there are the necessary wells and pipelines near Baytown to take advantage of the elastically available water. Such infrastructure commonly is very expensive to install or refurbish, and such efforts might not be cost-effective, considering that the total elastically

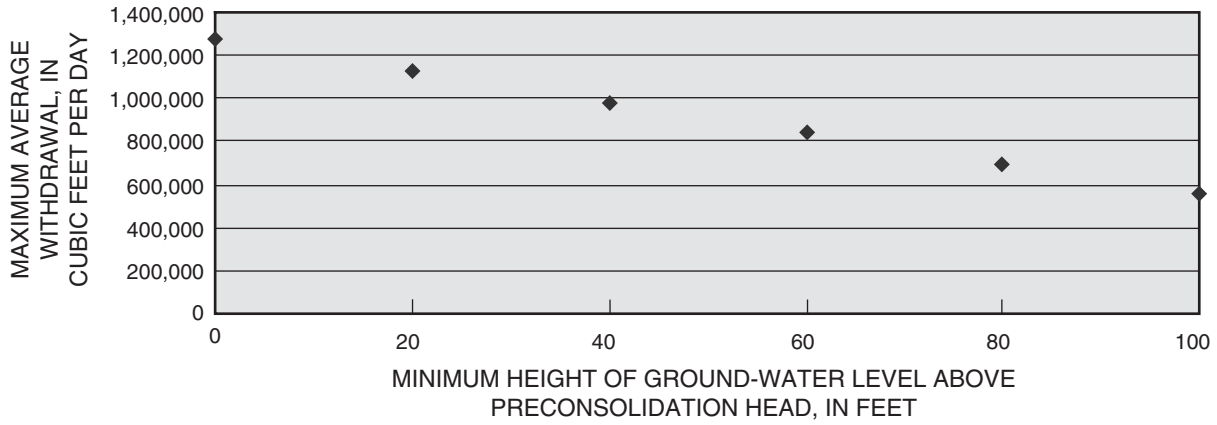

Figure 7. Maximum average withdrawal for different minimum heights of ground-water level above the preconsolidation head.

available water identified in this study is less than 0.5 percent of the total water demand in the Houston area.

Future work to better define the management alternatives of using elastically available ground water in the Houston area include varying pumpage at each site, adding additional well sites, and incorporating the costs necessary to produce and transport the ground water.

ACKNOWLEDGMENTS

The authors gratefully acknowledge support of this research by the City of Houston. Additionally, the authors thank and acknowledge Eve L. Kuniansky (USGS) for initiating the study and Robert K. Gabrysch (USGS retired and Harris-Galveston Coastal Subsidence District's consulting engineer) for his advice and insight on land-surface subsidence and hydrology in the Houston area.

Characterization and Modeling of Land Subsidence Due to Ground-Water Withdrawals From the Confined Aquifers of the Virginia Coastal Plain

By Jason P. Pope[1] *and* Thomas J. Burbey[2]

Abstract

High-resolution borehole extensometers were used in the southeastern Coastal Plain of Virginia to measure 24.2 millimeters of total compaction at Franklin from 1979 to 1995 (1.5 millimeters per year) and 50.2 millimeters of total compaction at Suffolk from 1982 to 1995 (3.7 millimeters per year). Analysis of the extensometer data reveals that the small rates of aquifer-system compaction appear to be correlated with withdrawals of water from several confined aquifers. One-dimensional vertical compaction modeling indicates that the measured compaction is the result of nonrecoverable hydrodynamic consolidation of the fine-grained confining units and interbeds as well as recoverable compaction and expansion of some portion of fine-grained units and all of the coarse-grained aquifer units. The modeling results also provide useful estimates of the specific storage and vertical hydraulic conductivity of individual hydrogeologic units that enhance understanding of the complex Coastal Plain aquifer system and should prove useful in future modeling and management of ground water in this area.

INTRODUCTION

Withdrawals of ground water from the confined aquifers of the Virginia Coastal Plain have increased dramatically over the past century, resulting in large declines in water levels (hydraulic heads) and gradual subsidence of the land surface. The small magnitude of subsidence measured in this area has been unnoticeable to most observers, and little effort has previously been devoted to its study. However, research in other areas experiencing subsidence has demonstrated that an understanding of the relations between ground-water withdrawals, hydraulic heads, and aquifer-system compaction reveals fundamental information about the properties and behavior of the system (Galloway and others, 1999). Consequently, a study was undertaken to measure and analyze aquifer-system compaction due to ground-water withdrawals in the Coastal Plain of Virginia. Total aquifer-system compaction was measured at two locations with high-resolution borehole extensometers, and related head and withdrawal data were collected and analyzed. A one-dimensional model was used to simulate the complex and time-dependent relation between hydraulic heads and compaction and to better characterize the hydrogeologic properties of individual units in this multilayered aquifer system. This report presents the compaction measurements and describes the results of the modeling.

The study area (fig. 1) includes about 10,000 km^2 of the southern part of the Coastal Plain physiographic province of Virginia. This area is bounded by the James River to the north and by North Carolina to the south. On the west, it is bounded by the Fall Line, which defines the western limit of the Coastal Plain province. To the east, it is bounded by the Chesapeake Bay and the Atlantic Ocean. Most of this area is of low elevation (less than 50 m above sea level) and low relief; the level terrain is characterized by a series of wave-cut terraces, broad river valleys, and wetlands.

The Coastal Plain of Virginia is underlain by a thick sedimentary wedge of unconsolidated to partially consolidated gravels, sands, silts, and clays ranging in age from Early Cretaceous to Holocene (Meng and Harsh, 1988). These sediments unconformably overlie the crystalline basement bedrock surface, which slopes gently to the east. The collective thickness of these sedimentary deposits ranges from almost zero at their western boundary along the Fall Line to more than 1,000 m below the Chesapeake Bay. A relatively thick

[1] U.S. Geological Survey, Richmond, Va.
[2] Department of Geological Sciences, Virginia Polytechnic Institute and State University, Blacksburg, Va.

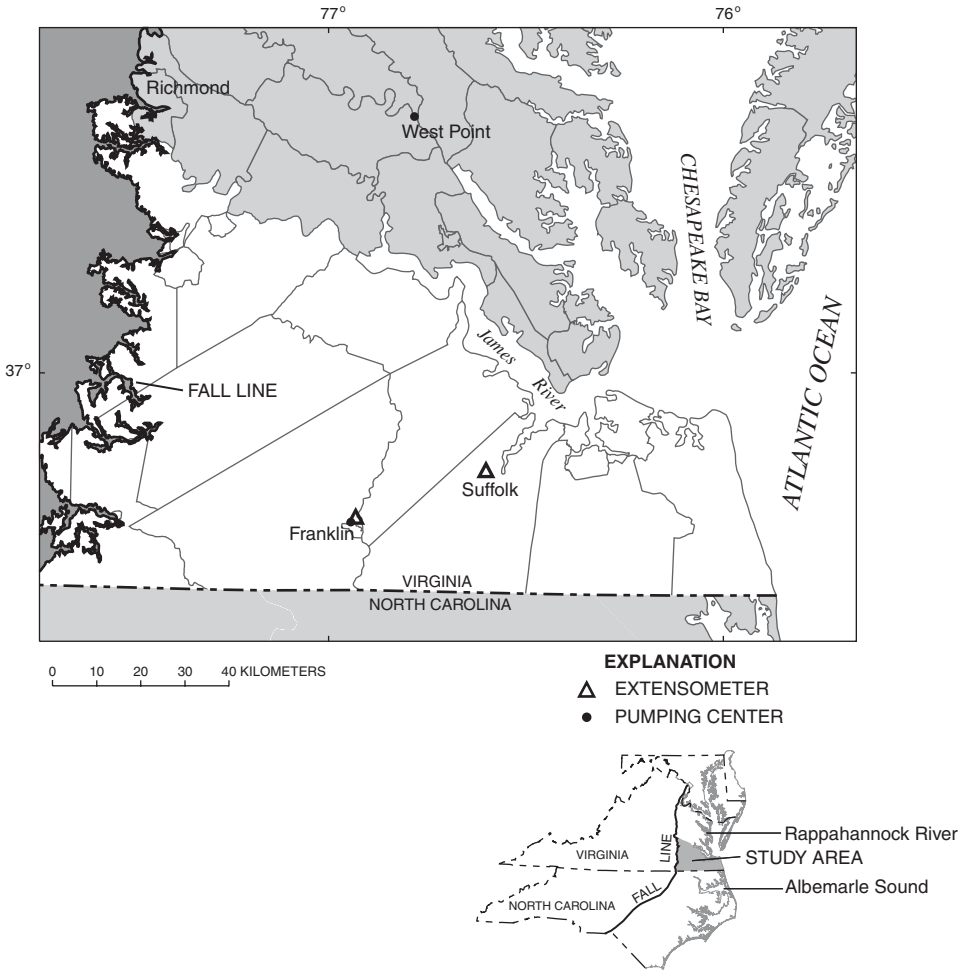

Figure 1. Study area in southeastern Virginia, showing locations of extensometers and major pumping centers.

sequence of continental, fluvial-deltaic deposits primarily of Cretaceous age is overlain by a much thinner sequence of marine deposits of Tertiary age and by a very thin layer of Quaternary sediments. These depositional units generally strike approximately parallel to the Fall Line, dipping and thickening to the east. Many of these units are disrupted northeast of the study area by the recently discovered Chesapeake Bay impact crater, which resulted from a meteorite about 35 million years ago near the present mouth of the Chesapeake Bay (Powars, 2000). Although the impact crater greatly affected the geology of eastern Virginia, its effects on aquifer-system compaction and land subsidence are unknown, because most of the water-level decline and measured compaction have occurred outside the known crater boundary.

In southeastern Virginia, the hydrogeologic framework includes a surficial unconfined aquifer, six confined aquifers, and six associated confining units (Hamilton and Larson, 1988; Meng and Harsh, 1988). Below the Quaternary deposits composing the unconfined Columbia aquifer, three confined aquifers and three confining units have been defined from Tertiary marine deposits of poorly sorted, glauconitic sand with varying amounts of shell, silt, and clay. The Yorktown-Eastover, Chickahominy-Piney Point, and Aquia aquifers are distinguished from their intervening confining units primarily by coarser grain size and higher shell content (McFarland, 1999). Similarly, three aquifers and three confining units have been defined from the underlying fluvial-deltaic deposits of Cretaceous age, which are composed of medium-to-coarse-grained quartz sand with varying amounts of gravel, silt, and

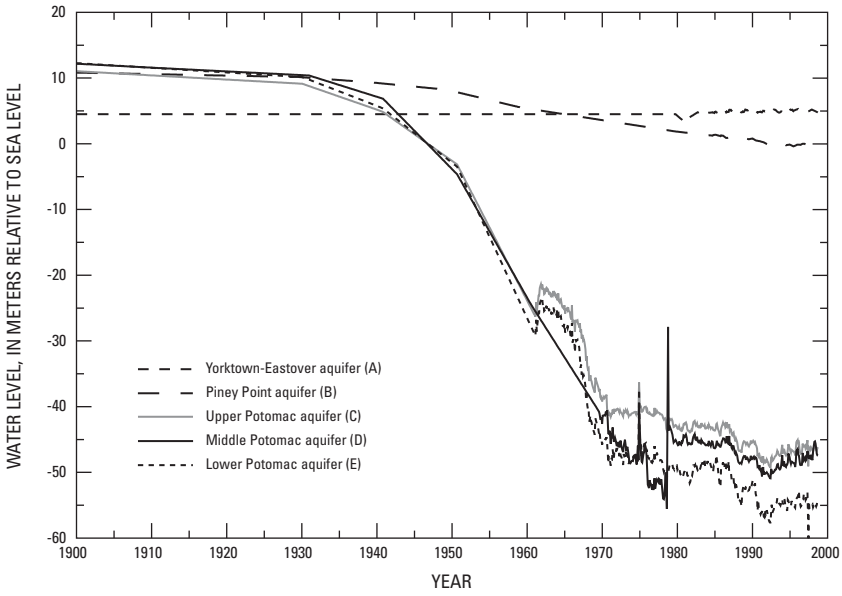

Figure 2. Estimated and measured hydraulic heads in the confined aquifers at Franklin, Virginia. Levels are approximated prior to 1980 for Yorktown-Eastover, prior to 1984 for Piney Point, prior to 1960 for Middle Potomac, and prior to 1969 for Lower Potomac; the entire Upper Potomac record is simulated. (Letters correspond to piezometers shown in figure 4.)

clay. In these Cretaceous deposits, the sand units of the Upper Potomac, Middle Potomac, and Lower Potomac aquifers are separated by discontinuous clay beds and lenses (McFarland, 1999). The discontinuous nature of these clay lenses has led to reconsideration of their function as distinct confining units, and it has been suggested that the three Potomac aquifers might be best characterized as one large aquifer system (E.R. McFarland, U.S. Geological Survey, oral commun., 2001).

The three Potomac aquifers are particularly important for water supply in eastern Virginia. These thick, coarse-grained deposits have very high transmissivities and are capable of supplying large volumes of water. Because of their depth, the Potomac aquifers typically have been used only by a small number of industries and municipalities that have been responsible for a large percentage of the withdrawals. Reported withdrawals from the confined Coastal Plain aquifers in Virginia have risen from less than 37,850 m^3/d (10 Mgal/d) in 1900 to their current total of over 378,500 m^3/d (100 Mgal/d). Together, withdrawals from the Potomac aquifers at Franklin (121,120 to 151,400 m^3/d; 32 to 40 Mgal/d) and West Point (52,990 to 64,345 m^3/d; 14 to17 Mgal/d) constitute close to one-half of that amount.

Increasing withdrawals from the Coastal Plain aquifers throughout the 20th century were accompanied by declining hydraulic heads. Until about 1940, heads in the Potomac aquifers were above land surface across much of eastern Virginia (Cederstrom, 1945). At Franklin, hydraulic head in the Middle Potomac aquifer declined from about 5 m above sea level in 1940 to almost 50 m below sea level in 1970. By the 1970s, pumping at Franklin, West Point, and elsewhere in the Coastal Plain had created a regional cone of depression in the potentiometric surfaces of the Potomac aquifers 190 kilometers (km) long and 95 km wide, extending from the Rappahannock River in northeastern Virginia to the Albemarle Sound in northeastern North Carolina (Hopkins and others, 1981). Withdrawal rates have stabilized since that time, and heads at Franklin have declined only moderately in the last 2 decades. A reconstruction of historical estimated and measured hydraulic heads in the confined aquifers at Franklin (fig. 2) provides an overview of the changing hydraulic conditions at that location. In other areas, increased pumping rates have led to continued local head declines and expansion of the cone of depression, although the heads in the

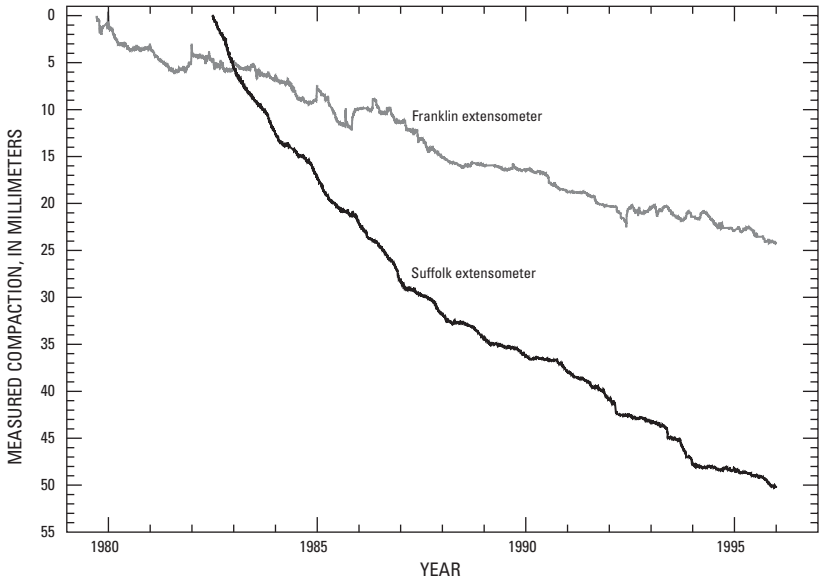

Figure 3. Aquifer-system compaction measured by borehole extensometers at Franklin (1979–95) and Suffolk (1982–95).

Potomac aquifers at Franklin remain the lowest in the region. Withdrawal rates from the other Coastal Plain aquifers have increased more slowly. Consequently, heads in these aquifers have declined much less than in the Potomac aquifers. Some of that head decline appears to have been induced by leakage of water into the underlying Potomac aquifers.

MEASUREMENT AND ANALYSIS OF COMPACTION

Land subsidence in the Coastal Plain of Virginia was first reported by Holdahl and Morrison (1974) on the basis of a study of geodetic and tidal data. They measured average annual rates of subsidence ranging from 1.2 to 4.0 mm between 1940 and 1971 and noted appreciable local variations in the rate of land-surface movement. The close correlation between measured subsidence and the locations of large withdrawals of ground water around Franklin and West Point was later noted by others (Davis, 1977, 1987) and ultimately led to further investigation of land subsidence and aquifer-system compaction in Virginia.

Borehole extensometers were installed at Franklin, Va., in 1979 and near Suffolk, Va. (fig. 1), in 1982 by the U.S. Geological Survey and the Virginia Department of Environmental Quality. The 262-m borehole extensometer at Franklin is located within 1 km of the large pumping center. It extends from land surface to bedrock and records total compaction in the aquifer system. The counter-weighted pipe extensometer was constructed following guidelines described by Riley (1986) to achieve high-strain sensitivity. In particular, the modified Stevens type-F recorder is equipped with a 50:1 gear ratio to increase instrument sensitivity to expected small changes in strain. The 514-m Suffolk pipe extensometer also extends from surface to bedrock and was constructed in a manner similar to the instrument at Franklin. However, its recorder was equipped with a 15:1 gear ratio, limiting its sensitivity. Both instruments provided continuous records of compaction data until measurements were discontinued at the end of 1995.

Monthly recorder charts from the extensometers were digitized to produce continuous records of total cumulative compaction at the two sites. Measured compaction from the two extensometers is presented in figure 3. Total cumulative compaction at Franklin from 1979 to 1995 was 24.2 mm, with a mean rate of about 1.5 mm/yr over the period of record. Total compaction at Suffolk from 1982 to 1995 was measured at 50.2 mm, with a mean rate of 3.7 mm/yr. In general, the greater rate of compaction at Suffolk over the period of record can be explained by the much greater thickness of the deposits of the aquifer system at that location and by

continued drawdown in the aquifer system. Franklin remains the approximate center of the regional depression of the potentiometric surface, although hydraulic heads at Franklin have declined very slowly in recent years. Heads at Suffolk have continued to decline, however, resulting in larger rates of compaction over the period of record.

Close correlation between the compaction and water-level records is apparent at both extensometer sites. Particularly noticeable are instantaneous compaction and expansion episodes resulting from short-term (hours to days) head changes in the heavily pumped Potomac aquifers. These episodes are thought to represent recoverable (elastic) deformation of coarse-grained aquifer units. However, examination of the data indicates that compaction cannot be defined simply in terms of concurrent declines in water levels in the Potomac system. A dominant trend of increasing cumulative compaction at Franklin is apparent even during periods of no net head decline, suggesting that ongoing, time-dependent residual compaction of the fine-grained confining units is an important component of compaction in this aquifer system. This behavior is consistent with that of many other systems experiencing compaction due to the withdrawal of ground water (Galloway and others, 1999; Sneed and Galloway, 2000).

An attempt was made to estimate recoverable (elastic) and nonrecoverable (inelastic) skeletal storage coefficients for the Coastal Plain aquifer system using the method established by Riley (1969). For a system that equilibrates rapidly to changes in pressure, a plot of applied stress (hydraulic head) versus vertical strain (compaction) reveals two dominant linear trends that represent the two components of the skeletal storage coefficient, S_{ke} and S_{kv} (Riley, 1969). For this system, the application of Riley's method revealed an inconsistent relation between the total measured compaction and the applied stress in any of the individual aquifers, suggesting the existence of a complex and time-dependent relation between multiple stresses and cumulative strain in the entire aquifer system.

ONE-DIMENSIONAL SIMULATION OF COMPACTION

Because of the complexity of the Coastal Plain aquifer system, a numerical model was needed to account for vertical variations in applied stress across numerous hydrogeologic units, to characterize the resulting time-dependent vertical variations in strain, and to discern the contributions of individual hydrogeologic units to the total observed compaction. The one-dimensional finite-difference numerical model developed by Helm (1975, 1976) uses the one-dimensional (vertical) form of the diffusion equation to compute the temporal distribution of compaction in a hydrogeologic unit from the history of applied stress on the upper and lower boundary of the unit, as well as the unit's properties of vertical hydraulic conductivity, specific storage (recoverable and nonrecoverable), and thickness. This model was used to evaluate the parameters of each of the units in the Virginia Coastal Plain by matching the total computed compaction of all units to the measured compaction of all units from extensometer data. Simulation of compaction was attempted for both the Franklin and Suffolk sites, but the paucity of water-level data at Suffolk constrained accurate representation of the aquifer system at that location, and limitations in the resolution of the measured compaction data from the Suffolk extensometer prevented satisfactory model calibration. Consequently, only the results of the Franklin simulations are presented here.

With Helm's model, a hydrogeologic unit can be simulated either as an aquifer containing one or more doubly draining fine-grained interbeds with identical stress conditions on the upper and lower boundaries, or as a separator (confining unit) affected by different stress conditions in the surrounding aquifers, above and below. In this case, the vertical discretization of the model for the Franklin site was influenced primarily by the availability of hydraulic head (boundary stress) data for the various aquifers. For the Franklin simulation, the system was divided into nine separate model units (fig. 4), and total compaction was computed as the sum of the simulated compaction in each of the nine units. For units simulated as fine-grained separators (confining units), time-dependent compaction was computed on the basis of the stress on both sides of the unit, as well as the thickness of the unit and its hydraulic parameters: vertical hydraulic conductivity (K_v), nonrecoverable skeletal specific storage (S_{skv}), recoverable skeletal specific storage (S_{ske}), and the initial distribution of past maximum (preconsolidation) stress. For units simulated as aquifer/interbed systems, compaction was computed as the sum of instantaneous compaction in the coarse-grained aquifer and time-dependent compaction of the fine-grained interbeds, on the basis of the parameters listed above. Multiple interbeds within a model unit

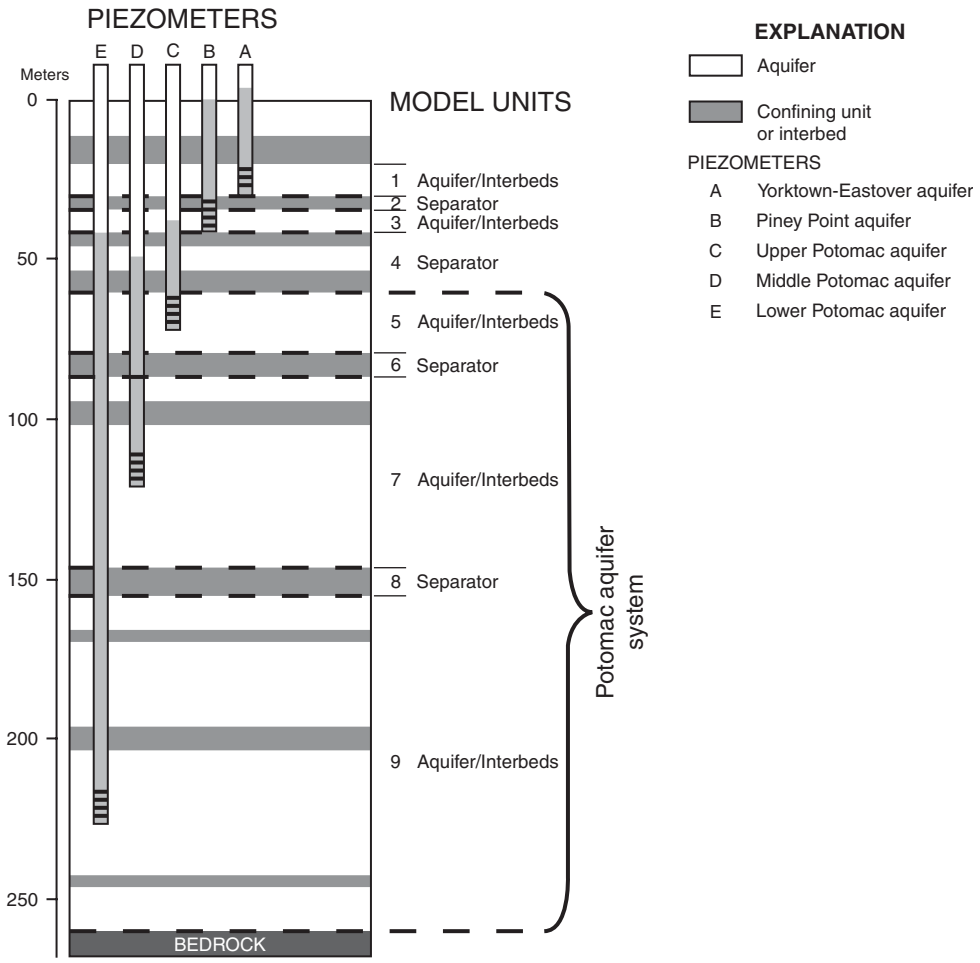

Figure 4. Model units for one-dimensional simulation of compaction at Franklin, Virginia. (Piezometers correspond with records of hydraulic head presented in figure 2.)

were simulated as one bed with an equivalent (weighted average) thickness, using the method described by Helm (1975).

The five hydraulic head records used as stresses in the model were constructed from measured data and historical reports, in an effort to simulate historical variations in head from predevelopment conditions to the present. Linear interpolation was used to fill gaps and produce complete records of monthly values from 1900 to 1998. The vertical locations of these five stress conditions are represented by the piezometers in figure 4, and the time distributions of the stresses are presented in figure 2.

The model was calibrated by trial and error, beginning with initial parameter values derived from published calculations and estimates. Parameter values for S_{skv}, S_{ske}, and K_v of each unit were adjusted to fit the total computed compaction to (1) the measured 1979 to 1995 record and (2) an estimated cumulative value derived from the Holdahl and Morrison benchmark data (about l36 mm from 1900 to 1998). The calibrated simulation results are shown in figure 5, along with the extensometer record of total compaction for comparison.

Results of the calibrated model reveal important information about the properties and behavior of the aquifer system. In general, S_{skv} for the fine-grained units is small but significant, decreasing with depth and ranging from 1×10^{-4} to 1.5×10^{-5} m^{-1}. Values of S_{skv} for the confining units of marine origin (model units 1, 2, 3, and 4) are about an order of magnitude higher than values for the continental deposits (model units 5 through 9), perhaps reflecting less historical preconsolidation of the younger and less deeply buried

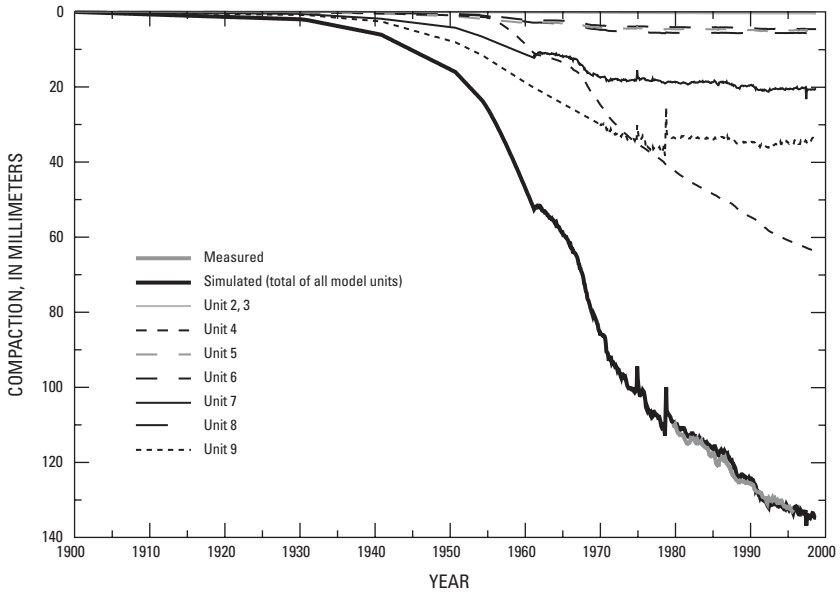

Figure 5. Simulated and measured aquifer-system compaction at Franklin, Virginia. (Records correspond to model units in figure 4.)

marine sediments. Simulated values of S_{ske} range from 4.5×10^{-6} to 6×10^{-6} m^{-1}, but some uncertainty is associated with the calibration of S_{ske} because heads have not recovered enough to cause substantial measurable elastic expansion of the fine-grained units. Vertical hydraulic conductivity values are low for all of the simulated confining units, ranging from 1.2×10^{-6} to 5.5×10^{-6} m/d, but the simulated total compaction record is not extremely sensitive to changes in K_v because most of the fine-grained units are relatively thin, particularly in the Potomac system. Simulation results indicate that the Potomac system, represented by model units 5, 6, 7, 8, and 9, has contributed more than 40 percent of cumulative historical compaction in the aquifer system but has contributed very little of the recent compaction, as heads in the Potomac aquifers have remained fairly constant for the past 3 decades. On the other hand, heads throughout the Potomac aquifers now approach the threshold of past maximum stress, indicating that even small declines in head beyond current levels could cause greater compaction of the Potomac system and subsequent land subsidence.

Notably, the fine-grained marine sediments (model unit 4) overlying the Potomac system appear to be responsible for a large part of the historical compaction and most of the ongoing compaction. Simulation results indicate that this unit is compacting slowly as withdrawals from the Potomac aquifers maintain a large head gradient, causing downward drainage of ground water through this interval. If correct, the simulation for model unit 4 indicates that small rates of residual compaction could continue for months or years even if hydraulic heads in the Potomac system do not decline beyond current levels. This conclusion is supported by time constants of about 15 years for unit 4 and of several months to several years for the other fine-grained units.

SUMMARY

Over the past century, large increases in groundwater withdrawals from the confined aquifers of the Virginia Coastal Plain have resulted in large head declines and small amounts of subsequent land subsidence. Measurement and simulation of aquifer-system compaction indicate that the magnitude and rate of compaction and the resulting land subsidence in this region are small compared with many other areas experiencing subsidence (Galloway and others, 1999). Nonetheless, analyses of extensometer measurements have confirmed that measured compaction is the result of ground-water withdrawals from the confined aquifers, and simulations have increased our understanding of the complex relation between measured hydraulic heads and compaction in this system. For example, simulation results explain the uneven spatial and

temporal distribution of compaction in the Coastal Plain system and reveal that compaction is not evenly distributed vertically throughout the aquifers and confining units. In addition, simulations have revealed that storage values for the fine-grained units in the Coastal Plain are larger than previously thought, suggesting that confining-unit storage appreciably affects ground-water flow in this complex aquifer system. These results are expected to be useful in ongoing efforts to simulate ground-water flow. Previous flow models of the Virginia Coastal Plain have not considered the effects of confining-unit storage, which might be important for accurate calibration of hydraulic heads, particularly for transient simulations.

Application of Nonlinear Regression Methods to Estimate Hydraulic Properties that Control Vertical Aquifer-System Deformation at the Lorenzi Site, Las Vegas, Nevada

By Michael T. Pavelko[1]

Abstract

The U.S. Geological Survey has continuously monitored water-level changes in three piezometers and vertical aquifer-system deformation with a borehole extensometer at the Lorenzi site, in Las Vegas, Nevada, since 1994. A one-dimensional ground-water-flow model of the aquifer system below the Lorenzi site was developed. Nonlinear regression methods were used to calibrate the model and estimate the vertical hydraulic conductivity of thick interbedded fine-grained deposits or interbeds, inelastic skeletal specific storage of interbeds, and elastic skeletal specific storage of interbeds in the coarser-grained aquifers. Water levels were used as system stresses in the model to simulate vertical aquifer-system deformation. Estimated and measured aquifer-system deformation data were used to minimize a weighted least-squares objective function and to estimate optimal property values.

Model results indicate that the vertical hydraulic conductivity of interbeds is 3×10^{-6} ft/d, the inelastic specific storage of interbeds is 4×10^{-5} ft^{-1}, the elastic specific storage of interbeds is 5×10^{-6} ft^{-1}, and the elastic specific storage of aquifers is 3×10^{-7} ft^{-1}. Regression statistics indicate that the model and data provide sufficient information to estimate the target properties, the model adequately simulates observed data, and the estimated property values are accurate and unique.

[1] U.S. Geological Survey, Las Vegas, Nev.

INTRODUCTION

Intensive ground-water pumping in Las Vegas Valley, Nev., has lowered water levels by as much as 300 ft from predevelopment conditions. These water-level declines have resulted in aquifer-system compaction and associated land subsidence and earth fissuring. The land surface in some areas has subsided more than 5 ft since the 1930s, causing millions of dollars in damage to roads, pipelines, homes, and other infrastructure.

Artificial ground-water-recharge programs were started in 1988 to efficiently manage existing supplies of imported Colorado River water and to reduce the rate of future subsidence by maintaining or increasing existing water levels. Artificial recharge of the local aquifer system occurs during periods of lower water use (October to April), and ground water is pumped from the aquifer system during periods of high water use (May to September). Results from current studies indicate that the artificial recharge programs have stabilized water levels and reduced subsidence rates; short periods of aquifer expansion and land-surface uplift have been observed during cycles of artificial recharge. Some land subsidence still is occurring because of residual aquifer-system compaction. The residual compaction is attributed to delayed drainage from thick interbeds within the aquifer system.

The State of Nevada, Las Vegas Valley Water District, and U.S. Geological Survey (USGS) are cooperatively collecting data to monitor water levels, aquifer-system compaction, and land subsidence, and are conducting studies to better understand and conceptualize processes controlling land subsidence in Las Vegas Valley. As part of these efforts, the USGS has continuously measured aquifer-system compaction and water levels at the Lorenzi site in northwest Las Vegas since 1994 (fig. 1). A one-dimensional (1–D) ground-water-flow model has been constructed for the Lorenzi

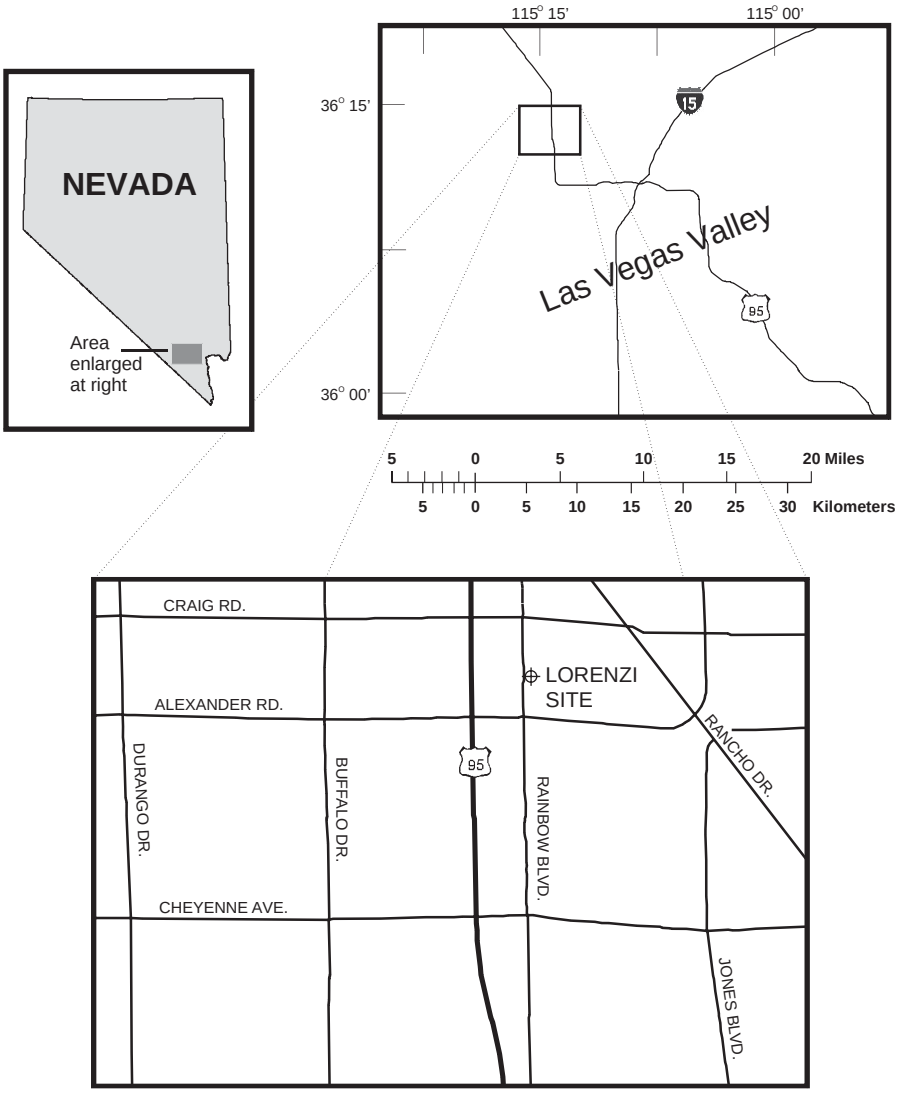

Figure 1. Location of the Lorenzi site, Las Vegas, Nevada.

site to estimate selected hydraulic properties of the aquifer system.

Purpose and Scope

The purpose of this report is to briefly document preliminary results of a study to estimate hydraulic properties that control land subsidence at the Lorenzi site. The estimated properties are vertical hydraulic conductivity of interbeds (K'_v), inelastic skeletal specific storage of interbeds (S'_{skv}), and elastic skeletal specific storage of interbeds (S'_{ske}) and aquifers (S_{ske}). (The primes denote interbed properties.) Values of the hydraulic properties were estimated by fitting numerical model results to observed land subsidence and aquifer-system compaction data. The numerical model is a 1–D, finite-difference, ground-water-flow model that also simulates aquifer-system compaction and expansion. Compaction and expansion in the model were inferred from storage changes caused by water-level fluctuations. Nonlinear regression methods were used to calibrate the model by minimizing differences between simulated and observed data. Observed data consist of estimated historical land-subsidence data and measured extensometer data.

Study Area

Las Vegas Valley, Nev., is a sediment-filled structural trough overlying carbonate bedrock. The

sediments are a complex assemblage of gravel, sand, silt, and clay formed by episodes of deposition, erosion, and fault movement. The mainly alluvial and fluvial sediments form a thick accumulation of interbedded and interfingered, coarse- and fine-grained sediments that, in places, exceed 5,000 ft in thickness (Plume, 1989) and form the Las Vegas Valley aquifer system.

Ground water is pumped mainly from the upper 2,000 ft of sediments. The principal aquifer, from about 200 to 2,000 ft below land surface, has been subdivided into shallow, middle, and deep zones that are hydraulically and lithologically separated by thick, low-permeability, fine-grained interbeds. An unconfined aquifer consisting of a 100- to 300-ft-thick section of clay, sand, and gravel overlies the principal aquifer in most places. The principal aquifer and the unconfined aquifer are separated by variably thick, laterally discontinuous interbeds (Maxey and Jameson, 1948; Malmberg, 1965; Harrill, 1976; Morgan and Dettinger, 1996).

The Lorenzi site consists of three nested piezometers, USGS–PZD, USGS–PZM, and USGS–PZS, and a vertical borehole extensometer, USGS–EXT1 (fig. 2). The site is within a 2-mile radius of 14 municipal wells used to pump ground water from about May through September and (or) to artificially recharge the aquifer system from about October through May (Pavelko, 2000).

Geophysical and lithologic logs from the Lorenzi extensometer borehole indicate the presence of three thick interbeds and three aquifers (Paillet and Crowder, 1996; Pavelko, 2000) that likely correspond to the three zones of the principal aquifer. The aquifer depths range from 255 to 308, 420 to 500, and 605 to at least 800 ft below land surface (fig. 2). The aquifers consist of sand and gravel with thin interbedded layers of silt and clay, and the thick interbeds consist mostly of silt and clay. There is no unconfined aquifer at the site (F.L. Paillet, U.S. Geological Survey, written commun., 1994).

ESTIMATING HYDRAULIC PROPERTIES

Nonlinear regression methods were applied to aquifer-system compaction and expansion data to calibrate a numerical ground-water-flow model and to estimate hydraulic properties. The numerical model was developed using MODFLOW, a modular finite-difference ground-water-flow model (McDonald and Harbaugh, 1988; Harbaugh and McDonald, 1996). UCODE, a computer program for inverse modeling (Poeter and Hill, 1998), was used for the nonlinear regression and hydraulic-property estimation. Four properties were estimated: K'_v, S'_{skv}, S'_{ske}, and S_{ske}.

Numerical Model

The numerical model represents a 735-ft-thick section of the aquifer system at the location of the Lorenzi extensometer. The simulated section is from 65 to 800 ft below land surface and includes three aquifers and three thick interbeds totaling 328 ft and 407 ft, respectively. Model cells range in thickness from 1 to 8 ft. Aquifer cells generally are thicker than interbed cells, and cells are thinnest near aquifer-interbed boundaries (fig. 2). The model uses variable discretization to better represent large, nonlinear head gradients in thick interbeds and to better simulate residual compaction.

The model simulates compaction from January 1, 1901, to November 19, 2000. The time discretization of the recent period, 1995–2000, is much finer than the historical period, 1901–1994, to better simulate seasonal compaction and expansion and to better utilize measured data during the nonlinear regression. Stress periods and time steps for the historical period are 1 year and 1 month, respectively, and for the recent period are 50 days and 3 hours, respectively.

The Flow and Head Boundary package (Leake and Lilly, 1997) was used to specify heads in cells at the margins of aquifers. Those heads control all simulated ground-water flow, including the formation of nonlinear head gradients in the thick interbeds. The slow equilibration of heads in the thick interbeds relative to head changes in the surrounding aquifers results in residual compaction. The Interbed-Storage package (Leake and Prudic, 1991) was used to assign preconsolidation heads (based on computed water levels) and elastic and inelastic skeletal storage values and to track compaction and expansion caused by changes in storage. When the head in a cell is above the preconsolidation head, the elastic skeletal specific storage is assigned and the preconsolidation head remains unchanged. When the head in a cell drops below the preconsolidation head, the inelastic skeletal specific storage is assigned and the current head becomes the new preconsolidation head.

Nonlinear Regression

UCODE (Poeter and Hill, 1998) was used to apply nonlinear regression methods to calibrate the numerical model and estimate property values. UCODE ran the numerical model in an iterative fashion using a

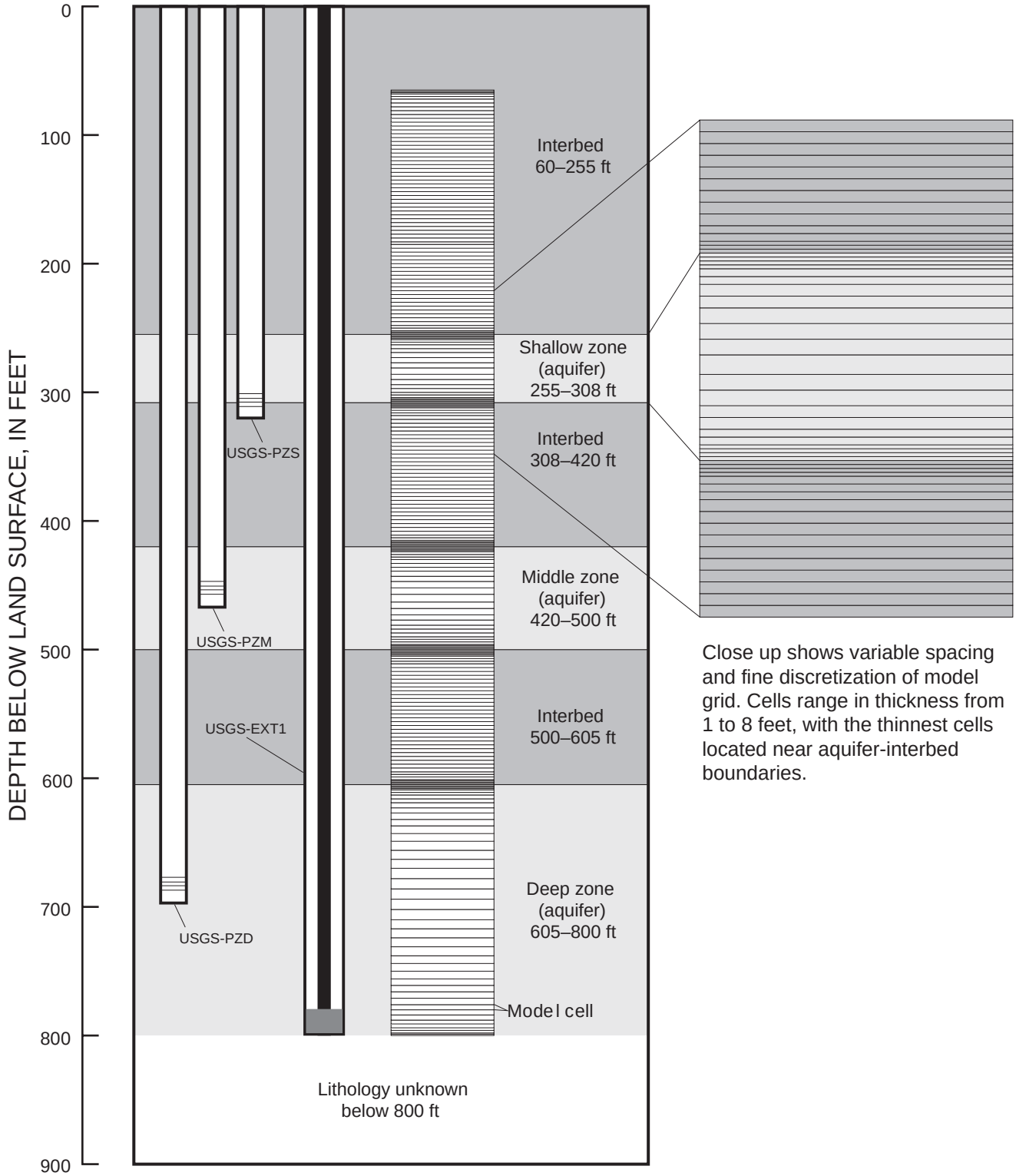

Figure 2. Schematic showing piezometer and extensometer depths, aquifer and interbed depths for the Lorenzi model grid, and a close up of the model cells.

modified Gauss-Newton method and systematically adjusted the estimated property values for each iteration. The results of each iteration were evaluated by UCODE to obtain the set of optimal property values with the minimum value of the objective function. The weighted least-squares objective function (S) used in UCODE is defined as:

$$S = \sum_{i=1}^{n} w_i [y_i - y'_i]^2, \quad (1)$$

where

n is the number of observation data values,
w_i is the i^{th} weight,
y_i is the i^{th} observation value, and
y'_i is the i^{th} simulated value.

The difference y_i - y'_i is the residual for the i^{th} observation.

For the historical period, 21 estimates of compaction derived from benchmark surveys (Malmberg, 1965; Mindling, 1971; Harrill, 1976; Bell, 1981b; Bell and Price, 1993; and Bell and others, 2000) were used as observation data. For the recent period, 72 extensometer measurements were used as observation data. The recent period observation data were short-term, seasonal, and long-term measurements, ranging from 25 days to 5.5 years. The extensometer observations are more accurate and more important to the regression than the estimated historical observations and, therefore, are more heavily weighted.

EVALUATIONS AND CONCLUSIONS

After the numerical model and UCODE were set up and the observation data and weights were determined, initial runs of UCODE were executed to evaluate the numerical model, the observation data, and the estimated property set. After the initial UCODE runs, the model fit was evaluated. For the purposes of this report, model and regression evaluation focus on the more accurately defined recent period, 1995–2000.

Composite scaled sensitivities (CSS) and parameter correlations computed for the initial UCODE runs were analyzed to determine whether the numerical model and observation data provided enough information to adequately estimate the selected properties (Hill, 1998). The CSS of an estimated parameter represents the change in model response to a change in property value and indicates the importance of all observation data to estimating the property value. The CSS values for the estimated properties of the Lorenzi model (table 1) indicate that the numerical model and observation data provided sufficient information to estimate the properties because the largest CSS value was less than 100 times the smallest CSS value (Hill, 1998).

Table 1. Composite scaled sensitivities and estimated values for the estimated properties of the Lorenzi model

[K'_v, vertical hydraulic conductivity of interbeds; S'_{skv}, inelastic skeletal specific storage of interbeds; S'_{ske}, elastic skeletal specific storage of interbeds; and S_{ske}, elastic skeletal specific storage of aquifers]

Property	Composite scaled sensitivity	Estimated value
K'_v	9	3×10^{-6} ft/d
S'_{skv}	33	4×10^{-5} ft^{-1}
S'_{ske}	6	5×10^{-6} ft^{-1}
S_{ske}	6	3×10^{-7} ft^{-1}

No parameters are correlated above 0.60, indicating that the model and observation data provide sufficient information to adequately estimate the parameter values and that the set of estimated values are unique.

The model fit was evaluated by comparing simulated and observed compaction data; the standard error of regression; and graphical analyses of weighted residuals. Compaction data simulated by the Lorenzi model compare well to observed data for the historical and recent periods (fig. 3).

The standard error of regression measures how well the simulated data match the observation data. If a model fit is consistent with the data accuracy, as indicated by the weighting, the expected value of the standard error is 1.0. The standard error of the Lorenzi regression is 0.36. Large deviations from 1.0 indicate that the fit may be inconsistent with the weighting. Standard error values less than 1.0 indicate that the regression fits observed data better than the weighting suggests, but do not indicate a lack of model error.

A plot of weighted residuals versus weighted simulated values should show points randomly distributed above and below zero (fig. 4), if the model reasonably fits observed data (Hill, 1998). Trends or grouping of points would indicate bias or systematic error in the model or field observations. A plot of weighted residuals versus time (fig. 5) also should show points

randomly distributed above and below zero (Hill, 1998). A discernible temporal trend would indicate temporal bias in observed data or the model regression was not an adequate fit.

Once the model fit was considered acceptable, the optimal property estimates (table 1) were analyzed. The accuracy of the estimated values is implied in the model fit to observed data, which is good, and can be further assessed by comparisons to values of other studies in similar settings (Tiedeman and others, 1998). The values estimated by this model are all within ranges estimated by previous studies of unconsolidated aquifer systems in arid environments (Riley, 1969; Hanson, 1989; Waichler and Cochran, 1993; Heywood, 1995; Morgan and Dettinger, 1996; and Sneed and Galloway, 2000). Together, the good model fit, lack of correlated parameters, and similarity to other reasonable estimates indicate that the property estimates for the Lorenzi site are accurate and unique.

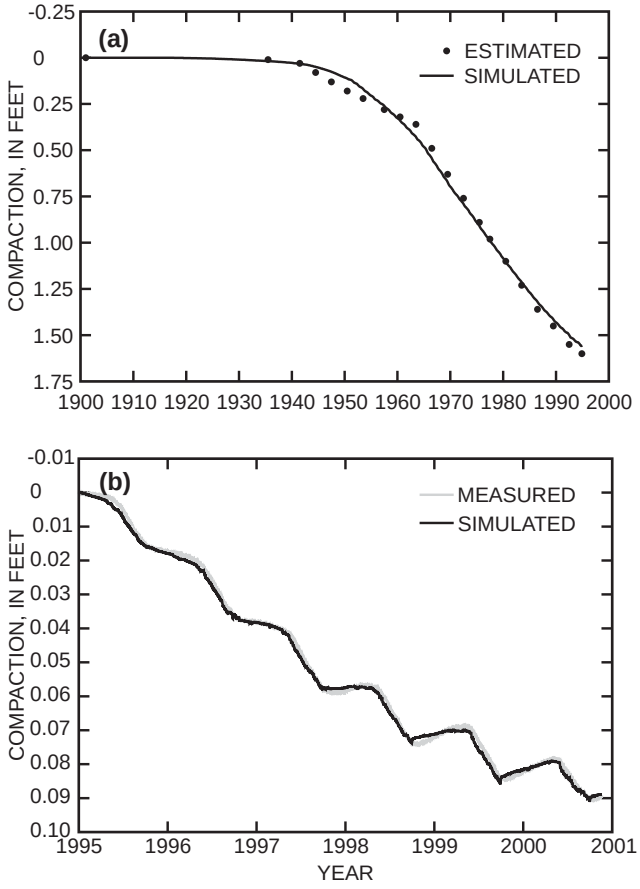

Figure 3. Estimated, measured, and simulated compaction at the Lorenzi site for (a) the historical period, 1901–94, and (b) the recent period, 1995–2000.

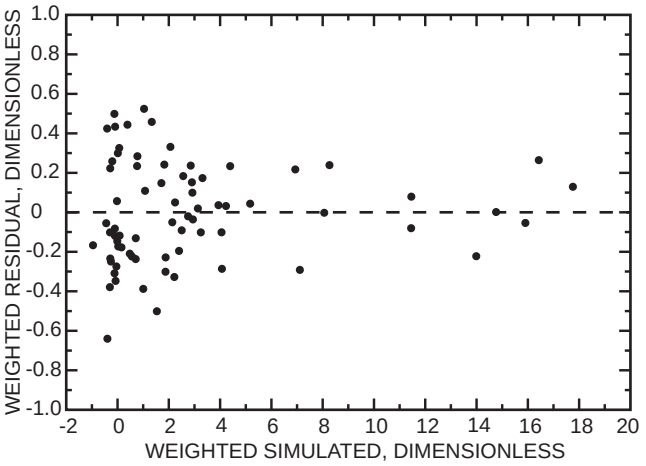

Figure 4. Weighted simulated versus weighted residual values for the recent period, 1995–2000, of the Lorenzi model.

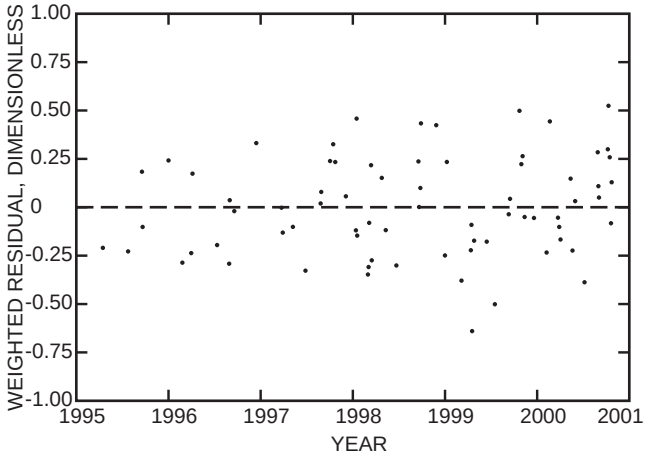

Figure 5. Temporal distribution of weighted residuals for the recent period, 1995–2000, of the Lorenzi model.

Sea-Level Rise and Subsidence: Implications for Flooding in New Orleans, Louisiana

By Virginia R. Burkett[1], David B. Zilkoski[2], *and* David A. Hart[3]

Abstract

Global sea-level rise is projected to accelerate two- to four-fold during the next century, increasing storm surge and shoreline retreat along low-lying, unconsolidated coastal margins. The Mississippi River Deltaic Plain in southeastern Louisiana is particularly vulnerable to erosion and inundation due to the rapid deterioration of coastal barriers combined with relatively high rates of land subsidence. Land-surface altitude data collected in the leveed areas of the New Orleans metropolitan region during five survey epochs between 1951 and 1995 indicated mean annual subsidence of 5 millimeters per year. Preliminary results of other studies detecting the regional movement of the north-central Gulf Coast indicate that the rate may be as much as 1 centimeter per year. Considering the rate of subsidence and the mid-range estimate of sea-level rise during the next 100 years (480 millimeters), the areas of New Orleans and vicinity that are presently 1.5 to 3 meters below mean sea level will likely be 2.5 to 4.0 meters or more below mean sea level by 2100.

Subsidence of the land surface in the New Orleans region is also attributed to the drainage and oxidation of organic soils, aquifer-system compaction related to ground-water withdrawals, natural compaction and dewatering of surficial sediments, and tectonic activity (geosynclinal downwarping and movement along growth faults). The problem is aggravated owing to flood-protection measures and disruption of natural drainageways that reduce sediment deposition in the New Orleans area.

Accelerated sea-level rise, the present altitude of the city, and high rates of land subsidence portend serious losses in property in the New Orleans area unless flood-control levees and pumping stations are upgraded. The restoration and maintenance of barrier islands and wetlands that flank New Orleans to the south and east are other adaptations that have the potential to reduce the loss of life and property due to flooding. Accurate monitoring of subsidence is needed to provide calibration data for modeling and predicting subsidence in coastal Louisiana, as well as for support for constructing and maintaining infrastructure and levees. GPS technology is being tested in the New Orleans region as a means for more frequent, less expensive subsidence monitoring.

INTRODUCTION

Accelerated sea-level rise is regarded as one of the most costly and most certain consequences of global warming. If sea-level rise increases at rates projected by the United Nation's Intergovernmental Panel on Climate Change (2001) during the next century, many of the world's low-lying coastal zones and river deltas could be inundated. Several of the world's most heavily populated coastal cities are particularly vulnerable to inundation due to human interactions with deltaic processes. Such is the case in the New Orleans metropolitan area, where more than 1 million people are protected from river floods and storm surge by levees and pumping stations, and where the land is gradually sinking at rates that exceed 20th century sea-level rise.

GEOMORPHOLOGIC SETTING

Most of the present landmass of southeast Louisiana was formed by deltaic processes of the Mississippi River. Over the past 7,000 years, during a period of relatively small fluctuations in sea level, the river deposited massive volumes of sediment in five deltaic

[1] U.S. Geological Survey, Lafayette, La.
[2] National Oceanic and Atmospheric Administration, National Geodetic Survey, Silver Spring, Md.
[3] University of Wisconsin, Madison, Wis.

complexes that now lie in various stages of abandonment (, 1967). The Chandeleur Island chain that lies to the southeast of the city of New Orleans is an erosional feature of one of these ancient deltas. A combination of levees, diversion structures, and reduced suspended sediment discharge have essentially halted the aggradation of the Mississippi River delta in southeast Louisiana.

Levees constructed along the banks of the Mississippi River from Cairo, Ill., to Venice, La., (about 30 km south of New Orleans) prevent the flooding of the adjacent land by sediment-laden river water, halting the depositional processes that naturally maintained the altitude of the land surface in southeast Louisiana above sea level. Three large diversion structures constructed upriver near Simmesport, La., now route up to one-third of the water and sediment load from the Mississippi River westward into the Atchafalaya River to protect New Orleans, Baton Rouge, and many other cities in southeast Louisiana from flooding. The volume of sediment delivered by the Mississippi River to Louisiana has been reduced by almost one-half since 1950 by the construction of reservoirs on the major tributaries of the Mississippi River (Meade, 1995).

Most of the land surface of the New Orleans Metropolitan Statistical Area (MSA), a region that includes all or parts of seven parishes, is sinking or "subsiding" relative to mean sea level. Subsidence of the land surface in the New Orleans region is also attributed to the drainage and oxidation of organic soils (Earle, 1975), aquifer-system compaction related to ground-water withdrawals (Kazmann, 1988), natural compaction and dewatering of surficial sediments (Gosselink, 1984), and tectonic activity (geosynclinal downwarping and movement along growth faults) (Howell, 1960; Jones, 1975).

SUBSIDENCE AND SEA-LEVEL TRENDS

Observations of local subsidence in the New Orleans region were derived from precise leveling data collected by the National Geodetic Survey (NGS) during 1951–55, 1964, 1984–85, 1990–91, and 1995. The subsidence network included a total of 341 benchmarks. Land-surface altitude data sets for each epoch (time period between surveys) were prepared using a minimum constraint least squares adjustment tied to a benchmark in eastern Orleans Parish (Zilkoski and Reese, 1986). Files containing the location of benchmarks and the differences in adjusted heights were converted into ArcView shapefiles and projected into Louisiana State Plane Coordinates, South Zone NAD83, in feet. The annual rate of subsidence at each benchmark was determined by dividing the differences in adjusted heights by the number of years between leveling.

Benchmark locations were integrated with generalized maps of soils and geology covering parts of Orleans Parish, which lies at the center of the New Orleans MSA. It is important to note that the soil and geology data sets were digitized from small-scale, paper, photocopied maps to test the initial concepts of using GIS to support development of a subsidence model (Hart and Zilkoski, 1994). The source of the geology map is "Geology of Greater New Orleans—Its Relationship to Land Subsidence and Flooding" by Snowden and others (1980), and the source of the soils map is the "Soil Survey of Orleans Parish, Louisiana" by the Soil Conservation Service (Trahan, 1989).

Figure 1 shows subsidence rates for 165 benchmarks that were consistently surveyed during the period from 1951 to 1995. Table 1 shows the number of benchmarks surveyed, mean annual subsidence rate, and standard deviation for soils and geologic units for each of the four epochs identified above. The average rate of subsidence among soil types was between 4.0 and 6.0 mm/yr for all but the Aquents soil classification, which makes up about 13 percent of the land area in the Parish (Trahan, 1989). There appears to be a noticeable decrease through time in the mean subsidence rate for the Clovelly-Lafitte-Gentilly soil classification as compared to the others. Also, the overall mean subsidence rate for all soil types increases from the 1951–64 epoch to the 1964–85 and 1985–91 epochs, and then apparent rebound is seen during the 1991–95 epoch. Precipitation was very heavy in the New Orleans region during 1991, which may be related to the apparent high rates of subsidence during 1985–91. Additional correlations may exist between land subsidence and other, more detailed and accurate soil and geology data sets, as well as other environmental factors that may have an effect on subsidence. These other environmental factors include drainage infrastructure, levee locations, drainage pumping-station operations, well locations and withdrawals, ground-water recharge, application of fill and overburden, land use, the history of human settlement and urban development, and the bulk and density of buildings.

The 1951–95 altitude data also showed some interesting differences among survey epochs and

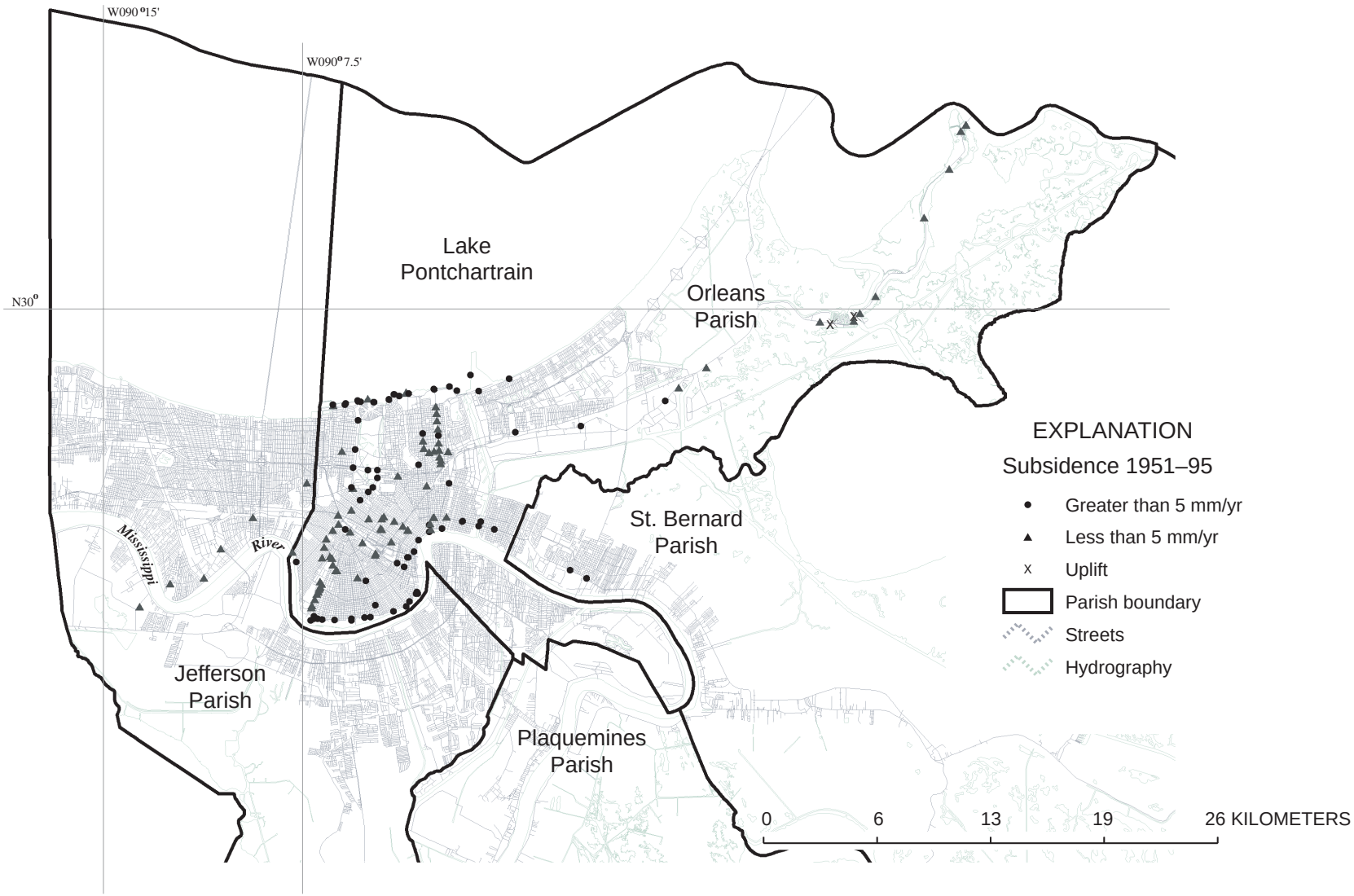

Figure 1. Mean annual local subsidence rates for five soil types and the four major geologic units in the New Orleans region.

Table 1. Mean annual subsidence rates for five soil types and the four major geologic units in the New Orleans region, 1951–95

[mm/yr, millimeters per year; mm, millimeters]

Soil type	1951–64			1964–85			1985–91			1991–95			1951–95		
	Number of benchmarks	Average annual difference (mm/yr)	Std. dev. (mm)	Number of benchmarks	Average annual difference (mm/yr)	Std. dev. (mm)	Number of benchmarks	Average annual difference (mm/yr)	Std. dev. (mm)	Number of benchmarks	Average annual difference (mm/yr)	Std. dev. (mm)	Number of benchmarks	Average annual difference (mm/yr)	Std. dev. (mm)
Sharkey-Commerce	161	-5.0	4.7	130	-6.4	3.8	176	-8.5	2.4	187	3.9	2.2	87	-4.8	2.8
Clovelly-Lafitte-Gentilly	13	-3.0	1.7	12	-2.2	1.9	17	-1.8	1.8	19	.6	2.3	8	-1.3	.8
Harahan-Westwego	36	-3.3	4.3	33	-3.3	9.2	58	-9.3	5.4	65	2.3	6.7	16	-4.0	3.2
Alemmands, drained—Kenner, drained	14	-5.5	4.3	10	-8.1	5.4	17	-8.5	2.7	17	2.1	4.3	4	-4.0	2.4
Aquents	56	-3.9	3.9	49	-9.4	4.8	66	-9.2	3.2	74	.8	3.3	33	-5.9	2.6
Total	280	-4.5	4.4	234	-6.5	5.4	334	-8.4	3.6	362	2.7	3.9	148	-4.8	2.9

Geologic unit	1951–64			1964–85			1985–91			1991–95			1951–95		
	Number of benchmarks	Average annual difference (mm/yr)	Std. dev. (mm)	Number of benchmarks	Average annual difference (mm/yr)	Std. dev. (mm)	Number of benchmarks	Average annual difference (mm/yr)	Std. dev. (mm)	Number of benchmarks	Average annual difference (mm/yr)	Std. dev. (mm)	Number of benchmarks	Average annual difference (mm/yr)	Std. dev. (mm)
Artificial fill	28	-4.8	2.1	26	-10.6	3.5	30	-9.7	1.1	30	2.2	1.8	20	-6.5	1.6
Alluvial soils	63	-3.9	3.4	56	-5.7	7.2	86	-8.6	2.4	98	2.5	5.6	36	-4.6	2.4
Lake fringe deposits	7	-8.1	8.3	3	-13.6	.4	6	-9.5	2.2	7	.5	2.7	3	-9.1	.7
Natural levee deposits	166	-5.6	5.1	124	-6.4	4.5	158	-9.2	3.6	171	4.1	2.4	73	-4.9	3.0
Total	264	-5.2	4.7	209	-6.8	5.5	280	-9.1	3.1	306	3.3	3.8	132	-5.2	2.8

geologic units (table 1). Mean annual subsidence in levee deposits, alluvial soils, artificial fill, and lake fringe deposits ranged from 4.6 to 9.1 mm/yr. It should be noted that one recent analysis of NGS Gulf Coast elevation data by Louisiana State University and NGS (Roy Dokka, Louisiana State University, oral commun., 2003) suggests that the absolute subsidence rates for the New Orleans region could be about 5 mm/yr or higher, but the relative differences would be the same. Relative differences in subsidence rates among the four survey epochs might be explained by a more thorough examination of rainfall data, ground-water extraction and recharge, land-use change, and other factors mentioned previously.

Global sea level has risen about 120 m as a result of melting of large ice sheets since the last glacial maximum about 20,000 years ago (Fairbanks, 1989). The most rapid rise occurred during the late and post-glacial periods followed by a period of relatively stable sea level during the past 6,000 years (Mimura and Harasawa, 2000). During the past 3,000 years, sea level rose at an average rate of about 0.1 to 0.2 mm/yr, but by the end of the 20th century the rate had increased to approximately 1.0 to 2.0 mm/yr or 100 to 200 mm per century (Gornitz, 1995; Intergovernmental Panel on Climate Change, 1996). The Intergovernmental Panel on Climate Change (2001) projects a two- to four-fold acceleration of sea-level rise over the next 100 years, with a central value of 480 mm.

The rate of land subsidence in the New Orleans region (average 5 mm/yr) and the Intergovernmental Panel on Climate Change (2001) mid-range estimate of sea-level rise (480 mm) suggests a net 1.0-m decline in elevation during the next 100 years relative to present mean sea level (fig. 2). A storm surge from a Category 3 hurricane (estimated at 3 to 4 m without waves) (National Oceanic and Atmospheric Administration, 2002) at the end of this century, combined with mean global sea-level rise and land subsidence, would place storm surge at 4 to 5 m above the city's present altitude. The effect of such a storm on flooding in the New Orleans MSA will depend upon the height and integrity of the regional levees and other flood-protection projects at that time.

An additional factor to be considered when evaluating the future vulnerability of New Orleans to inundation is the current altitude of the land surface. Much of the heavily populated area in Orleans and St. Bernard Parishes lies below mean sea level. At the intersection of Morrison Road and Blueridge Court (located in lake fringe deposits of eastern Orleans Parish), for example, which is presently about 2.6 m below local mean sea level, the cumulative effects of land subsidence, sea-level rise, and storm surge from a Category 3 hurricane at the end of this century place storm surge 6 to 7 m above the land surface (fig. 2). Such a storm would exceed the design capacity of the existing flood-protection levees. The storm surge of a Category 5 hurricane, generally greater than 5 m (National Oceanic and Atmospheric Administration, 2002), would pose more serious flooding danger. Hurricane Camille, a Category 5 hurricane that made landfall in Mississippi in 1969, increased water levels in coastal Mississippi by as much as 7 m (U.S. Army Corps of Engineers, 1970). Landfall of a Category 5 hurricane in New Orleans would place the Morrison Road/Blueridge Court intersection at least 9 m below storm-surge level today and, based on the same sea-level rise and land-subsidence trends discussed above, at 10.5 m or more below storm-surge level by the end of the 21st century.

In addition to the decline in land-surface altitude, the loss of marshes and barrier islands that dampen storm surge and waves during hurricanes increases the risks of flood disaster in New Orleans and vicinity. Since 1940, approximately 1 million acres of coastal wetlands have been converted to open water in southern Louisiana as a result of natural and human-induced environmental change (Burkett and others, 2001). The extensive loss of coastal marshes and bald cypress forests that once flanked the hurricane-protection levees of St. Bernard and Plaquemines Parishes has increased the threat of storm-surge flooding for the 94,000 residents in the southern part of the New Orleans MSA. Several barrier island and wetland restoration projects are planned by the State of Louisiana, local governments, and Federal agencies.

ADAPTATIONS THAT MINIMIZE FLOODING

Most of the New Orleans MSA is protected from flooding by levees constructed since 1879 by local sponsors and the U.S. Army Corps of Engineers under five different Congressional authorizations. Levee design heights range from about 4.5 to 6 m above mean sea level. The levees along the Lake Pontchartrain shoreline are designed at a height that exceeds the surge and waves of a Category 3 hurricane. The levee design criteria assume no increase in mean sea level and no subsidence (Alfred C. Naomi, U.S. Army Corps of Engineers, oral commun., 2001). The city of New

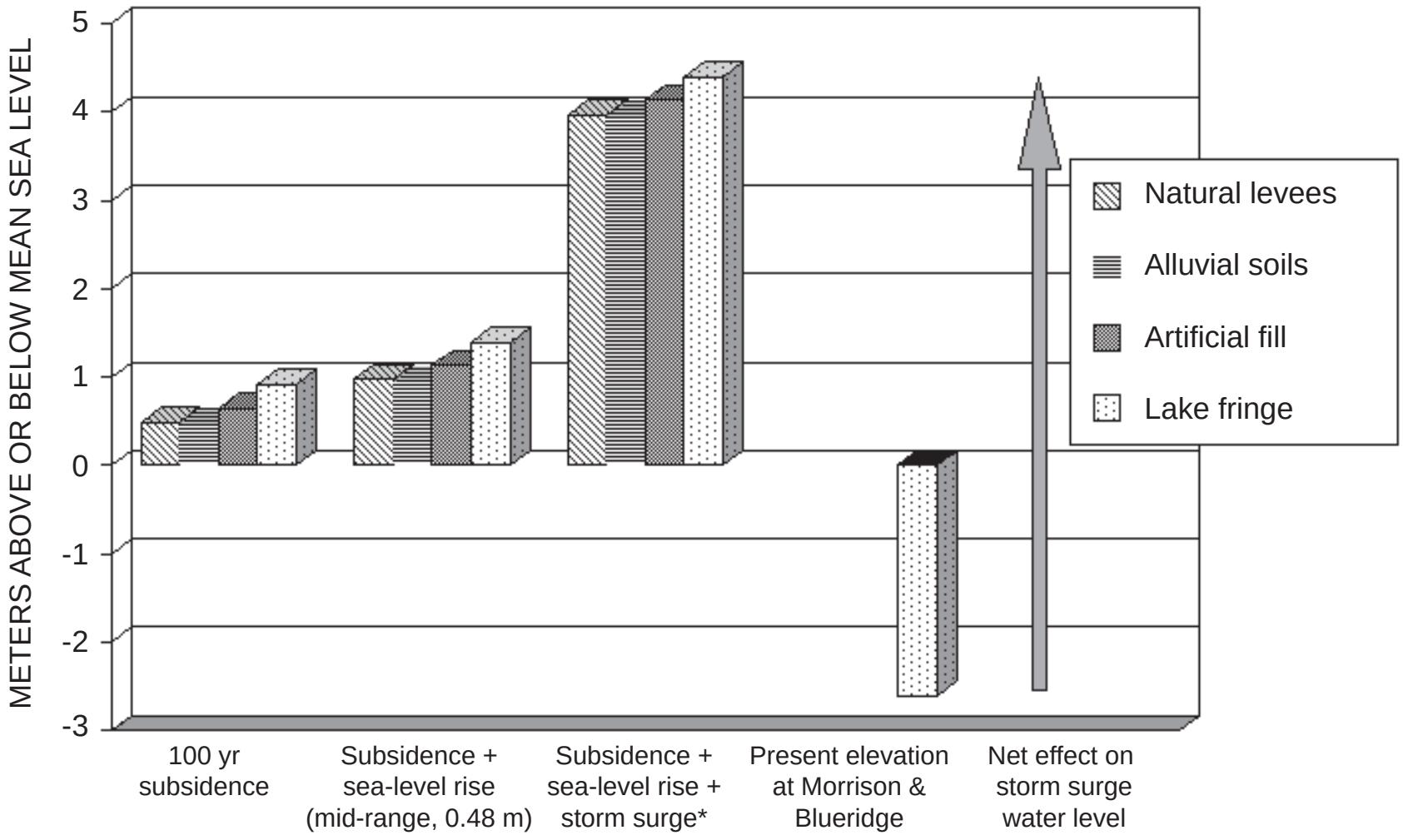

Figure 2. Local subsidence and sea-level projections for New Orleans and vicinity through 2100. Arrow on right represents the cumulative influence of land-surface elevation change and sea-level rise on storm-surge level *(Category 3 hurricane) at the Morrison Road/Blueridge Court intersection, which is presently about 2.6 m below mean sea level.

Orleans is drained by an extensive network of drainage canals (108 km of surface and subsurface canals) with 22 pumping stations. Most of the stormwater drainage is pumped over the flood-protection levees into Lake Pontchartrain (Sewerage and Water Board of New Orleans, 2001).

The following adaptation strategies would aid in reducing, but not eliminate, the vulnerability of the New Orleans MSA to flood disaster:

1. Upgrade levees and drainage systems to withstand Category 4 and 5 hurricanes.
2. Design and maintain flood protection on the basis of historical and projected rates of local subsidence, rainfall, and sea-level rise.
3. Minimize drain-and-fill activities, shallow subsurface fluid withdrawals, and other human developments that enhance subsidence.
4. Improve evacuation routes.
5. Protect and restore coastal defenses.
6. Encourage flood proofing of buildings and infrastructure.
7. Develop flood-potential maps that integrate local elevations, subsidence rates, and drainage capabilities (for use in the design of ordinances, greenbelts, and other flood-damage reduction measures).

GPS SOLUTIONS FOR MONITORING SUBSIDENCE IN LOUISIANA

Accurate monitoring of land subsidence over time is vital to providing data for calibrating models of land subsidence and predicting subsidence, as well as providing information for planning, constructing, and maintaining infrastructure and levees. Historically, geodetic differential leveling has been used to measure subsidence in the New Orleans MSA; it was very accurate but also very expensive. Over the past decade, GPS surveying techniques have proven to be so efficient and accurate that they are now routinely used in place of classical line-of-sight surveying methods for establishing horizontal control. Understandably, interest has also been growing in using GPS techniques to establish accurate vertical control. Progress, however, has been hampered due to difficulties in obtaining sufficiently accurate geoid height differences to convert GPS-derived ellipsoid height differences to accurate orthometric height differences.

These factors have recently been resolved, making GPS-derived orthometric heights a viable alternative to classical line-of-sight geodetic differential leveling techniques for many applications. Additional information is available at the following web sites on the topics of

- completion of the general adjustment of NAVD 88 (http://www.ngs.noaa.gov/PUBS_LIB/NAVD88/navd88report.htm),
- development of NGS guidelines for establishing GPS-derived ellipsoid heights to meet 2- and 5-cm standards (http://www.ngs.noaa.gov/PUBS_LIB/NGS-58.html), and
- computation of an accurate, nationwide, high-resolution geoid model, GEOID99 (http://www.ngs.noaa.gov/GEOID/).

A cooperative study between the Harris-Galveston Coastal Subsidence District (HGCSD) and the NGS is using GPS methods to measure subsidence at a fraction of the cost of the previous method. Due to the magnitude of subsidence in the Houston-Galveston region of southeastern Texas, there are no stable benchmarks in the area. Therefore, stable borehole extensometers were equipped with GPS antennas to provide a reference frame to measure subsidence at other stations in the area. These stations are known as local GPS Continuously Operating Reference Stations (CORS).

The NGS/HGCSD project uses dual-frequency, full-wavelength GPS instruments and geodetic antennas. Data are collected at 30-second sampling intervals and averaged over long periods, generally 24 hours. The goal is to yield differential vertical accuracy of less than 10 mm in a totally automated mode operated by HGCSD personnel. Data have now been collected from the three CORS sites and four portable GPS measuring stations called Port-A-Measures (PAMS), at 20 sites, for more than 4 years in the Houston-Galveston region. Results between CORS and PAMS indicate that some geodetic monuments are subsiding as much as 70 mm/yr and correlate well with extensometer data. The joint NGS/HGCSD GPS subsidence project is described in more detail by Zilkoski and others (p. 13 of these proceedings).

Louisiana's greatest environmental problem is the continuing loss of its coast. To address these problems, NGS in partnership with Louisiana State University

through a newly created Louisiana Spatial Reference Center (LSRC) is building a statewide network of GPS CORS similar to the HGCSD network. Like the HGCSD network, the LSRC GPS CORS will be referenced to the National Oceanic and Atmospheric Administration (NOAA) national CORS. The national GPS CORS will provide the framework for the LSRC CORS to measure yearly subsidence rates at the 10-mm level. In addition to the continuously operating GPS CORS and PAMS, specially designed GPS network surveys adhering to NGS guidelines will be performed to estimate the subsidence in local areas.

CONCLUSIONS

Increases in mean sea level, coupled with the current low altitude of the land surface and land-subsidence trends in the region, portend serious losses of life and property in the New Orleans MSA unless flood-control levees and drainage systems are upgraded. The maintenance of barrier islands and wetlands that flank New Orleans to the south, west, and east is another adaptation that will likely minimize the potential loss of life and property due to flooding. The changes in sea level that are predicted to accompany increasing global temperature are statistically and practically significant to those responsible for designing flood-control works and coastal protection strategies for New Orleans, Houston, Amsterdam, and other rapidly subsiding coastal areas. The application of GPS technology for determining orthometric height differences should enhance the utility and cost effectiveness of land-subsidence monitoring in flood-protection design.

Simulation of Land Subsidence in a Glacial Aquifer System Above a Salt Mine Collapse Redux: A Post Audit

By Richard M. Yager[1]

Abstract

The bedrock ceiling in parts of the Retsof salt mine in the Genesee Valley in western New York collapsed in March and April 1994, and water from overlying glacial aquifers began to flow into the mine at rates of as much as 1,300 liters per second. Water-level declines within the aquifer system and the accompanying increase in effective stress caused compaction of fine-grained sediments in two confining units. By February 1996, as much as 24 centimeters of land subsidence was measured 1 kilometer south of the mine.

One-dimensional, transient simulations were conducted with MODFLOW and the IBS1 package to represent vertical fluid flow and sediment compaction in the confining units at two locations—one near a borehole instrumented with pressure transducers and a second at a survey monument. Vertical hydraulic conductivity and skeletal specific storage of the confining units were estimated through nonlinear regression from observations of pore-fluid pressure and subsidence. Computed fluid-pressure changes were in close agreement with measured pressures, and the maximum computed subsidence at the survey monument was about 6 percent less than that observed. About 92 percent of the computed subsidence was the result of compaction in the lower confining unit, of which 90 percent was attributed to inelastic compaction.

Estimated values of vertical hydraulic conductivity and specific storage of confining-unit sediments were incorporated into a three-dimensional, ground-water-flow model calibrated with MODFLOWP to measured water-level declines in wells and estimated ground-water discharges to the salt mine. The computed subsidence in February 1996 along a survey transect compared favorably with the measured subsidence. As much as 3 centimeters of the simulated subsidence had occurred by February 1996 over a 41-square-kilometer area that extended 8 kilometers north and 11 kilometers south of the collapse area.

Measurements of fluid pressure and subsidence recorded from 1998 to 2001 indicate that the one-dimensional models simulate fluid-pressure changes and land surface recovery quite well, despite this relatively simple characterization of the complex aquifer system.

INTRODUCTION

The 1994 collapse and flooding of a salt mine near Retsof, N.Y. (fig. 1), caused land subsidence resulting from both collapses (March and April 1994) into the mined cavity and the rapid compaction of sediments in the overlying aquifer system in response to water-level drawdown. The salt mine, which had been in operation since 1885, was sealed after the mine became completely flooded in January 1996. Subsidence rates more than 15 cm/yr during a 20-month period were attributed to sediment compaction, comparable to subsidence rates within pumped aquifer systems measured over several decades in Houston, Tex. (10 cm/yr; Holzer, 1984) and the San Joaquin Valley, Calif. (20 cm/yr; Poland and others, 1975). Comprehensive monitoring of this catastrophic event provided a unique opportunity to simulate the response of an aquifer system to rapid drawdowns initiated by a mine collapse and thereby estimate the mechanical and hydraulic properties of overlying aquifers and confining units.

[1] U.S. Geological Survey, Ithaca, N.Y.

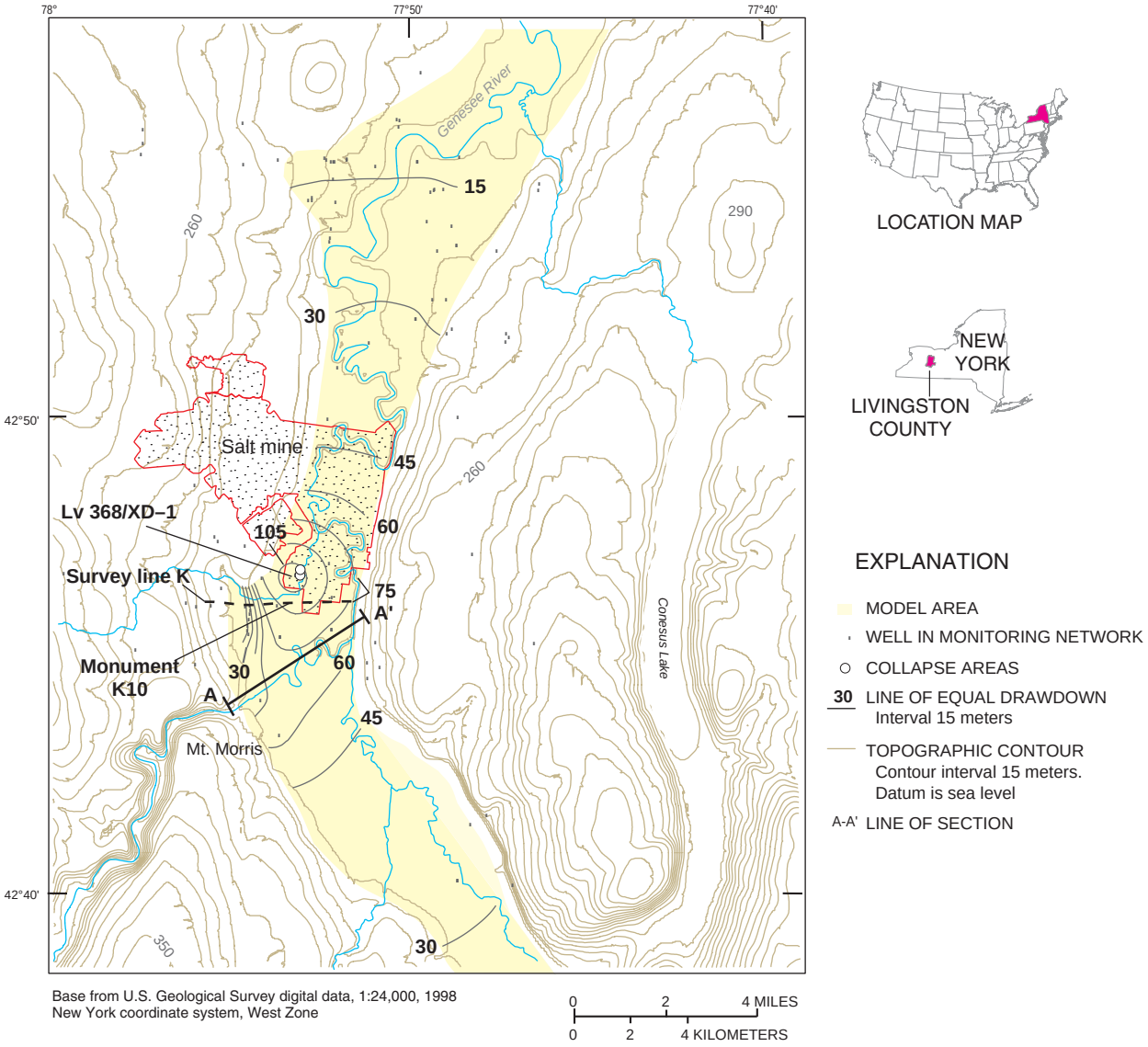

Figure 1. Extent of mined area, site of collapse, and distribution of drawdown in lower aquifer in January 1996 in response to mine flooding.

HYDROGEOLOGIC SETTING

The glacial aquifer system within the Genesee Valley consists of three aquifers separated by two confining units and underlain by water-bearing zones in bedrock (fig. 2). The glacial aquifers are hydraulically connected at the edges of the confining units near the bedrock valley walls. The uppermost (unconfined) aquifer consists of alluvial sediments 6 to 18 m thick; a middle confined aquifer consists of glaciofluvial sand and gravel 3 to 5 m thick, and a lower aquifer consists of glaciofluvial sand and gravel about 7.5 m thick overlying the bedrock valley floor. The upper and middle aquifers are separated by an upper confining unit of lacustrine sediments and till as much as 75 m thick, and the middle and lower aquifers are separated by a lower confining unit of undifferentiated glaciolacustrine sediments as much as 75 m thick.

EFFECTS OF MINE COLLAPSE

The effects of the mine collapse and subsequent flooding included (1) land subsidence, (2) severe water-level declines, (3) changes in ground-water quality, and (4) exsolution of natural gas. The effects of the mine

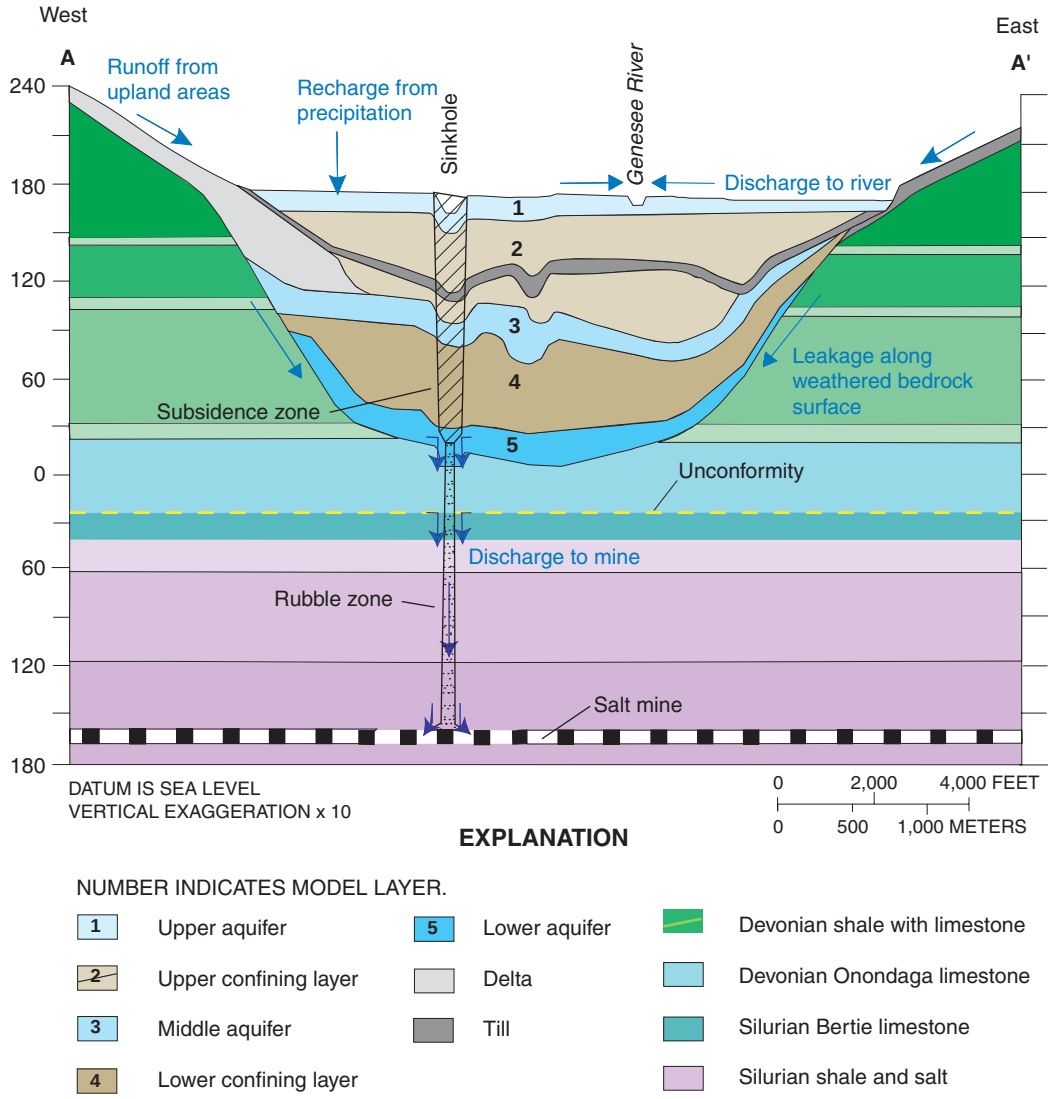

Figure 2. Generalized section showing aquifers and confining units in the Genesee Valley (line of section shown in fig. 1).

collapse on the aquifer system are described in Yager and others (2001). Possible causes and effects of the collapses are discussed in Nieto and Young (1998) and Gowan and others (1999).

The collapses in the mine allowed water to cascade into the mine from the lower aquifer at the bedrock surface, which is 150 m lower than water levels at the north (downgradient) end of the Genesee Valley. Water levels in the lower aquifer had dropped as much as 120 m by January 1996 when the mine was completely flooded, and several wells screened in the middle aquifer went dry. Drawdowns of 15 to 40 m were recorded at wells 10 km north and south of the collapse area (fig. 1). Water levels in the collapse area had recovered 90 m (75 percent) about 2 years after drainage to the mine had ceased.

Collapse of the overlying rock and sediment propagated from the mine to land surface, leaving two 90-m-diameter sinkholes (fig. 1) as much as 21 m deep that damaged nearby structures. Subsidence ranged from 24 cm or less south of the mined area to as much 5 m over the uncollapsed mined area. The subsidence south of the mine is attributed to compaction of fine-grained sediments in the confining units, although most of the subsidence over the mine was caused by closure of the mine cavity, a process that was accelerated by the dissolution of the salt pillars by water that flooded the mine.

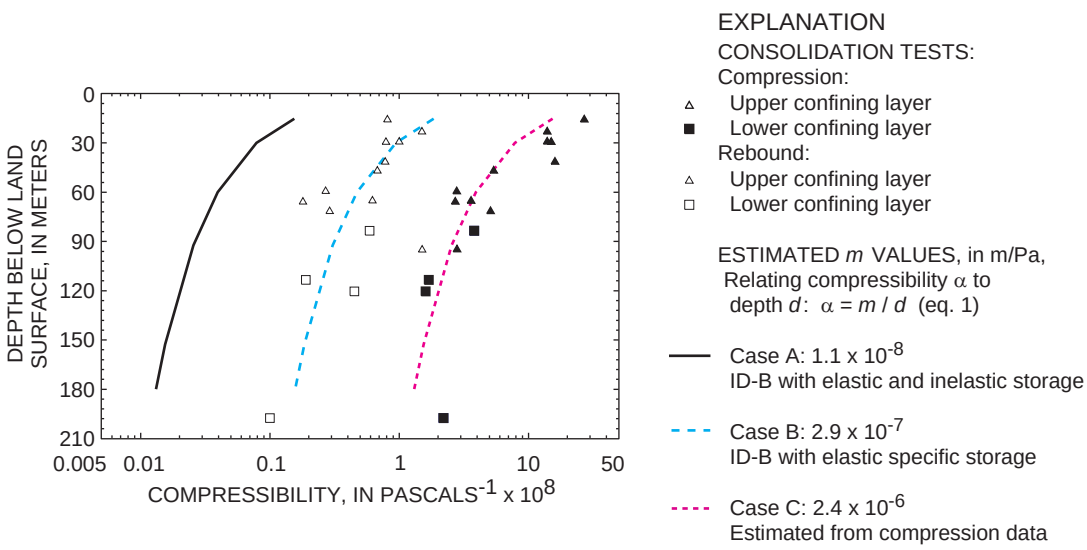

Figure 3. Relation of compressibility to depth as derived from consolidation curves of confining-unit sediments in Genesee Valley aquifer system.

Consolidation curves for lower confining-unit sediments indicated that the stress resulting from water-level declines after the mine collapse corresponded to the transition from the elastic to the inelastic stress range (Yager and others, 2001). The increased stress in the upper confining unit was not much greater than the ambient stress because less drawdown occurred in the upper confining unit. Compressibility of confining-unit sediments under ambient stress was computed from consolidation curves for 15 samples of confining-unit sediments (Alpha Geoscience, 1996) (fig. 3). Compressibility generally declined with increasing effective stress at increasing burial depths, as expected from empirical relations given in Neuzil (1986). The relation of compressibility, α, to depth, d, is

$$\alpha = \frac{m}{d}, \qquad (1)$$

where

m = constant (meters per Pascal).

An m value of 2.4×10^{-6} m/Pa gives the compressibility values computed from consolidation curves during compression with a correlation coefficient (r^2) of 0.94 (fig. 3, case C).

SIMULATION OF GROUND-WATER FLOW

Ground-water flow within the aquifer system was simulated using a three-dimensional (3D) model using MODFLOWP (Hill, 1992) to represent flow conditions before and after the mine collapse (Yager and others, 2001). Hydraulic heads computed by steady-state simulation representing conditions prior to the mine collapse provided initial conditions for a transient-state simulation representing drainage from the aquifer system to the mine (March 1994 through December 1995) and recovery of water levels after the mine completely flooded (January 1996 through August 1996).

Model Design and Calibration

The three aquifers and two confining units within the aquifer system (fig. 2) were represented by five model layers. Recharge to the unconfined aquifer (model layer 1) was represented by a constant-flux boundary at land surface with larger rates specified along valley walls to account for recharge from upland runoff. The contact between the aquifer system and the shale bedrock at the valley wall was represented by a no-flow boundary. Vertical leakage through permeable deposits and (or) bedrock fractures along the valley wall was represented by hydraulic connections between adjacent model layers.

In transient-state simulations, constant-head boundaries were specified at the two collapse sites in the lower aquifer (model layer 5) to represent drainage from the aquifer system to the mine from March 1994 through December 1995. Six parameters were estimated

through transient-state simulations from 354 water-level measurements recorded in 51 wells and two estimates of ground-water discharge to the mine in March and September 1994 (table 1).

Simulated Response of Aquifers

The computed distribution of drawdown in January 1996 was similar to the measured distribution; the standard error in heads was 10 m. Computed drawdowns near the collapse area (123 m) were overpredicted by less than 3 m, and the predicted change in drawdown with time was in close agreement with measured drawdowns at individual wells (fig. 4). Drawdowns 10 km to the north (10 m) and 12 km to the south (15 m) were generally underpredicted by about 5 m and 18 m, respectively.

Computed discharges to the mine in April 1994 (570 L/s) were 100 percent greater than the values estimated from the observed rate of mine flooding, and computed discharges to the mine in September 1994 (790 L/s) were 40 percent less than the estimated values. The computed water budget indicated that ground water released from storage provided 73 percent of the water discharged to the mine, and that most of the inflow was from storage in the lower aquifer (58 percent), with releases from storage in confining units contributing less than 10 percent of the total.

Values of specific storage, S_s, estimated for the middle and lower aquifers (2.3 X 10^{-4} m^{-1} and 9.5 X 10^{-4} m^{-1}, respectively) were much larger than the range of values (2.3 X 10^{-6} m^{-1} to 7 X 10^{-6} m^{-1}) estimated for other sand and gravel aquifers from borehole extensometer data (Riley, 1998). (Specific storage consists of two summed components owing to the compressibility of the fluids (water or gas) and the compressibility of the skeleton or matrix of the aquifer-system sediments.) Assigning a lower value of specific storage greatly increased model error (fig. 4), however, and no combination of the remaining parameter values was found through nonlinear regression that provided an acceptable match to the measured water levels. The larger values of specific storage estimated by the regression

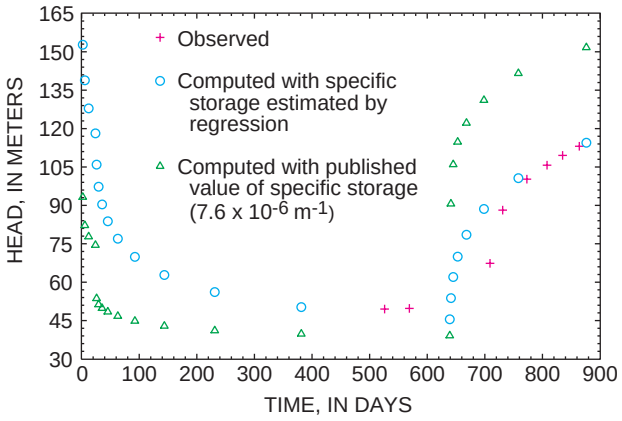

Figure 4. Water levels predicted from two alternative values of S_s and measured in the lower aquifer at well Lv368 near the collapse area.

Table 1. Optimum parameter values estimated for confined aquifer system (model layers 2 through 5) through nonlinear regression in transient-state simulation and their approximate confidence intervals at 95-percent level

[m/d, meters per day; m^{-1}, 1/meter]

Variable	Value	Approximate individual confidence interval	Coefficient of variation (percent)[1]
Hydraulic conductivity, m/d			
Middle aquifer	1.1	0.4–3.4	30
Lower aquifer	91	55–150	26
Vertical hydraulic conductivity of lower confining layer, m/d			
Collapse area	8 X 10^{-3}	7 X 10^{-5} – .94	37
Remainder of layer	3.7 X 10^{-4}	.2 X 10^{-4} – 9.7 X 10^{-4}	4
Specific storage, m^{-1}			
Middle aquifer	2.3 X 10^{-4}	4.3 X 10^{-5} – 1.2 X 10^{-3}	5
Lower aquifer	9.5 X 10^{-4}	4.6 X 10^{-4} – 2.0 X 10^{-3}	3

[1] Coefficient of variation on log-transformed parameter.

Table 2. Parameter values estimated for confining layers in one-dimensional models 1D–A (borehole XD–1) and 1D–B (monument K10), approximate confidence intervals at 95-percent level, and mean values specified in 3D model

[m/d, meters per day; --, not applicable or not measured; m^{-1}, 1/meter; m, meters; cm, centimeters]

Aquifer property	Value estimated in 1D models	Approximate individual confidence interval	Mean values specified in 3D model
Vertical hydraulic conductivity, m/d			
Upper confining layer	2.1×10^{-6}	$1.3 \times 10^{-6} – 3.4 \times 10^{-6}$	3.0×10^{-6}
Lower confining layer	[1] 3.7×10^{-4}	--	3.7×10^{-4}
Mean elastic specific storage, m^{-1}			
Upper confining layer	7.5×10^{-6}	$4.6 \times 10^{-6} – 1.3 \times 10^{-5}$	[2] 7.2×10^{-5}
Lower confining layer	3.6×10^{-6}	$2.6 \times 10^{-6} – 5.6 \times 10^{-6}$	[2] 2.6×10^{-5}
Preconsolidation head, m	125	110–140	--

[1] Fixed value in regression.

[2] Estimated in regression with one-dimensional models, case B.

Subsidence (monument K10)	Model 1D–B	Measured subsidence	3D model
Upper confining layer, cm	1.8	--	1.5
Lower confining layer, cm	20.4	--	15.2
Total	22.2	23.8	16.7

probably resulted from gas exsolution. Releases of methane from several wells suggest that gas was present as a free phase over a wide area during water-level declines. The expansion and exsolution of the gas partially dewatered the confined aquifers, releasing water from storage. The effect of gas exsolution on specific storage in the Genesee Valley aquifers is discussed in Yager and Fountain (2001).

SIMULATION OF LAND SUBSIDENCE

Two one-dimensional (1D) models were developed using MODFLOW (McDonald and Harbaugh, 1988; Harbaugh and McDonald, 1996) with the interbed-storage package IBS1 (Leake and Prudic, 1991) to estimate hydraulic properties of the confining units from observations of (1) pore-fluid pressure near the collapse area and (2) land subsidence 850 m south of the collapse area. Estimates of hydraulic values derived from calibration of the two 1D models were then substituted in the 3D model described earlier to depict the spatial and temporal distribution of land subsidence.

Two pressure transducers were installed in September 1995 in borehole XD–1 (fig. 1) within the upper confining unit at a depth of 66 m, about 30 m above the top of the middle aquifer. The transducers were placed within a saturated sand pack, and the borehole was sealed to land surface with an expansive grout to isolate the monitored interval from atmospheric pressure and other hydrologic influences (Alpha Geoscience, 1996). Land-surface altitudes were surveyed along survey line K (fig. 1) from September 1994 through July 1996 (K. Cox, Akzo Nobel Salt, Inc., written commun., 1997).

Model Design and Calibration

Model 1D–A for borehole XD–1 represented only the upper confining unit and used a column of 257 cells 30 cm thick. Model 1D–B for survey monument K10 represented both the upper and lower confining units with a column of 446 cells 30 cm thick. Aquifer boundaries in both models were assigned hydraulic heads generated from transient-state simulations with the 3D model. Subsidence resulting from compaction of the confining units was computed as the sum of the volume of water released from storage assuming the storage changes were attributable to the compressibility of the skeleton (granular matrix) of the aquifer system, rather than the expansion of water.

The confining units in each 1D model were assigned values of vertical hydraulic conductivity, K_v, and skeletal specific storage, S_{sk}. The K_v value for the upper confining unit in both models was obtained through the nonlinear regression method described below, and the K_v value for the lower confining unit (model 1D–B) was fixed at the value estimated from the 3D model (3.7×10^{-4} m/d). The S_{sk} values assigned to both confining units were chosen to represent both the elastic and inelastic stress ranges. Values of elastic skeletal specific storage, $S_{ske}(i)$, were computed for each cell i using compressibility values from equation 1 with the depth below land surface, $d(i)$, and an m value estimated by nonlinear regression. Values of inelastic or virgin skeletal specific storage, $S_{skv}(i)$, were specified to be either 30 or 50 times greater than $S_{ske}(i)$ values on the basis of published values (Riley, 1998). The magnitude of stress (preconsolidation head, H_{pc}) at which the transition from elastic to inelastic storage occurred was also estimated in the regression.

A nonlinear regression method (PEST; Doherty and others, 1994) was used to estimate three parameters (K_v, m, and H_p) in both 1D models using eight observations of pore-fluid pressure at borehole XD–1 (model 1D–A) and four observations of subsidence at monument K10 (model 1D–B). Weights were assigned to the pressure and subsidence observations to account for differences in the measurement ranges (pressure [expressed as equivalent head of freshwater]: 123 to 132 m; subsidence 5.5 to 24 cm). Parameters were estimated through a 12.4-year transient-state simulation representing post-collapse conditions.

The K_v value for the upper confining unit estimated by the PEST regression was close to that specified in the 3D model (table 2). Mean elastic skeletal specific-storage values for the upper and lower confining units agree with a specific storage, S_s, estimated for a confining unit of glacial drift in Anchorage, Alaska (7.5×10^{-6} m^{-1}) from borehole extensometer measurements made during an aquifer test (Nelson, 1982). The preconsolidation head of 125 m corresponds to a prior loading of the sediments equivalent to about 46 m of water and indicates that the confining-unit sediments are overconsolidated; this result is consistent with the presence of till in the upper confining unit that was probably deposited during a temporary glacial advance during the Pleistocene. Specifying values of inelastic skeletal specific storage that were either 30 or 50 times the S_{ske} values resulted in little difference in model error.

Simulated Response of Confining Units

Computed pore-fluid pressure changes in the upper confining unit (model 1D–A) were in close agreement with pressures measured in borehole XD–1 during drainage of the confined aquifer system and the subsequent recovery that began once the mine was flooded in January 1996 (fig. 5). The maximum residual was about 1.5 m, and the mean error was 0.64 m, less than 2 percent of the computed 44-m drawdown. The predicted subsidence at monument K10 (model 1D–B) closely matched the observed subsidence, and the maximum simulated subsidence (22 cm) was about 6 percent less than that observed (24 cm) (fig. 6). About 90 percent of

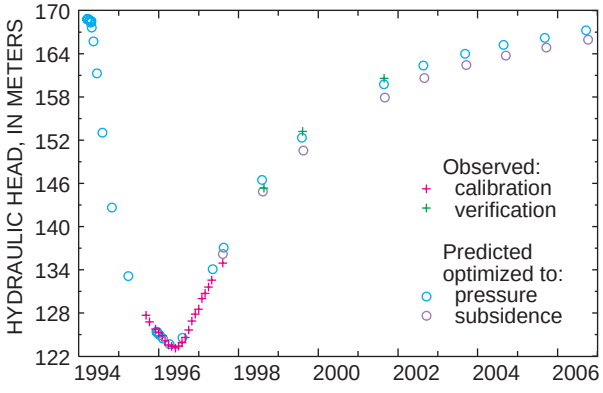

Figure 5. Hydraulic head in upper confining unit near collapse area as computed by one-dimensional model 1D–A and measured at borehole XD–1.

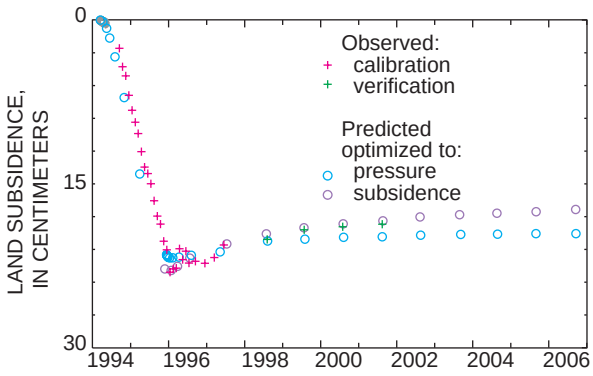

Figure 6. Subsidence computed by one-dimensional model 1D–B and measured land subsidence at monument K10, 850 m south of collapse area.

Table 3. Parameter values estimated for confining layers in one-dimensional models 1D–A (borehole XD–1) and 1D–B (monument K10) with additional data 1998 to 2001, and optimized to pressure or subsidence

[m/d, meters/day; m^{-1}, 1/meter; m, meters]

Variable	Optimized to pressure	Optimized to subsidence	Constant specific storage[1]
Vertical hydraulic conductivity, m/d			
Upper confining layer	4.9×10^{-6}	5.5×10^{-6}	2.7×10^{-5}
Mean elastic specific storage, m^{-1}			
Upper confining layer	7.2×10^{-6}	2.5×10^{-5}	2.0×10^{-5}
Lower confining layer	3.3×10^{-6}	9.5×10^{-6}	1.1×10^{-6}
Preconsolidation head, m	128	116	126

[1] Separate values of S_s estimated for each confining layer.

the simulated subsidence was owing to inelastic, nonrecoverable compaction.

The 1D models were initially calibrated with pore-fluid pressure and subsidence data from 1994 to 1997. A post-audit of the model's prediction capability was made possible by more recent measurements collected from 1998 to 2001, which indicate that model predictions match the recovery of fluid-pressure and uplift of land surface remarkably well (figs. 5 and 6). A more accurate match of the fluid-pressure recovery was obtained in an additional regression that included the recent data with the pressure data weighted more heavily than the land-surface-altitude data (subsidence and uplift or rebound); the increase in accuracy was gained at the expense of additional error in the prediction of land-surface uplift, however. A similar, but opposite pattern was observed in a second regression in which the land-surface-altitude data were weighted more heavily than the fluid-pressure data. Both the fluid-pressure recovery and land-surface uplift were matched equally well in a third regression in which separate values of specific storage were specified for the upper and lower confining units. This regression used S_s values that were constant and did not vary with depth, as in the other regressions. The ratio of estimated values for the upper and lower confining units in this regression was 18 (table 3)—a difference much larger than suggested by the consolidation tests. In contrast, the ratios from the other two regressions (2.2 and 2.6) were more consistent with consolidation-test results.

Elastic compressibility values computed from the m value of 1.1×10^{-8} m/Pa estimated by the regression (case A, fig. 3) were about one order of magnitude

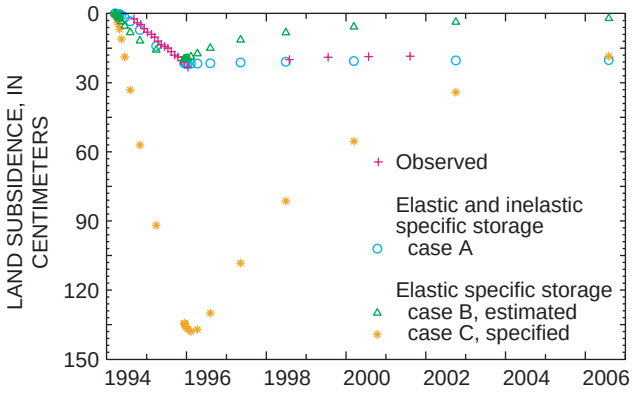

Figure 7. Land subsidence measured at monument K10 and predicted by model 1D–B in three alternative regressions.

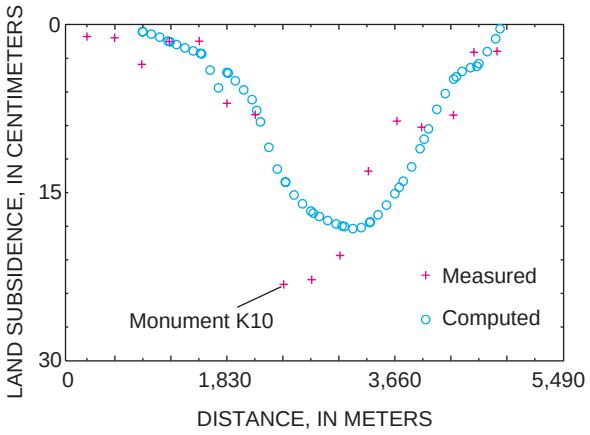

Figure 8. Land subsidence along survey line K as measured in February 1996 and as computed by three-dimensional model.

less than those calculated for confining-unit sediments during the rebound phase of the consolidation tests. Model sensitivity to skeletal specific storage was investigated in two alternative regressions in which the observed subsidence was assumed to result solely from elastic compaction. The mean S_{ske} values obtained in these regressions were larger than those computed in case A, which represented both elastic and inelastic compaction. Results of the two alternative regressions matched the pressure response observed at bore-hole XD–1 (model 1D–A) equally well; however, because estimated K_v values also were larger than in case A, the vertical hydraulic diffusivity (K_v/S_s) was unchanged.

Case B, with the estimated m value of 2.9×10^{-7} m/Pa, yielded a maximum subsidence of 20 cm at monument K10—about 85 percent of the measured value, and elastic skeletal compressibilities matched reasonably well with the values calculated for the rebound phase of consolidation tests. This case indicates that the compacted sediments would expand elastically, causing the land surface to rebound, approaching its pre-mine collapse elevation after water levels had begun to recover—a result that was not observed (figs. 6 and 7). Case C, with a specified m value of 2.4×10^{-6} m/Pa estimated from the compression phase of consolidation tests, resulted in a maximum subsidence of 1.5 m, about six times greater than the measured value (fig. 7).

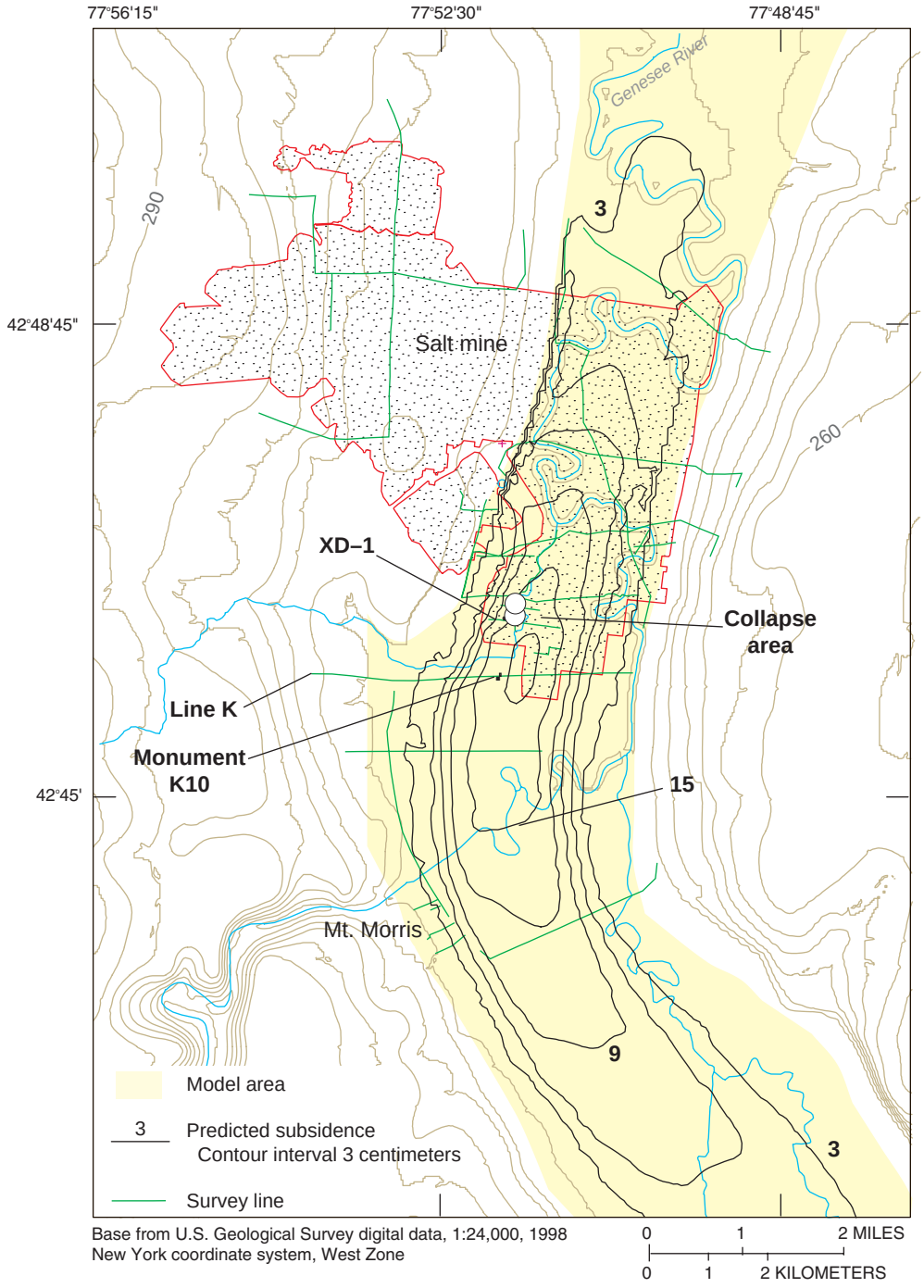

Figure 9. Distribution of maximum land subsidence in Genesee Valley in February 1996, as computed by three-dimensional model.

Spatial Distribution of Simulated Subsidence

The 1D models indicate that land subsidence south of the mine was the result of both elastic and inelastic compaction, but the program MODFLOWP, which was used to construct the 3D model, allows only one storage value for each model cell. The S_s values specified in the 3D model for the upper and lower confining units (3.3×10^{-5} m^{-1} and 1.6×10^{-5} m^{-1}, respectively) are close to the mean S_{se} values computed in case B in which only elastic compaction was simulated. In case B, the close match between computed and maximum subsidence at monument K10 indicates that an approximate value for the volume of water released from storage in the confining units can be obtained from a single S_s value. Values of K_v and S_s estimated assuming elastic compaction (case B) were therefore incorporated into the 3D model to compute the spatial distribution of subsidence when water-level drawdown was a maximum. The subsidence at each cell was computed as the sum of the volume of water released from storage in each confining unit (model layers 2 and 4) divided by the cell area.

The maximum subsidence at monument K10 as computed by the 3D model (17 cm, table 2) is about 70 percent of that observed (24 cm). The cumulative subsidence in February 1996 along survey line K as computed by the 3D model was reasonably consistent with the measured subsidence (fig. 8), although offset 900 m to the east. The 900-m discrepancy in the location of maximum subsidence along survey line K suggests that the confining-unit thickness specified in the 3D model does not accurately represent the actual thickness of fine-grained confining-unit sediments.

The 3D model indicates that as much as 3 cm of subsidence had occurred by February 1996 over an area covering about 41 km^2 that extended 13 km north and 11 km south of the collapse area (fig. 9); as much as 15 cm of subsidence occurred over an area covering about 3.6 km^2. Simulated subsidence closely matched the measured subsidence in Mt. Morris, 5 km south of the collapse, where as much as 9 cm of subsidence was measured. Subsidence was greatest near the collapse area and in the center of the Genesee Valley, where deposits of fine-grained sediments are thickest.

CONCLUSIONS

Skeletal specific storage was estimated for confining-unit sediments through simulation of pore-fluid pressure and subsidence measured at two locations near a salt mine collapse where severe water-level drawdowns resulted from mine flooding. One-dimensional simulations indicated that land subsidence resulted mainly from inelastic compaction, but an alternative simulation indicated that the maximum subsidence could be computed considering solely elastic compaction using an elastic skeletal specific storage value. This elastic storage value was incorporated into a 3D flow model in which the confining units were represented by single model layers. The subsidence computed from the volume of water released from storage in the confining units agreed reasonably well with measured subsidence, suggesting that the 3D model could be used to simulate the distribution of the maximum subsidence resulting from mine flooding. Estimated elastic-compressibility values were about one order of magnitude less than those computed for confining-unit sediments during the rebound phase of the consolidation tests, suggesting that values derived from consolidation tests do not accurately represent the actual compressibilities under field conditions. A post-audit of the model's predictive capability, made possible by additional measurements of pressure and subsidence recorded from 1998 to 2001, after the model calibration period, verifies that the 1D models simulate fluid-pressure and land-surface recovery quite well, despite this fairly simple characterization of the complex aquifer system.

ACKNOWLEDGMENTS

This study was conducted in cooperation with the Livingston County Department of Health. Measurements of laboratory consolidation tests, water levels, pore-fluid pressures, and subsidence were provided by Akzo Nobel Salt, Inc.

Separating Ground-Water and Hydrocarbon-Induced Surface Deformation From Geodetic Tectonic Contraction Measurements Across Metropolitan Los Angeles, California

By Gerald W. Bawden[1]

Abstract

Following the 1987 Whittier Narrows and 1994 Northridge earthquakes that revealed blind thrust faults threaten metropolitan Los Angeles, California, an array of 250 continuously recording GPS stations (Southern California Integrated GPS Network) was deployed to detect and monitor the displacements associated with deep slip on both blind and surface faults. This report augments the GPS time series with InSAR imagery. After removing the deformation associated with extraction of subsurface fluids and known strike-slip faulting, there is 4.4±0.8 millimeters per year of N.36±5°E.-oriented uniaxial contraction across the Los Angeles Basin, perpendicular to the major strike-slip faults. This suggests that the contraction is primarily accommodated on the thrust faults rather than on northeast-trending strike-slip faults. Ground displacements accompanying the widespread pumping for ground water and oil obscures, and in some cases mimics, the tectonic signals expected from the blind thrusts. In the 40-kilometer-long Santa Ana Basin, ground-water withdrawal and re-injection produces about 20 millimeters per year of long-term aquifer-system compaction and land subsidence, accompanied by ±55 millimeters of vertical and ±8 millimeters of horizontal summer-to-winter seasonal oscillations. The timing of the long-term subsidence correlates with an increase in ground-water pumpage that began in 1995–96.

[1] U.S. Geological Survey, Menlo Park, Calif.

INSAR OVERVIEW

Satellite InSAR is a remote sensing technique that maps where the Earth's surface has moved either toward or away from the radar antenna on the satellite (line-of-sight range change). The satellite emits radar pulses and then listens for the radar "echo" to return. The SAR platform on the satellite can precisely measure the amount (amplitude) of the signal that is reflected back to the antenna and the fraction of a wavelength (5.6 cm for the European Space Agency ERS 1/2 satellites) that is returned in the radar echo for each point on the ground (pixel posting typically is 30 to 90 m). An interferogram is a map of how the phase at stable radar reflectors (pixels) on the ground changes between two radar scenes imaged at different times. Interferograms are formed by precisely aligning the amplitude component of two SAR scenes, differencing the phase information at each point on the ground in both radar images (fig. 1a), and correcting for the effects of topography. The ERS 1/2 satellites have a look angle that is about 23° from vertical, which means that the satellites are most sensitive to vertical deformation: uplift and subsidence. The line-of-sight unit vector for descending ERS 1/2 satellites in Los Angeles, Calif., is—North:East:Up, -0.08:0.39:0.92, respectively.

An interferogram typically is depicted as repeating color bands or fringes, where relative surface displacements can be determined between two regions by counting the number of full (one complete color cycle) and partial fringes and then multiplying by a scale factor that represents the magnitude of displacement for one full color fringe. This value is arbitrary, but typically the value 28.3 mm (1.1 in.) (fig. 1b) is used as it represents one-half the wavelength of the C-band radar used by ERS 1/2 and the maximum displacement that

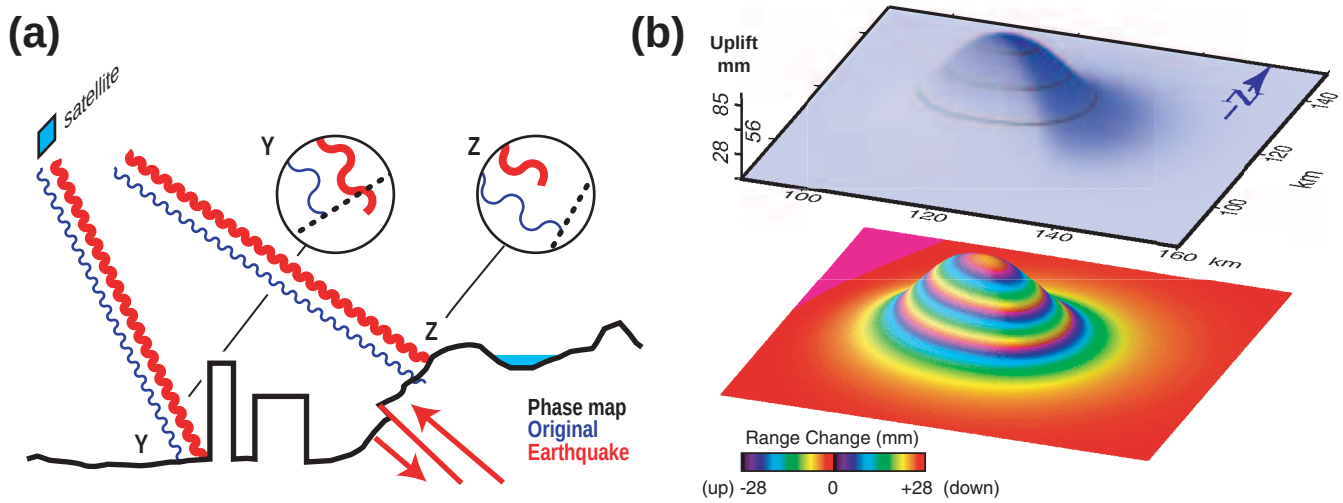

Figure 1. Interferometric phase mapping for (a) an earthquake and (b) modeled uplift. (a) The sine waves transmitted by the radar depict the position of the Earth's surface before and after an earthquake—the thin blue sine waves, before an earthquake, and the thick red sine waves, after an earthquake. In the footwall (Y) the ground moved away from the satellite about 0.5 wavelength and in the hanging wall (Z) the surface moved toward the satellite about 0.75 wavelength. By evaluating each point on the ground a complete, smooth map of the phase change can be generated—an interferogram. (b) Shallow inflation of 10 cm at depth would produce an uplift pattern (top image) that would be seen as a series of repeating color bands in an interferogram (lower image). To read an interferogram, select a point outside of the deformation feature (for example in the lower right corner) and count the number of fringes (repeating color bands) to the center of the feature (three in this example). Multiply the number of fringes by the color-scale factor, 28.3 mm or 1.1 in. (3 x 28.3 mm~85 mm). Next determine the direction of motion (up or down in this example) by matching how the colors change in the feature with the InSAR scale bar. In this example, moving from the lower right corner toward the feature, the colors cycle from red-yellow-green-blue-violet and back to red. This color pattern goes from right to left on the InSAR scale which means that the surface is decreased in range (getting closer to the satellite) and therefore uplifted.

can be unambiguously measured from pixel to pixel. If there is no surface deformation between the two radar scenes, then the interferogram will be flat—all the same color. However, if the ground elevation changed, then the resulting interferogram is a map of satellite-to-ground range change between neighboring pixels on the ground (fig. 1b). Interferograms are not only sensitive to motion of the Earth's surface, but also topography and atmospheric moisture. The effects of topography can be removed with either a digital elevation model or another SAR scene imaged close in time to one of the paired images used to develop the interferogram. The effects of atmospheric moisture can be assessed by producing several interferograms of the target region and inspecting each interferogram. An atmospheric artifact will be associated with only one scene, while true surface deformation will persist in many scenes.

INSAR OBSERVATIONS

Anthropogenic deformation across metropolitan Los Angeles is evident from a series of 1997–99 interferograms that reveal ongoing subsidence of the Wilmington oil field near Long Beach (Clarke and others, 1987) and seasonal uplift and subsidence of the Santa Ana Basin, the primary ground-water source for Orange County (fig. 2). The 5-km-wide Wilmington oil field (W in fig. 2b) undergoes episodic subsidence (up to 30 mm over 175 days). The 20 X 40 km Santa Ana Basin displays seasonal fluctuations of 50 mm of basin uplift during late fall through mid-spring (figs. 2b and 2c) and 60 mm of subsidence during late spring and mid-fall (figs. 2e and 2f). The extent of the deformation is similar in each seasonal episode, with the greatest fluctuations near the city of Santa Ana and at the northwestern extent of the basin. A profile shows that uplift mirrors the subsidence and that a net annual

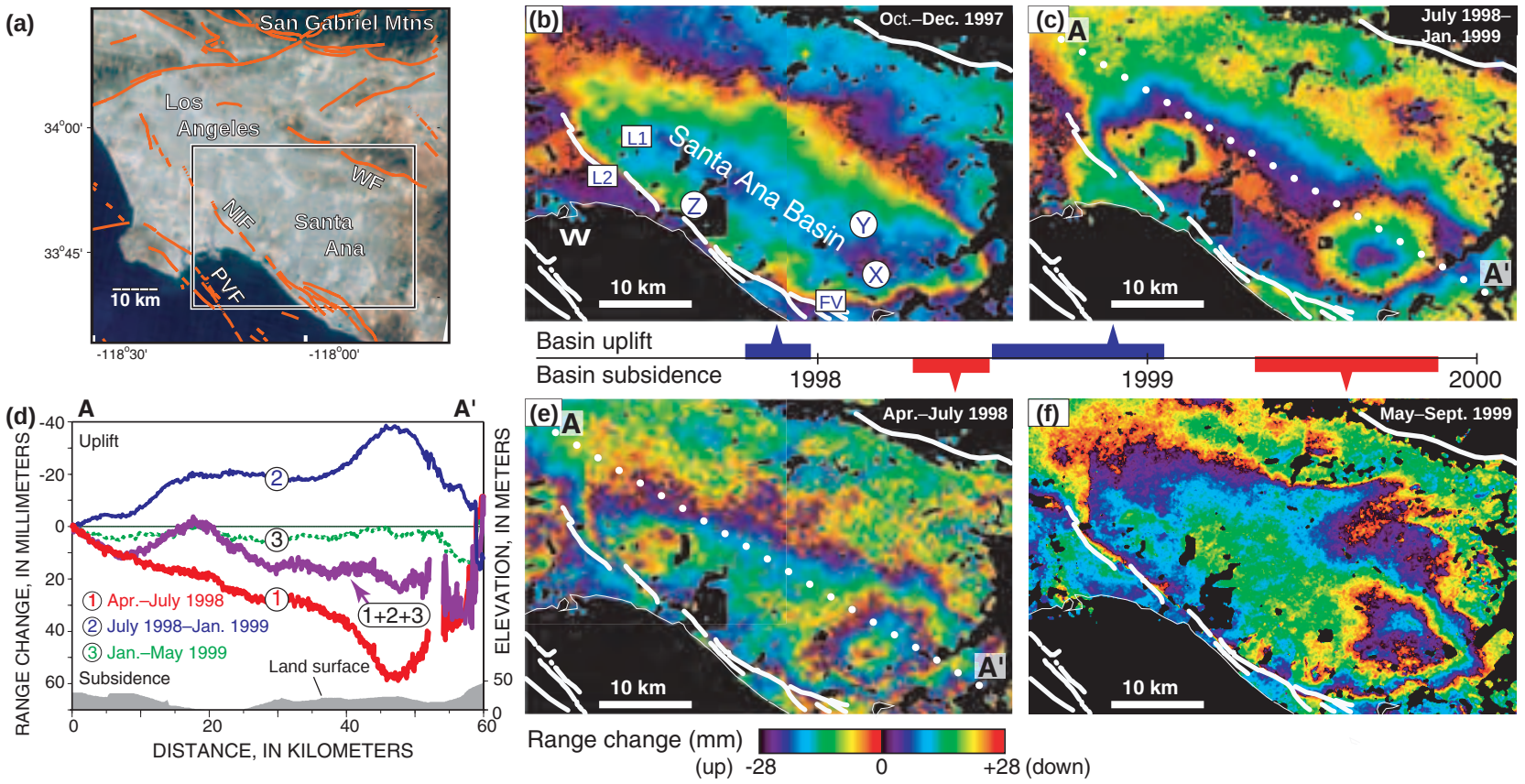

Figure 2. Seasonal deformation in the Santa Ana Basin. (a) Location map for interferograms in figure 2 (black/white frame) and for figures 3 and 6 (full frame); Faults: PVF, Palos Verdes; NIF, Newport-Inglewood; and WF, Whittier. The interferograms (b–c, e–f) represent line-of-sight range changes between the surface and satellite. One color cycle from red through violet represents a decrease in the range of 28 mm between the ground and the satellite. The time history bar in the center of the figure shows the period that each image spans and summarizes the type of motion observed in the Santa Ana Basin. Blue bar denotes uplift (winter months) and red bar denotes subsidence (summer months). (b) Oct.–Dec. 1997 (70 days). This image shows up to 34 mm of uplift in the Santa Ana Basin. W, Wilmington oil field; L1, L2, and FV are GPS sites; X, Y, and Z are water-supply wells. (c) July 1998–Jan. 1999 (175 days). The regions of maximum uplift are at the northwestern and southeastern ends of the basin, with 30 and 50 mm of uplift, respectively. (e) Apr.–July 1998 (105 days). Two regions show up to 60 mm of subsidence. (f) May–Sept. 1999 (105 days). The maximum subsidence is 60 mm. (d) Unwrapped range-change profiles along the Santa Ana Basin, where unwrapping corrects for phase discontinuities as the phase cycles through increments of 2π. Profile location A–A' is shown on (c). The deformation is independent of topography and is thus not an artifact of elevation-dependent atmospheric delays or an inaccurate digital elevation model. All data are from descending ERS 1/2 track 170, frame 2925.

subsidence of about 16 mm occurred between April 1998 and May 1999 (fig. 2d).

Sites of likely long-term anthropogenic deformation in metropolitan Los Angeles are revealed by a 5-year interferogram (fig. 3a) with subsidence rates up to 34 mm/yr and uplift rates as high as 9 mm/yr. Long-term year-to-year subsidence is seen in the Santa Ana Basin (6 to 13 mm/yr), as well as in the Wilmington (W, 28 mm/yr) and the Beverley Hills (B, 11 mm/yr) oil fields. Ground-water pumping near Chino (C) results in a subsidence rate of about 34 mm/yr (Ferretti and others, 2000). The Santa Fe Springs (SF) and parts of the Baldwin Hills (BH) oil fields are uplifting at 5 to 9 mm/yr. Since 1993, fluid injection has exceeded withdrawal in the Baldwin Hills oil field, and the observed uplift could be explained by increased fluid pressures and decreased effective stresses in the injection zones. The uplift mechanism for the Santa Fe Springs oil field is unclear: The 1984–99 extraction rates are 9 percent larger than the injection rates; there is no seasonal component to the uplift; and the uplift rate is much larger than the expected tectonic slip rate (Shaw and Shearer, 1999). The Newport-Inglewood fault forms a sharp boundary to the deformation (figs. 2 and 3). The sense of displacement across the fault seasonally reverses, indicating that the deformation is associated with a cyclical stress such as ground-water pumping rather than slip along the Newport-Inglewood fault. The steep deformation gradient across the fault suggests that ground-water flow is impeded by a low hydraulic conductivity zone associated with this active fault.

GROUND-WATER-LEVEL OBSERVATIONS

Seasonal ground-water-level fluctuations in the Santa Ana Basin are affected by the distribution and magnitude of ground-water discharge and recharge and indicate an association between aquifer management practices and surface deformation, which has been observed in other ground-water basins (Galloway and others, 1998; Galloway and others, 1999; Ireland and others, 1984). Water levels in wells near locations where the largest seasonal changes in land-surface elevation occur exhibit the greatest seasonal ground-water-level fluctuations, and wells elsewhere in the basin have proportionally smaller ground-water-level and land-surface-elevation changes (fig. 4a). The aquifer is artificially recharged year-round and is pumped during May–September to meet the demand for water in the summer. During 1996–97 about 78 percent of the water pumped from the basin came from artificial recharge (Mills and others, 1999). On the basis of the correlation between the measured surface deformation, ground-water-level changes and ground-water discharge and recharge (fig. 4), as well as the geometry of the regional aquifer system (Poland and Piper, 1956), it is likely that the seasonal deformation of the Santa Ana Basin results from repeat cycles of ground-water extraction and replenishment.

Most of the annual subsidence in the Santa Ana Basin likely is caused by the present ground-water-level declines, although a component of the land subsidence northeast of Santa Ana might be residual compaction. Residual compaction is related to the time-dependent fluid-pressure equilibration between the aquifer and any thick, fine-grained interbeds and confining units associated with historical ground-water-level declines (fig. 3b). The water level time series shows a pronounced response to seasonal pumping beginning in 1995, with the water levels reaching new lows in each successive summer through 1999 (fig. 5). A 2-year interferogram that precedes this period shows a few localized pockets of subsidence in the Santa Ana Basin (fig. 3b) but lacks the widespread subsidence features observed after 1995. Therefore, the longer-term subsidence shown in the 5-year interferogram (fig. 3a) is a recent feature that began after July 1995 and is not a result of residual compaction in response to historical ground-water-level declines. This implies that the 60 mm of subsidence observed in the 5-year interferogram took place in 3 years and that the subsidence rates near Santa Ana are about 20 mm/yr. Much of the annual deformation presumably occurs from inelastic compaction (largely irreversible) and fluid-pressure equilibration between the coarser-grained aquifers and thin, more compressible, fine-grained interbeds within the aquifer.

GPS OBSERVATIONS

GPS sites on the margin of the Santa Ana Basin undergo seasonal horizontal motion toward and away from the basin, while sites within the basin undergo seasonal uplift and subsidence, consistent with a simple elastic model of basin behavior. The GPS site FVPK, for example, located on the southern margin of the basin is pulled to the northeast (fig. 4b) when water levels decline in the summer (fig. 4a) and is pushed to the southwest when water levels rise in the winter,

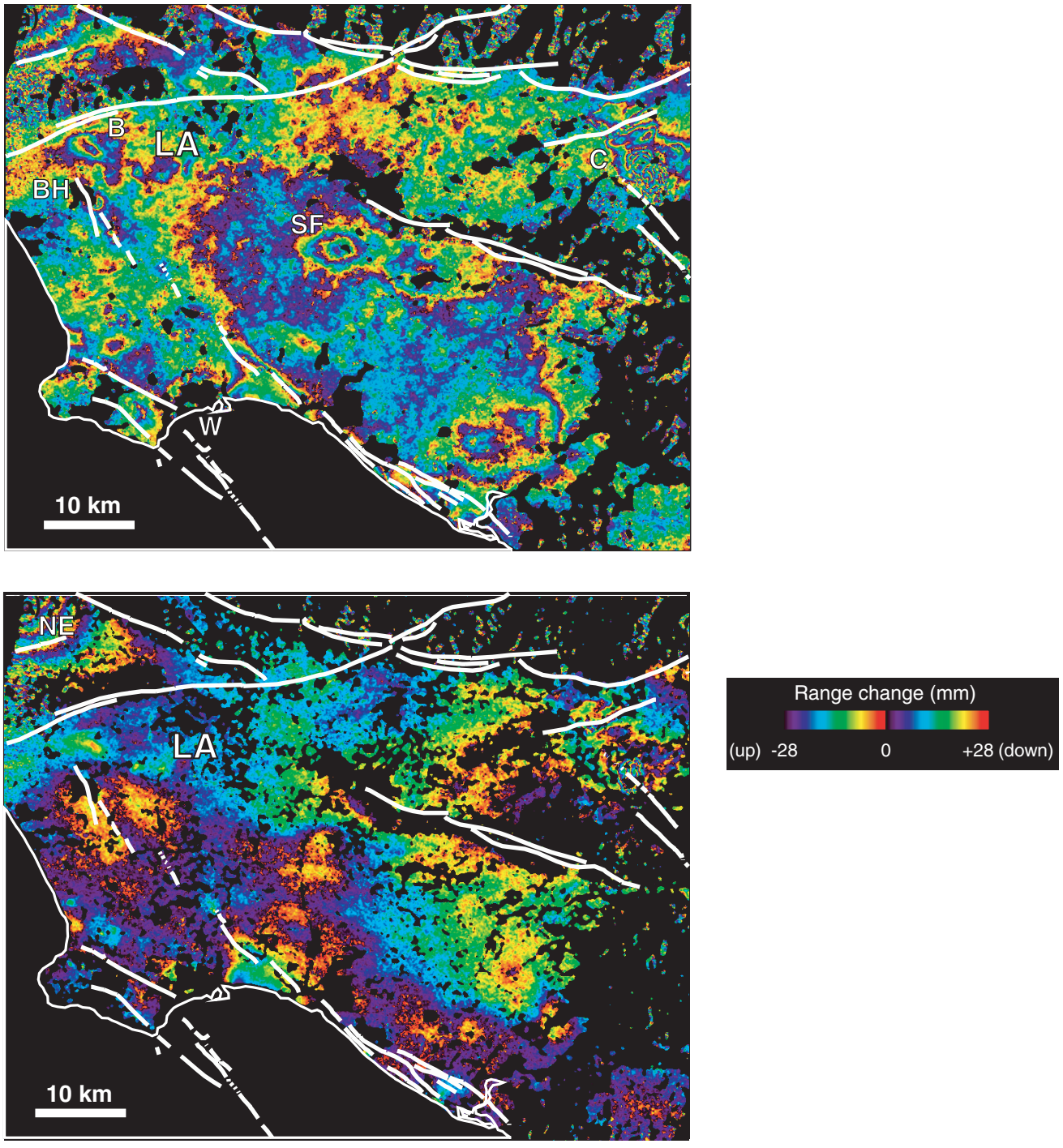

Figure 3. Long-term differential interferograms for metropolitan Los Angeles. (a) 5-year interferogram, Oct. 1993–Oct. 1998, shows more than 60 mm of subsidence at the southeastern end of the Santa Ana Basin during this time period (fringes in the upper left-hand corner are from the uplift associated with the 1994 Northridge earthquake). (b) 2-year interferogram, July 1993–June 1995. B, Beverley Hills; BH, Baldwin Hills; C, Chino; LA, Los Angeles; NE, Northridge earthquake; SF, Santa Fe Springs; and W, Wilmington oil fields. The incidence angle of the ERS satellites is 23° from the vertical, thus the interferograms are most sensitive to vertical motion. (The unit vector components in the satellite look direction are: North = -0.08, East = 0.39, and Up = 0.92.)

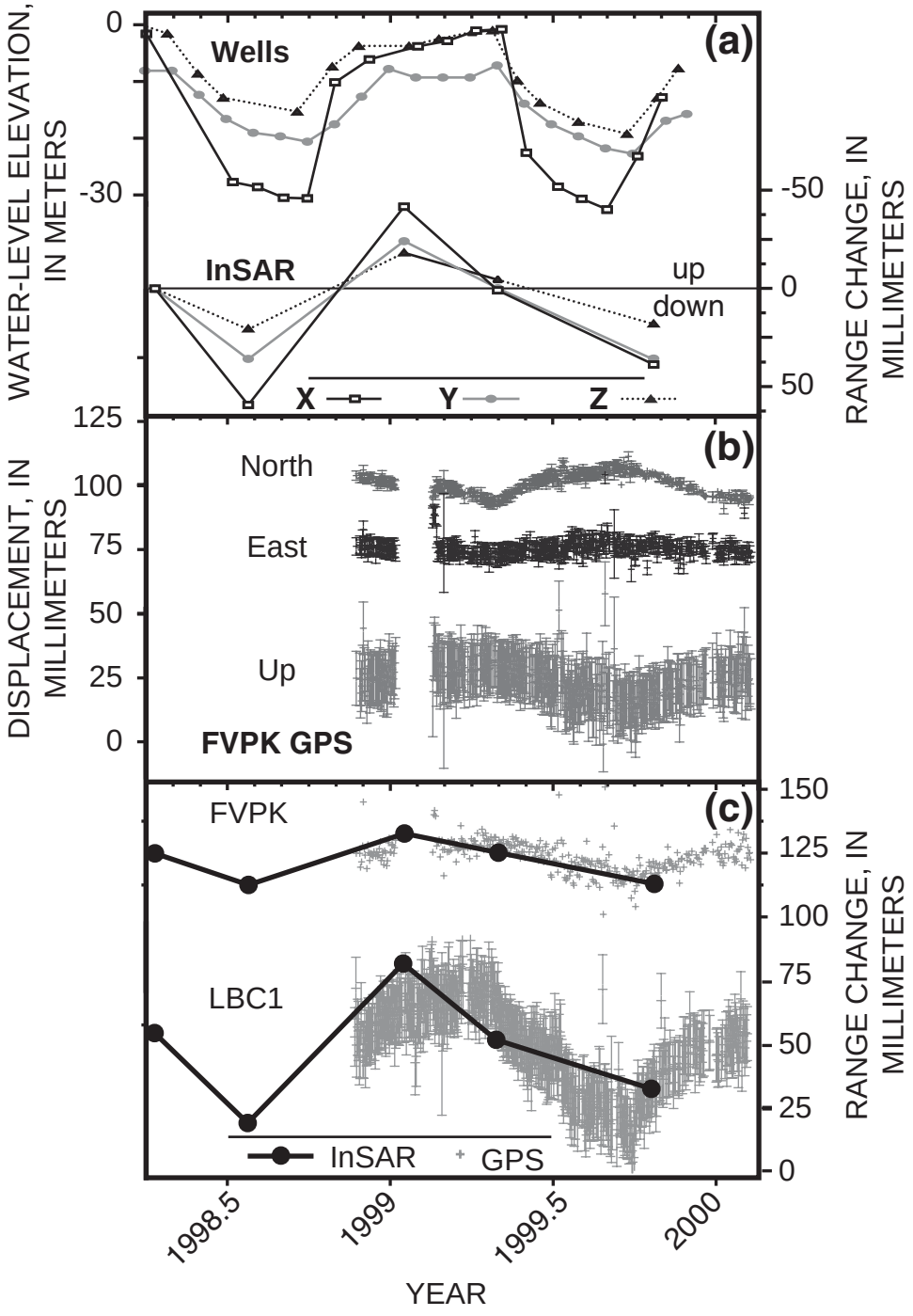

Figure 4. Comparison of ground-water-level fluctuations, InSAR range change, and detrended GPS time series. (a) Seasonal water-level changes for three wells located in the Santa Ana Basin (top) (wells shown in fig. 2b) compared with unwrapped InSAR range change time series corresponding to each well location (bottom). (b) The north, east, and vertical GPS components for the site FVPK (FV in fig. 2b). (c) The three-component GPS vector projected onto the InSAR line-of-site vector at FVPK and LBC1 (L1 in fig. 2b). An average linear trend has been removed from each horizontal component of the GPS time series. Water-level data are from the Orange County Water District. Wells: X, IRWD-6/1; Y, SA-35/1; Z, SCWC-LAYT/1.

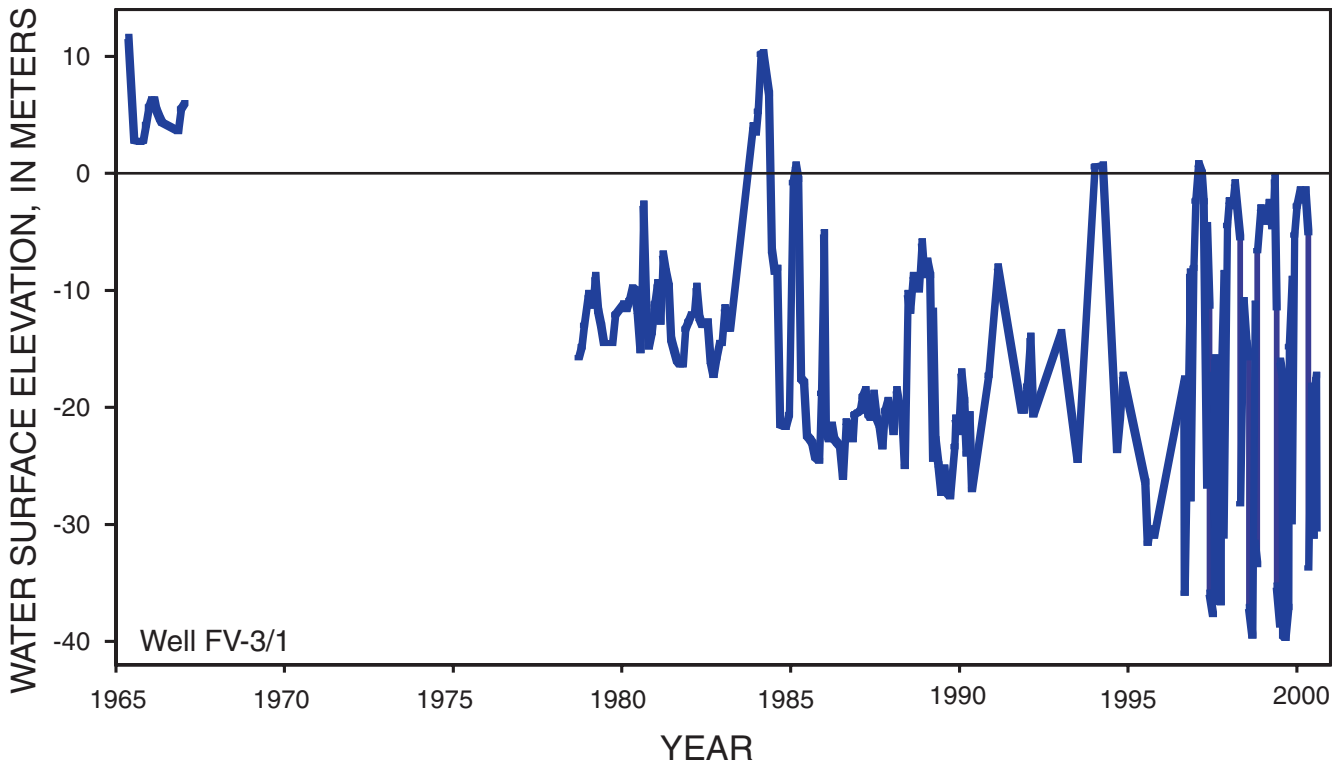

Figure 5. Historic water-level fluctuations for well FV-3/1, Santa Ana Basin. Other wells in the region show similar trends. Well is near well X shown in figure 2b.

producing 14 mm of horizontal and 15 mm of vertical movement. Conversely, the GPS site LBC1 located within the basin exhibits little seasonal horizontal movement (±3 mm) but large seasonal vertical motions (±30 mm) (fig. 4c). Such a pattern, with a high horizontal strain-rate gradient near the periphery of an aquifer system, also observed elsewhere (Carpenter, 1993), can be approximated by the response of a thin aquifer system embedded in an elastic half-space (Young's modulus = 10^4 MPa and Poisson's ratio = 0.25) to ground-water-level variations caused by pumping or recharge (Bawden and others, 2001). The simulated and observed displacement fields agree throughout the basin, with the largest horizontal motions occurring on the basin margins and the largest vertical motions occurring within the basin.

RESOLVING TECTONIC CONTRACTION ACROSS THE LOS ANGELES BASIN

About 50 percent of the continuous GPS sites in the Los Angeles Basin exhibit superposed effects of tectonic motion and deformation associated with the extraction of subsurface fluids. Removing deformation associated with right-lateral strike-slip faults from the Southern California Integrated GPS Network (SCIGN) velocity field (Bock and others, 1997; Prescott, 1996), sites outside the major zones where pumping takes place, show a N.36±5°E. contraction across the Los Angeles Basin (fig. 6a). GPS sites north of Los Angeles exhibit an average southward velocity of 4.4±0.8 mm/yr relative to the Palos Verdes peninsula (PV, fig. 6a), with no discernible contraction between the Palos Verdes and Catalina Island sites 31 km to the south. In contrast, sites that are within or on the periphery of the uplift or subsidence regions have large residual velocities that generally are oriented perpendicular to the local uplift/subsidence gradient (fig. 6b). Ironically, most of the sites that exhibit motion associated with anthropogenic activity lie above the Puente Hills, Elysian Park, and Compton blind thrust faults, limiting our ability to infer their geometry (fig. 6b). (The Puente Hills thrust fault structurally overlies the Elysian Park thrust fault and is not shown in figure 6.) Knowing which GPS sites are affected by human-induced deformation permits either the elimination of

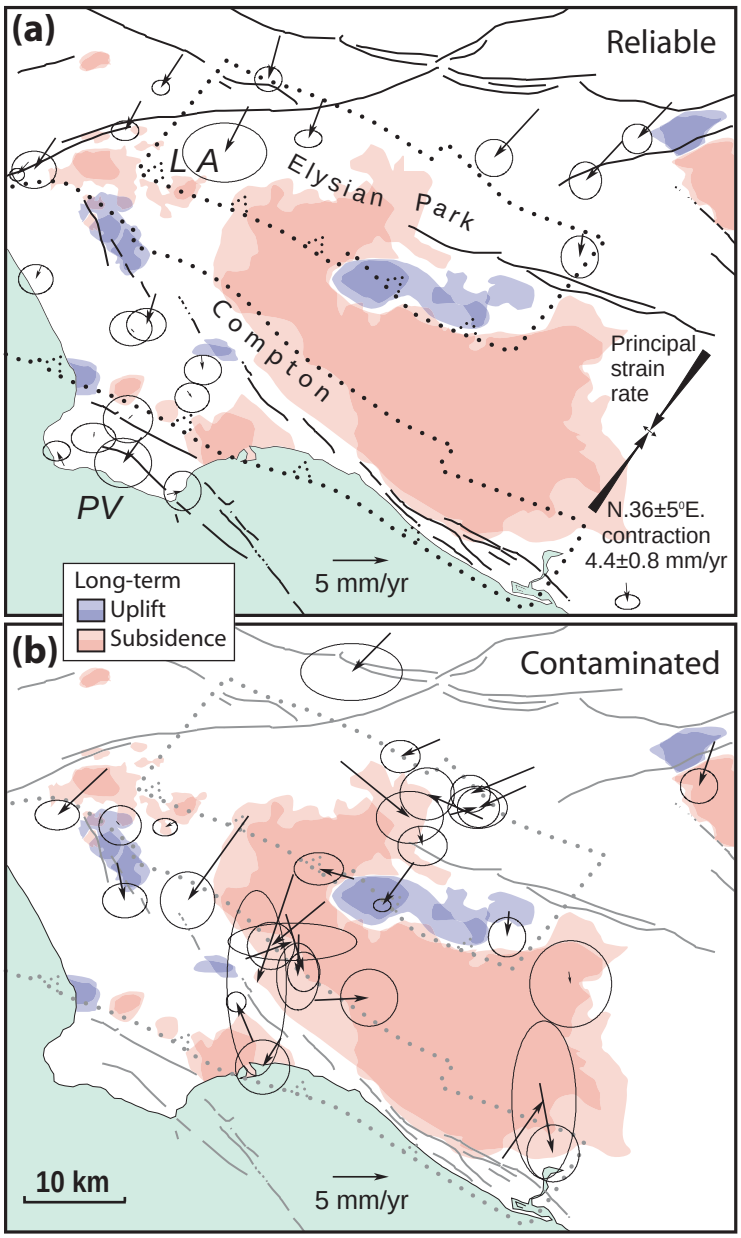

Figure 6. GPS residual velocities, after removal of motion associated with strike-slip faults, superimposed on long-term uplift and subsidence features deduced from InSAR. Formal velocity uncertainties were multiplied by 4.5 to account for flicker noise in GPS time series (Zhang and others, 1997). The displacement field caused by the San Andreas, San Jacinto, and Elsinore faults was removed from the SCIGN site velocities by using a simulated dislocation in an elastic half-space locked above 20-km depth and slipping below at the estimated Holocene slip rates (Jackson and others, 1995) except for the Mojave segment of the San Andreas fault, where a slip rate of 25 mm/yr was used. A 10-km locking depth was used for the Palos Verdes (2.5 mm/yr), Newport-Inglewood (1.0 mm/yr), and Whittier (2.5 mm/yr) faults. Deeper locking depths produced large misfit/noise ratios for the Holocene slip rates. The dotted lines are the surface projections of the Elysian Park and Compton thrust faults (CT) (Shaw and Shearer, 1999; Shaw and Suppe, 1996). For simplicity, the segmented Puente Hills thrust fault (Shaw and Shearer, 1999), which lies above the Elysian Park thrust with a more easterly strike, is not shown. (a) SCIGN sites outside the margins of the aquifers and oil and gas reservoirs are classified as reliable. (b) Sites contaminated with seasonal variations in their horizontal (3 mm/yr) and vertical (8 mm/yr) time series are located near or within regions of long-term uplift or subsidence.

these suspect sites, the placement of future GPS stations outside areas of human-induced uplift and subsidence, or the eventual correction of the artifacts. Irrespective of the placement of GPS stations, InSAR will be needed to discriminate between tectonic and non-tectonic signals in the spatially aliased SCIGN array.

Residual GPS velocities that are free of seasonal and anthropogenic effects exhibit nearly uniaxial contraction oriented perpendicular to both the San Andreas and major strike-slip faults. The contraction rate is smaller and rotated 36° clockwise from that determined by Argus and others (1999). This difference arises because, in addition to the San Andreas and San Jacinto faults, interseismic slip was included on the Palos Verdes, Newport-Inglewood, and Whittier faults to minimize right-lateral GPS displacement gradients. Argus and others (1999) used a smaller GPS dataset to infer that regional contraction across downtown Los Angeles is confined to a 30-km-wide zone between the San Gabriel Mountains and downtown Los Angeles, but it was found that the GPS sites needed to resolve the southern boundaries of the contraction region are affected by human activities (fig. 6b). Walls and others (1998) argued that no more than one-half the geodetically observed contraction, or less than 2.5 to 3.5 mm/yr, is due to thrust faulting, with the remainder accounted for by conjugate strike-slip faults in the northern Los Angeles Basin. Results of this study indicate that the residual contraction is larger than that inferred by Walls and others (1998), but because the NE.-oriented contraction strain rate (56±7 nanostrain/yr) is eight times larger than the NW.-oriented extension rate and the contraction is oriented normal to the strike-slip faults (N.36±5°E.), the residual contraction cannot be explained by strike-slip faulting that was not simulated (fig. 6a). Instead, the contraction is optimally oriented to accommodate slip on the regional blind and surface-cutting thrust faults. Further densification of the SCIGN outside the subsidence zones might enable discrimination of competing thrust fault models, which will be vital to seismic hazard assessment in this major urban corridor.

ACKNOWLEDGMENTS

This work was supported by the National Aeronautics and Space Administration (NASA) Solid Earth and Natural Hazards Program. Ground-water and well data were provided by the Orange County Water District. The author acknowledges the Southern California Integrated GPS Network (SCIGN) and its sponsors, the W.M. Keck Foundation, NASA, National Science Foundation, U.S. Geological Survey, and Southern California Earthquake Center for providing GPS data used in this study. GPS velocity data were provided by Scripps Orbit and Permanent Array Center (SOPAC) with assistance from Yehuda Bock. The author is grateful to Charles Wicks (U.S. Geological Survey) for sharing his InSAR expertise, and John Shaw and Andreas Plesch (Harvard University) for providing Puente Hills thrust fault data. Nearly one-half of the findings presented in this manuscript first appeared in Bawden and others (2001). The new material presented here constrains the timing of the human-induced subsidence, which helps to delineate the mechanism driving the surface motions.

Aquifer-System Characterization Using InSAR

By Michelle Sneed[1], Sylvia V. Stork[1], *and* Randell J. Laczniak[2]

Abstract

InSAR is a powerful technique that uses radar data acquired at different times to measure land-surface deformation, or displacement, over large areas at a high level of spatial detail and a high degree of measurement resolution. InSAR displacement maps (interferograms), in conjunction with other hydrogeologic data, have been used to determine aquifer-system characteristics for areas where surface deformation is the result of stress-induced changes in the granular skeleton of the aquifer system. Interferograms and measurements of aquifer-system compaction from borehole extensometers, and ground-water levels in wells in Santa Clara Valley, California, have shown that land-surface changes caused by aquifer-system deformation for September 23, 1992–August 2, 1997, are elastic (reversible): During the summer when water levels are declining, the land surface subsides, and during the winter when water levels are recovering, the land surface uplifts, resulting in no net surface deformation. Interferograms used with fault maps of Santa Clara Valley and of Las Vegas Valley, Nevada, have shown that the extent of regional land-surface changes caused by aquifer-system deformation may be partially controlled by faults. Interferograms of Yucca Flat, Nevada, show subsidence associated with the recovery of elevated hydraulic heads caused by underground weapons testing at depths of more than 600 meters.

For these selected case studies, continuing or renewed deformation of the aquifer system is coupled with pore-fluid-pressure changes. When applied stresses (water-level changes) can be measured accurately for periods that the interferograms show displacement, stress-strain relations, and thus bulk storage properties, can be evaluated. For areas where additional ground-water-level, land-surface-elevation, aquifer-system-compaction, or other environmental data are needed, the interferograms can be used as a guide for designing appropriate monitoring networks. Aquifer-system properties derived from stress-strain relations and identification of hidden faults, other structural or stratigraphic controls on deformation and ground-water flow, and other hydrogeologic boundaries in the flow system can be used to constrain numerical ground-water flow and subsidence simulations. Managing aquifer systems within optimal limits may be possible if regions susceptible to ground-water depletion and the accompanying land subsidence can be identified and characterized.

INTRODUCTION

Land subsidence is a gradual settling or sudden sinking of the Earth's surface owing to subsurface movement of earth materials. The principal causes of land subsidence are aquifer-system compaction, drainage of organic soils, underground mining, hydrocompaction, natural compaction, sinkholes, and thawing permafrost. Land subsidence, and associated earth fissuring, can damage buildings, roads, pipelines, and other infrastructure; negatively affect aquifer-system storage, wetlands, flood-prone areas, and tidal areas; and spur litigation as a result of the environmental and civil damages. In the United States, about 45,000 km^2 have been affected by land subsidence, an estimated 80 percent of which is a consequence of our Nation's water-use practices, much of which is caused by ground-water depletion and the associated water-level declines in unconsolidated aquifer systems (Galloway and others, 1999). The mechanical processes within an unconsolidated aquifer system that cause land

[1] U.S. Geological Survey, Sacramento, Calif.
[2] U.S. Geological Survey, Las Vegas, Nev.

subsidence can be reversible (elastic) or permanent (inelastic), depending on the properties and water-level history of the affected aquifer system. Under certain conditions, land-surface uplift occurs when water levels rise (Galloway and others, 1999).

InSAR data have been used successfully to map land subsidence and uplift caused by water-level fluctuations. InSAR is a powerful technique that uses radar data acquired at different times to measure land-surface deformation, or displacement, over large areas at a high level of spatial detail (typically 40 m X 40 m pixel resolution is attainable) and a high degree of measurement resolution (5 to 10 mm). InSAR measures displacement by differencing or "interfering" the phase components of two SAR scenes imaged at different times to formulate a "change" interferogram (Galloway and others, 2000).

The interferograms, combined with other hydrogeologic data, have been used to evaluate aquifer-system characteristics including aquifer-system elastic storage properties and geologic controls on ground-water flow and aquifer-system deformation. Aquifer-system characteristics can be used to constrain conceptual and numerical models of ground-water flow and aquifer-system deformation (Hoffmann and others, p. 103 of these proceedings). For areas where additional ground-water level, land-surface elevation, aquifer-system compaction, or other environmental data are needed, interferograms can be used as a guide for designing appropriate monitoring networks. Information derived from interferograms can be used by water-resource managers and urban planners to more effectively preserve the ground-water resource and to help minimize land subsidence and associated damages.

CHARACTERIZING AQUIFER SYSTEMS USING INSAR: CASE STUDIES

Three selected case studies, Santa Clara Valley, Calif.; Las Vegas Valley, Nev.; and Yucca Flat, Nev., are presented in this paper to illustrate the use of interferograms to better understand aquifer systems.

Santa Clara Valley, California

Santa Clara Valley was the first area in the Nation where land subsidence caused by ground-water withdrawal was recognized (Tolman and Poland, 1940). Between 1910 and 1995 nearly 5 m of subsidence had accrued at one location in downtown San Jose, though much of this occurred prior to 1970. In 1969, rapid subsidence was arrested by artificially recharging the aquifer system with imported surface water. Owing to aggressive water-resource management practices, in part to mitigate subsidence, ground-water levels have recovered more than 70 m and are near predevelopment levels throughout most of the aquifer system.

Two interferograms of Santa Clara Valley are presented in this paper: one represents nearly 5 years (September 23, 1992–August 2, 1997) of displacement, and the other represents about 8 months (January 4, 1997–August 2, 1997) of displacement and is a temporal subset of the 5-year interferogram (fig. 1) (Ikehara and others, 1998; Galloway and others, 2000). The 5-year interferogram shows 5 to 10 mm of uplift over much of the area and corresponds to a period of water-level recovery throughout the valley (fig. 1a). The 8-month interferogram shows a subsidence area centered southeast of San Jose where as much as 30 mm of displacement has occurred; water levels in this area declined about 10 m during the same period (fig. 1b) (Ikehara and others, 1998). The displacement pattern is consistent with the historical subsidence pattern (1934–67) and with more recent measurements from borehole extensometers in Sunnyvale and San Jose (Ikehara and others, 1998). The 8-month interferogram also shows about 15 mm of uplift on the east side of the valley, which has been attributed to recharge through percolation ponds and streams in this area (fig. 1b) (Galloway and others, 2000).

Analyses of the two interferograms revealed that, in the range of water levels corresponding to the 5-year interferogram, short-term subsidence is recoverable and the extent of land-surface deformation in the east may be constrained by the Silver Creek Fault and (or) associated faults. The 5-year interferogram shows no subsidence, and, therefore, the subsidence shown in the 8-month interferogram is inferred to be a recoverable seasonal response—a conclusion confirmed by measurements from extensometers in San Jose and Sunnyvale (Ikehara and others, 1998). The eastern limit of subsidence is nearly coincident with the inferred trace of the Silver Creek Fault; the displacement profiles show steep gradients at or near this fault boundary. Surface geophysical (seismic reflection/refraction) surveys confirmed the presence of additional faults at or near this boundary that probably constitute the Silver Creek fault zone (Catchings and others, 2000). The Silver Creek fault zone may control the eastern extent of displacement. The fault zone may separate sediments of differing compressibilities and (or) may act as a

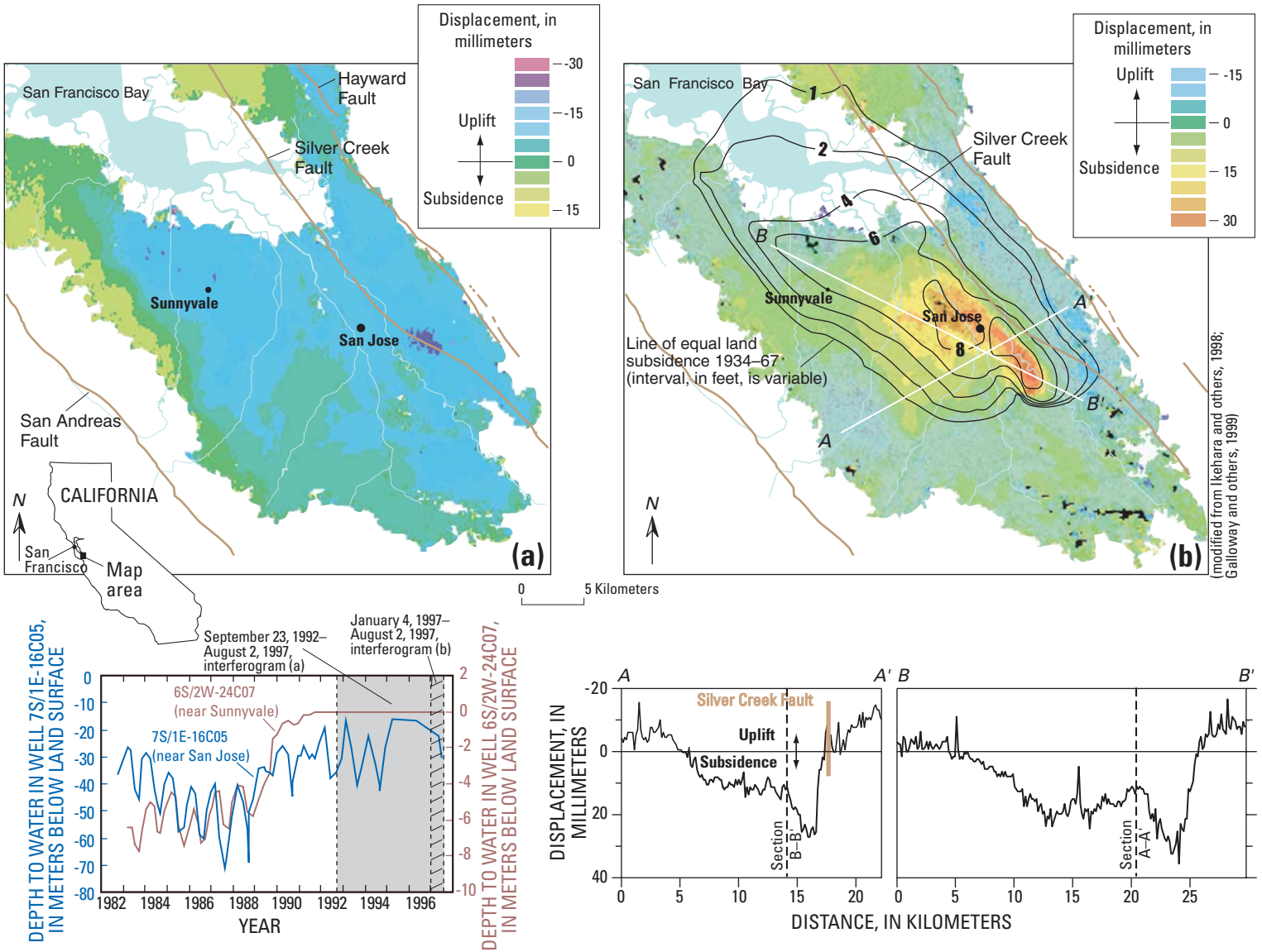

Figure 1. Land-surface displacement and hydrographs for wells 7S/1E–16C05 and 6S/2W–24C07 in Santa Clara Valley, California. (a) Interferogram for September 23, 1992–August 2, 1997 (5 years). (b) Subsidence contours for 1934–67 and interferogram and two cross sections for January 4, 1997–August 2, 1997 (8 months).

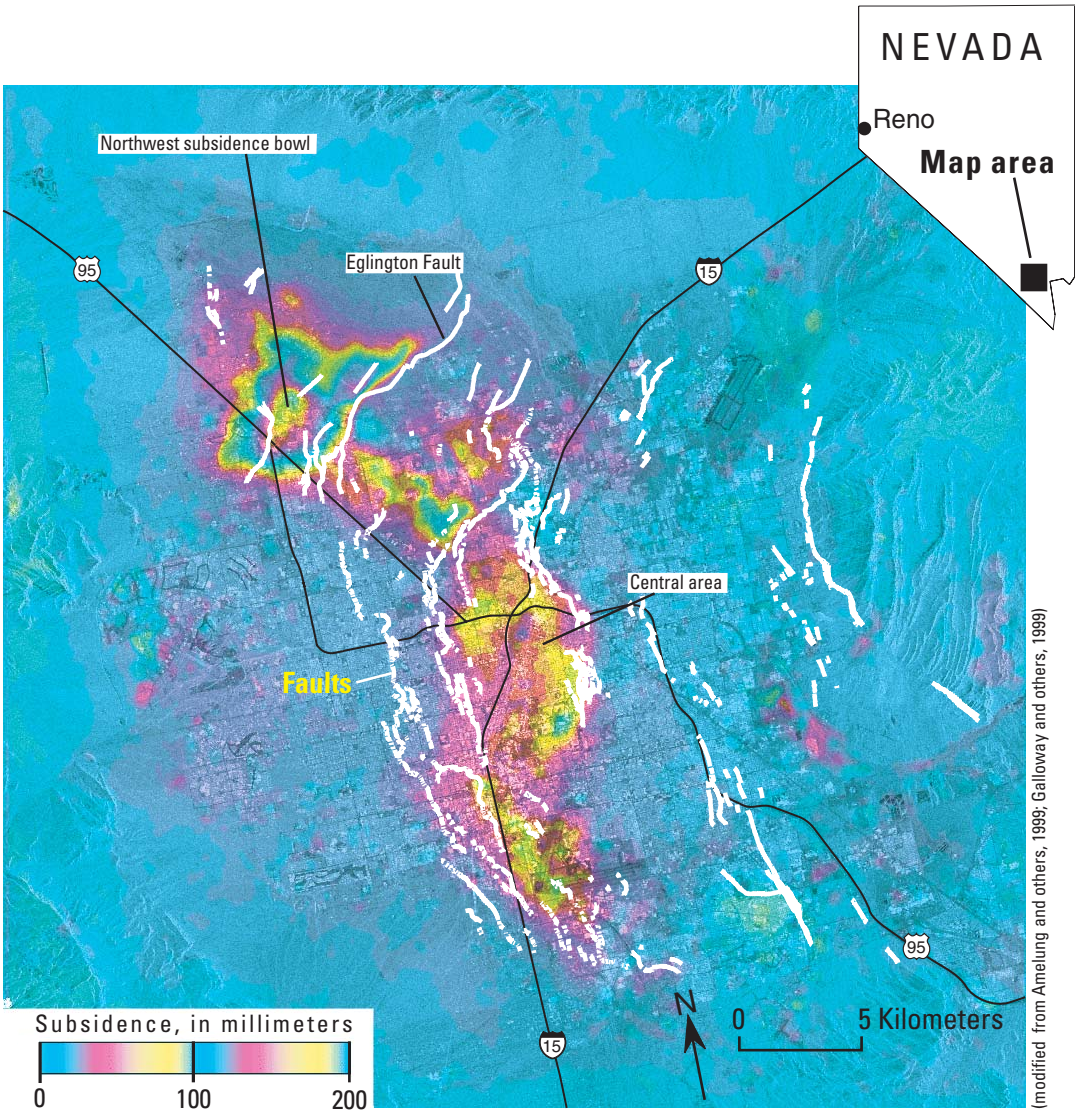

Figure 2. Interferogram showing subsidence for April 21, 1992–December 5, 1997, in Las Vegas Valley, Nevada.

hydrologic barrier to ground-water flow (Ikehara and others, 1998; Catchings and others, 2000).

Las Vegas Valley, Nevada

Las Vegas Valley is the fastest growing metropolitan area in the Nation. Since the 1950s, annual ground-water withdrawals have exceeded the estimated natural recharge. In the late 1800s, several springs flowed in the valley and most wells were artesian. Today, the springs are dry, and locally, water levels are more than 100 m below land surface. The ground-water-level declines have caused widespread aquifer-system compaction and nearly 2 m of land subsidence in some areas (Bell and others, 2000).

One interferogram for Las Vegas Valley is presented in this paper; it represents displacement for April 21, 1992–December 5, 1997 (fig. 2) (Amelung and others, 1999). The interferogram is a composite produced by summing, or stacking, three shorter-period, time-consecutive interferograms.

Many other interferograms (Hoffmann and others, 2001) for Las Vegas Valley indicate changing magnitudes and patterns of displacement and show the locations and the effectiveness of geologic controls on displacement. Ten interferograms presented by

Hoffmann and others (2001) for Las Vegas Valley show recurring large-scale patterns exhibiting varying magnitudes of displacement. The large-scale patterns, which can be seen in figure 2, include a subsidence bowl in the northwest area and several coalescing bowls in the central area of the valley. Eight of the interferograms, covering four summer and four winter seasons during the 1990s, indicate that subsidence rates throughout Las Vegas Valley generally decreased or stabilized with each successive summer interferogram and that uplift rates in the central area generally increased or stabilized with each successive winter interferogram. Two other interferograms representing two consecutive annual periods (May 1996–May 1997 and May 1997–April 1998) show that residual aquifer-system compaction and land subsidence occurred in the northwest bowl, as ground-water levels measured in the aquifers were recovering in the area during these periods (Hoffmann and others, 2001). These two interferograms also show minimal displacement in the central area in the 1996–97 interferogram and uplift in the 1997–98 interferogram, indicating that little or no residual compaction or land subsidence occurred in this area, which is consistent with the stabilized or recovering water levels in this area (Las Vegas Valley Water District, 1998).

In the central area, devoid of residual compaction and where recoverable (elastic) deformation was evident on the interferograms, Hoffmann and others (2001) used the interferograms as strain measurements and paired these with water-level, or stress, measurements to calculate bulk elastic skeletal storage coefficients of the aquifer system for selected locations by using stress-strain methods (Riley, 1969).

The interferograms for Las Vegas Valley indicate that the lateral extent of displacement is partially controlled by faults. The Eglington Fault controls the southeasterly extent of the displacement of the northwest subsidence bowl (fig. 2). From other hydrogeologic information, no significant differences in hydrologic properties of the sediments across the Eglington Fault have been observed: subsidence on the northwestern side of the fault likely is related to heavy pumping in nearby areas north of the fault, but the hydrogeologic relations responsible for the subsidence barriers are poorly understood (Amelung and others, 1999).

Yucca Flat, Nevada

Yucca Flat is about 160 km northwest of Las Vegas and is part of the Nevada Test Site, an area where underground weapons testing was done at depths of more than 600 m until September 1992 (Laczniak and others, p. 121 of these proceedings). Although not all of the post-test processes affecting the subsurface are fully understood, it is believed that most of the underground tests caused collapse of the subsurface test chambers and vents resulting in crater-like depressions at land surface that are observable on digital elevation models of the area. Comparison of time-consecutive interferograms for April 24, 1992–June 18, 1993; June 18, 1993–June 11, 1995; and June 11, 1995–June 16, 1997 (fig. 3) indicates that there has been land subsidence around the craters since the initial collapse. Ground movements along surface faults and the development of fissures at the land surface also have been noted in areas surrounding the craters. One likely explanation for the post-seismic displacement is the compression of low-permeability tuff units in the saturated zone of the aquifer system following pore-fluid pressurization caused by the tests and subsequent delayed drainage and depressurization (Laczniak and others, p. 121 of these proceedings). Some of the displacement appears to be bounded by faults, which likely play a role in controlling the lateral extent of subsidence in this area.

The interferogram for April 24, 1992–June 18, 1993, coincides with the detonation of three tests, two for which—Galena and Divider—the interferogram reveals the coseismic collapse features believed to be associated with the test blasts (figs. 3a and 4). A concentric subsidence signal around the Galena test suggests that the aquifer system may be laterally homogeneous (fig. 4a). A four-lobed deformation signal with oppositely sensed displacement between adjacent lobes around the Divider test (fig. 4b) is similar to that expected for displacement on a strike-slip fault, and suggests that the Divider test triggered faulting or fault reactivation (Laczniak and others, p. 121 of these proceedings).

The interferograms for June 18, 1993–June 11, 1995, and June 11, 1995–June 16, 1997, each span consecutive 2-year periods and show slightly decreasing amounts of displacement (fig. 3b, c). Together the three interferograms support the likelihood of continued post-seismic deformation, possibly at a decreasing rate. In general, the rate of post-seismic deformation is consistent with rates of head decline based on water-level measurements in the area (Laczniak and others, p. 121 of these proceedings).

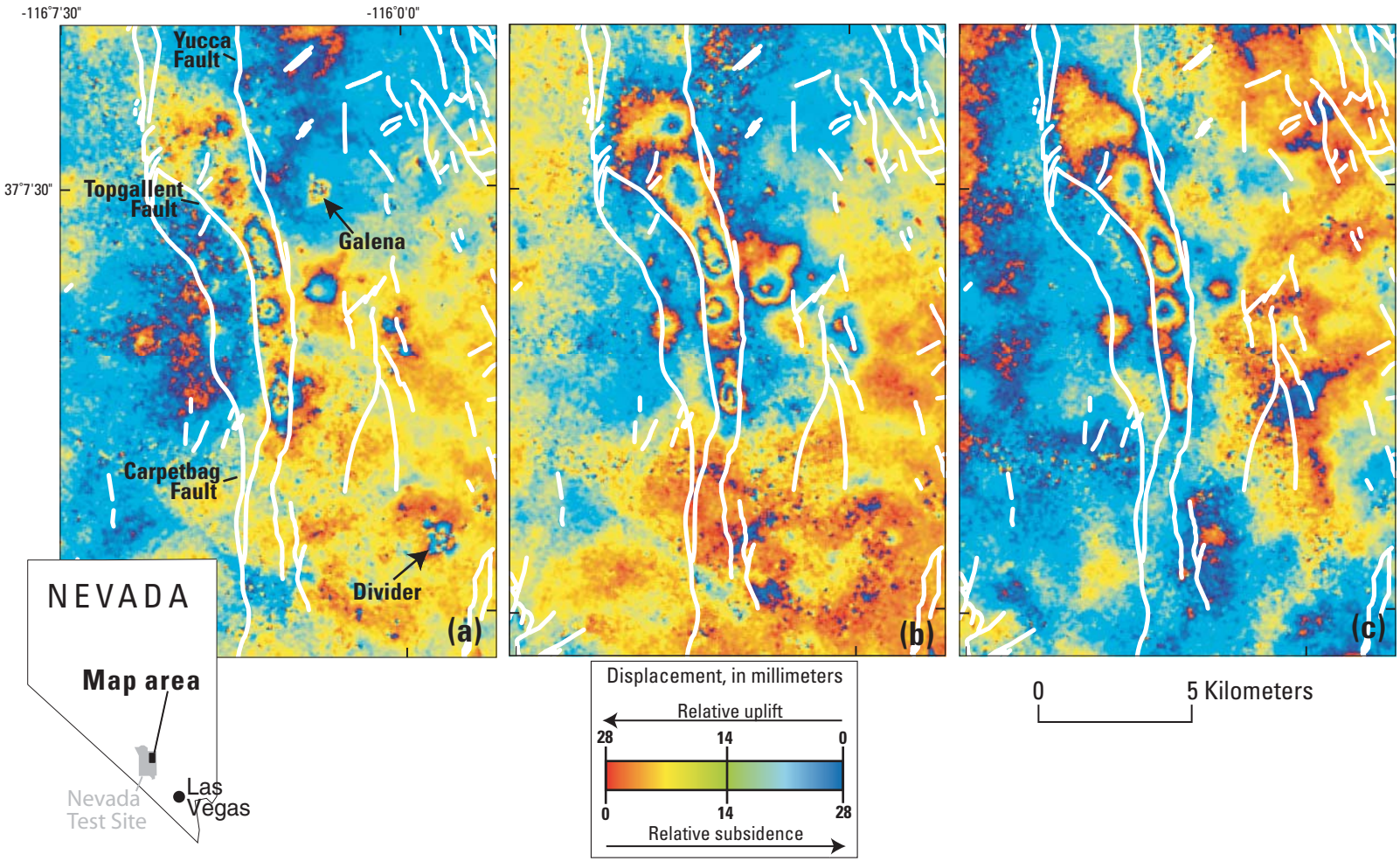

Figure 3. Interferograms showing displacement in Yucca Flat, Nevada. (a) April 24, 1992–June 18, 1993. (b) June 18, 1993–June 11, 1995. (c) June 11, 1995–June 16, 1997.

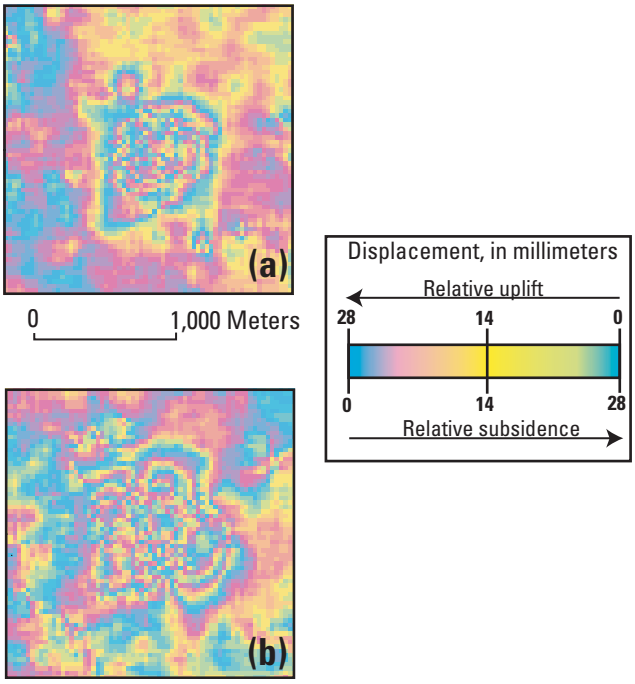

Figure 4. Interferograms showing displacement for April 24, 1992–June 18, 1993, caused by two underground weapons tests in Yucca Flat, Nevada. (a) Galena test. (b) Divider test. See figure 3a for locations of the two interferograms.

CONCLUSIONS

InSAR is being used to map the magnitude of land-surface displacement over large areas at a high level of spatial detail and a high degree of measurement resolution: such mapping has been used successfully in the Santa Clara Valley, Calif., and for Las Vegas Valley and Yucca Flat, Nev. Where land-surface displacement is the result of ground-water-level changes, the InSAR maps (interferograms), in conjunction with other hydrogeologic data, have been used to characterize the aquifer systems.

In conjunction with other hydrogeologic data the interferograms have been used to document elastic and inelastic deformation within aquifer systems at seasonal and multiyear time scales. The interferograms have been used to better define the heterogeneity of aquifer systems, including the distribution of compressible sediments and the presence of geologic features controlling ground-water flow and land-surface displacement. Storage properties, which typically are difficult to measure in the field, costly to measure in the laboratory, and largely unrepresentative because of the limited spatial extent of the measurements, can be calculated using InSAR data and accurately measured water levels. Information gained from interferograms can improve conceptual models of aquifer systems and better constrain numerical models of ground-water flow and aquifer-system deformation. For areas where additional ground-water-level, land-surface-elevation, subsurface-compaction, or other environmental data are needed, interferograms can be used as a guide for designing appropriate monitoring networks. The identification, characterization, and monitoring of regions susceptible to the land subsidence that accompanies ground-water-level declines, afforded by InSAR, should provide valuable information to water-resources managers who attempt to manage aquifer systems within optimal limits.

Use of InSAR to Identify Land-Surface Displacement and Aquifer-System Compaction, Paso Robles Area, California

By Jill N. Densmore[1], Devin L. Galloway[1], *and* David W. Valentine[2]

Abstract

Steady population growth and land-use conversion from dry farming and grazing to irrigated vineyards and urban development has increased the water demand in the Paso Robles area. Increased ground-water pumping to meet the demand has resulted in seasonal water-level declines that have raised concerns about potential land subsidence related to aquifer-system compaction. Spaceborne InSAR was used to reveal land-surface displacements and identify potential differential aquifer-system compaction related to geological structures or variably compressible sediments. This information can be used to enhance the conceptualization of the hydrologic system and constrain the calibration of ground-water-flow models.

INTRODUCTION

Spaceborne InSAR provides a cost-effective means of remotely sensing detailed land-surface displacement over broad areas. InSAR interferograms, created by differencing the phases from two SAR images obtained at different times, show change in the distance between the land surface and the satellite and can be viewed as a spatially detailed displacement map. A brief discussion on how InSAR works and how the mapped displacements are scaled onto repeating color fringes is presented in the paper by Bawden and others (p. 81 of these proceedings). Previous studies (Galloway and others, 1998; Amelung and others, 1999; Bawden and others, 2001; Hoffman and others, 2001) in other ground-water basins have shown that the interferogram can reveal subcentimeter-level vertical land-surface displacement.

Background

The Paso Robles area is about 230 mi northwest of Los Angeles, Calif. (fig. 1). The main water-bearing units in the area are Quaternary alluvium and Quaternary/Tertiary continental sediments of the Paso Robles Formation. Several faults crossing the area are the Rinconada and La Panza Faults (fig. 2; Campion and others, 1983).

APPROACH

InSAR was used to identify land-surface displacements associated with ground-water level declines and possible differential compaction. From the patterns of differential displacements, some insight can be gained into the shape and location of subbasin boundaries that are typically related to the presence of geological structures, such as faults, or facies changes that control the distribution of compressible sediments (Galloway and others, 1998; Amelung and others, 1999; Bawden and others, 2001). Seasonal and longer-term changes in ground-water levels in the Paso Robles area were compared to interferograms of the area to detect the presence of subsidence owing to aquifer-system compaction. Subsidence can include both elastic (recoverable) and inelastic (permanent) compaction.

METHODS

For this study, SAR data from the European Remote Sensing satellites ERS–1 and ERS–2 were used to create 5-, 7-, 15-, and 20-month interferograms, using techniques described by Zebker and others (1994), Peltzer and Rosen (1995), Peltzer and others (1996), and Galloway and others (1998). Only the 5-month image (fig. 2) from March 28 to August 15, 1997, showed coherent phase signatures that warranted further examination.

[1] U.S. Geological Survey, Sacramento, Calif.

[2] Davidson Library, Map and Imagery Laboratory, University of California, Santa Barbara, Calif.

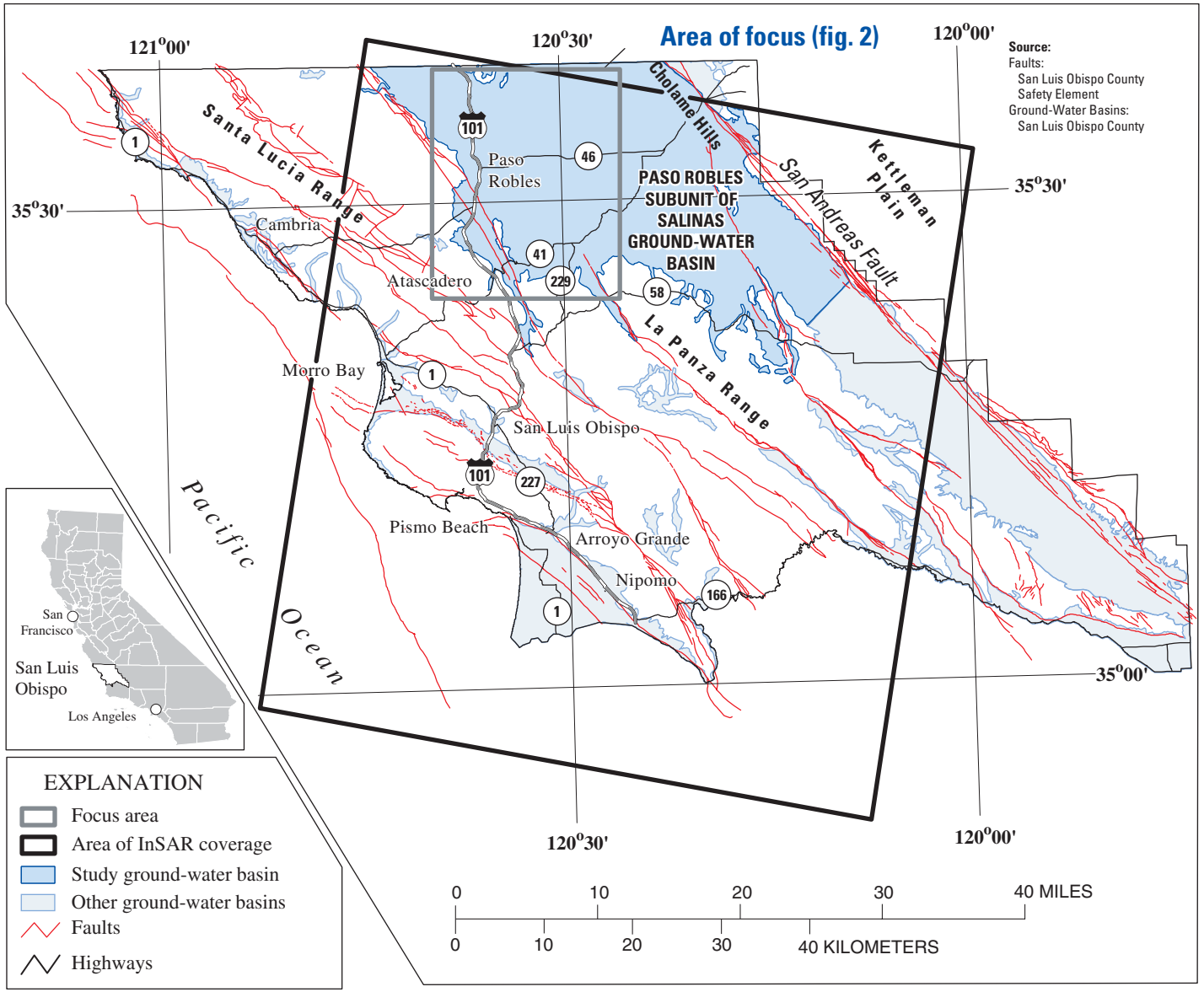

Figure 1. Paso Robles area, California.

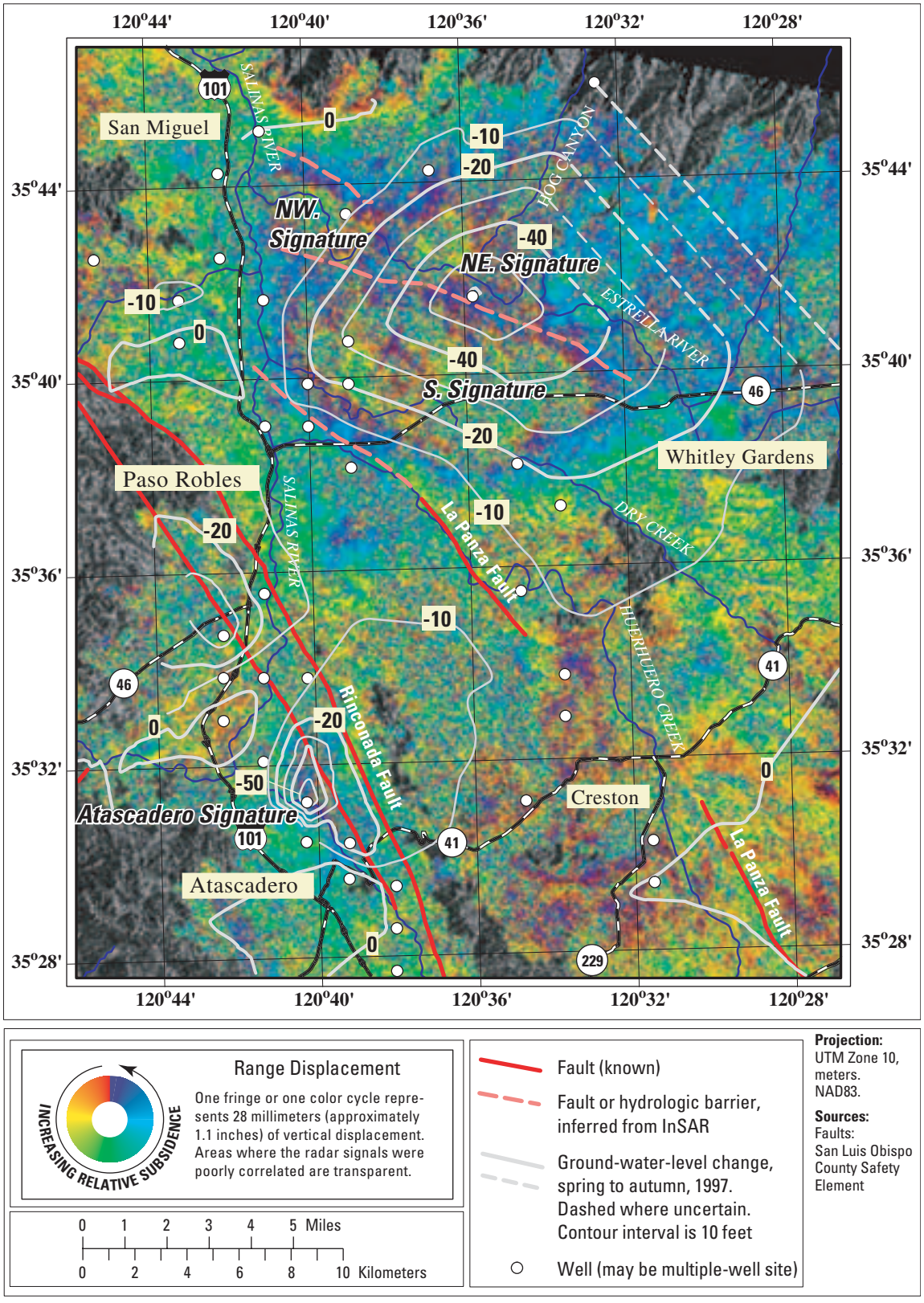

Figure 2. InSAR image of the Paso Robles region with seasonal ground-water-level change for spring to autumn, 1997.

A comparison was made with ground-water-level change between spring and autumn of 1997 (fig. 2).

Findings

The 5-month interferogram shows land-surface displacement during the summer pumping season in two main areas. Four distinct interferometric signatures in these two areas indicate that subsidence occurred and that three of the subsiding areas roughly correspond with areas of seasonal water-level decline indicating aquifer-system compaction due to ground-water withdrawal. Three of the signatures from an area northeast of Paso Robles show a relative land-surface change of about 2 in. These three signatures coincide with an area of seasonal water-level declines as great as 62 ft. The south signature is subparallel to an extension of the La Panza Fault (Dibblee, 1974). The northwest and northeast signatures may be separated from the south signature in the Paso Robles area by a ground-water-flow barrier, other geologic boundary, or an irregular distribution of pumping occurring between the signature areas. The Atascadero signature, located south of Paso Robles, shows relative subsidence of about 1 in. and coincides with an area of seasonal water-level declines as great as 54 ft. This area is bordered by the San Marcos Fault and might act as a hydraulic or tectonic boundary. It is unknown if the subsidence identified by InSAR is permanent or recoverable. No previous subsidence has been identified in these areas.

DISCUSSION

InSAR-derived displacement maps can reveal subsiding areas and previously unidentified boundaries, providing information that can be used to enhance the conceptualization of the hydrologic system and to constrain parameter estimation and calibration of coupled ground-water-flow and aquifer-system compaction models. The sense and magnitude of the displacements can be used to determine key parameter values governing compaction and the release from or uptake to storage of ground water in compressible interbeds and confining units (Hoffmann and others, p. 103 of these proceedings).

Inverse Modeling of Regional Aquifer-System Compaction Based on Land Subsidence Measurements, Antelope Valley (Mojave Desert), California

By Jörn Hoffmann[1], Devin L. Galloway[2], *and* Howard A. Zebker[1]

Abstract

Observations of land subsidence from repeatedly surveyed benchmarks and InSAR-derived displacement maps are used to calibrate spatially-varying time constants and storage coefficients for interbeds within the aquifer system in Antelope Valley, California. A previously calibrated ground-water-flow and subsidence model was modified to account for the delayed drainage of thick, slowly draining, compressible fine-grained deposits—interbeds. The observed subsidence cannot be satisfactorily explained without explicitly accounting for delayed compaction caused by slowly equilibrating fluid pressures in thick, compacting interbeds. The observed subsidence patterns reflect both the spatial distribution of drawdowns and the spatially-varying storage coefficients. In Antelope Valley, subsidence observations over long time periods are necessary to constrain the large time constants (tens of years) associated with the compaction of the thick, compressible interbeds. Thus, the usefulness of the InSAR observations, which in this study covered only a 3-year time period, is limited in determining these time constants. This problem will be alleviated as more synthetic aperture radar acquisitions become available in the future or where time constants are small. The inelastic storage coefficients that best reproduce the observed land subsidence show significant spatial variations. The most important limitation of the approach presented here is the potential error in the poorly constrained, simulated drawdowns that bias the resulting parameter estimates.

INTRODUCTION

Land subsidence caused by the compaction of susceptible aquifer systems has been linked to the development of ground-water resources and the accompanying ground-water-level declines (Tolman and Poland, 1940; Riley, 1969; Poland and others, 1975; Poland and Ireland, 1988; Holzer, 1984; Holzer and others, 1979; Bell and Price, 1993; Ikehara and Phillips, 1994; Galloway and others, 1998). With the advent of InSAR techniques, the extent of land-surface deformations caused by ground-water pumpage have become more easily observed and quantified in spatial detail. Previous investigations have detected and mapped land subsidence using InSAR interferograms (Galloway and others, 1998; Amelung and others, 1999). More recently, InSAR has also been used to determine storage coefficients for elastically deforming aquifer systems (Hoffmann and others, 2001) and to define structural geologic controls on aquifer systems (Bawden and others, 2001; Lu and Danskin, 2001). Many studies have used historical subsidence data obtained from borehole extensometers (for example Helm, 1975, 1976; Nelson, 1982; Epstein, 1987; Hanson, 1989; Heywood, 1995, 1997; Sneed and Galloway, 2000; Pavelko, p. 57 of these proceedings; Pope and Burbey, p. 49 of these proceedings), and repeat surveys of benchmarks (Williamson and others, 1989; Hanson and Benedict, 1994; Nishikawa and others, 2001; Kasmarek and Strom, 2002; Leighton and Phillips, 2003) to calibrate ground-water-flow and subsidence models. No work to date has attempted to use InSAR-derived land subsidence data to model regional ground-water flow and aquifer-system compaction.

[1] Department of Geophysics, Stanford University, Stanford, Calif.

[2] U.S. Geological Survey, Sacramento, Calif.

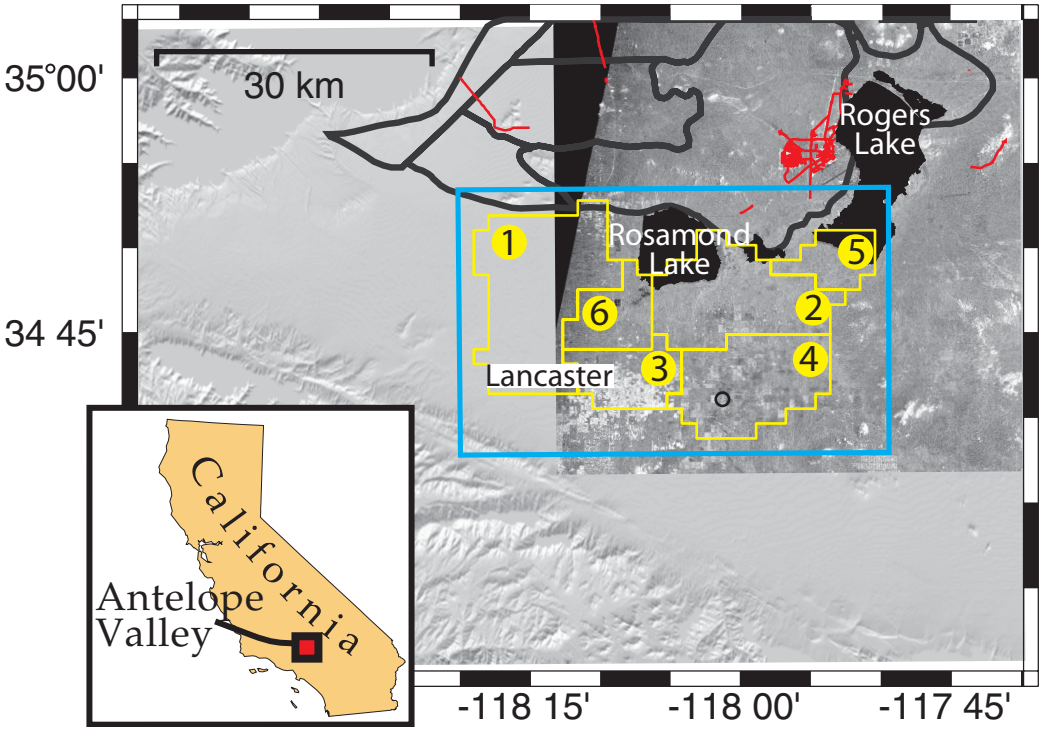

Figure 1. Location map, Antelope Valley, California. The blue frame encloses the area shown in figures 3 and 4. The radar amplitude image covers the area within the model region that is covered by the interferograms. Major roads (red) and the playas (dry lakes) are shown for reference. The bold black lines delineate ground-water subbasins defined by Bloyd (1967). The black circle indicates the location where data shown in figure 2 was obtained. The yellow lines delineate the six parameter zones used in the estimation of the time constants.

Antelope Valley is a topographically closed basin about 80 km northeast of Los Angeles, Calif. The sedimentary basin is bounded by mountain ranges to the northwest and southwest and by lower hills to the east. The structural basin has been filled to depths of 1 km or more with fluvial and lacustrine sediments, forming the aquifer system that now provides much of the water supply for agricultural irrigation and the growing communities in the valley. The valley floor has little topographic relief and is dominated by two large playas, Rosamond Lake and Rogers Lake.

Bloyd (1967) conceptually subdivided the basin into many ground-water subbasins based mostly on geologic structure (fig. 1). The largest and most important subbasin in terms of ground-water pumpage and land subsidence is the Lancaster subbasin. In early studies the aquifer system was divided into a principal (unconfined) aquifer and a mostly confined deep aquifer (Durbin, 1978). In a large part of the Lancaster subbasin the two aquifers are separated by a laterally extensive lacustrine clay unit that extends from south of Rogers Lake, where it is very close to the land surface, down dip to the southwest. Where the lacustrine clay is present, it acts as a confining unit for the underlying deep aquifer.

Recent studies (Sneed and Galloway, 2000; Nishikawa and others, 2001; Leighton and Phillips, 2003) use additional data to define three aquifers, the upper, middle, and lower aquifer. The middle and lower aquifers combined represent the deep aquifer in earlier studies, and the upper aquifer represents the principal aquifer. An important conceptual difference between these two representations of the aquifer system is that earlier studies consider the unconfined principal aquifer the most productive aquifer. Recent studies consider the upper aquifer as generally unproductive with most water produced from the confined middle aquifer. Low-permeability interbeds of varying thickness of fine-grained deposits are interspersed throughout all three aquifers. Owing to increasing overburden stress (geostatic load) with depth of burial, these deposits are more consolidated at depth; the shallower deposits are relatively less consolidated and thereby more

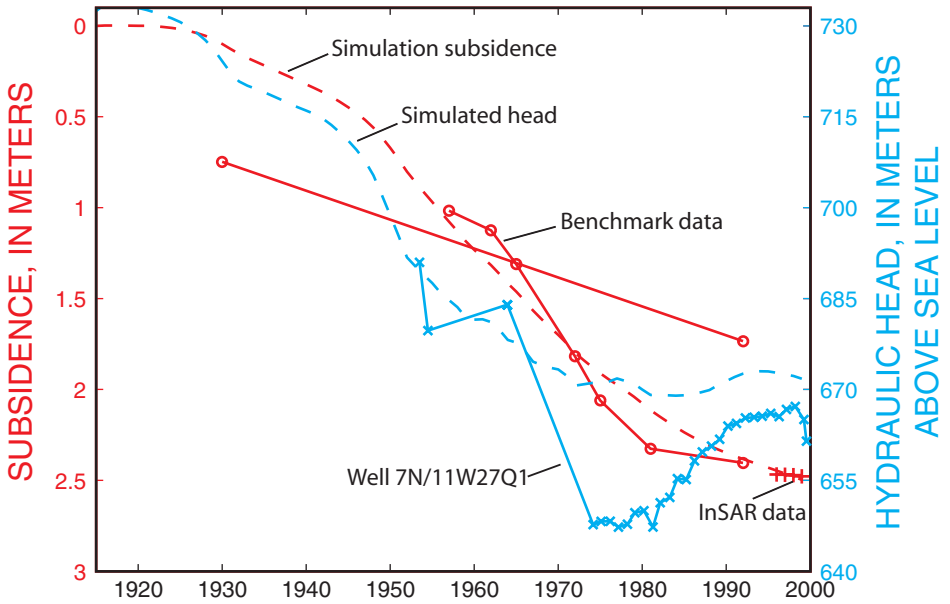

Figure 2. Measured and simulated head and subsidence values in model layer 2 at the location marked by the black circle in figure 1. The measured head values shown as blue x's are observations from a well near the indicated location. The subsidence values shown as red circles are the kriged subsidence values, determined from repeat surveys at benchmarks near that location. The kriged values derived from the estimated subsidence between 1930–92 are shown separately from the other subsidence values, because they are much less reliable. The red pluses are the subsidence values derived from the interferograms at that location. The dashed lines indicate simulated heads (blue) and subsidence (red).

compressible. A more detailed description of this study is published in Hoffman and others (2003).

DELAYED COMPACTION

In aquifer systems containing thick, compressible interbeds with low vertical hydraulic conductivity, the equilibration of pore-fluid pressures within the interbeds lags the head declines in the surrounding aquifers. Most investigations of land subsidence to date have ignored these delays. However, because a significant part of the land subsidence may be due to compaction occurring within these thick interbeds, in many cases it is important to account for the effect of delayed dissipation of the residual, excess pore-fluid pressures within these units with respect to the fluid pressures in the surrounding, hydraulically stressed aquifers—the coarser-grained, more permeable deposits within the aquifer system. (Pore-fluid pressure (p) is related to hydraulic head (h) by Z, where Z is the elevation head referenced to an arbitrary datum. Water levels measured in wells open to the atmosphere typically are used to determine hydraulic heads in aquifer systems and generally are a measure of the heads in the more permeable aquifers in the aquifer system.) Figure 2 shows that subsidence is observed despite recovering water levels in at least part of the valley. Although the water levels ceased declining by 1975 and then recovered many meters after 1980, subsidence continues as observed in both the benchmark and InSAR data. This cannot be explained without a time-delay between the measured hydraulic head in the aquifer and the head in the interior of compacting interbeds.

The delayed dissipation of residual, excess pore-fluid pressures from interbeds can be simulated in MODFLOW (McDonald and Harbaugh, 1988) with the Interbed Storage 2 (IBS2) package developed by Leake (1990). This package has been released for use with MODFLOW–2000 (Harbaugh and others, 2000) as the subsidence (SUB) package (Hoffmann and others, in press). The package is based on the Terzaghi (1925) theory of one-dimensional consolidation (the process of consolidation, whether expansion or compression, is referred to herein as compaction, where compression or decreasing thickness is positively signed, and expansion

is negatively signed). For stresses (measured as changes in hydraulic head) greater than the preconsolidation stress, the compaction of a single interbed can be written as

$$s(t) = S_{kv} \bullet \Delta h \bullet \left(1 - \frac{8}{\pi^2} \sum_{n=0}^{\infty} \frac{\exp\left(-\frac{\pi^2}{4} \frac{t}{\tau_n} \right)}{(2n+1)^2} \right), \quad (1)$$

where

$$S_{kv} = b_0 \bullet S_{skv}, \quad (2)$$

where

S_{kv} is the inelastic skeletal storage coefficient of the interbed,

b_0 is the thickness of the interbed,

S_{skv} is the inelastic skeletal specific storage,

Δh is the step change in hydraulic head of the surrounding aquifer,

t is time,

n is the index for the infinite series, and

τ_n is

$$\tau_n = \frac{\left(\frac{b_0}{2}\right)^2 S_{skv}}{K_v (2n+1)^2}, \quad (3)$$

where

K_v is the vertical hydraulic conductivity of the interbed.

The quantity $\tau = \tau_0$ is the time constant of the interbed.

Helm (1975) used an equivalent thickness of interbeds,

$$b_{equiv} = \sqrt{\frac{1}{N} \sum_{i=1}^{N} b_i^2}, \quad (4)$$

to represent the time constant of a system of N interbeds, where b_i is the thickness of the i^{th} interbed.

Using b_{equiv} in equation 3 results in one time constant for the entire aquifer system containing the N interbeds. Note, however, that b_{equiv} cannot be used to compute the total inelastic skeletal storage coefficient from equation 2. Instead the inelastic skeletal storage coefficient for all the N interbeds is

$$S^*_{kv} = S_{skv} \sum_{i=1}^{N} b_i, \quad (5)$$

where the asterisk denotes the property for all interbeds in the aquifer system. In this study it was assumed that S_{skv} is the same for all interbeds. From equation 4, it follows that b_{equiv} is always greater than the largest b_i and less than the cumulative interbed thickness, $\sum_{i=1}^{N} b_i$. The case $b_{equiv} = b_1$ is the limiting case for $N = 1$.

APPROACH

A previously calibrated ground-water-flow and subsidence model of Antelope Valley (Leighton and Phillips, 2003) was modified to improve the simulated land subsidence by modifying the way interbed storage was represented. The IBS2 package was used instead of the IBS1 package (Leake and Prudic, 1991) used in the Leighton and Phillips (2003) model. The IBS2 package simulates transient movement of water from or into interbed storage, rather than an instantaneous release from or uptake to storage in the interbeds corresponding to a step decrease or increase of hydraulic head in the surrounding aquifer, as is simulated in the IBS1 package. The IBS2 package, therefore, simulates the more realistic, time-dependent compaction owing to the slow dissipation of pore fluid from thick interbeds. The storage properties assigned to the interbeds were determined by the parameter estimation scheme described below. Historical subsidence measurements from repeat surveys of sparsely distributed benchmarks (Ikehara and Phillips, 1994) and more recent, spatially-detailed InSAR measurements were used to constrain a nonlinear regression for spatially-variable estimates of the time constants, τ, and inelastic storage coefficients, S^*_{kv}, of the compacting interbeds using the general-purpose parameter estimation code, UCODE (Poeter and Hill, 1998).

The original model developed by Leighton and Phillips (2003) is based on a grid that extends 97 km (60 mi) from west to east and 69 km (43 mi) from south to north. The modeled area is shown in figure 1. Three model layers are used to simulate ground-water flow.

Stresses on the aquifer system are caused by hydraulic-head variations related to ground-water pumping from the top two model layers. The simulation of aquifer-system compaction is limited to the upper two model layers, as deeper interbeds are generally far more consolidated and thus less compressive.

Observational Constraints

Twenty-two interferograms were formed from 17 SAR scenes acquired by the European Space Agency ERS-2 satellite between January 26, 1996, and May 1, 1999. Of these interferograms, 13 were combined (stacked) to create three composite images measuring subsidence from about January of each of the years 1996, 1997, and 1998 to the beginning of the reference year 1999. Each of the composite images was created from 3 to 6 individual interferograms, thereby significantly reducing noise and the effects of atmospheric signal contributions that are random from one scene to another. Satellite-SAR data suitable for interferometry has been widely available since 1992. This time period proved too short to adequately characterize the delays between water-level decline and subsidence in parts of Antelope Valley. The InSAR observations can be simulated using a wide range of parameter values, therefore, it was not possible to constrain estimates of the time constants of the aquifer system, τ, using only InSAR observations. However, the InSAR data were used to help define appropriate zones of constant parameters within the model domain for the estimation of the time constants and to constrain the estimation of the spatially-varying inelastic skeletal storage coefficients.

There have been several benchmark leveling surveys in Antelope Valley conducted by different agencies and with various standards of precision. Ikehara and Phillips (1994) compiled a comprehensive dataset of subsidence values from various surveys. Their table 9 contains subsidence magnitudes for more than 250 benchmarks during the six time periods 1957–62, 1962–65, 1965–72, 1972–75, 1975–81, and 1981–92. These periods correspond to the dates of major spirit leveling surveys and a GPS survey in 1992. Ikehara and Phillips also provide an estimate for subsidence during 1930–92 for 195 benchmark locations. This estimate is significantly less reliable than the observations from the measured time periods.

In order to better constrain the regression at different locations and to more easily assign relative weights to benchmark and InSAR observations, kriging was used to interpolate subsidence at locations away from the benchmarks for each of the seven time periods listed above. The number and spatial distribution of subsidence observations vary for the seven time periods listed above, limiting the area for which an interpolated subsidence value could be determined. The resulting subsidence maps for all but the estimated 1930–92 period are shown in figure 3. It is important to note, however, that the results of this interpolation do not afford the spatial detail that is suggested by the map presentation. Unlike the spatially-detailed InSAR displacement maps, the interpolation approach smooths localized subsidence changes caused by small-scale structure or localized head changes. Similarly, the resulting kriging map is biased by benchmarks sampling localized subsidence that is not necessarily representative for the surrounding areas.

Though drawdown data from observations in wells were used to calibrate the Leighton and Phillips (2003) model, in the model presented here, adjustments to the interbed storage did not significantly alter the simulated heads in aquifers. As such, it was not possible to improve upon the agreement between measured and simulated heads in the aquifers by varying the interbed storage parameters in the model. Therefore, the drawdown data were not used as observational constraints.

Parameterization

According to equations 1 and 5 the compaction in a system of interbeds owing to a step decrease in hydraulic head depends on the time constant, τ, and the inelastic skeletal storage coefficient of the aquifer system, S^*_{kv}. The time constant governs the timing of the compaction, and the storage coefficient affects the magnitude of compaction and governs how much water is released from interbed storage to the surrounding aquifers. The actual subsidence is essentially a convolution of the subsidence in equation 1 and the drawdown history in the aquifer, assuming, as was done here, that stress-dependencies of the time constant and storage coefficient are negligible.

Because different combinations of K_v, S_{skv}, and b_{equiv} result in identical time constants (equation 3), these parameters cannot be independently determined using only observations of hydraulic head and subsidence. Similarly, S_{skv} cannot be uniquely resolved from the measurement of cumulative compaction at the land surface and changes in hydraulic head. Therefore only the time constant, τ, and the inelastic skeletal storage

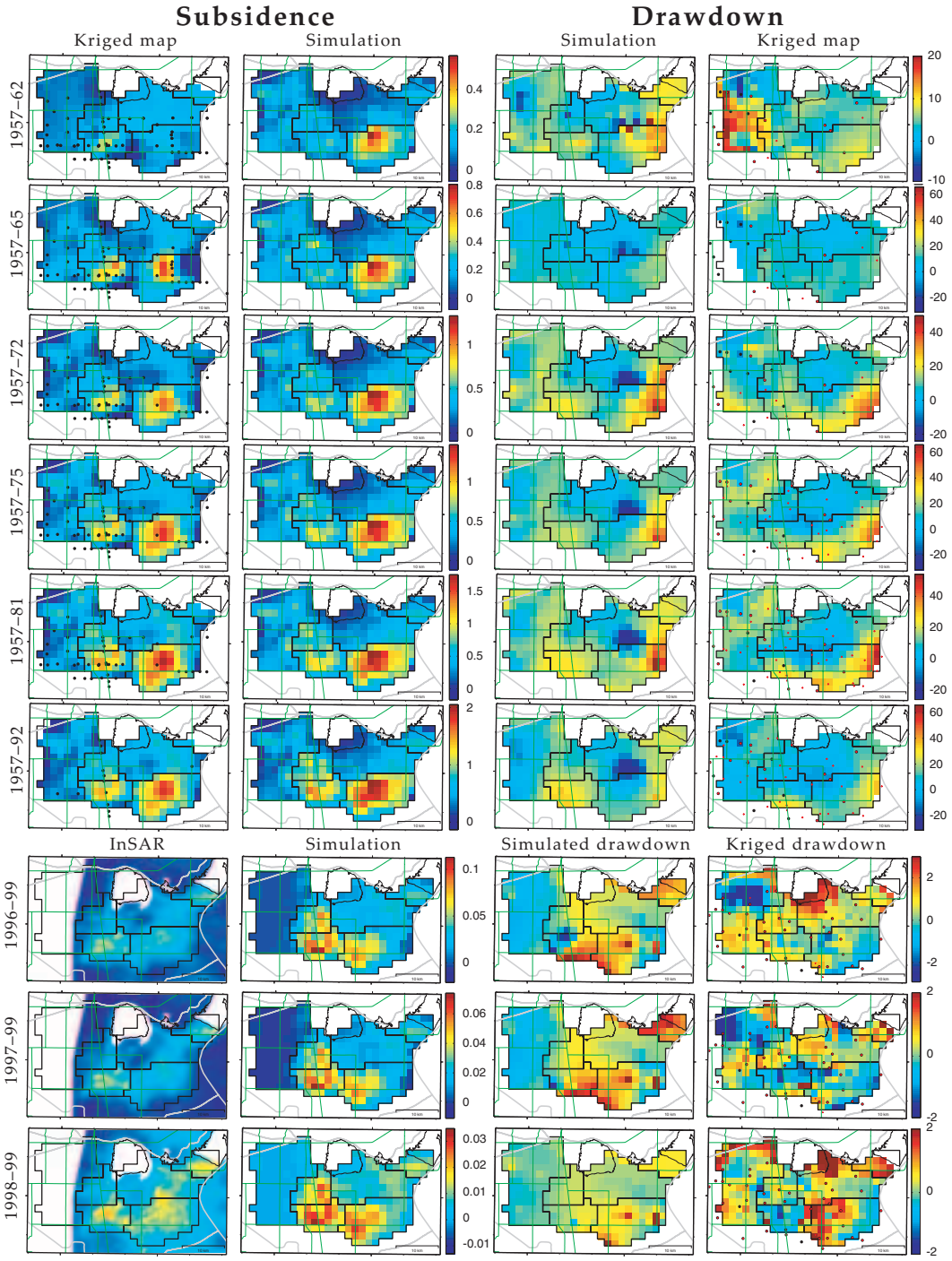

Figure 3. Comparison of simulated and kriged subsidence and drawdown values (in meters) for nine time periods. The first 6 rows correspond to the times of major repeat surveys of benchmarks. The last 3 rows show time periods covered by the composite interferograms. The columns show from left to right: 1. Subsidence values from kriging of available benchmark data (the solid black dots show locations of benchmarks) for the first 6 rows, and InSAR-derived displacements for the last 3 rows; 2. Simulated subsidence values corresponding to the final model-derived parameter values (fig. 4); 3. Simulated drawdowns in the second model layer; and, 4. Kriged drawdown maps based on selected wells in the area (the solid black and red symbols show the locations of observation wells used in kriging heads at the beginning and end of each time period, respectively).

coefficient of the aquifer system, S^*_{kv}, were estimated. Using independent estimates for the inelastic skeletal specific storage, S_{skv}, the S^*_{kv} estimates can be translated into the cumulative thickness of compressible sediments (equation 5).

ZONING AND PARAMETER ESTIMATION

Spatial gradients of hydraulic head and subsidence, measured by benchmark surveys and InSAR, indicate spatial heterogeneity of the skeletal storage coefficients within the aquifer system. InSAR-derived subsidence maps provide the spatially-detailed subsidence observations necessary to constrain spatially-variable parameter estimates. However, observations over time periods on the order of the time constants for interbed compaction are necessary to reliably estimate these time constants. The 3 years covered by the InSAR maps used in this study proved to be too short to estimate the time constants for inelastic deformation in Antelope Valley. Therefore, the estimation of the time constants using this model relied primarily on the benchmark leveling data, covering a large part of the century. Because the spatial detail afforded by the historical subsidence observations is limited, six zones (fig. 1) with separate time-constant parameters were defined in the model. These zones were based on a zonation of interbed storage by Leighton and Phillips (2003), which was modified slightly on the basis of spatially-variable subsidence observed in the InSAR images and initial regression results. The value of S^*_{kv} was allowed to vary for each of the 282 grid cells within the six parameter zones during the regression.

Estimating 282 storage coefficients and six time constants using nonlinear regression is computationally daunting. However, given the aquifer's head-decline history and a time constant, the subsidence is linearly related to the inelastic skeletal storage coefficient (equation 1). Although this is only approximately true in the presence of elastic deformation, it is a good approximation for interbeds, where the ratio of S_{skv} to S_{ske} (the elastic skeletal specific storage) is generally large. This recognition enabled the much more efficient two-step estimation procedure described in the following paragraph.

The general-purpose parameter estimation program UCODE (Poeter and Hill, 1998) was used to estimate the time constants in all six parameter zones. Within each UCODE iteration a linear weighted least-squares estimate of S^*_{kv} was obtained at each of the 282 grid cells using all available subsidence observations. Thus, up to 10 temporal subsidence observations were used for each location; three InSAR observations at cells within the area covered by the images and benchmark values for up to seven time periods. The observational-data covariance matrix (the weight matrix for the weighted least-squared estimation) varied spatially. The data variance used for the benchmark data was the kriging variance at the center of the grid cell. The smallest variance allowed for these data was the variance within 2.6 km^2 (1 mi^2) (using the variogram model). The off-diagonal elements of the data covariance matrix are the covariances between observations for different time periods. The subsidence observations for different time periods are correlated because subsidence is computed by differencing observations of land-surface elevations from subsequent leveling surveys. However, because of the high precision of leveling surveys, this covariance is negligible compared to the much larger kriging variances, which quantify the variance due to interpolation.

The variance of the InSAR-derived displacement maps is assumed to be 50 mm^2. Although this value is a somewhat subjective choice, it addresses an attempt to include two separate error sources. The first error is the measurement variance, assumed to be at the level of about 25 mm^2 in the composite images. The second error is due to the averaging of all InSAR observations within a model grid cell. The median observation may not be the best representation of the subsidence value for the grid cell. A variance of 25 mm^2 was subjectively assigned to this effect. The data covariance was also accounted for because all three InSAR-derived maps share one reference year (1999).

The vertical hydraulic conductivity, K_v, of the interbeds and the inelastic skeletal specific storage, S_{skv}, were assumed constant over the entire model domain and equal to the values determined by Sneed and Galloway (2000, table 3) at a borehole extensometer, the Holly site, south of Rogers Lake. Using these values, the equivalent thickness, b_{equiv}, of the compacting interbeds can be computed from the estimated time constants. As mentioned above, b_{equiv} is by definition less than or equal to the cumulative interbed thickness. At model cells where the estimated S^*_{kv} corresponded to a cumulative thickness smaller than the equivalent thickness of the interbeds (determined by the time constant), the time constant was reduced slightly at that location and the linear estimation repeated, until the resulting

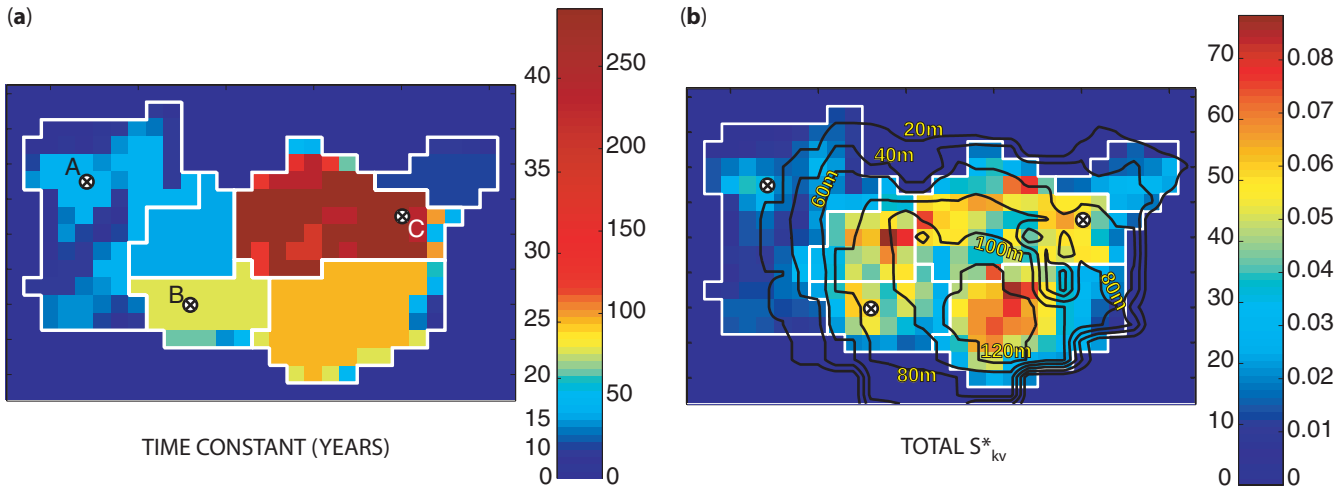

Figure 4. Final model-derived parameter values for (a) time constants, and (b) inelastic skeletal storage coefficients of interbeds, S^*_{kv}. The labels on the left-hand side of the left colorscale show the equivalent thicknesses (in meters) corresponding to the time constants (equation 3). The labels on the left-hand side of the right colorscale show the cumulative thickness (in meters) of all interbeds computed using an inelastic skeletal specific storage of 1.148 x 10^{-2} m^{-1}. The labels on the right-hand side of the colorscales are the time constants (in years) and S^*_{kv}, respectively, in (a) and (b). The time constants are not strictly constant within each parameter zone because a constraint that the total storage must amount to at least the equivalent thickness, b_{equiv} (determined from the resulting time constant), using S_{skv} = 1.148 x 10^{-2} m^{-1} and K_v = 4.233 x 10^{-11} m·$s^{-1}$was enforced. The black contours on the right show the thickness and distribution of the lacustrine clay unit as mapped by Durbin (1978). The locations of the curves in figure 5 are marked by the ⊗.

cumulative interbed thickness was greater than or equal to the equivalent thickness. This explains why the time constants shown in figure 4a are not strictly constant within each zone.

Table 1. Time constants and nonlinear confidence intervals estimated with UCODE for six parameter zones in the model. The confidence intervals are larger where fewer measurements at benchmarks are available to constrain the subsidence history (for example, zone 2)

Zone	τ (years)	95-percent confidence interval (years)
1	40.8	[38.3, 43.5]
2	284.9	[207.8, 550.3]
3	77.3	[73.1, 81.6]
4	94.7	[91.4, 97.7]
5	20.5	[10.2, 30.7]
6	39.1	[29.0, 49.3]

RESULTS

The estimated time constants are shown in figure 4a and table 1. Values range from 3 to 285 years, which correspond to an equivalent thickness between 3.8 and 36.4 m assuming an inelastic skeletal specific storage of 1.148×10^{-3} m^{-1}.

The resulting spatially-variable inelastic skeletal storage coefficient for the interbeds, S^*_{kv}, is shown in figure 4b. Values range from zero at the boundaries of the simulated domain to a maximum value of about 9×10^{-2} in zone 6.

The estimation variance computed in the linear estimation of the storage coefficients varies spatially. These variations reflect observational-data variances and the goodness of fit. They do not include any uncertainties related to the simulated heads used in the regressions and subsidence simulation. The final parameter estimates result in the subsidence histories shown in the second column of figure 3. They are compared to the kriged subsidence maps for the corresponding time periods. The simulated drawdowns driving the simulations and kriged maps of drawdowns from a number of

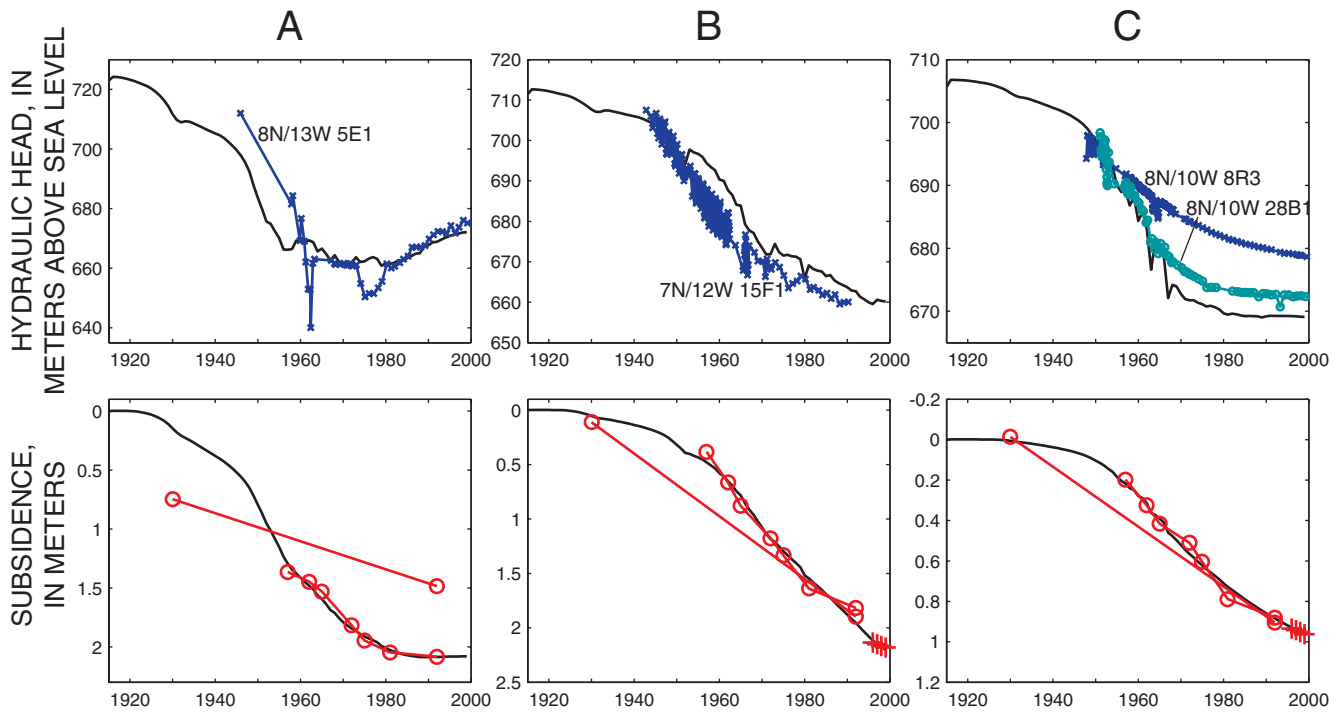

Figure 5. Measured and simulated head and subsidence values for the three locations (A–C) indicated in figure 4. The black curves show the simulated heads, and the blue and green lines correspond to nearby water-level observations. In the subsidence plots the black line shows the simulated results, the red circles denote measurements at benchmarks, and the red pluses denote InSAR-derived subsidence measurements. An offset has been added to the differential subsidence observations to better compare them to the simulations. The 1930–92 subsidence estimate from Ikehara and Phillips (1994) is shown independently of the shorter measured time intervals because of its much higher uncertainty. A separate arbitrary offset has also been added to this estimate.

observation wells in the study area are shown for reference. The simulated subsidence is also compared with the observational-data constraints for three locations in figure 5.

The simulated subsidence for the final parameter values (fig. 3) captures the main subsidence patterns and the timing of the subsidence. However, important differences remain and highlight the weaknesses of the approach presented here. Particularly, comparison of simulated and measured subsidence for the relatively short time periods spanned by the InSAR images (bottom three rows in fig. 3) clearly indicates that the simulation cannot adequately reproduce short-term subsidence.

DISCUSSION

The resulting parameter estimates reflect the spatial heterogeneity of interbed storage in the aquifer system, resulting in a spatially-varying distribution of subsidence caused by large-scale declines, both in magnitude and distribution, of hydraulic head. The observed subsidence is not solely an expression of spatially-variable drawdowns, but clearly represents the spatially-variable skeletal storage coefficients of the interbeds.

Though the simulation reproduces the main subsidence features over the long term, short-term subsidence features are not adequately reproduced. This observation points to the most important problem in estimating the storage parameters and interpreting the results, namely the uncertainty of the simulated heads that drive the subsidence simulation. The parameter estimates are strongly biased where the simulated heads are unrepresentative of heads in the aquifers surrounding the interbeds. Replacing simulated heads with measured heads is not a reasonable alternative because reliable head-measurement data are scarce and would have to be extrapolated spatially and temporally to

provide the necessary inputs for the subsidence simulation, adding yet another similar and likely larger element of uncertainty. It was beyond the scope of this study to improve on the simulated hydraulic heads. Nevertheless the results represent important physical properties of the aquifer system. The modifications to the original Leighton and Phillips (2003) model lead to a very large improvement in the accuracy of the simulated subsidence both in magnitude and distribution.

The contour lines in figure 4b show the thickness of a lacustrine clay unit that confines the deep aquifer in parts of the valley (Durbin, 1978). The correlation between the thickness of the confining unit and the distribution of model-estimated S^*_{kv} can be clearly seen. It is likely that some, possibly even most, of the observed subsidence is realized by compaction of the confining unit and not in interbeds as simulated. Compaction of the confining unit was not simulated in the Leighton and Phillips (2003) model, nor in the model reported on here. In a separate, one-dimensional simulation of aquifer-system compaction at the Holly site (south of Rogers Lake), Sneed and Galloway (2000) computed time constants of less than 1 year for aquitards less than 5.5 m thick and a time constant of about 60 years for a 19.2-m-thick aquitard. The time constant they computed for a 20.1-m-thick confining unit, which accounted for 31 percent of the subsidence in their historical simulation (before 1991), was 350 years. In comparison the time constants determined in this study (3 to 285 years) seem relatively large, likely owing to slow compaction occurring in the confining unit, which in the regression is attributed to the interbeds. Another possible explanation for the fairly large time constants estimated in this study is that the simulated drawdowns in the aquifers are not sufficiently representative of the actual drawdowns at the interfaces between the compacting interbeds and the aquifers that drive interbed compaction. Unfortunately, the vertical distribution of hydraulic head in the aquifer system is generally not well known and therefore poorly constrained in groundwater-flow models. Furthermore, the historical development of the head declines is difficult to assess accurately from the available head observations that are typically derived from wells open to multiple aquifers. Because these historical head declines affect the simulated subsidence, any error in the assumed head-decline history will bias the estimates of time constants (and consequently the estimate of storage coefficients). This bias could be either an overestimation or underestimation, depending on the difference between the actual and simulated hydrographs.

The InSAR data were helpful in mapping recent subsidence and defining the parameter zones, but their importance for determining the time constants was limited by the short period of time spanned by InSAR acquisitions. InSAR has been used successfully to estimate elastic storage coefficients (Hoffmann and others, 2001) in areas undergoing predominantly elastic deformation, where heads are above the preconsolidation stress and time delays in the equilibration of pore-fluid pressures in the interbeds are small. As more SAR data become available in the future, interferograms covering longer time periods could replace the benchmark data used in this study and would provide a more complete subsidence dataset—both in space and time—likely providing more robust parameter estimates.

SUMMARY AND CONCLUSIONS

Land subsidence measurements from repeat surveys of benchmarks and InSAR data were used to derive spatially-varying estimates for the inelastic skeletal storage coefficient, S^*_{kv}, and time constants of thick interbeds in the Antelope Valley aquifer system. An inverse approach was used to estimate S^*_{kv} at 282 locations in a model of ground-water flow and aquifer-system compaction (using MODFLOW with the IBS2 package). An independent estimate of the inelastic skeletal specific storage, S_{skv}, obtained from a previous study was used to compute the cumulative interbed thickness in each zone based on the model-derived S^*_{kv}.

The estimated time constants, typically on the order of tens of years to more than 200 years, were larger than expected and, in part, might be biased by simulated heads used in the regressions that are potentially unrepresentative of the true distribution of hydraulic head. The available head observations were temporally and spatially inadequate to constrain the simulated head distribution.

The model-derived S^*_{kv} and time constants reproduced the observed timing and distribution of subsidence in Antelope Valley. The simulation more accurately reproduced the subsidence observations over longer time periods, which can be explained by the fact that short-term fluctuations of aquifer hydraulic head are not reproduced as adequately as the long-term trends.

Owing to the limited temporal coverage of satellite SAR data and the large time constants of interbeds in Antelope Valley, the use of InSAR to estimate interbed time constants presently is limited. However, as more SAR data become available in the future, the role of the spatially-detailed InSAR-derived displacement maps in the characterization of aquifer-system properties governing compaction and resulting land subsidence is likely to increase.

Land Subsidence in Las Vegas Valley, Nevada: Evolution, Spatial Patterns, and Rates Through 2000

By John W. Bell[1] *and* Falk Amelung[2]

Abstract

Land subsidence in Las Vegas Valley, Nevada, has been geodetically monitored since 1935, and several generations of maps have depicted more than1.7 meters of total subsidence. New geodetic data reveal insights into the spatial distribution and magnitude of subsidence through 2000. In particular, InSAR and GPS studies demonstrate that subsidence is localized within four bowls each bounded by Quaternary faults. Conventional level-line surveys across the faults further indicate that these spatial patterns have been present since at least 1978, and on the basis of the new geodetic data a revised map showing subsidence during 1963–2000 has been developed.

An analysis of subsidence rates based on conventional, InSAR, and GPS data indicates that rates have significantly declined since 1991. Ground-water-use data indicate that the rate decline in large part is caused by an artificial recharge program which injects as much as 3.4 cubic kilometers of water per year into the aquifer system. The rates in the northwestern part of the valley have declined from more than 5 to 6 centimeters per year to about 2.5 to 3 centimeters per year, a reduction of 50 percent; in the central and southern parts of the valley, rates have declined from about 2.5 centimeters per year to only a few millimeters per year, a reduction of more than 80 percent. An additional effect of the recharge program has been the seasonal rebound (uplift) of some areas undergoing intensive recharge.

INTRODUCTION

Las Vegas Valley is located in a structurally controlled alluvial basin containing hundreds of meters of unconsolidated sediment of Pliocene through Holocene age. Coarse-grained (sand and gravel) alluvial-fan deposits derived from the surrounding mountain ranges form broad piedmonts around the periphery of the valley, and predominantly fine-grained (silt and clay) compressible deposits underlie the central part of the valley (fig. 1).

Intercalated sequences of both coarse- and fine-grained deposits within the basin constitute the principal aquifers from which nearly all ground water is pumped. Impermeable caliche horizons within the alluvial-fan deposits and poorly permeable clay horizons within the fine-grained basin fill create confined and semiconfined aquifer conditions and artesian heads and flowing artesian wells in a few locations. A series of north- to northeast-trending, east-dipping Quaternary faults cut the valley floor creating a succession of prominent scarps as much as 50 m high.

Las Vegas was the fastest growing metropolitan area in the United States during 1990–2000. The growth rate was 62 percent, and the population increased from 852,000 to more than 1.3 million according to the 2000 U.S. Census. It is located in a 1,300-km^2 alluvial valley in southern Nevada that receives from 12 to 20 cm average annual precipitation, producing average natural recharge originally estimated to be in the range of 3.1 to 4.3 km^3/yr (Maxey and Jameson, 1948). Ground water has supported development in Las Vegas since 1905 when the first wells were drilled, and by the late 1960s, ground-water withdrawals had increased to more than 10.8 km^3/yr. Beginning in 1972, ground-water resources were

[1] Nevada Bureau of Mines and Geology, University of Nevada, Reno, Nev.

[2] Hawaii Institute of Geology and Physics, University of Hawaii, Honolulu, Hawaii

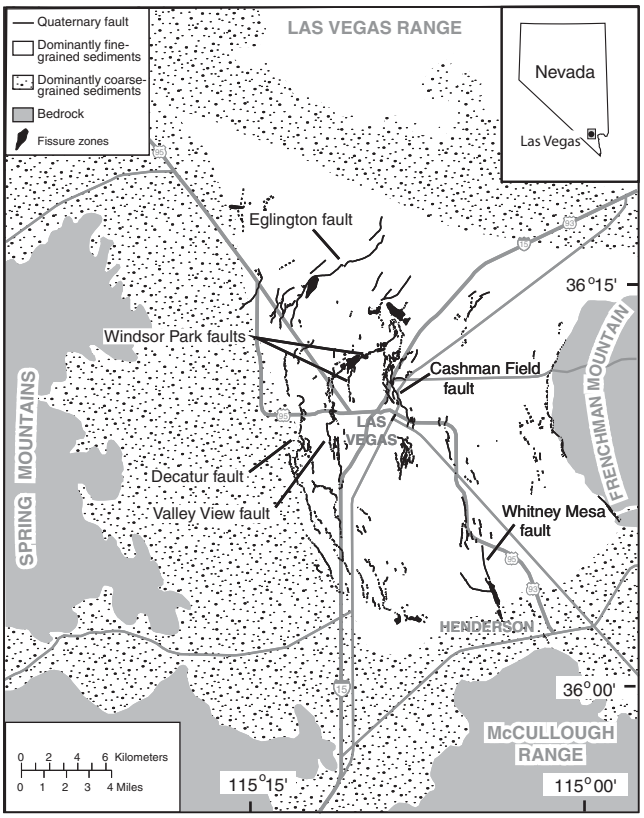

Figure 1. Distribution of fine- and coarse-grained deposits and location of principal Quaternary faults, and earth fissures in Las Vegas Valley.

supplemented with as much as 43 km^3/yr of imported water from the Colorado River, which provides for the continuing population growth in the area. Since the 1970s, however, withdrawals have remained between 7.4 and 9.3 km^3/yr, consistently exceeding estimated natural recharge by a factor of about two. These withdrawals have resulted in long-term depressurization of the aquifer system, regional decline of water levels, development of earth fissures, and more than 1.7 m of land subsidence.

SUBSIDENCE 1935–2000

Evolution and Spatial Patterns

On the basis of first-order-accuracy leveling of benchmarks established in 1935, early subsidence maps showed that as much as 60 cm of subsidence had occurred in the central part of Las Vegas Valley by 1963 (Malmberg, 1964). By 1980, surveys of the benchmarks indicated that subsidence had evolved from a singular central bowl to a broad valleywide bowl punctuated by three localized bowls each of which exhibited 60 to 78 cm of movement for the 1963–80 period (fig. 2; Bell, 1981b). The original Central bowl remained fixed near the downtown Las Vegas region, while the Northwest and Southern bowls developed in other parts of the valley affected by extensive ground-water withdrawals occurring since the early 1960s.

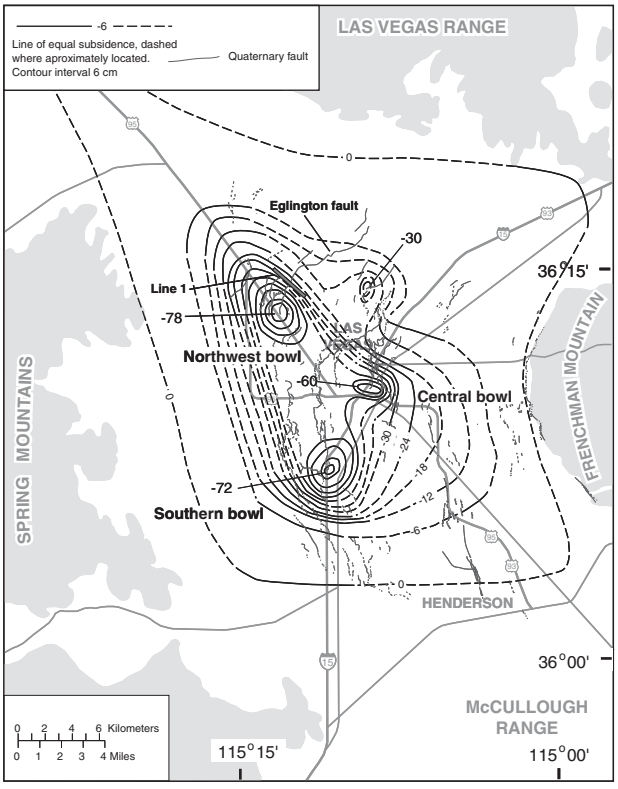

Figure 2. Subsidence contour map for 1963–80 showing maximum subsidence in three principal localized bowls in Las Vegas Valley (from Bell, 1981b).

The localization of the subsidence bowls was believed to be related to concentrated pumping, and subsidence was inferred to be uniformly distributed about the pumping centers (Harrill, 1976; Bell, 1981b).

In a study conducted in the early 1990s, a subsidence map covering the period 1963–87 showed that the three principal localized bowls had become more pronounced and more extensive (Bell and Price, 1991). On the basis of first-order leveling data, a fourth subsidence bowl (North Las Vegas) was identified. In

addition, the Northwest subsidence bowl was found to be the dominant subsidence zone in the valley, having subsided more than 1.5 m for the 24-year period and exceeding the total amount occurring since 1935 in the original Central subsidence bowl.

On each of the early subsidence maps, elevation changes were assumed to be uniformly distributed about the benchmarks, with subsidence contours drawn by conventional interpolation of values between benchmarks. The 1935–63 (Malmberg, 1964) and 1963–80 (Bell, 1981b) subsidence maps used more than 100 benchmarks to contour subsidence in the valley. By 1987, however, the number of recoverable benchmarks was fewer than 30 due to the loss of benchmarks caused by construction related to urbanization. The uniform spatial patterns inferred for the early subsidence maps were consistent with areas of known intensive ground-water pumping in the valley, with the elastic properties of the aquifer system, and with comparable patterns in similar ground-water basins of the arid United States (Schumann and Poland, 1970).

Despite the assumption that subsidence was uniformly distributed about the principal pumping centers, some evidence suggested that the faults that cut the basin floor were possible sites of differential movement. Beginning in 1978, a series of 1.5- to 4-km-long, second-order-accuracy, vertical-control lines were established across the fault scarps to determine whether the faults were potential sites for subsidence-induced fault slip, such as found on the Picacho fault in central Arizona (Holzer and others, 1979). The lines were resurveyed annually until 1989 and then repeated in 1991, 1997, and 1999. The results showed that although the faults were moving in response to subsidence, the movement was distributive in nature and generally in the opposite direction to the sense of fault displacement. In particular, line 1, which extended across the Eglington fault in the Northwest bowl (fig. 2), showed a total elevation change of 36 cm for the 1978–85 period, with movement down on the northwestern side of the east-dipping fault (fig. 3).

Based on the level-line data, the fault movement was believed to be one element contributing to the overall pattern of the localized subsidence bowls; the principal consequence of the fault movement was associated with the development of earth fissures (Bell and Price, 1991). A statistical analysis of the spatial distribution of subsidence-related fissures in the valley

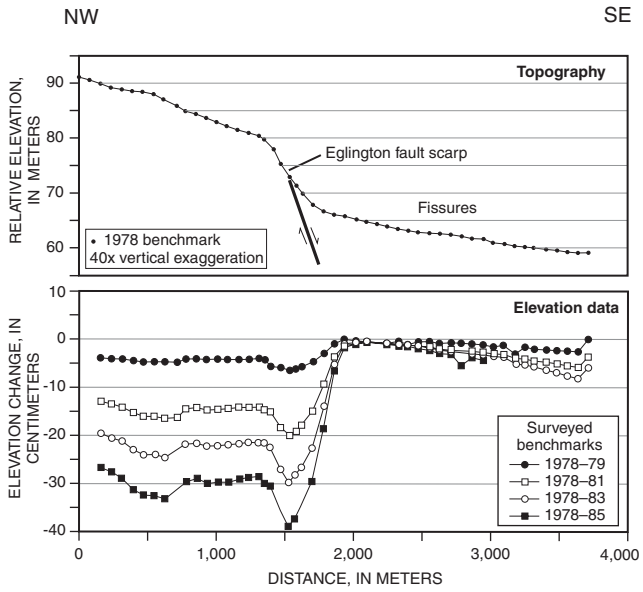

Figure 3. Topography and elevation change for level line 1 across the Eglington fault (fig. 2) for the period 1978–85.

showed that the fissures were preferentially developing near and along the faults. More than 18,000 m of fissures were included in the analysis, which showed that 90 percent of mapped fissures occurred within 600 m of a fault, strongly suggesting that the faults were sites of structural weakness that contributed to the development of fissures.

InSAR Studies

Several satellites have been acquiring 56-mm wavelength microwave SAR images of the earth's surface since 1992. Two SAR scenes acquired at different time periods are accurately co-registered, and by comparing changes in reflected radar wave phases, small (<1 cm) changes in the ground surface can be detected through the use of phase change maps or SAR interferograms. The use of InSAR is now considered a mature geodetic technique and is routinely used to monitor a wide range of crustal deformation processes. Beginning in 1998, InSAR studies of Las Vegas Valley were initiated that used ERS-1 and -2 satellite data to produce a series of interferograms showing subsidence for the period 1992–97 (Amelung and others, 1999). A composite interferogram covering the April 1992–November 1993, November 1993–February 1996, and January 1996–December 1997 intervals revealed new

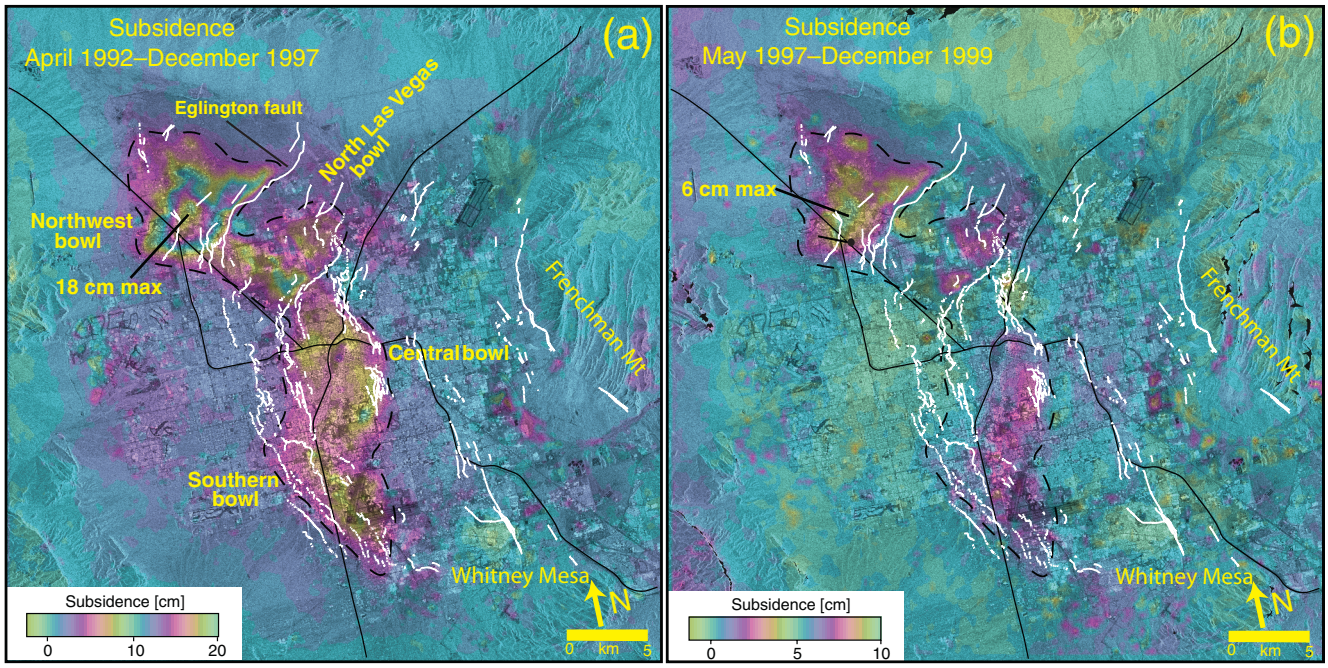

Figure 4. Composite interferograms of Las Vegas Valley for (a) April 1992–December 1997 (from Amelung and others, 1999) and (b) May 1997–December 1999. Faults are shown in white.

insights into the spatial distribution and structural control of subsidence in Las Vegas Valley (fig. 4a).

The 1992–97 interferogram shows that subsidence was occurring in a series of elongated bowls that coalesce to form a 5- to 10-km-wide, north-northwest-trending depression along the axis of the valley. The greatest amount of movement occurred in the Northwest bowl where a maximum displacement of 18 cm was observed for the 5.7-year period; the Central bowl exhibited about 10 cm of movement for the same period. A composite interferogram produced for the 1997–99 period shows similar, but smaller, elevation changes; during this period, 5 to 6 cm of subsidence was measured in the Northwest bowl, and 2 to 3 cm of subsidence was measured in the Central bowl (fig. 4b).

The fine spatial detail of the InSAR studies revealed several new elements of the subsidence patterns that were not evident in earlier conventional contouring studies. Most importantly, they showed that the spatial pattern of subsidence is much more strongly controlled by the faults than previously believed. The InSAR data clearly indicated that subsidence is occurring in a series of four elongated, localized bowls controlled almost entirely by the faults that cut the basin floor. The Northwest subsidence bowl is sharply bounded on the southeast side by the Eglington fault, which appears to act as a subsidence barrier with almost all movement occurring on the northwest side of the fault. This observation is consistent with the surveying results from line 1 (fig. 3) and indicates that the InSAR pattern is representative of the long-term deformation pattern.

The 1963–87 subsidence map (Bell and Price, 1991) was revised to more closely reflect the spatially detailed patterns revealed by InSAR, while remaining consistent with conventional benchmark data (fig. 5). The location, shape, and areal extent of the localized subsidence bowls were derived from the InSAR pattern, and the contour values were based on the conventional benchmark and level-line data.

EFFECTS OF ARTIFICIAL RECHARGE

Reduction in Subsidence Rates

A comparison of conventional leveling and InSAR data for the 1978–99 period shows that subsidence rates have declined significantly in most parts of the valley since 1991 (fig. 6). The most active

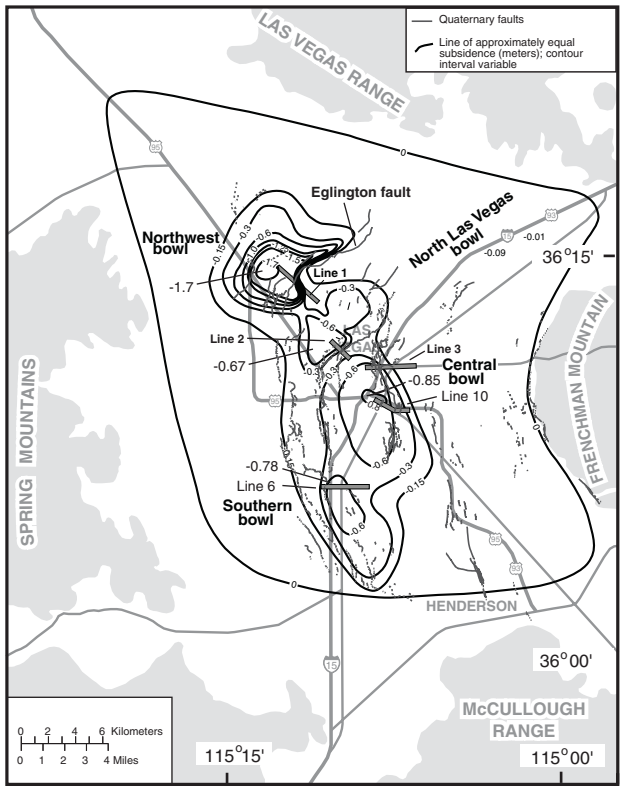

Figure 5. Revised subsidence contour map for Las Vegas Valley, 1963–2000, showing maximum subsidence measured in four localized bowls and location of level lines.

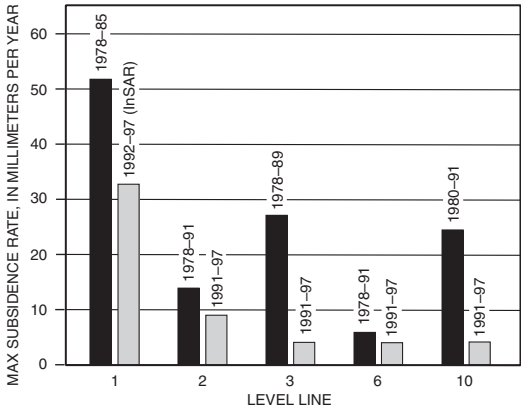

Figure 6. Histogram showing maximum subsidence rates measured along level lines 1, 2, 3, 6, and 10 (fig. 5) for the period 1978–97. Pre- and post-1991 rates are compared for each line on the basis of conventional leveling results, except for line 1 which is based on post-1991 InSAR measurements.

subsidence zone, the Northwest bowl, had a rate decline from 5 to 6 cm/yr to 2.5 to 3 cm/yr, a reduction of 50 percent. The largest reductions have occurred in the Central bowl where rates have declined as much as 80 percent. Based on analysis of water-use data, it is evident these reductions can be attributed to the artificial recharge program initiated by the Las Vegas Valley Water District (LVVWD)/Southern Nevada Water Authority in 1990–91, which has produced a general rise in water levels of as much as 18 to 20 m in most parts of the valley.

Artificial Recharge Causes Uplift of Land Surface

Evidence for seasonal uplift associated with artificial recharge was first detected in 1992–97 InSAR data in the Amelung and others (1999) study (fig. 4a), and as much as 2.5 cm of uplift was measured on the 1997–99 composite interferogram (fig. 4b). Similar data were presented by Hoffmann and others (2001); the InSAR data collectively showed that much of the present-day aquifer-system deformation is elastic and fully recoverable. To further investigate the elastic recovery of the aquifer system, this study examined continuous GPS data collected at the LVVWD main well field near the point of intensive artificial recharge in 1999–2000. The LVVWD station data were coprocessed with continuous GPS data collected at two stable bedrock sites operated by the California Institute of Technology BARGEN network between April 1999 and September 2001. The results (fig. 7) show a systematic GPS ellipsoid height increase of 11 cm of the LVVWD station between November 1999 and April 2000. An analysis of the timing of the uplift with water levels in three nearby artificial recharge wells in the main well field further shows that the ground uplift was coincident with about a 32-m maximum rise in water levels.

The elastic properties of the Las Vegas Valley aquifer system were analyzed by Hoffmann and others (2001) who computed elastic skeletal storage coefficients (S_{ke}) from contemporaneous InSAR and water-level observations for several wells; an S_{ke} of 3.41×10^{-3} was computed for a well near the LVVWD station. In this analysis, the 1999–2000 GPS height change of +0.11 m and the water-level change of +32 m yield an S_{ke} of 3.44×10^{-3}, a value in close agreement with the value computed by Hoffmann and others (2001).

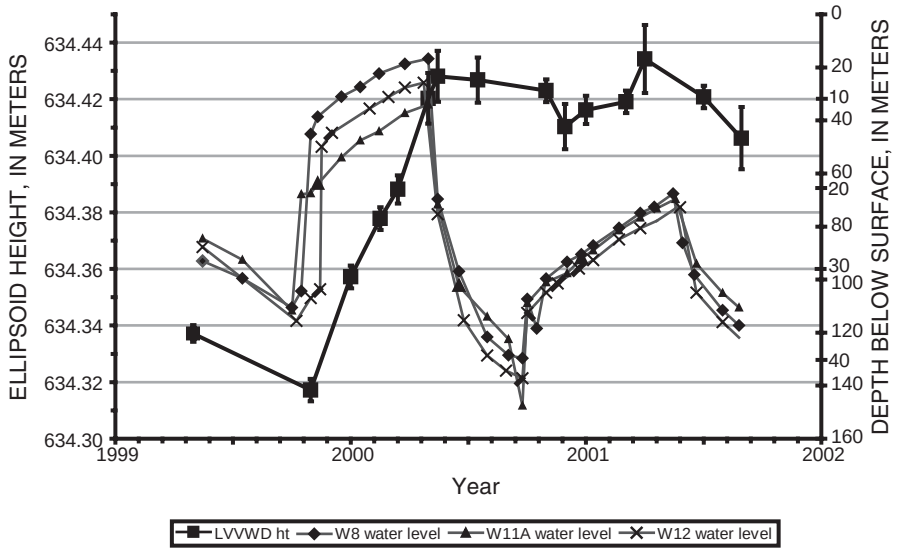

Figure 7. Ellipsoid height change of LVVWD GPS station and water-level fluctuations in three adjacent artificial recharge wells. Water-level data were provided by Las Vegas Valley Water District. Error bars on ellipsoid heights are 1-σ.

Although water levels subsequently declined during 2000–2001, the height of the LVVWD station has remained elevated, suggesting that anisotropy affects elastic recovery of the aquifer system (Donald C. Helm, Morgan State University, written commun., 2002).

ACKNOWLEDGMENTS

Helpful reviews of this paper and earlier versions were provided by Mike Pavelko and Terry Katzer. The study was supported by the Las Vegas Valley Water District/Southern Nevada Water Authority.

InSAR Detection of Post-Seismic and Coseismic Ground-Surface Deformation Associated With Underground Weapons Testing, Yucca Flat, Nevada Test Site

By Randell J. Laczniak[1], Devin L. Galloway[2], *and* Michelle Sneed[3]

Abstract

Underground weapons testing in Yucca Flat at the Nevada Test Site (NTS) has resulted in considerable deformation of the ground surface. The most visible deformation features are craters (fig. 1) resulting from coseismic and immediate post-seismic collapse of the subsurface chimney and test cavity. The testing of nuclear weapons was suspended in September 1992, and since that time no nuclear weapons have been detonated at the NTS. Displacement maps (interferograms) for three sequential periods derived from four satellite-acquired SAR images (April 24, 1992; June 18, 1993; June 11, 1995; and June 16, 1997) reveal small-magnitude (as much as 140 millimeters in 5 years) subsidence (figs. 2 and 3). This small-magnitude subsidence is characterized by oval-shaped patterns, generally surrounding one or many test locations and spread over a broad area (figs. 2 and 3). In Yucca Flat, most of this subsidence is concentrated in the region between the Yucca and Topgallant faults (figs. 1 and 2). These faults likely are major controls on the areal extent of test-generated subsidence throughout the area (figs. 2 and 3).

One likely explanation for post-seismic deformation is elastic compression of low-permeability tuff units within the aquifer system. Elastic compression results from delayed drainage and depressurization of the tuff units following coseismic pore-fluid pressurization. These low-permeability tuff units are most prevalent in the saturated zone between the Yucca and Topgallant faults and are referred to as the "tuff pile" (fig. 1). The tuff pile was the location of many weapons tests detonated near or below the water table (fig. 1). At about the time testing was suspended, measured water levels in wells penetrating the tuff units near weapons-test sites were greatly elevated, some by more than 400 meters above pre-testing static levels. Since the suspension of testing, water levels in these same wells have declined steadily, some by as much as 50 meters (fig. 4, UE-4t1 and UE-3e4-1). These declines in water level, along with the dissipation of measured pressures throughout the tuff-pile area, support the concept of water draining from the low-permeability tuff unit. Some of this drainage collects in subsurface cavities as indicated by a 45-meter rise in the water level measured in a hole drilled into a test-generated cavity (fig. 4, U-4u PS 2A).

The earliest interferogram (figs. 3, 5, and 6), developed for the period April 24, 1992–June 18, 1993, captures deformation resulting from the three most recent weapons tests (Galena, Divider, and Victoria) in Yucca Flat. All three tests were detonated above the water table during the period spanned by the interferogram. The interferogram clearly shows coseismic ground-surface deformation in the vicinity of Galena and Divider (fig. 5). These two weapons tests formed coseismic craters 130 and 120 meters in diameter and 8 and 3 meters deep, respectively (fig. 6). Subsidence signals observed in the interferogram extend well beyond the rims of these surface craters to a diameter of

[1] U.S. Geological Survey, Henderson, Nev.
[2] U.S. Geological Survey, Sacramento, Calif.
[3] U.S. Geological Survey, Sacramento, Calif.

about 1 kilometer. About 20 millimeters of subsidence is detected between the outer diameter of the Galena signal to an inner diameter of about 600 meters. The pixel-to-pixel displacement exceeds the maximum pixel-to-pixel measurement resolution of the C-band radar (28 millimeters) and renders the signal ambiguous within 600 meters of the test. Centered on Divider, the signal shows a four-lobed deformation pattern with oppositely sensed displacement between adjacent lobes similar to what is expected for slip on a strike-slip fault. This pattern suggests that Divider triggered faulting. The capability of InSAR to capture coseismic signals underscores its potential in monitoring associated with the Comprehensive Test Ban Treaty.

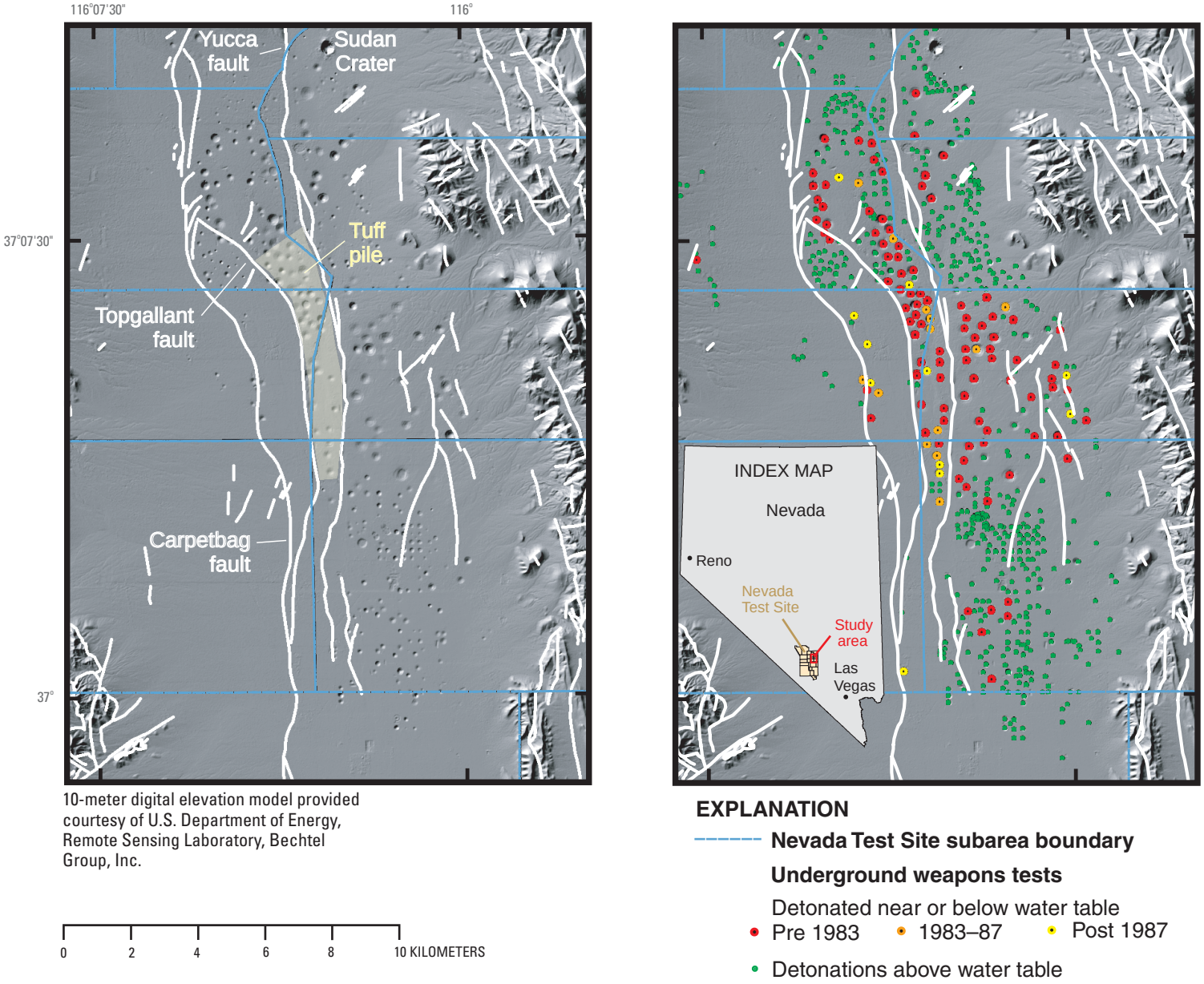

Figure 1. Location of underground weapons tests in Yucca Flat. First map shows location and distribution of craters caused by underground testing. Second map shows spatial distribution of tests, the position of tests relative to the water table, and temporal distribution of tests detonated below the water table.

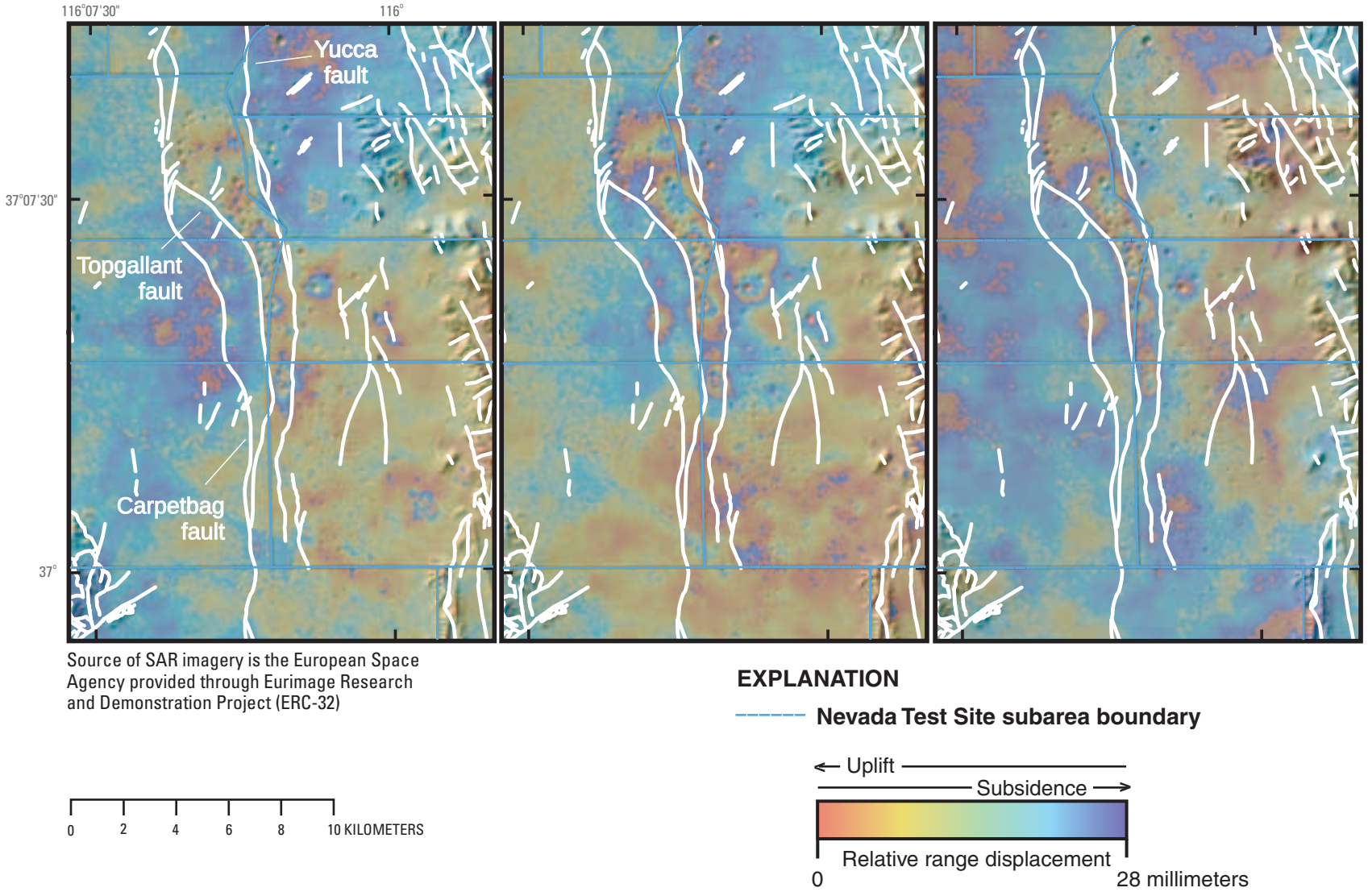

Figure 2. InSAR-generated displacement patterns (interferograms) of Yucca Flat area for three sequential periods spanning 1992–97. First interferogram spans period April 24, 1992–June 18, 1993, and is inclusive of the last weapons tests detonated in Yucca Flat area. Remaining two interferograms span sequential periods following the suspension of weapons testing, June 18, 1993–June 11, 1995, and June 11, 1995–June 16, 1997, respectively.

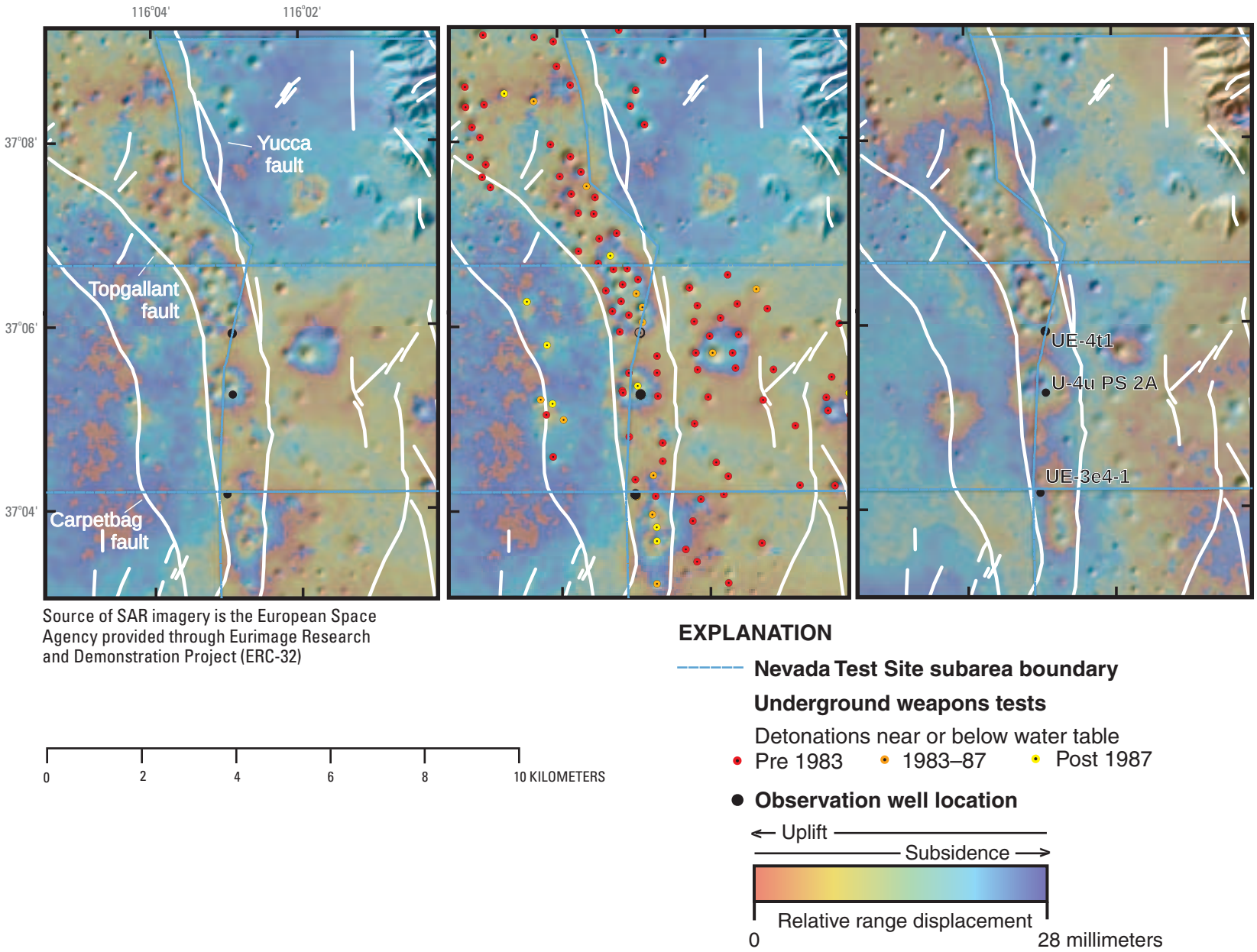

Figure 3. InSAR-generated displacement patterns (interferograms) in tuff-pile area of Yucca Flat for three sequential periods spanning 1992–97. First interferogram spans period inclusive of last weapons tests detonated in Yucca Flat area. Middle interferogram shows distribution of tests detonated below water table. Last interferogram identifies long-term observation wells used to measure water-level responses in tuff-pile area.

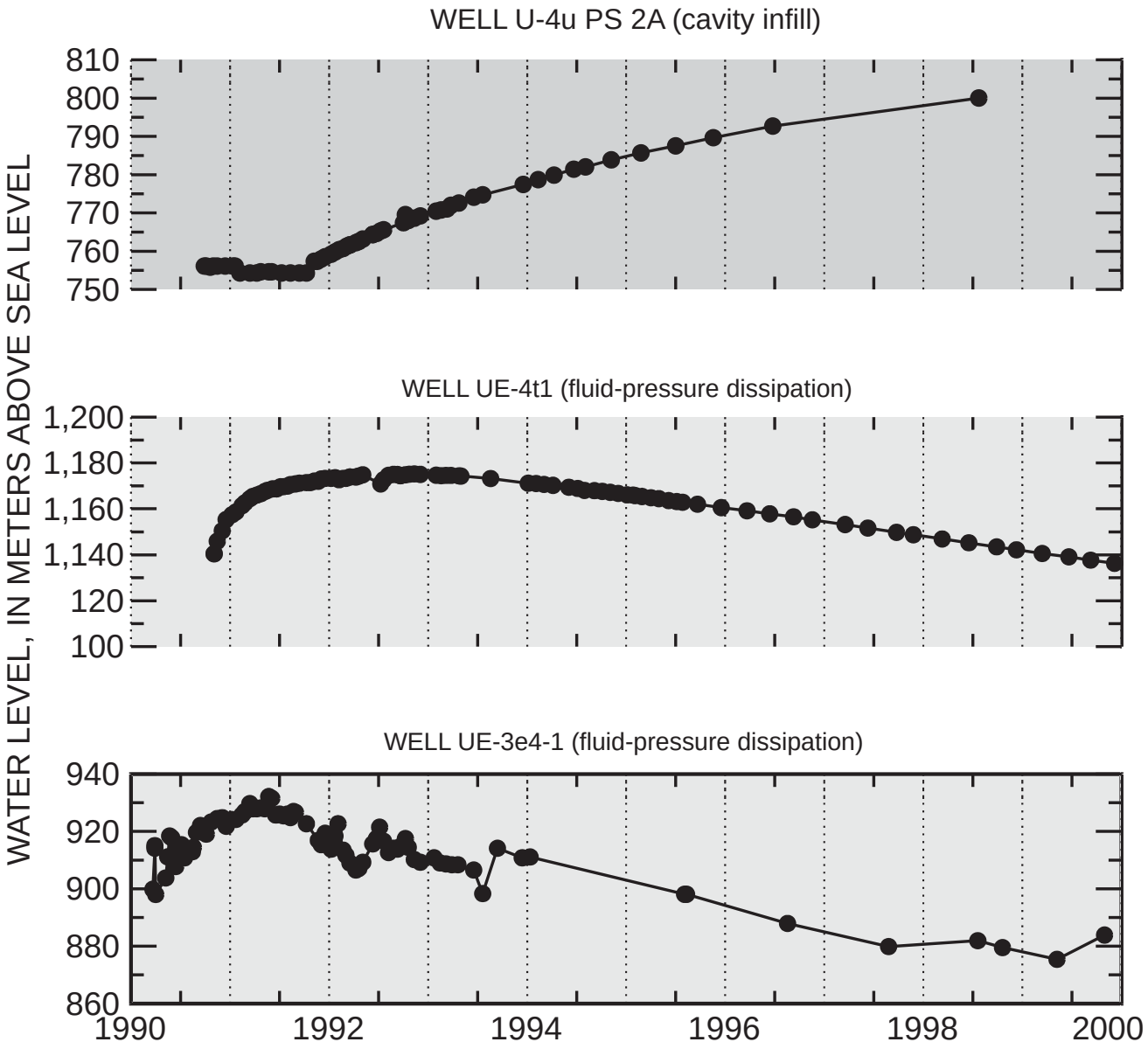

Figure 4. Wells in tuff-pile area exhibiting appreciable water-level changes in response to nearby underground weapons tests. Declines are attributed to the dissipation of fluid pressures from low-permeability units and recovery from drainage into a test-generated cavity. Upper graph shows infilling response characteristic of wells drilled into and open to a test cavity. Lower two graphs show characteristic rise and fall of the water level in wells open to low-permeability units in tuff-pile area. Well locations shown in figure 3.

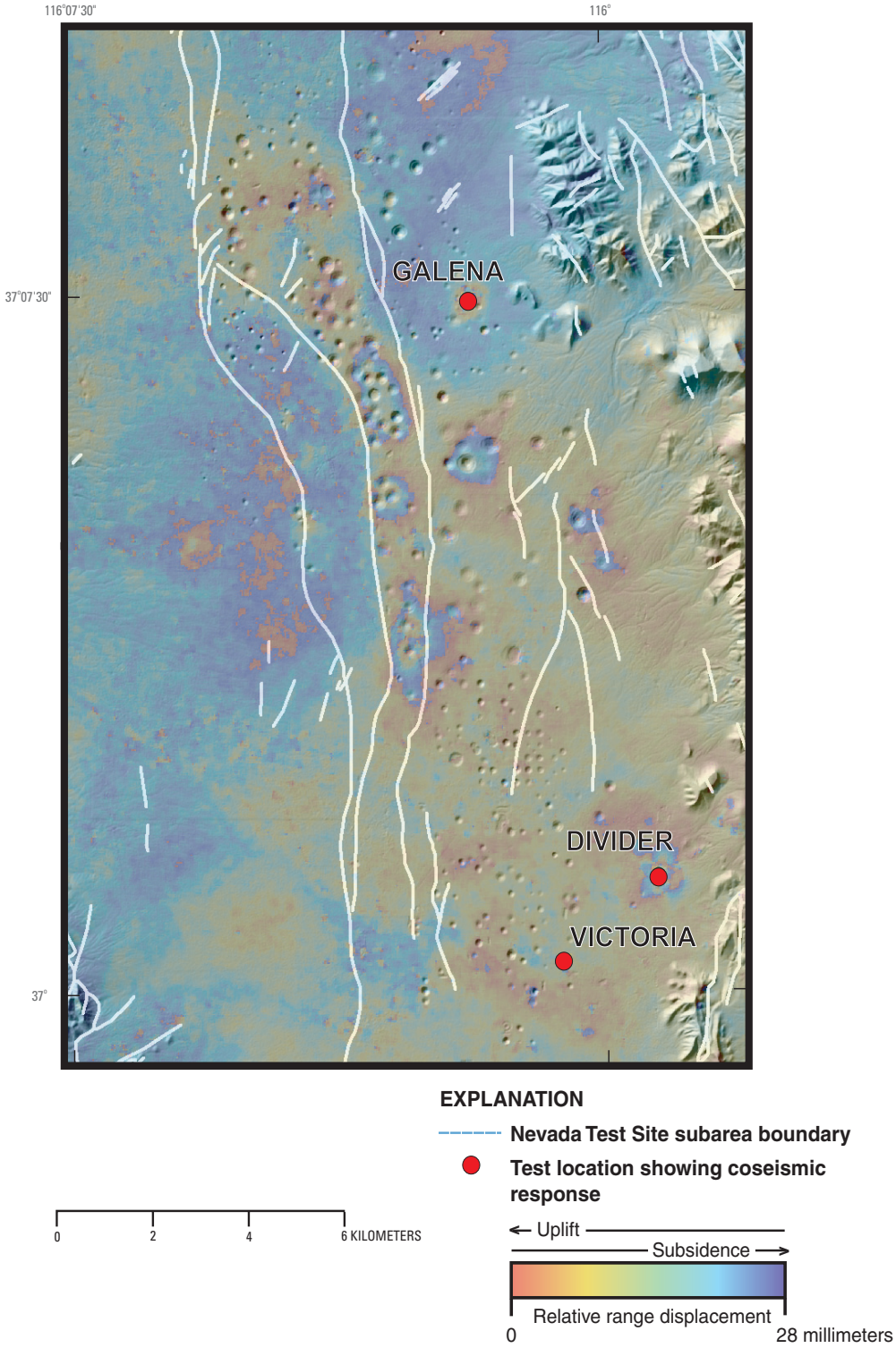

Figure 5. Location of three weapons tests detonated in 1992. All three tests were detonated above the water table. Interferogram spans period of tests April 24, 1992–June 18, 1993

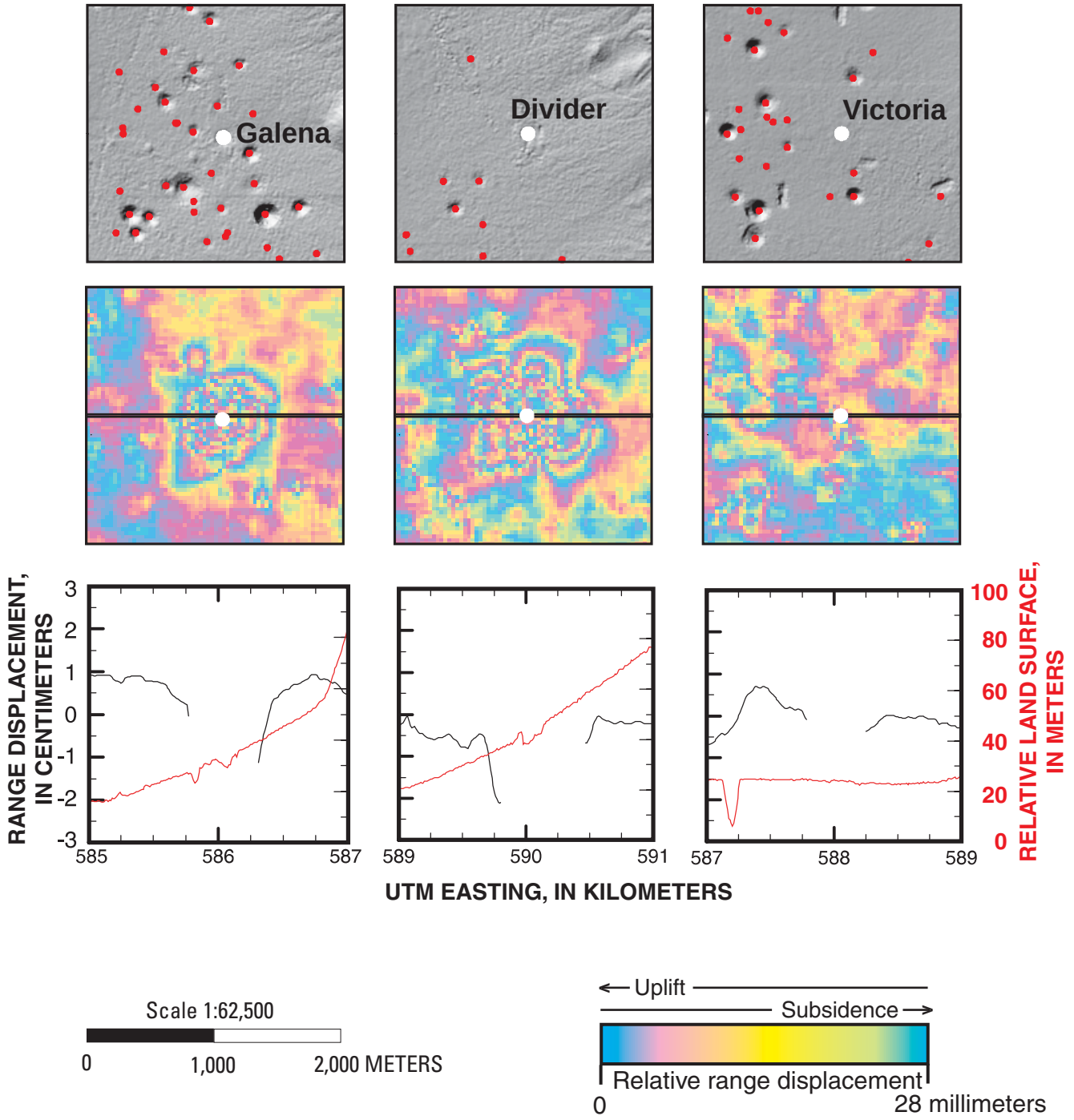

Figure 6. InSAR-detected coseismic deformation at three underground weapons tests detonated during 1992 in Yucca Flat. Upper panel shows hill shade of 10-meter digital elevation model (DEM) constructed from aerial photography flown in 1998 (U.S. Department of Energy Remote Sensing Laboratory, Bechtel Group, Inc.). Test locations shown as white circles. Nearby weapons tests shown as red circles. Middle panel shows InSAR-detected deformation for period April 24, 1992–June 18, 1993. Lower panel shows topographic profiles along cross section shown as black line on middle panel. Black curves (lower panel) are sensed range displacement constructed from interferogram. Red curves (lower panel) are changes in land-surface altitude constructed from 10-meter DEM (upper panel).

InSAR-Derived Temporal and Spatial Patterns of Land Subsidence and Uplift Caused by Aquifer-System Deformation Controlled in Part by Ground-Water-Level Variations and Geologic Structures Near Albuquerque, New Mexico

By Charles E. Heywood[1], Devin L. Galloway[2], *and* Sylvia V. Stork[3]

Abstract

Six synthetic aperture radar images were processed to form five unwrapped InSAR images of the greater metropolitan area in the Albuquerque Basin. Most interference patterns in the images were caused by range displacements resulting from changes in land-surface elevation. Loci of land-surface-elevation changes correlate with changes in aquifer-system water levels and largely result from the elastic response of the aquifer-system skeletal matrix to changes in measured pore-fluid pressure. The magnitude of the observed subsidence and uplift suggests that aquifer-system deformation resulting from ground-water withdrawals in the Albuquerque area probably has remained in the elastic (recoverable) range of stress from July 1993 through September 1999. Evidence of inelastic (permanent) subsidence in the Rio Rancho area exists, but its relation to compaction of the aquifer system is inconclusive because of insufficient water-level data. Patterns of elastic deformation in both Albuquerque and Rio Rancho suggest that intrabasin faults impede ground-water flow at seasonal time scales and at local and regional spatial scales.

INTRODUCTION

Permanent land subsidence caused by the inelastic compaction of overdrafted alluvial aquifer systems is a global problem. In many ground-water basins in the arid to semiarid western United States, permanent regional-scale subsidence has resulted from mining ground water for agricultural, municipal, and industrial water supplies (Galloway and others, 1999). Notable examples are the Antelope (Mojave Desert) (Ikehara and Phillips, 1994; Galloway and others, 1998; Sneed and Galloway, 2000; Hoffman and others, 2003), Santa Ana (Bawden and others, 2001), San Joaquin (Poland and others, 1975; Ireland and others, 1984), and Santa Clara (Poland and Ireland, 1988) Valleys in California; the Las Vegas Valley (Bell, 1981a, b; Bell and Price, 1993; Amelung and others, 1999; Bell and others, 2002) in Nevada; and several basins in south-central Arizona (Laney and others, 1978; Carpenter, 1999). Presently, the maximum historical subsidence in these basins ranges from about 2 to 9 m. In each of these examples, large volumes of ground water extracted to irrigate crops and provide municipal-industrial water supplies caused ground-water levels to decline below critical thresholds, leading to the onset of permanent subsidence. Conjunctive use of local ground-water supplies and imported surface-water supplies has helped decrease or halt permanent subsidence in each of these basins.

Short of permanent subsidence, reversible, elastic deformation occurs in all aquifer systems subject to pore-fluid pressure variations. From other alluvial basins subjected to daily and seasonal pumping stresses where aquifer-system deformation has been studied and monitored, these elastic displacements typically are about 1 to 5 mm for daily periods and can exceed 30 to 60 mm for seasonal periods.

Geomorphic evidence suggests that the Rio Grande has eroded as much as 100 m of sediment of Pleistocene age from a pre-existing fluvial-alluvial plain, of which the present *Llano de Albuquerque* (fig. 1) is a relict. Underlying sediment was pre-consolidated by the weight of this sedimentary

[1] U.S. Geological Survey, Richmond, Va.
[2] U.S. Geological Survey, Sacramento, Calif.
[3] U.S. Geological Survey, Sacramento, Calif.

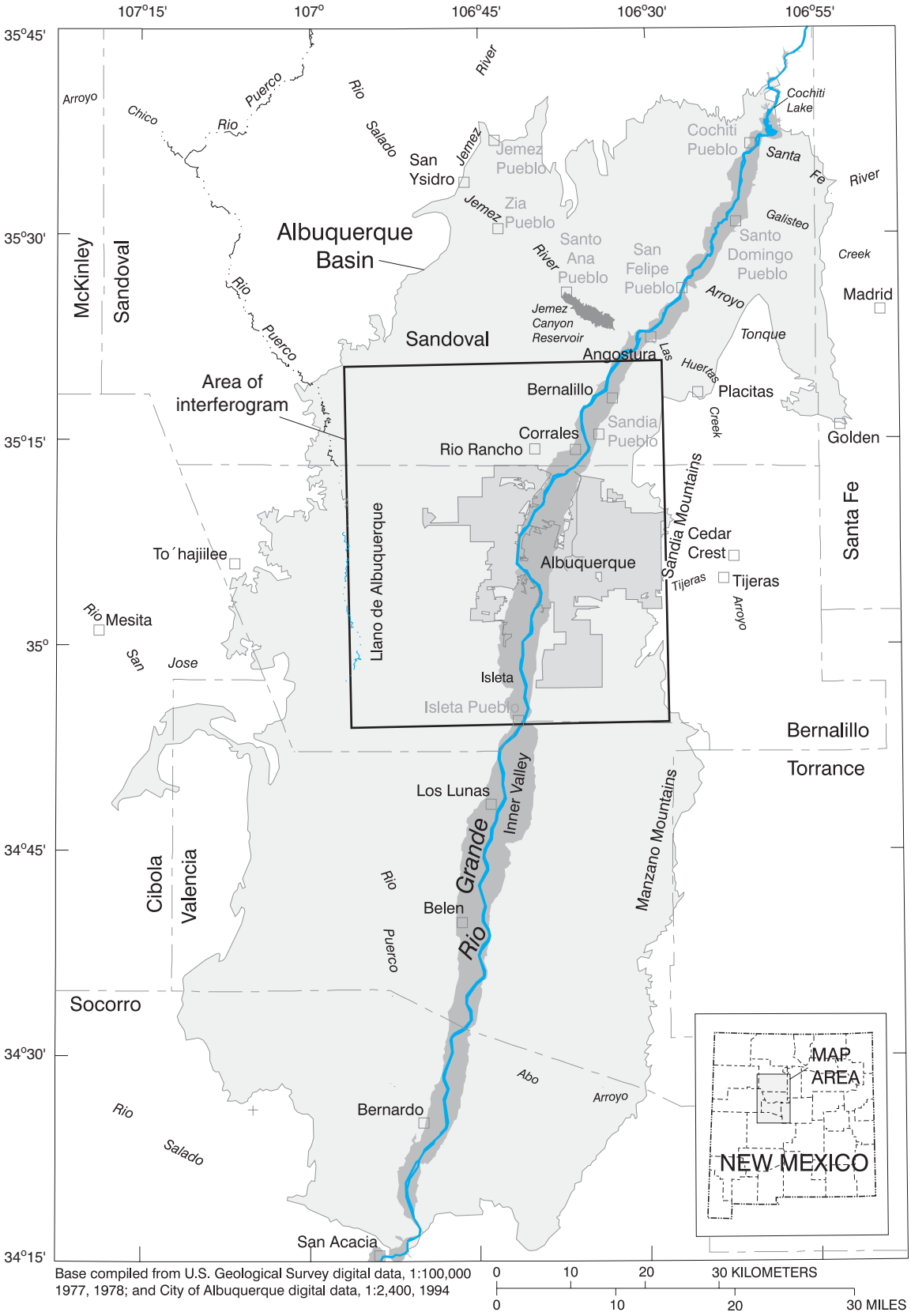

Figure 1. Area of interferogram coverage in the Albuquerque Basin, central New Mexico.

overburden and is now over-consolidated after erosion of the overburden. Aquifer-system deformation resulting from ground-water-level declines are therefore likely to remain in the elastic range until such declines cause aquifer-system effective stresses to exceed the pre-consolidation stress thresholds. The magnitude of water-level decline required to exceed these thresholds can be estimated using simple assumptions (Terzaghi, 1925). By assuming similar depths to the paleo-water and modern water tables, an average grain density of 2.7 g/cm^3, and porosity of 0.3, the equivalent water-level decline under confined conditions is about 1.2 times the thickness of the missing overburden or about 120 m. By 1996, ground-water levels had declined as much as 50 m from steady-state conditions in some areas of Albuquerque (Bartolino and Cole, 2002).

This paper summarizes the results of Heywood and others (2002), a study to determine potential land-surface displacement in and near Albuquerque, N. Mex., related to ground-water-level variations. SAR data were acquired from earth-orbiting satellites, and the InSAR technique was used to derive spatially detailed maps (interferograms) of ground-surface displacements to detect small-scale deformation of the aquifer system in the upper Albuquerque Basin. This technique has been successfully applied to investigations of land subsidence and uplift caused by deforming aquifer systems accompanying ground-water discharge and recharge in unconsolidated basin-fill deposits (for example, Amelung and others, 1999; Galloway and others, 1998, 2000; Hoffman and others, 2001; Hoffmann and others, 2003). Five interferograms of the Albuquerque area are presented for selected time intervals between July 1993 and September 1999. Radar data for this study were obtained from the European Space Agency (ESA), distributed through Eurimage Corporation for purposes of research and development.

RADAR INTERFEROMETRY

Five interferograms were processed using SAR data (track 98, frame 2907) acquired by the ERS–1 and ERS–2 satellites operated by ESA. Six SAR scenes with similar acquisition geometries were paired to form five interferograms covering the period July 2, 1993, to September 13, 1999. Interferometric processing was done on a subarea of the full SAR frame to focus on the Albuquerque area (fig. 1). To eliminate some of the noise in the interferograms the individual SAR images were averaged, resulting in a 40- x 40-m spatial (pixel) resolution.

The phase component of the complex-valued interferogram contains not only information about coherent displacements of reflectors imaged by the radar but also topography and signal propagation delays owing to spatially and temporally variable tropospheric water content. The effects of topography were removed by simulating a topographic interferogram in the geometry of the SAR scenes using an existing 30-m digital elevation model (DEM) of the study area and subtracting it from each SAR scene. The effect of variable tropospheric delays was minimized by selecting SAR scenes acquired during periods of dry weather on the basis of local meteorological data. The interferograms were processed using the PRISME/DIAPASON software (Centre National d'Etudes Spatiales, 1997) and the two-pass approach described by Massonnet and others (1994) and Massonnet and Feigl (1998). The coherent phase component of the resulting interferograms represents range (line-of-sight) displacements, mapped modulo 2π (or 28 mm, one-half the wavelength of the C-band radar). Prior to unwrapping, the interferograms were smoothed using a spectral smoothing algorithm (Z. Lu, U.S. Geological Survey, written commun., 2000). The smoothed interferograms were unwrapped using the *Escher* algorithm (Shindle, 1999). The resulting interferograms were transformed from the geometry of the radar to cartographic coordinates (Lambert central meridian = -106) and resampled at 30-m resolution on the registered grid of the DEM.

Assuming that all the observed range displacement was owing to vertical ground displacements, the vertical component of the displacement field was computed from the range displacements using the ERS radar incident angle (~23° from vertical). Interferogram values were internally referenced to areas of stable (zero displacement) bedrock outcrops.

GROUND-DISPLACEMENT OBSERVATIONS

InSAR Measurements

The five interferograms are shown in color draped over a gray-scale shaded-relief image of the area in figures 2a–e. (Areas in which an interferogram could not be unwrapped are transparent in these figures, thereby providing geographic reference from the underlying shaded relief image.) The interferograms cover

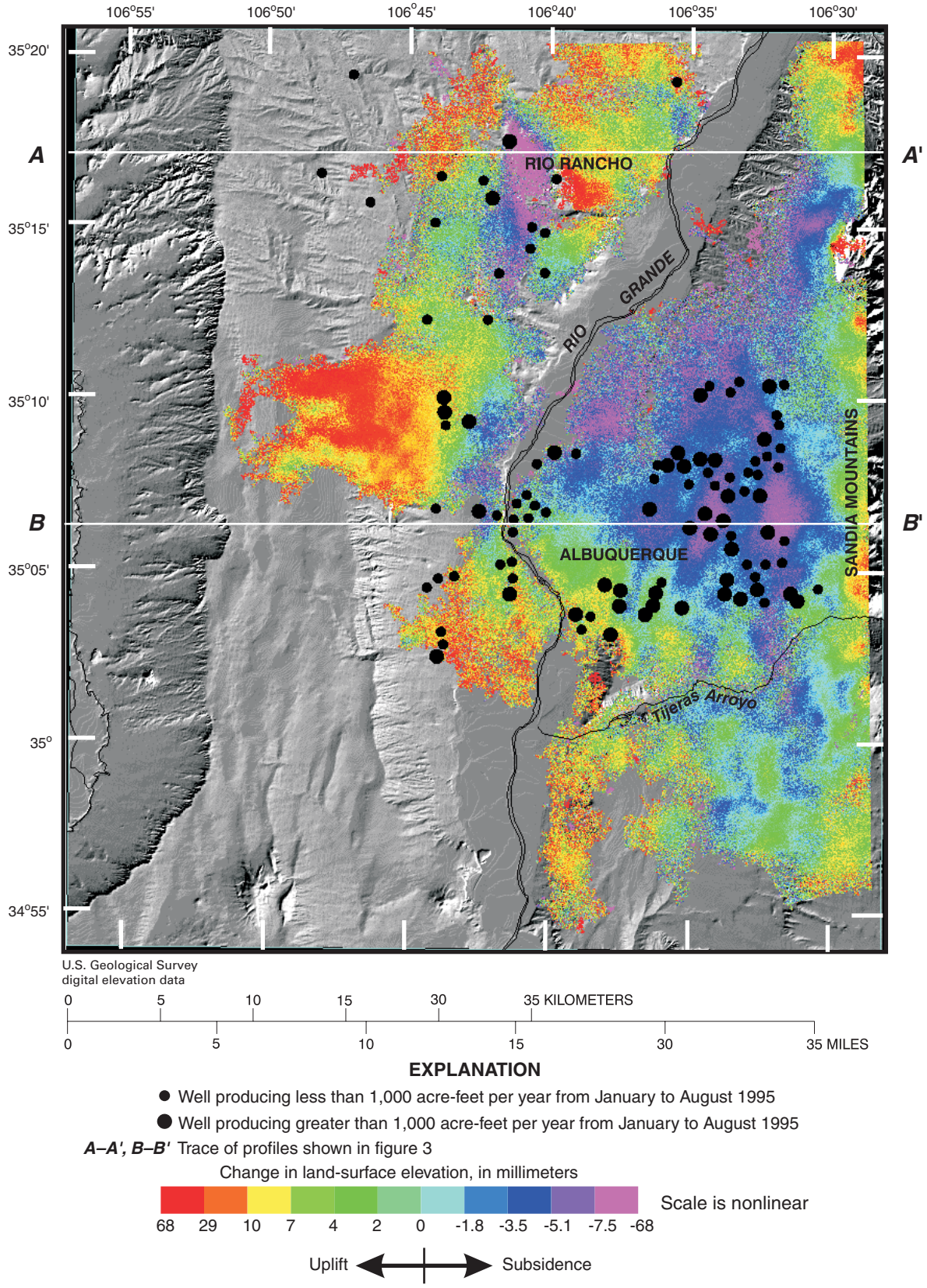

Figure 2a. 793-day interferogram (July 2, 1993–September 3, 1995).

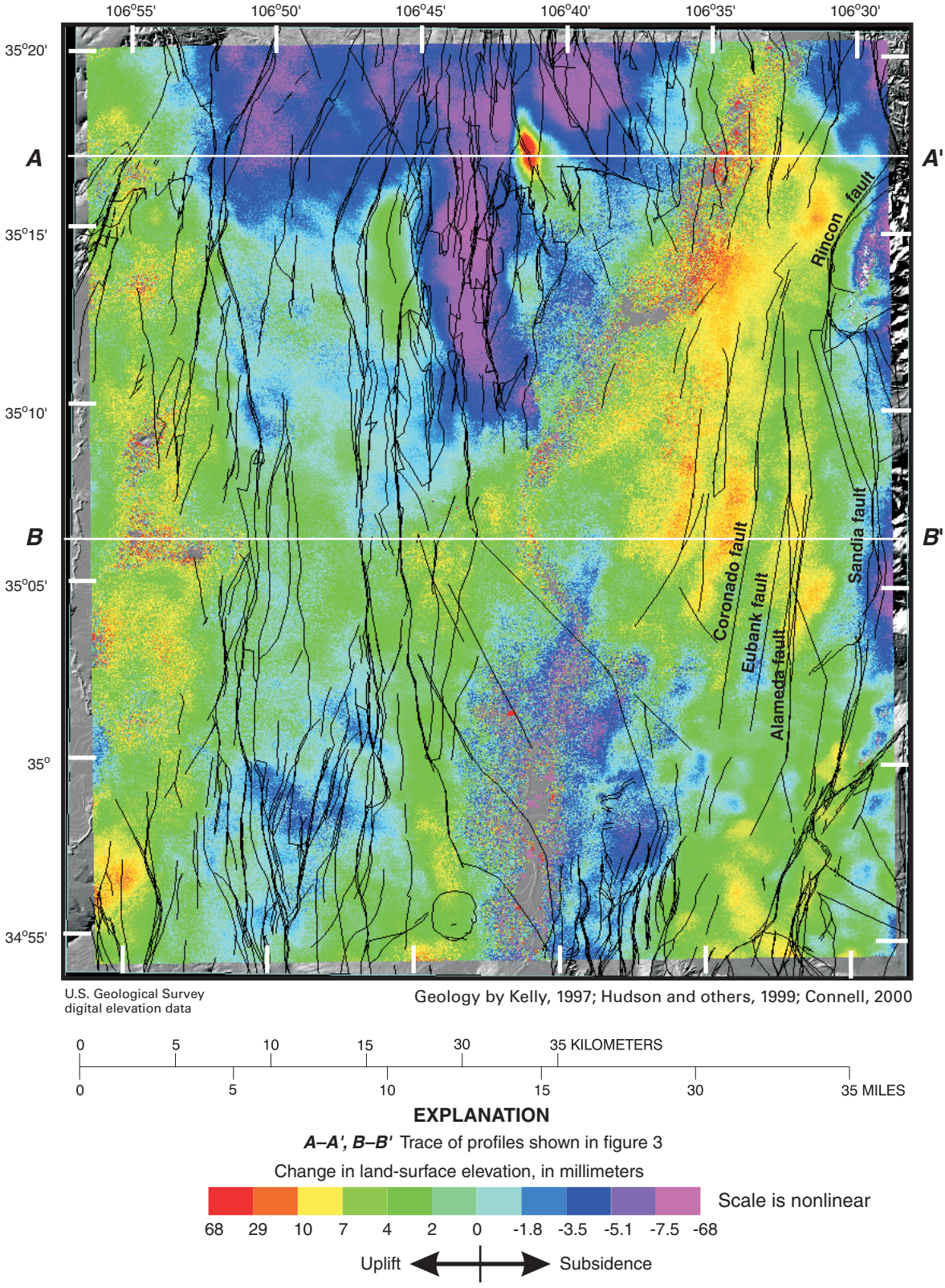

Figure 2b. 211-day interferogram (September 3, 1995–April 1, 1996).

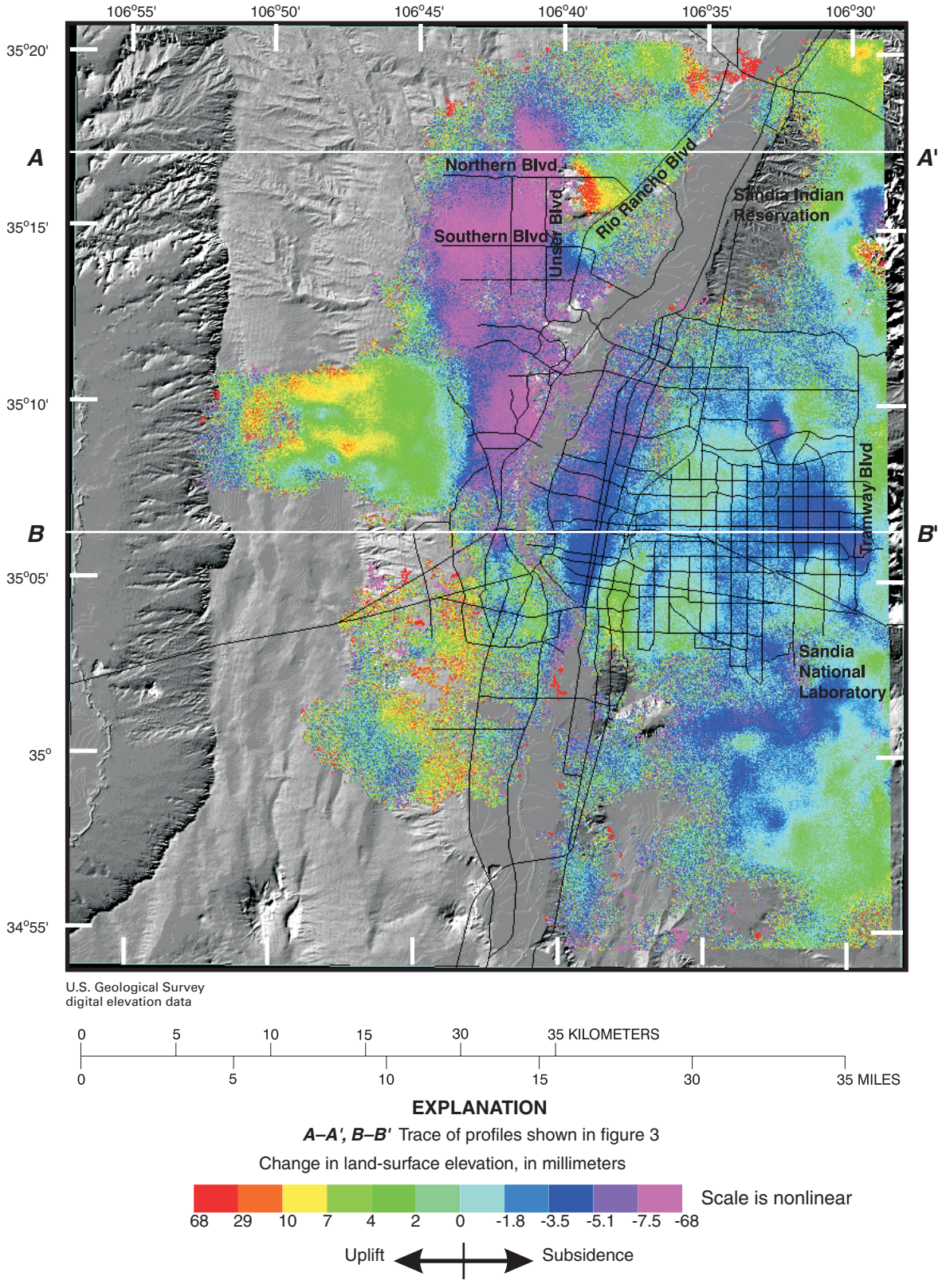

Figure 2c. 1,004-day interferogram (July 2, 1993–April 1, 1996).

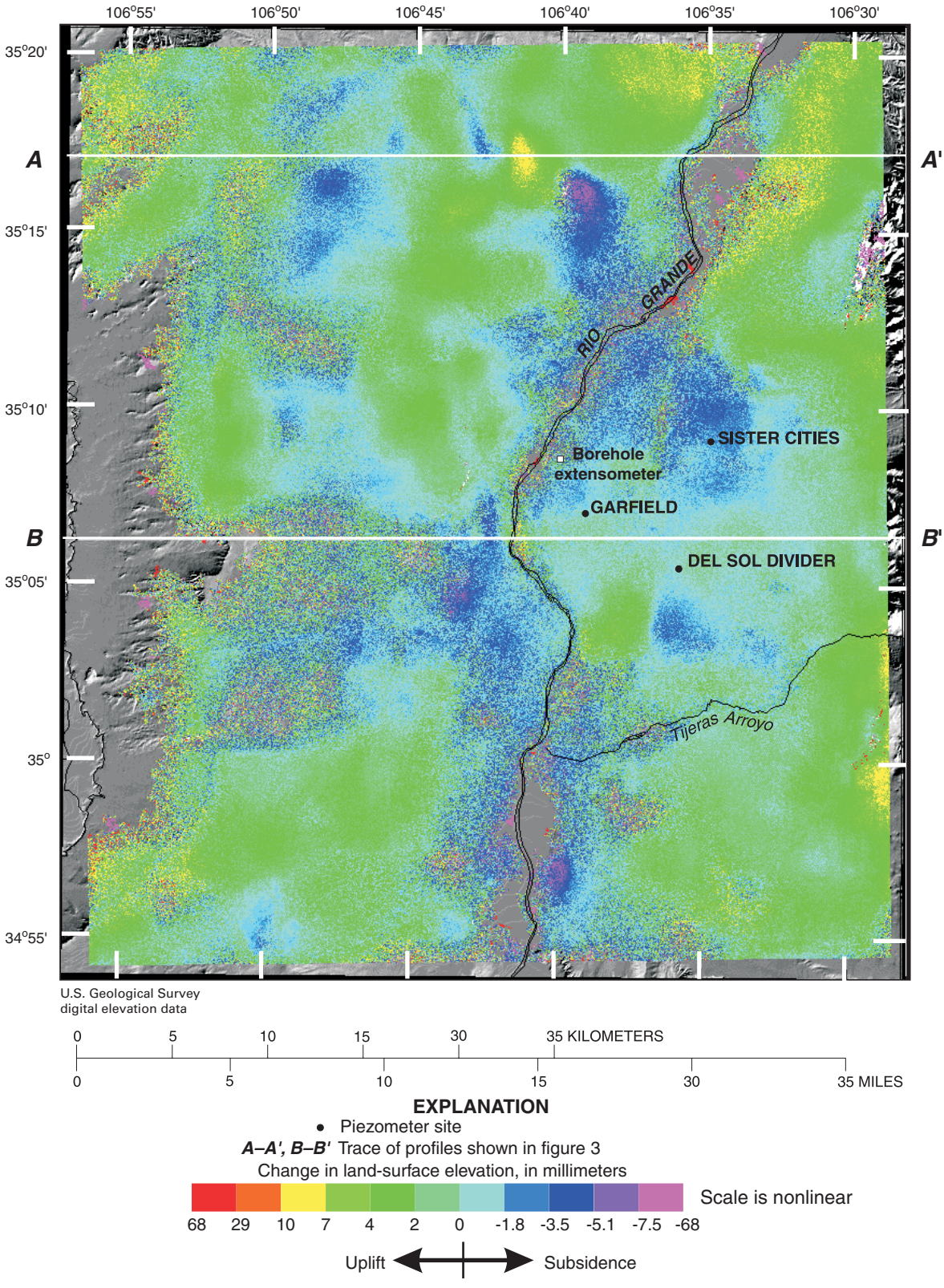

Figure 2d. 385-day interferogram (February 10, 1997–March 2, 1998).

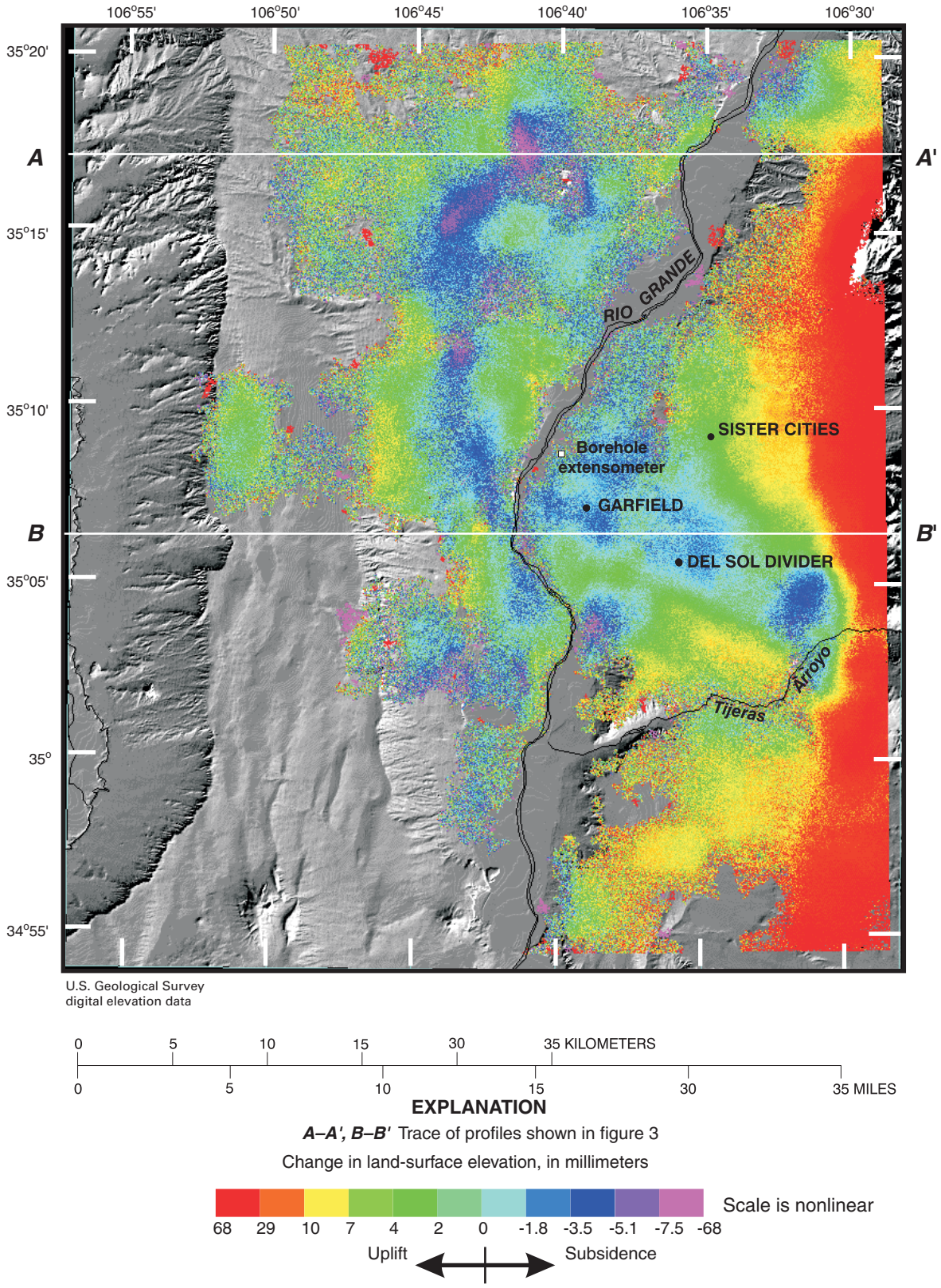

Figure 2e. 560-day interferogram (March 2, 1998–September 13, 1999).

the periods July 2, 1993–September 3, 1995 (793 days, fig. 2a); September 3, 1995–April, 1, 1996 (211 days, fig. 2b); July 2, 1993–April, 1, 1996 (1,004 days, fig. 2c); February 10, 1997–March 2, 1998 (385 days, fig. 2d); and March 2, 1998–September 13, 1999 (560 days, fig. 2e). The color bar on these interferograms was scaled to resolve variations of small-amplitude displacements, while encompassing the total range on all interferograms. Profiles of the displacements are shown in figures 3 and 4 for two east-west oriented cross sections (fig. 2) for each of the interferograms.

Local and regional subsidence and uplift are evident on the interferograms and profiles. In the Rio Rancho area, where as much as 48 mm of subsidence was observed (fig. 2a), seasonal-scale effects are evident by comparing displacement sense between interferograms spanning periods containing differing proportions of summer (figs. 2a, 2e, 3) and winter seasons (figs. 2b, 2d, 3). Ground-water pumpage decreases from summer highs to winter lows. The 793-day interferogram (fig. 2a) is biased toward a summer-season response because it includes two extra summer months in 1995 relative to the July 1993 beginning date. The 1,004-day interferogram (figs. 2c, 3, 4), though it contains more winter than summer seasons, indicates about 21 mm of subsidence in the Rio Rancho area and very little displacement in the Albuquerque area. (The expected noise level of these interferograms is on the order of ±5 mm.) These observations are discussed in detail below in the context of ground-water-level variations and geologic controls on the magnitudes and patterns of displacement.

Other Measurements

A borehole extensometer completed in December 1994, east of the Rio Grande (fig. 2d) in Albuquerque (Heywood, 1997, 1998), continuously measures and records compaction and water levels in the interval 5 to 315 m below land surface. The displacement time series shows daily and seasonal variations of about 1 to 2 mm in response to water-level variations at a nearby production well. For the time corresponding to the 211-day interferogram (fig. 2b), accounting for the 1,748-hour (Greenwich Mean Time) orbital pass-over, 1.7 mm of uplift was measured on the extensometer. The interferometrically derived displacement in the pixel containing the extensometer is 2.1 mm of uplift; averaging of 2 X 2 pixels and 4 X 4 pixels centered on the extensometer site yields 1.3 and 1.4 mm of uplift, respectively. The U.S. Geological Survey and City of Albuquerque installed a geodetic land-subsidence monitoring network in 1993, which was surveyed using GPS in 1993 and 1994. For 1993–94, the maximum computed benchmark-elevation change of -2 cm was observed near a well in Rio Rancho. Other computed benchmark-elevation changes were less than 2 cm, which was considered the limit of resolution of the differential GPS survey. The time span between the GPS surveys is less than, and contained within, the period of the 793-day interferogram (fig. 2a). The negligible vertical displacements measured at discrete benchmarks using GPS during 1993–94 agree with those in the 793-day interferogram.

CORRELATION WITH GROUND-WATER-LEVEL VARIATIONS

Ground-water levels in the Albuquerque area exhibit annual periodicity superimposed on a long-term decline. Hydrographs of selected piezometers (fig. 5) reveal that deep ground-water levels (that is, in wells screened more than 100 m below the water table) recover during fall and early winter months and typically attain their maximum levels in January and February. Deep ground-water levels decline during spring and early summer months and typically reach minimum levels in July and August. Seasonal variations in municipal ground-water pumping contribute to this cyclic response. Land-surface-elevation changes observed in the interferograms (figs. 2a–e, 3, 4) follow these trends in deep ground-water-level changes. This spatial and temporal correspondence suggests that observed apparent land-surface-elevation changes result from elastic compression and expansion of the skeletal matrix of the aquifer system resulting from pore-fluid pressure changes. At the Garfield piezometer site (figs. 2d, 5a) in the Rio Grande Valley, seasonal variations of the water table and deeper water levels are out of phase, emphasizing the vertical impedance to ground-water flow and pressure equilibration between the water table and the deeper confined aquifer system.

The 793-day interferogram (fig. 2a) corresponds to a period during which net annual ground-water levels declined relatively rapidly in the Albuquerque and Rio Rancho areas. Few observation wells existed in the area at that time, but water-level records from Albuquerque production wells indicate that annual declines were about 1 to 2 m. Two full seasonal periods of water-level recovery are encompassed in this interferogram, during

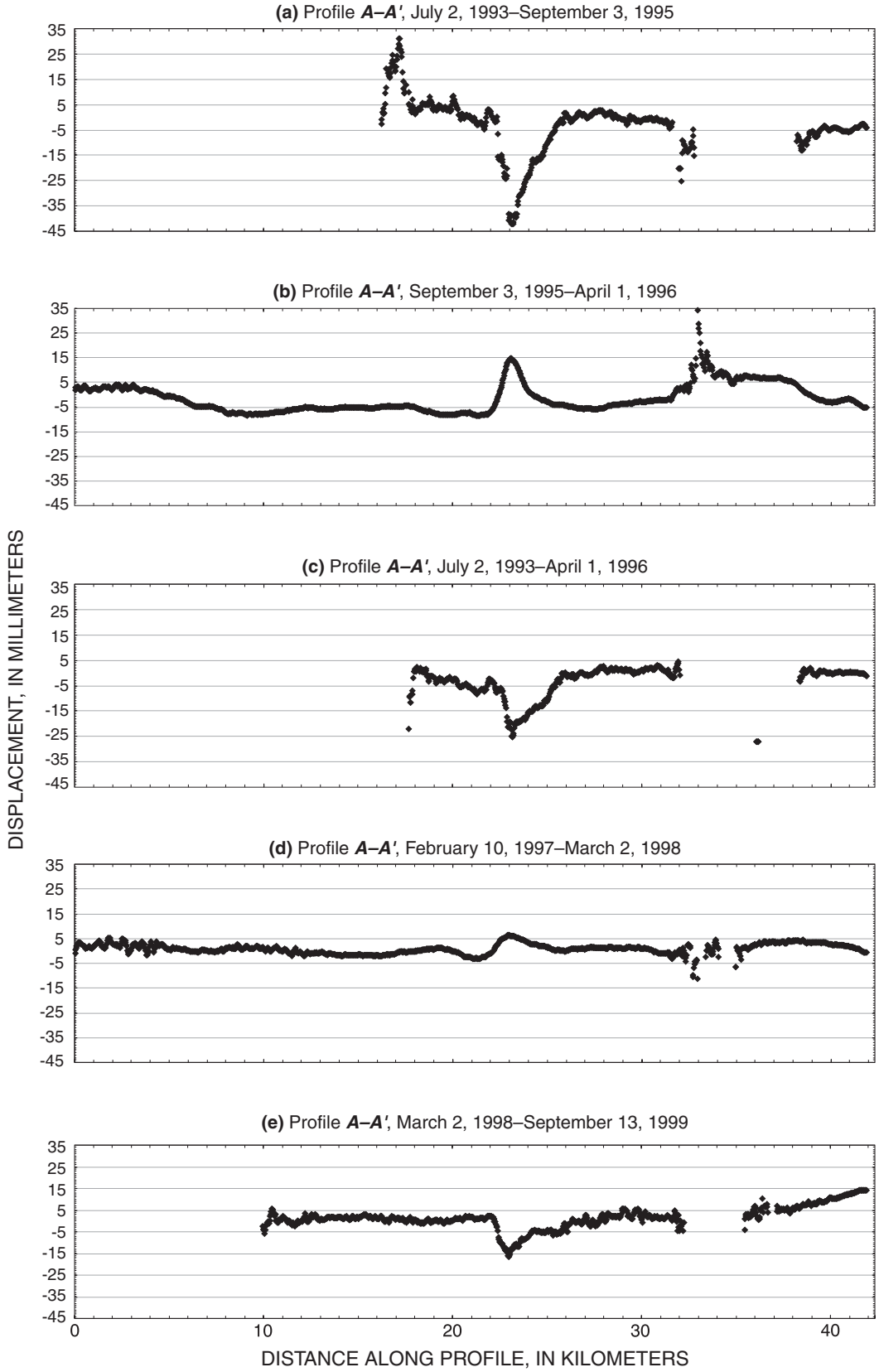

Figure 3. Vertical displacement along profile *A*–*A*' from July 2, 1993, to September 13, 1999.

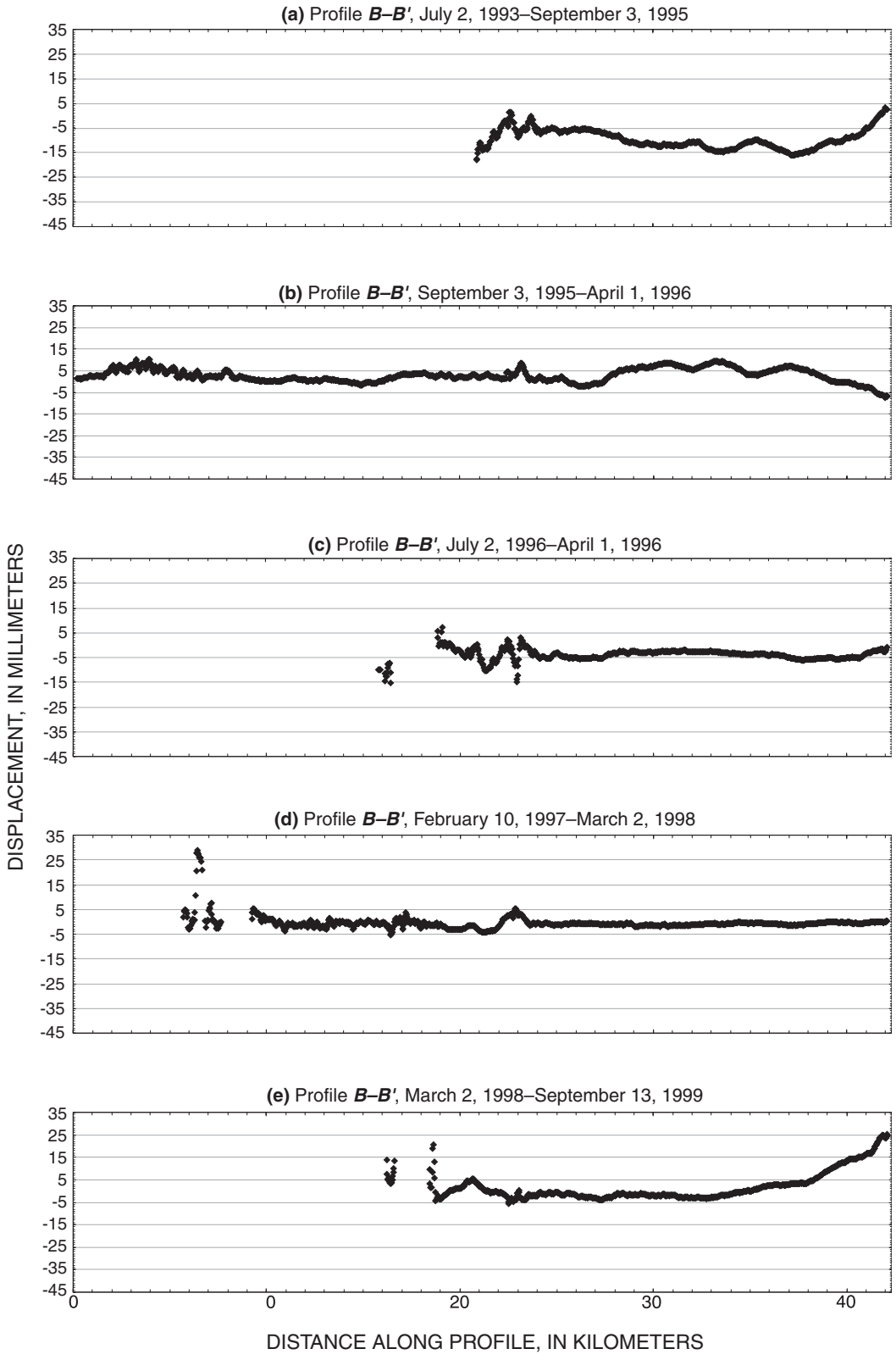

Figure 4. Vertical displacement along profile *B–B'* from July 2, 1993, to September 13, 1999.

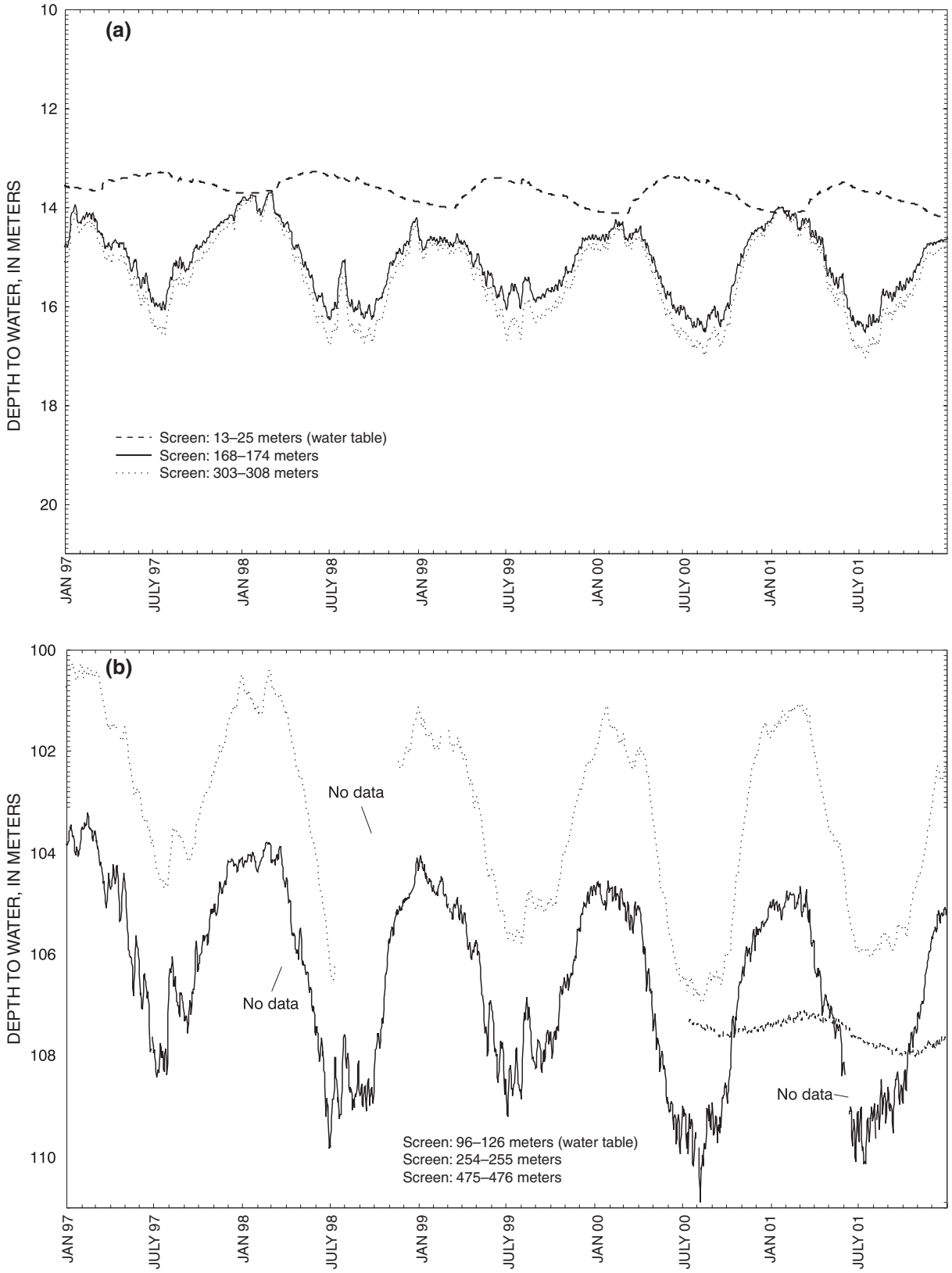

Figure 5. Depth to water in (a) Garfield piezometers and (b) Del Sol Divider piezometers. (Location of piezometer sites in figure 2d.)

which ground water flowed locally toward the loci of previous withdrawals. The observed subsidence features are therefore biased toward ground-water withdrawals that occurred during the final period of seasonal water-level declines. To evaluate correlation between ground-water withdrawals and subsidence, withdrawals from ground-water supply wells were totaled for January through August 1995. The subsequent 211-day (September 3, 1995, to April 1, 1996; fig. 2b) interferogram encompasses a period of seasonal water-level recovery. The reversed sense of deformation (that is, uplift in locations of subsidence features observed in the previous 793-day interferogram) is the elastic response of the aquifer system to recovering water levels.

The 1,004-day interferogram (fig. 2c) encompasses 2 years of long-term water-level decline with an extra seasonal recovery period superimposed. Although subsidence and uplift features are observed in this interferogram, subsidence features predominate. Considering the summer to late-winter seasonal span of the interferogram and the widespread uplift observed in the 211-day interferogram (fig. 2b) (presumably during a period of water-level recovery), it is probable that permanent (inelastic) compaction and subsidence are accumulating over yearly or longer time scales. This is partly corroborated by the subsidence observed in the 793-day interferogram (fig. 2a). Because water-level data do not exist in these areas during the time spanned by these interferograms, it is not possible to determine conclusively whether the subsidence is recoverable (elastic) or permanent. In Rio Rancho, profile *A–A'* crosses the prominent quadrilateral-shaped feature for which the magnitude of subsidence observed in the 793-day interferogram (figs. 2a, 3) and subsequent elastic rebound observed in the 211-day interferogram (figs. 2b, 3) is about 48 and 24 mm, respectively. The 385-day interferogram (figs. 2d, 4) closely encompasses one cyclic period of seasonal water-level change. Minimal net water-level change was observed in the Garfield and Del Sol Divider piezometers (figs. 5a, 5b) during this time, and insignificant ground displacements are observed at these locations of the interferogram. The water level in the Sister Cities 1 piezometer (site location shown in fig. 2d) declined 1.74 m during this period; subsidence is observed in this area of north Albuquerque. Displacement features in Rio Rancho exhibit both subsidence and elastic rebound, presumably in response to net ground-water-level changes. This suggests that a zone of reduced permeability that impedes ground-water flow might separate the two areas. This effect also is evident in figure 2c.

The 560-day interferogram (fig. 2e) also encompasses a period with both long-term and seasonal water-level changes superimposed. Hydrographs from deeper piezometers at the Garfield and Del Sol Divider sites (figs. 5a, 5b) indicate about 2 and 4 m, respectively, of net water-level decline during this period. Relatively small and uniform subsidence is observed in this area of the interferogram.

CORRELATION WITH GEOLOGIC STRUCTURES

The quadrilateral-shaped displacement feature observed in Rio Rancho in all five interferograms, particularly the 211-day interferogram (fig. 2b), correlates with the location of the Zia Horst, a known fault-bounded, local structural uplift. This horst juxtaposes relatively permeable, well-sorted Zia Formation sand of Tertiary age against outlying, stratigraphically younger sediment. Greater diagenetic cementation (Sean Connell, New Mexico Bureau of Geology and Mineral Resources, oral commun., 2001) in the outlying sediment might have imparted a lower permeability and compressibility to this sediment; horst-bounding faults also appear to impede ground-water flow. Subsidence is observed over the Zia Horst in the 793-day interferogram (fig. 2a), presumably owing to pumpage from a well near the west fault-bounded side of the structure. The subsequent 211-day interferogram (fig. 2b) shows elastic rebound over this structure as ground-water levels recovered. The light blue subsidence lobes northwest and northeast of this block of relatively high permeability suggest that water levels declined in those areas during this 211-day period, although no significant ground-water withdrawals occurred. These water-level declines might be a response to drawdown in this area during the previous interferogram period, which was delayed by the low permeability of the block-bounding faults. This interpretation suggests the possibility that the water-level response inferred from a continuous series of short, temporal-baseline interferograms could be used to estimate the effective hydraulic conductivity of a fault "flow barrier" in an elastically deforming aquifer system.

On the east side of the interferograms, the Rincon and Sandia normal faults (fig. 2b) are basin bounding structures that separate crystalline rock of Precambrian age to the east from basin-fill alluvium of Tertiary and

Quaternary age (Kelly, 1977) to the west; the eastern limit of the observed InSAR-derived displacements in Albuquerque corresponds with this boundary. The Alameda, Eubank, and Coronado Faults are north-trending, west-dipping normal faults that make up the East Heights Fault Zone (EHFZ). Offsets in deposits of Tertiary and Quaternary age observed in borehole lithologic and geophysical logs were used to map these faults. The boundaries of the displacement lobes observed in the 793- and 211-day interferograms (figs. 2a, 2b) correlate well with the mapped extent of these faults, suggesting that the faults have low permeability, which impedes flow and the propagation of water-level changes. As previously noted, these apparent subsidence and elastic-rebound lobes could be artifacts resulting from localized tropospheric delays in the September 3, 1995, SAR data. An additional interferogram spanning a time with similar water-level variations would help discriminate between these alternatives. The 385-day interferogram (fig. 2d) does not span a time with significant seasonal water-level change. The 560-day interferogram (fig. 2e) does span a seasonal change, but is contaminated by atmospheric effects in the area of interest. An interferogram processed from SAR data collected in January and August 1997 would span a time with seasonal water-level variation and might further illuminate the presence of permeability barriers in the Albuquerque and Rio Rancho areas.

The north-south trends of faults in the EHFZ (fig. 2b) are from a compilation by Hudson and others (1999). Connell (2000) interpreted a northwesterly trend divergence of these faults in north Albuquerque, in accordance with a regional structural interpretation (John Hawley, Hawley GeoMatters, oral commun., 2000). The northwesterly trend of the eastern boundary of the subsidence lobe in figure 2a might support this interpretation. Because water-level change (and consequent observed elastic compression) is a convolved response to pumping and spatially variable aquifer-system hydraulic diffusivities, it is difficult to discriminate the hydraulic effect of these structural alternatives without ground-water-flow modeling. Plummer and others (2001) mapped zones of different water quality in the Albuquerque area. Differences in stable isotopes discriminate zones containing ground water recharged from the Sandia Mountains versus the Rio Grande River. The boundary between the two zones generally corresponds with the EHFZ location, further suggesting that ground-water flow from the mountain front is impeded by low-permeability faults such as the Alameda, Eubank, and Coronado strands of the EHFZ.

CONCLUSIONS

Interferometric measurements of land-surface-elevation change suggest that aquifer-system compression resulting from ground-water withdrawals in the Albuquerque area probably has remained elastic (recoverable) from July 1993 through September 1999. Evidence suggests that some inelastic (permanent) compaction and land subsidence might have occurred in the Rio Rancho area, but this cannot be concluded because of the absence of contemporaneous ground-water-level data. Patterns of subsidence and uplift in both Albuquerque and Rio Rancho suggest that intra-basin faults might impede ground-water diffusion at seasonal time scales. Alternatively, apparent patterns of compression and elastic rebound might result from spatially coincident tropospheric delay effects in the September 3, 1995, SAR data. An additional interferogram spanning the time from January to August 1997 might help discriminate between these alternatives.

Status of Radar Interferometry for Operational Subsidence Monitoring

By Sean M. Buckley[1]

Abstract

Repeat-pass differential InSAR is a satellite imaging technique that can provide wide-area mapping (100- by 100-kilometer individual SAR scenes) of natural and anthropogenic earth-surface deformation at high spatial detail (<100- by 100-meter pixels are typically attainable) and measurement resolution (~1 centimeter). InSAR measurements of subsidence associated with ground-water pumping have been made in several metropolitan areas in the United States and elsewhere, demonstrating the potential for InSAR to provide valuable information for use in urban and water-resources management and planning. This paper presents an overview of current InSAR capabilities and limitations as they pertain to operational monitoring of land subsidence.

HISTORICAL DEVELOPMENT AND LIMITATIONS

Historical Development

Radar interferometry uses multiple SAR images to measure earth-surface topography and deformation. The SAR instrument works by alternately transmitting microwave pulses and receiving the backscattered signals from the surface. The radar coherently measures the return signal—that is, the received pulse amplitude and phase are preserved. In InSAR, the differences in the phases of nearly-coincident SAR images collected at different times are related to surface topography and deformation measured along the radar line-of-sight. The deformation phase signatures are isolated by removing the topography with another interferogram or an independent digital elevation model (Rosen and others, 2000).

[1] Center for Space Research, The University of Texas, Austin, Tex.

Building on the U.S. Seasat mission in 1978 (satellite failure after 100 days) and the U.S. Shuttle Imaging Radar missions in the 1980s and 1990s, several civilian satellite SAR missions have been launched. These missions include the European ERS–1 (1991–2000), ERS–2 (1995–present), and Envisat (launched in early March 2002 and followed by a 7- to 9-month commissioning phase); the Japanese JERS–1 (1992–98); and the Canadian Radarsat (1995–present). ERS–1/2 have provided the majority of usable InSAR data to date with several future missions planned to collect SAR data for interferometry applications.

The range and sophistication of InSAR earth-science applications have advanced greatly during the past decade. InSAR has developed into a viable and valuable tool for measurement of earth-surface deformation through study of natural and anthropogenic hazards such as seismic activity (Bürgmann and others, 1998; Peltzer, Crampé, and Rosen, 2001; Sandwell and others, 2000; Zebker and others, 1994) and subsidence associated with subsurface fluid withdrawal (Amelung and others, 1999; Bawden and others, 2001; Fielding and others, 1998; Galloway and others, 1998; Hoffmann and others, 2001). InSAR scientific studies have progressed from single interferogram investigations of line-of-sight deformation over a given time period (Massonnet and others, 1993) to multi-interferogram reconstructions of three-dimensional displacements (Fialko and others, 2001) and InSAR time series of continuous but variable deformation (Amelung and others, 1999; Bawden and others, 2001; Berardino and others, 2001; Hoffmann and others, 2001).

Radar interferometry processing algorithms also have matured. Analyses of tens of interferograms for a given study area have been the result of the general availability of interferometry software packages from, for example, the Jet Propulsion Laboratory (ROI_PAC), Delft Institute for Earth-Oriented Space Research (DORIS), Centre National d'Etudes Spatiales (DIAPASON), Vexcel Corporation (Phase and Focus)

and Gamma Remote Sensing (ISP and DIFF&GEO). Although these software packages are available with varying levels of robustness and cost, the most common current (2001) higher-level InSAR product is the differential interferogram.

Limitations

The primary limitations of repeat-pass InSAR are decorrelation and the presence of interferometric phase artifacts (Sandwell and Sichoix, 2000, table 1). Random rearrangement of individual scatterers within a pixel results in temporal decorrelation. At the ERS C-band wavelength (5.6 cm), urban areas generally are well correlated but widespread decorrelation is observed in vegetated areas. At longer wavelengths, for example L-band (24 cm), signal penetration of vegetation is possible and generally results in higher coherence in vegetated areas, although cultivated agricultural fields might still decorrelate over time. Geometric decorrelation is a result of the relation between the interferometric baseline (differences in positions of the SAR antenna phase centers at the two times when the target was imaged) and the maximum correlation between the SAR images. In other words, the maximum correlation decreases to zero at the critical baseline. For ERS, the critical perpendicular baseline is about 1,100 m, with a practical perpendicular baseline limit of about 400 m for conventional InSAR applications. Geometric decorrelation can be mitigated by maintaining the satellite repeat-orbit path sufficiently less than the critical baseline. For example, more stringent orbit control has resulted in significantly more ERS–1/2 InSAR data relative to the Radarsat and JERS–1 satellites.

The most prominent interferometric phase artifacts can be attributed to the atmosphere and imprecise knowledge of the interferometric baseline. Atmospheric artifacts are associated with variations in the ionosphere and troposphere, with spatial and temporal variations in water vapor typically being the largest source of error. These variations occur with varying power at all spatial scales. Examples include kilometer-scale artifacts that appear similar to localized subsidence features and large-scale phase ramps spanning much of the interferogram. Imprecise knowledge of the baseline results in similar broad-scale residual phase ramps across the flattened interferogram. However, these phase ramps typically are removed using a few topographic or deformation control points distributed across the image.

Atmospheric phase artifacts complicate the interpretation of differential interferograms. For differential interferogram phase signatures greater than the largest phase signatures associated with the atmosphere (about one cycle of phase) and spatial extent less than the size of the interferogram, visual inspection of a few interferograms can be used to confirm that the signature is surface deformation. In other words, phase signatures that are persistent across several independent interferograms likely are related to deformation. For analyses of many interferograms and more subtle and complex deformation (for example, millimeter- to centimeter-scale interseismic displacement or time-varying subsidence), these qualitative comparisons are neither satisfying nor tractable.

The capability of conventional InSAR for detecting and measuring regional-scale land subsidence, as well as InSAR's failings in vegetated and agricultural areas, have been demonstrated in several areas in the United States: Antelope Valley (Galloway and others, 1998), Coachella Valley (Sneed and others, 2001), and Los Angeles (Bawden and others, 2001) in California; Las Vegas, Nev. (Hoffmann and others, 2001); Phoenix, Ariz. and Houston, Tex. (Buckley, 2000). Although the densely urban areas in Houston remain coherent over time, vegetation in the less-developed coastal areas between Houston and Galveston decorrelate over time. In Phoenix and the Coachella Valley, maximum subsidence and water-level declines are in agricultural areas. However, temporal decorrelation occurs in these areas, making it difficult to image the full extent of the subsidence using InSAR. In addition, differential subsidence associated with growth faults in Houston and earth fissures in Phoenix and Antelope Valley can be transient, making it more difficult to distinguish from atmospheric artifacts. In summary, decorrelation and atmospheric artifacts can make it difficult to resolve temporally and spatially varying land subsidence from conventional InSAR without careful consideration of several interferograms.

RECENT AND POTENTIAL FUTURE DEVELOPMENT

Alternative strategies for mapping subtle and complex deformation using InSAR data have been identified in recent studies. What has been published is

discussed in this section and indicates the great potential for these post-processing strategies.

Multi-Track Interferogram Combination

Whereas a single interferogram captures the component of surface deformation along the radar line-of-sight and might not completely span a deformation feature of interest, combinations of multiple tracks of InSAR data can be used to determine a fuller extent of the deformation. For example, spaceborne SAR systems can collect data over a given location on both ascending and descending satellite passes or for combinations of adjacent and overlapping tracks. Interferograms made from ascending and descending image pairs can provide a sense of whether the observed deformation has mixed vertical and horizontal components. Fialko and others (2001) reveal the three-dimensional coseismic displacement field of the October 1999 Hector Mine earthquake through the use of InSAR from ascending and descending passes and the SAR image-pair registration offset information. Peltzer and others (1999) used data from three adjacent satellite tracks to capture the 170-km-long surface rupture associated with the November 1997 Manyi, Tibet, earthquake: A combination of multi-track interferogram measurements can provide a synoptic view of regional subsidence and potentially might reveal horizontal deformation associated with subsurface pumping, although this has not been demonstrated satisfactorily.

Interferogram Stacking

Interferogram stacking techniques use single-track, multi-interferogram combinations to reduce noise and enhance topographic and deformation signatures of interest. These techniques borrow from seismic stacking techniques and have been used to extract information from InSAR data from the ERS–1/2 missions. For example, Sandwell and Price (1998) and Sandwell and Sichoix (2000) used stacking of the InSAR phase gradient for topographic and deformation mapping. In addition, Peltzer, Crampé, Hensley, and Rosen (2001) have further manipulated a stack of interferograms to assess the accuracy of their deformation estimates through a "jackknife" procedure in which an interferogram is removed and an uncertainty computed for the reduced stack. This and other statistical methods can be used to determine an optimal set of interferograms to minimize the stack uncertainty. In more general terms, interferogram stacking is a problem of determining the optimal weights to apply to each interferogram in the stack and will depend, in part, on the nature of the signature of interest and its behavior over time.

Interferogram Time Series Analysis

Recent InSAR research has focused on interferometry time series analysis. Of the various techniques developed over the past few years, permanent scatterer analysis has garnered the most attention. As noted previously, the presence of vegetation results in widespread decorrelation over time for C-band InSAR. However, hundreds to thousands of sub-pixel scatterers, such as isolated buildings in vegetated areas, remain coherent over time. Ferretti and others (2000, 2001) have shown, and others have confirmed, that a time series analysis of these permanent scatterers yield viable InSAR point measurements of surface deformation. The technique works by using tens of SAR images to jointly estimate the surface deformation, topographic height, and atmospheric delay associated with each permanent scatterer over time. Whereas geometric decorrelation limits the maximum usable baseline in conventional InSAR, isolated subpixel-size dominant scatterers (relative to other scatterers within the SAR pixel) remain coherent over time and for baselines larger than the critical baseline. Consequently, the advantage of permanent scatterer analysis over traditional InSAR is its ability to use high spatial baseline interferograms and isolated points of correlation that would otherwise be unused. However, this comes at the cost of abandoning significant amounts of the original InSAR data.

Additional time series techniques have been applied to a series of interferograms in their entirety. For example, Amelung and others (1999); Bawden and others (2001); and Hoffmann and others (2001) have used time-sequential and nearly time-sequential interferograms to produce time series of land-surface displacements (subsidence and uplift) over deforming aquifer systems. In addition, Berardino and others (2001) have shown that multiple sets of small-spatial-baseline interferograms can be combined using a least-squares and single-value decomposition strategy to produce an InSAR time series. The result is a history of deformation, relative to a given reference image date, at each of the subsequent SAR acquisition dates and broadly applied to areas of generally good coherence.

OPEN ISSUES FOR OPERATIONAL USE

Integration of Higher-Level InSAR Products

With the routine generation of differential interferograms now possible, attention must now turn toward providing higher-level subsidence products of more direct value to the water-resource and infrastructure management communities. For example, instead of distributing several differential interferograms, profiles through the data, and an interpretation based on careful consideration of the dates of the radar acquisitions, research groups and software vendors are beginning to produce GIS-format deformation time series at selected points or over a given area. Other useful products might include deformation maps with decorrelated areas filled and associated error estimates based on ancillary atmospheric information. In addition, recent attention has focused on integrating InSAR deformation measurements into ground-water-flow and aquifer-system-compaction models (Galloway and others, 1998; Hoffmann and others, 2003). It remains an open question as to what form, at what stage, and how best to use InSAR subsidence measurements in the modeling process. Finally, InSAR has been used repeatedly to report on past deformation. A future use of InSAR would be as a predictive tool—subsidence risk maps based on the temporal and spatial evolution of InSAR-observed subsidence, projected water-use patterns, and subsidence prediction from coupled ground-water-flow and aquifer-system-compaction models. InSAR-derived data products of these types would integrate into the water resource and infrastructure management decision-making process.

Dedicated InSAR Missions

The most critical open questions related to the future applicability of InSAR to monitoring subsidence caused by aquifer-system compaction are also the most basic: Will there be consistent, periodic SAR measurements made in the future to conduct InSAR subsidence monitoring of critical subsidence-prone areas? If so, will the next generation of SAR satellite platforms provide usable data in vegetated and agricultural areas? The decade-long ERS–1/2 missions are nearing an end. Envisat, the next European C-band SAR satellite, was launched in early March 2002. Another Canadian C-band Radarsat mission as well as a Japanese L-band ALOS mission are planned. These satellites will carry advanced SAR systems with flexibility in the choice of temporal and spatial coverage, spatial and radiometric resolutions, imaging geometries, and polarizations. However, the myriad of imaging options decreases the likelihood that consistent SAR measurements will be made for use in an InSAR time series analysis of deformation over a given area. To develop radar interferometry into a reliable subsidence-monitoring tool requires an operational SAR satellite program dedicated to preserving cross-platform interferometry and single-mode collection reliability. The choice of radar frequency will be a trade-off between greater sensitivity to deformation for C-band platforms versus the capability to map subsidence in more vegetated areas for L-band platforms.

International Land Subsidence Data Base

By Keith R. Prince[1], Roy Sonenshein[2], *and* George Karavitis[3]

Abstract

In 1975 the International Association of Hydrological Sciences and the United Nations Educational Scientific and Cultural Organization developed a four-page questionnaire designed to collect information on the occurrence, location, causes, and other ancillary data related to land subsidence cases. Periodic distribution of the questionnaire has resulted in the documentation of nearly 100 cases of land subsidence worldwide. This data base represents a wealth of information about the spatial and temporal distribution of land subsidence, with the potential for being a significant resource for public works administrators, engineering agencies, resource managers, and scientists throughout the world. Unfortunately, this valuable data base exists only as paper files, making it nearly inaccessible for broad beneficial use.

The U.S. Geological Survey has constructed a digital relational data base on land subsidence to facilitate the compilation of existing data and the collection of new information about international case studies, and to make the data widely available over the World Wide Web for analysis and synthesis. Users have unrestricted access to retrieve data over the Internet using Web browser software and can enter new case studies and data through the data base Web interface. Newly entered data will be verified prior to being made available for retrieval. Eight broad categories were established for the relational data base on the basis of the content and structure of the original paper questionnaire. These are: location of subsidence, probable cause of subsidence, subsidence details, description of subsidence area, observation and measurement, effects of subsidence, bibliography regarding reported subsidence, and reporting party. In addition, the data base has the capability to store images of location maps and photographs.

INTRODUCTION

Problems related to the sinking of the land surface as a result of anthropogenic activities have been recognized for centuries. Increased exploitation of natural resources in the 20th century has caused an increase in the occurrence and magnitude of human-induced land subsidence. The seriousness of land subsidence has long been recognized by many scientific organizations and political entities, and in 1965 the United Nations Educational, Scientific and Cultural Organization (UNESCO) included land subsidence as one of the topics to be studied during the International Hydrological Decade (IHD) 1965–74. When the IHD concluded in 1974, UNESCO launched the International Hydrological Programme (IHP), the first phase of which was from 1975 to 1980. The subject of land subsidence was included in the framework of the IHP and has been retained in the work plan for each subsequent phase of the Programme.

In 1975, the Intergovernmental Council for the IHP established a Working Group for coordination of the IHP subproject "Investigation on land subsidence due to ground-water exploitation." One of the tasks of the group was the publication of a guidebook on land subsidence due to ground-water withdrawal (Poland, 1984). The guidebook included an introduction to the processes that control land subsidence, a table summarizing 42 worldwide occurrences of land subsidence, and detailed descriptions of nine case studies. The primary source of information on the 42 occurrences of land subsidence was a questionnaire that had been developed and distributed worldwide by the International Association of Hydrological Sciences (IAHS). In addition to land subsidence caused by aquifer-system compaction resulting from ground-water withdrawal, the IAHS questionnaire was designed to collect information on land subsidence as a result of the extraction of oil, gas, and brine, as well as geothermal development, the drainage of organic soils, mining, the dissolution and collapse of carbonate and evaporite (karst) rocks, and other causes of land subsidence.

[1] U.S. Geological Survey, Menlo Park, Calif.
[2] U.S. Geological Survey, Miami, Fla.
[3] U.S. Geological Survey, Ft. Meyers, Fla.

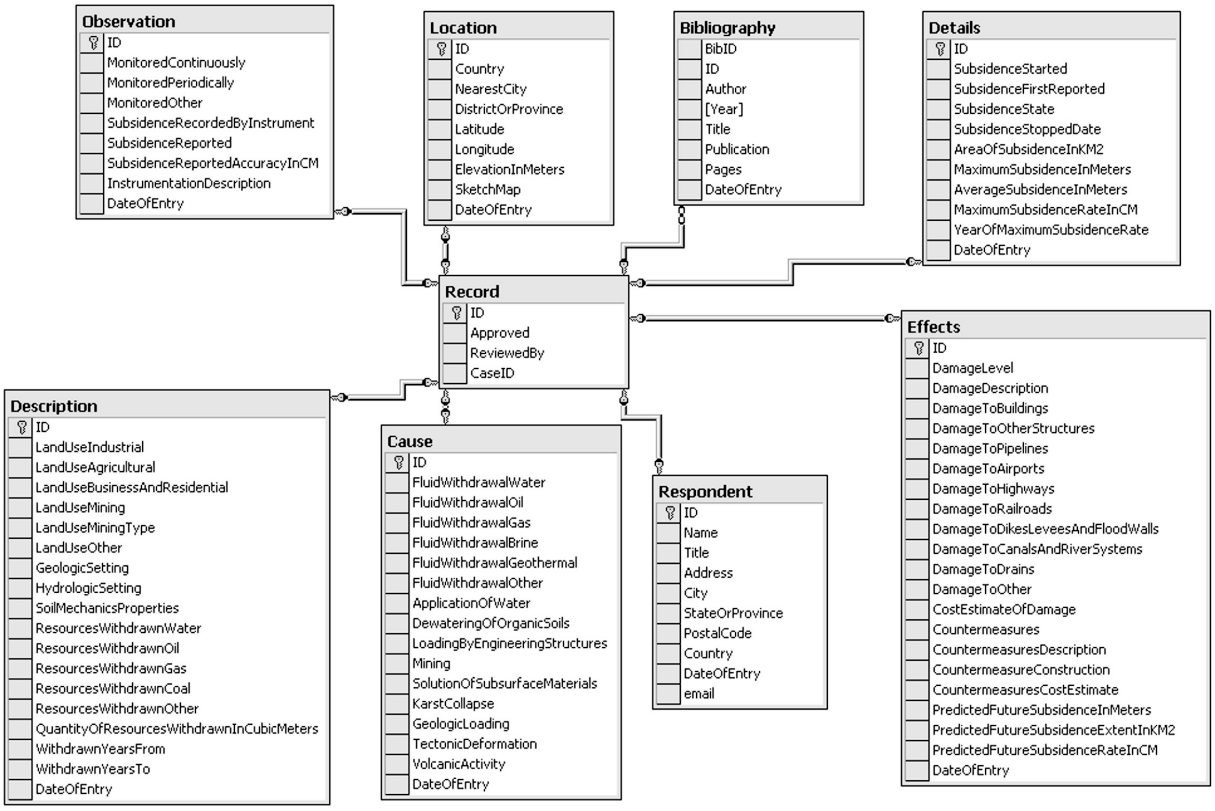

Figure 1. Diagram showing data base functional relations.

The questionnaires have been distributed worldwide at international symposia and conferences since 1975, and nearly 100 case studies of land subsidence in more than 20 countries have been documented. Unfortunately, the information contained in the questionnaires exists only as paper files, making it nearly inaccessible for broad beneficial use. Furthermore, the information cannot be easily synthesized or summarized. The U.S. Geological Survey (USGS) has constructed a digital relational data base on land subsidence to make the existing information about international case studies widely available for analysis and synthesis, and to facilitate the collection of new information about other case studies.

ELECTRONIC DATA BASE CONCEPT

The primary goals for constructing the data base were to (1) organize and store the existing information in a way that would promote data synthesis and analysis, (2) facilitate the collection and storage of new information on occurrences of land subsidence, (3) make the data readily accessible to the widest possible audience, and (4) effectively archive the information. A relational data base was constructed and coupled with a World Wide Web interface to expedite queries and the entry of new case studies. The data reside on a Windows® 2000 server using Microsoft® Enterprise Relational Data Base SQL Server software.

The initial design, content, and structure of the data base are based on the original paper questionnaire that was distributed by the IAHS. Each occurrence or case study of land subsidence is described by an individual record. Descriptive data on land subsidence for each case study are organized into eight major categories (fig. 1). These categories are location of subsidence, probable cause of subsidence, subsidence details, description of subsidence area, observation and measurement, effects of subsidence, bibliography regarding reported subsidence, and reporting party. In addition, the data base has the capability to store images

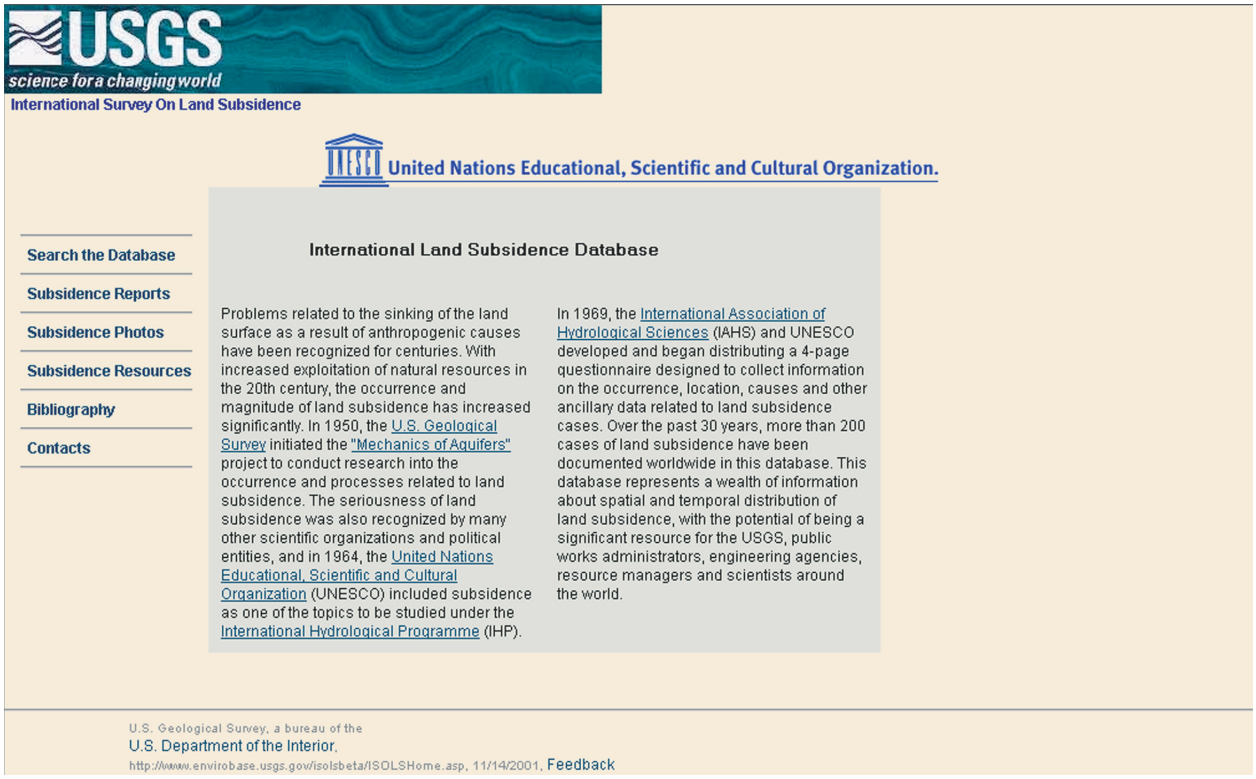

Figure 2. Screen capture showing a prototype of the Internet gateway page to the International Land Subsidence Data Base, as it appeared November 2001.

of location maps and photographs. The data base design is flexible to allow for future expansion of functionality, such as adding new tables or altering existing data tables. Future data base enhancements might include the addition of a geographic information system interface.

DATA BASE WEB INTERFACE

The data base is available to the public through the World Wide Web using widely available Internet browser software. Version 6.0 and newer versions of Microsoft® Internet Explorer or Netscape Navigator are recommended to obtain all the benefits of the data base Web interface. The Web site and data base are accessible at http://isols.usgs.gov/, or through the USGS Ground Water Information Pages Web site at http://water.usgs.gov/ogw. Figure 2 shows the Internet gateway page to the data base as it appeared November 2001; the layout and content of this prototype page might change. Users have unrestricted access to retrieve data over the Internet using several available query screens, and information for new case studies of land subsidence can also be entered. However, for quality control reasons, the data base manager will verify newly entered data before they are made available to the public for retrieval.

Data Base Query Features

The data base can be queried using the "Search" button on the data base gateway page (fig. 2). Selecting the "Search" button displays a new page with options to search the data base by country, list all records in the data base, or retrieve the available data for all records or case studies in Microsoft® Excel format (fig. 3). Individual case study reports can be obtained by selecting the desired record from the results of the "Search by Country" or "List all Records" options. The case study report lists all the available data for the selected record on a single Web page. The data can be read by scrolling down the page or can be printed by selecting the print function of the user's Web browser. The "Search" function works well for browsing the data base for information but is not ideal for downloading

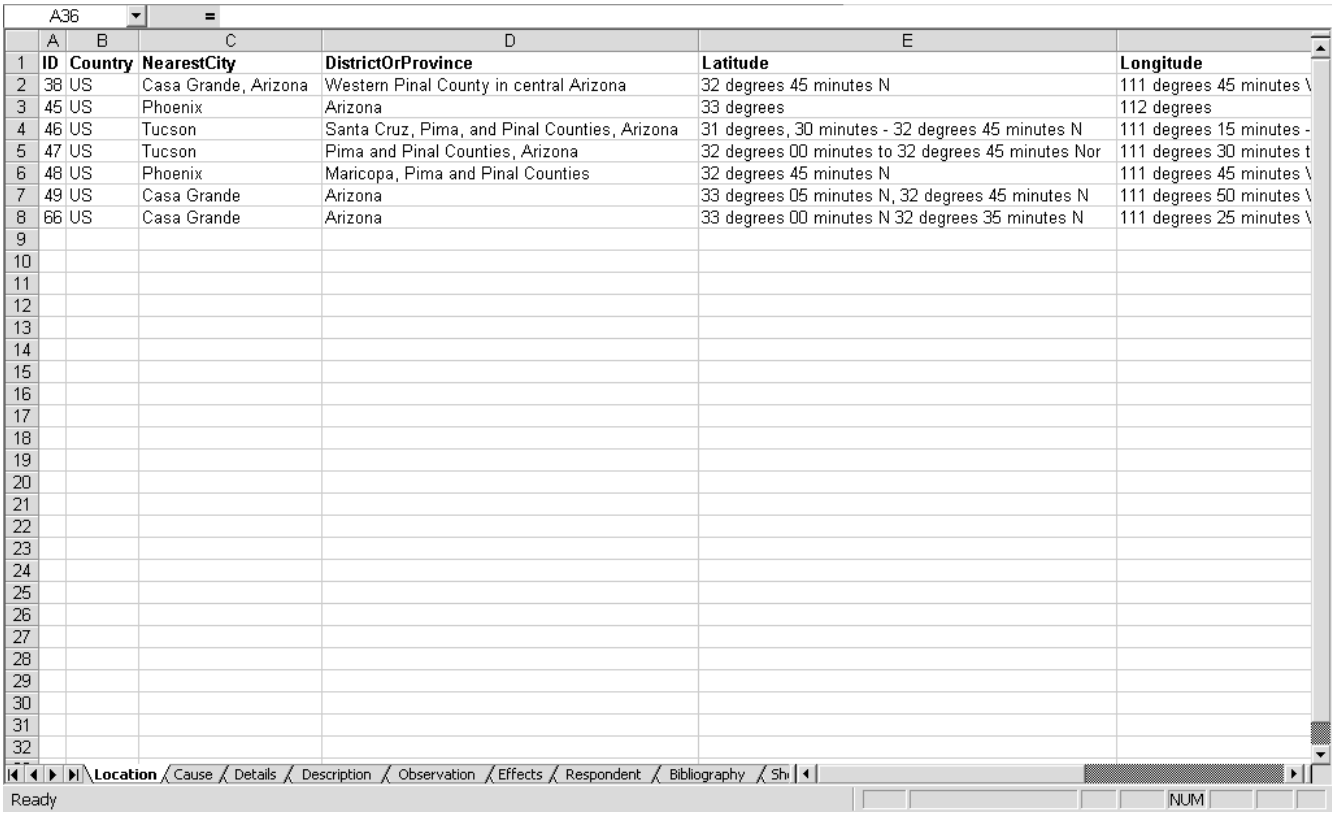

ID	Country	NearestCity	DistrictOrProvince	Latitude	Longitude
38	US	Casa Grande, Arizona	Western Pinal County in central Arizona	32 degrees 45 minutes N	111 degrees 45 minutes \
45	US	Phoenix	Arizona	33 degrees	112 degrees
46	US	Tucson	Santa Cruz, Pima, and Pinal Counties, Arizona	31 degrees, 30 minutes - 32 degrees 45 minutes N	111 degrees 15 minutes -
47	US	Tucson	Pima and Pinal Counties, Arizona	32 degrees 00 minutes to 32 degrees 45 minutes Nor	111 degrees 30 minutes t
48	US	Phoenix	Maricopa, Pima and Pinal Counties	32 degrees 45 minutes N	111 degrees 45 minutes \
49	US	Casa Grande	Arizona	33 degrees 05 minutes N, 32 degrees 45 minutes N	111 degrees 50 minutes \
66	US	Casa Grande	Arizona	33 degrees 00 minutes N 32 degrees 35 minutes N	111 degrees 25 minutes \

Figure 3. Screen capture showing a prototype of the Microsoft® Excel export format, as it appeared November 2001.

data for manipulation and analysis. Users planning to analyze or manipulate the data should use the Excel spreadsheet capability to download the data in digital form.

Reporting Case Studies

Data base users can submit case studies and additional information by selecting the "Subsidence Reports" button on the data base gateway page (fig. 2). The user is then given the option to either print the original IAHS questionnaire for submittal by mail, or enter the data interactively using the Web browser. For quality control reasons, data entered interactively are not available for public access from the data base until the data have been verified by the data base manager.

The data required to enter a case study (table 1) are extensive. Users are cautioned not to begin entry of data for a case study until all the available data have been gathered and organized. To aid the user in identifying the information needed to enter a new case study, a complete list of required data can be displayed and printed by selecting the "Review Required Information" button. To enter data interactively, the user selects the "Submit a New Subsidence Report" button on the "Subsidence Reports" Web page. A series of interactive data entry forms are then displayed that must be filled in by the user to complete the subsidence report.

Entry of data for a new case study does not have to be completed in a single session. The user can begin a data entry session, suspend that session at anytime after the first screen has been completed, and return at a later date to add more data or complete the case study. Key to suspending and resuming a data entry session is the unique case study identifier. Once the first screen of data identifying the respondent has been entered, the unique case study identifier is displayed. The user should record the unique identifier so that the correct record can be accessed for data entry later. To return to entering data for a partially completed case study, the user must navigate to the page for entering a new case study and enter the unique case study identifier where

Table 1. Entry fields for new subsidence case study records

RESPONDENT	DETAILS	OBSERVATION
Name	Subsidence started	Monitored continuously
Title	Subsidence first reported	Monitored periodically
Address	Subsidence state	Monitored other
City	Subsidence stopped date	Subsidence recorded by instrument
State or Province	Area of subsidence	Subsidence reported
Postal code	Maximum subsidence in meters	Subsidence reported accuracy
Country	Average subsidence in meters	Instrument description
Date of entry	Maximum subsidence rate	
Email address	Year of maximum subsidence rate	**EFFECTS**
	Land use industrial	Damage level
LOCATION	Land use agricultural	Damage to buildings
Country	Land use business and residential	Damage to other structures
Nearest City	Land use mining	Damage to pipelines
District or Province	Land use mining type	Damage to airports
Latitude	Land use other	Damage to highways
Longitude	Geologic setting	Damage to railroads
Elevation in meters	Hydrologic setting	Damage to dikes, levees, etc.
Sketch map	Soil mechanics properties	Damage to canals and rivers
	Resources withdrawn water	Damage to drains
CAUSE	Resources withdrawn oil	Damage to other
Fluid withdrawal water	Resources withdrawn gas	Cost estimate of damage
Fluid withdrawal oil	Resources withdrawn coal	Countermeasures
Fluid withdrawal gas	Resources withdrawn other	Countermeasures description
Fluid withdrawal brine	Quantity of resources withdrawn	Countermeasures construction
Fluid withdrawal geothermal	Withdrawn years (from)	Countermeasures cost estimate
Fluid withdrawal other	Withdrawn years (to)	Predicted future subsidence
Application of water		Predicted future subsidence extent
Dewatering of organic soils		Predicted future subsidence rate
Loading by engineered structures		
Mining		**BIBLIOGRAPHY**
Solution of subsurface materials		Author
Karst collapse		Year
Geologic loading		Title
Tectonic deformation		Publication
Volcanic activity		Number of pages

requested (fig. 4). Data entry will then begin at the point where data entry was suspended during the previous session.

As currently implemented, the data base does not have time-series capabilities. The data base can only store information on a given case study for a single time. For example, the maximum observed subsidence (and many other subsidence descriptors) cannot be updated if subsidence continues in an area once a case study has been entered. At this subsequent time, the only way new information can be entered is by creating a new case study. Future data base enhancements are planned that

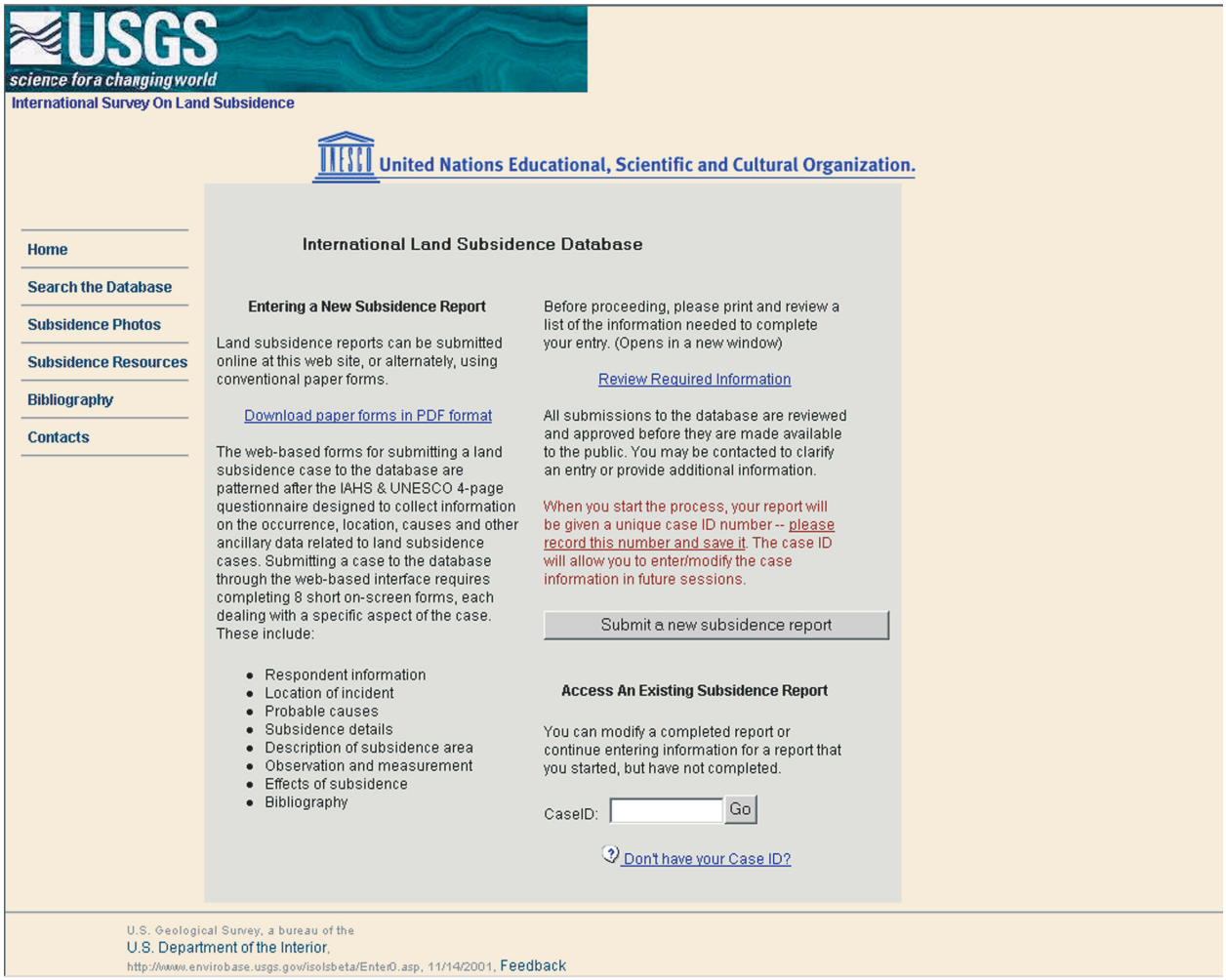

Figure 4. Screen capture showing the prototype web page used to begin entering a new subsidence case study, as it appeared November 2001.

will allow users revisiting an area that has already been entered into the data base to enter new information for case studies.

Photo Gallery

Digital photographs of subsidence-related features can be stored in the data base. Those that are related to case studies that reside in the data base can be linked to the appropriate case study. Available photos can be viewed and downloaded by selecting "Subsidence Photos" from the data base gateway page (fig. 2). The next page displayed will list case studies that have photos stored in the data base. Photos that are not linked to stored case studies are listed under the category "General Photos." The user can display the available photos in thumbnail form by selecting the desired case study, and a larger version of each photo can be viewed by selecting the desired thumbnail photo. The displayed photo can be downloaded by right-clicking on the photo and selecting "Save Image as" on the drop-down menu.

Online instructions for storing photos in the data base can be accessed by selecting "Submission Instructions" on the Subsidence Photos page. All photos submitted for storage in the data base must be in the public domain or must include written permission from the copyright holder to display the photos on the International Survey on Land Subsidence (ISOLS) Web site. Photos must be submitted for inclusion in the data base as attachments to an e-mail to the ISOLS data base administrator (isols@usgs.gov). The following

information must be included with each photo submitted for inclusion in the data base:

- The case study identifier of the related subsidence event in the ISOLS data base, or "None" if entering a general subsidence photo (not related to a specific case).
- The date and location the photo was taken.
- A short description of what is shown in the scene.
- Credits or copyright information.
- The name and organizational affiliation of the person submitting the photo.
- Authorization to display the photo.

Bibliography

The data base includes a bibliography that is linked to the case studies stored in the data base. The bibliography can be accessed and displayed by selecting "Bibliography" on the data base gateway page (fig. 2). Each bibliographic entry includes a link to display the related case study details, which are identical to the information displayed when selecting a case study under the "Search Data Base" capability.

Subsidence Resources

Selecting "Subsidence Resources" from the data base gateway page (fig. 2) provides access to a listing of subsidence-related resources and information, including links to Web pages and subsidence reports that are available on the Web. Selecting either the subsidence-related Web pages or Subsidence Reports option opens a new Web browser window in which the selected resource is displayed. Reports are made available from the ISOLS data base Web site in HTML or PDF formats only. Links also are available on the "Subsidence Resources" page to allow users to report either new Web links and reports or broken links.

REFERENCES CITED

Ahlfeld, D.P., and Mulligan, A.E., 2000, Optimal management of flow in groundwater systems: San Diego, Calif., Academic Press, 185 p.

Alpha Geoscience, 1996, Geologic and hydrogeologic investigation of the Genesee River valley: Albany, N.Y., Alpha Geoscience, Project no. 95132, 31 p.

Amelung, Falk, Galloway, D.L., Bell, J.W., Zebker, H.A., and Laczniak, R.J., 1999, Sensing the ups and downs of Las Vegas—InSAR reveals structural control of land subsidence and aquifer-system deformation: Geology, v. 27, no. 6, p. 483–486.

Argus, D.F., Heflin, M.B., Donnellan, Andrea, Webb, F.H., Dong, Danon, Hurst, K.J., Jefferson, D.C., Lyzenga, G.A., Watkins, M.M., and Zumberge, J.F., 1999, Shortening and thickening of metropolitan Los Angeles measured and inferred by using geodesy: Geology, v. 27, no. 8, p. 703–706.

Baguelin, F., Jezequel, J.F., and Shields, D.H., 1978, The pressuremeter and foundation engineering: Clausthal, Germany, Trans Tech Publications, 617 p.

Bartolino, J.R., and Cole, J.C., 2002, Ground-water resources of the middle Rio Grande Basin, New Mexico: U.S. Geological Survey Circular 1222, 132 p.

Bawden, G.W., Thatcher, Wayne, Stein, R.S., Hudnut, K.W., and Peltzer, Gilles, 2001, Tectonic contraction across Los Angeles after removal of groundwater pumping effects: Nature, v. 412, p. 812–815.

Bell, J.W., 1981a, Results of leveling across fault scarps in Las Vegas Valley, Nevada, April 1978–June 1981: Nevada Bureau of Mines and Geology Open-File Report 81–5, 7 p.

_____1981b, Subsidence in Las Vegas Valley: Nevada Bureau of Mines and Geology Bulletin 95, 84 p., 1 pl.

Bell, J.W., Amelung, Falk, and Ramelli, A.R., 2000, Land subsidence in Las Vegas, Nevada, USA—New geodetic data reveal localized spatial patterns, structural controls, and reduced rates, *in* Carbognin, L., Gambolati, G., and Johnson, A.I., eds., Land subsidence—Proceedings of the Sixth International Symposium on Land Subsidence, Ravenna, Italy, September 24–29, 2000: V. II, p. 127–138.

Bell, J.W., Amelung, Falk, Ramelli, A.R., and Blewitt, Geoff, 2002, Land subsidence in Las Vegas, Nevada, 1935–2000—New geodetic data show evolution, revised spatial patterns and reduced rates: Environmental and Engineering Geoscience, v. 8, no. 3, p. 155–174.

Bell, J.W., and Price, J.G., 1991, Subsidence in Las Vegas Valley 1980–1991: Nevada Bureau of Mines and Geology Open-File Report 93–5, 182 p.

_____1993, Subsidence in Las Vegas Valley, 1980–91—Final project report: Nevada Bureau of Mines and Geology, Open-File Report 93–4 [variously paged], 9 pls., scale 1:62:500.

Berardino, P., Fornaro, G., Fusco, A., Galluzzo, D., Lanari, R., Sansosti, E., and Usai, S., 2001, A new approach for analyzing the temporal evolution of Earth surface deformations based on the combination of DIFSAR interferograms, *in* International Geoscience and Remote Sensing Symposium, Proceedings: Institute of Electrical and Electronics Engineers, v. 6, p. 2,551–2,553.

Bloyd, R.M., Jr., 1967, Water resources of the Antelope Valley East-Kern Water Agency area, California: U.S. Geological Survey Open-File Report, 69 p.

Bock, Yehuda, Fang, Peng, Behr, Jeff, Dean, Jeff, Williams, Simon, Jie, Zhang, and Aki, Keiitti, 1997, Southern California Integrated GPS Network (SCIGN)/Permanent GPS Geodetic Array (PGGA)—The 1996 SCEC annual report: Progress reports from Southern California Earthquake Center (SCEC) scientists, v. II 14–08–001–A0899.

Buckley, S.M., 2000, Radar interferometry measurement of land subsidence: Austin, University of Texas, Ph.D. dissertation, 229 p.

Bürgmann, Roland, Fielding, E.J., and Sukhatme, J., 1998, Slip along the Hayward fault, California, estimated from space-based synthetic aperture radar interferometry: Geology, v. 26, no. 6, p. 559–562.

Burkett, V., Ritschard, R., McNulty, S., O'Brien, J.J., Abt, R., Jones, J., Hatch, U., Murray, B., Jagtap, S., and Cruise, J., 2001, Potential consequences of climate variability and change for the southeastern United States, *in* National Assessment Team, U.S. Global Research Program, eds., Climate change impacts in the United States—Potential consequences of climate variability and change, foundation document: Cambridge, United Kingdom, Cambridge University Press, 620 p.

Campion, L.F., Chapman, R.H., Chase, G.W., and Youngs, L.G., 1983, Resource investigation of low- and moderate-temperature geothermal areas in Paso Robles, California: California Department of Mines and Geology, Open File Report 83–11 SAC, 54 p.

Carpenter, M.C., 1993, Earth-fissure movements associated with fluctuations in ground-water levels near the Picacho Mountains, south-central Arizona, 1980–84: U.S. Geological Survey Professional Paper 497–H, 49 p.

_____1999, South-central Arizona—Earth fissures and subsidence complicate development of desert water resources, *in* Galloway, D.L., Jones, D.R., and Ingebritson, S.E., eds., Land subsidence in the United States: U.S. Geological Survey Circular 1182, p. 65–78.

Carr, J.E., Meyer, W.R., Sandeen, W.M., and McLane, I.R., 1985, Digital models for simulation of ground-water hydrology of the Chicot and Evangeline aquifers along the Gulf Coast of Texas: Texas Department of Water Resources Report 289, 101 p.

Catchings, R.D., Goldman, M.R., Gandhok, G., Rymer, M.J., and Underwood, D.H., 2000, Seismic imaging evidence for faulting across the northwestern projection of the Silver Creek Fault, San Jose, California: U.S. Geological Survey Open File Report 00–125, 29 p.

Cederstrom, D.J., 1945, Geology and ground-water resources of the Coastal Plain in southeastern Virginia: Virginia Geological Survey Bulletin 63, 484 p.

Centre National d'Etudes Spatiales (C.N.E.S), 1997, PRISME/DIAPASON software, version 1.0: Toulouse, France.

Clarke, D.D., Henderson, C.P., and Strehle, Rick, 1987, Road log to the Long Beach area—Geologic field guide to the Long Beach area (guidebook): Pacific Section, American Association of Petroleum Geologists, v. 58, p. 135–159.

Connell, S.D., 2000, Geology of the Alameda quadrangle, Bernalillo and Sandoval Counties, New Mexico: Socorro, New Mexico Bureau of Mines and Mineral Resources Open-File Map GM–10, 1 sheet, scale 1:24,000.

Davis, G.H., 1977, Potential for land subsidence due to reduction of artesian head in the Atlantic Coastal Plain, *in* Hydraulics in the Coastal Zone, American Society of Civil Engineers Specialty Conference, College Station, Texas, August 10–11, 1977: American Society of Civil Engineers, p. 152–160.

_____1987, Land subsidence and sea level rise on the Atlantic Coastal Plain of the United States: Environmental Geology and Water Science, v. 10, no. 2, p. 67–80.

Denby, G.M., and Hughes, J.M.O., 1982, Horizontal stress interpretation of pressuremeter tests, *in* Saxena, S.K., ed., Updating subsurface samplings of soils and rocks and their in-situ testing: Engineering Foundation publication, p. 227–244.

Dibblee, T.W., 1974, Regional geologic map of San Andreas and related faults in Carrizo Plain, Temblor, Caliente, and La Panza ranges and vicinity, California: U.S. Geological Survey Miscellaneous Geologic Investigations Map I–757, scale 1:125,000.

Doherty, J., Brebber, L., and Whyte, P., 1994, PEST—Model-independent parameter estimation: Ipswich, Australia, Watermark Computing, 135 p.

Durbin, T.J., 1978, Calibration of a mathematical model of the Antelope Valley ground-water basin, California: U.S. Geological Survey Water-Supply Paper 2046, 51 p.

Earle, D.W., 1975, Land subsidence and maintenance costs to homeowners in east New Orleans, Louisiana: Baton Rouge, La., Louisiana State University, Ph.D. dissertation.

Epstein, V.J., 1987, Hydrologic and geologic factors affecting land subsidence near Eloy, Arizona: U.S. Geological Survey Water-Resources Investigations Report 87–4143, 28 p.

Fairbanks, R.G., 1989, A 17,000-year glacio-eustatic sea level record—Influence of glacial melting rates on the Younger Dryas event and deep ocean circulation: Nature, v. 342, no. 7, p. 637–642.

Ferretti, Alessandro, Prati, Claudio, and Rocca, Fabio, 2000, Nonlinear subsidence rate estimation using permanent scatters in differential SAR interferometry, *in* International Geoscience and Remote Sensing Symposium, Proceedings: Institute of Electrical and Electronics Engineers, v. 38, no. 5, p. 2,202–2,212.

_____2001, Permanent scatterers in SAR interferometry, *in* International Geoscience and Remote Sensing Symposium, Proceedings: Institute of Electrical and Electronics Engineers, v. 39, no. 1, p. 8–20.

Fialko, Yuri, Simons, Mark, and Agnew, D., 2001, The complete (3-D) surface displacement field in the epicentral area of the 1999, M_w 7.1, Hector Mine earthquake from space geodetic observations: Geophysical Research Letters, v. 28, no. 16, p. 3,063–3,066.

Fielding, E.J., Blom, Ron, and Goldstein, R.M., 1998, Rapid subsidence over oil fields measured by SAR interferometry: Geophysical Research Letters, v. 25, no. 17, p. 3,215–3,218.

Frazier, D.E., 1967, Recent deltaic deposits of the Mississippi River—Their development and chronology: Transactions of the Gulf Coast Association of Geological Societies, v. 17, p. 287–315.

Freeze, R.A., and Cherry, J.A., 1979, Groundwater: Englewood Cliffs, N.J., Prentice Hall, 604 p.

Gabrysch, R.K., 1979, Approximate altitude of water levels in wells in the Chicot and Evangeline aquifers in the Houston area, Texas, spring 1977 and spring 1978: U.S. Geological Survey Open-File Report 79–334, 4 sheets.

Gabrysch, R.K., and Bonnet, C.W., 1975, Land-surface subsidence in the Houston-Galveston region, Texas: Texas Water Development Board Report 188, 19 p.

Galloway, D.L., Hudnut, K.W., Ingebritsen, S.E., Phillips, S.P., Peltzer, Gilles, Rogez, Francois, and Rosen, P.A., 1998, Detection of aquifer-system compaction and land subsidence using interferometric synthetic aperture radar, Antelope Valley, Mojave Desert, California: Water Resources Research, v. 34, no. 10, p. 2,573–2,585.

Galloway, D.L., Jones, D.R., and Ingebritsen, S.E., 1999, Land subsidence in the United States: U.S. Geological Survey Circular 1182, 175 p.

_____2000, Measuring land subsidence from space: U.S. Geological Survey Fact Sheet 051–00, 4 p.

Gornitz, V., 1995, Sea-level rise—A review of recent past and near-future trends: Earth Surface Processes and Landforms, v. 20, p. 7–20.

Gosselink, J.G., 1984, The ecology of delta marshes in coastal Louisiana—A community profile: U.S.

Department of Interior, Fish and Wildlife Service, FWS/OBS–84–09, p. 134.

Gowan, S.W., Trader, S.M., and Van Sambeek, L.L., 1999, An apparent brine pool associated with anomalous closure patterns and the eventual failure of the Retsof Salt Mine, *in* Solution Mining Research Institute Fall Meeting, Proceedings: Encinitas, Calif., p. 241–272.

Hamilton, P.A., and Larson, J.D., 1988, Hydrogeology and analysis of the ground-water flow system in the Coastal Plain of southeastern Virginia: U.S. Geological Survey Water-Resources Investigations Report 87–4240, 175 p.

Hanson, R.T., 1989, Aquifer-system compaction, Tucson Basin and Avra Valley, Arizona: U.S. Geological Survey Open-File Report 88–4172, 69 p.

Hanson, R.T., and Benedict, J.F., 1994, Simulation of ground-water flow and potential land subsidence, upper Santa Cruz Basin, Arizona: U.S. Geological Survey Water-Resources Investigations Report 93–4196, 47 p.

Hantush, M.S., 1956, Analysis of data from pumping tests in leaky aquifers: Transactions American Geophysical Union, v. 37, no. 6, p. 702–714.

_____1959, Nonsteady flow to flowing wells in leaky aquifer: Journal of Geophysical Research, v. 64, no. 8, p. 1,043–1,052.

_____1960, Modification of the theory of leaky aquifers: Journal of Geophysical Research, v. 65, no. 11, p. 3713–3725.

Hantush, M.S., and Jacob, C.E., 1954, Plane potential flow of ground water with linear leakage: Transactions American Geophysical Union, v. 35, no. 6, p. 917–936.

_____1955, Nonsteady radial flow in an infinite leaky aquifer: Transactions American Geophysical Union, v. 36, no. 1, p. 95–100.

Harbaugh, A.W., Banta, E.R., Hill, M.C., and McDonald, M.G., 2000, Modflow–2000, the U.S. Geological Survey modular ground-water model—Users guide to modularization concepts and the ground-water flow process: U.S. Geological Survey Open-File Report 00–092, 121 p.

Harbaugh, A.W., and McDonald, M.G., 1996, User's documentation for MODFLOW–96, an update to the U.S. Geological Survey modular finite-difference ground-water flow model: U.S. Geological Survey Open-File Report 96–485, 56 p.

Hardy, H.R., Jr., and Leighton, F.W., 1977, eds., Proceedings, first conference on acoustic emission/microseismic activity in geologic structures and materials: Clausthal, Germany, Trans Tech Publications, 489 p.

Harrill, J.R., 1976, Pumping and ground-water storage depletion in Las Vegas Valley, Nevada, 1955–74: Nevada Department of Conservation and Natural Resources, Division of Water Resources Bulletin 44, 70 p., 1 pl.

Harris-Galveston Coastal Subsidence District, 1998, Ground-water management plan: Friendswood, Tex., 72 p.

_____1999, District regulatory plan, 1999: Friendswood, Tex., 17 p.

Hart, D., and Zilkoski, D., 1994, Mapping a moving target—The use of GIS to support the development of a subsidence model in the New Orleans Region: Urban and Regional Information Association, URISA 1994, p. 555–569, accessed September 5, 2001, at URL http://spatialodyssey.ursus.maine.edu/gisweb/spatdb/urisa/ur94049.html.

Helm, D.C., 1975, One-dimensional simulation of aquifer system compaction near Pixley, California—Part 1. Constant parameters: Water Resources Research, v. 11, no. 3, p. 465–478.

_____1976, One-dimensional simulation of aquifer system compaction near Pixley, California—Part 2. Stress-dependent parameters: Water Resources Research, v. 12, no. 3, p. 375–391.

_____1994, Horizontal aquifer movement in a Theis-Thiem confined system: Water Resources Research, v. 30, no. 4, p. 953–964.

Heywood, C.E., 1995, Investigation of aquifer-system compaction in the Hueco basin, El Paso, Texas, USA, *in* Barends, F.B.J., Brouwer, F.J.J., and Schroder, F.H., eds., Land subsidence—Proceedings of the Fifth International Symposium on Land Subsidence, The Hague, October 1995: International Association of Hydrological Sciences Publication 234, p. 35–45.

_____1997, Piezometric-extensometric estimations of specific storage in the Albuquerque Basin, New Mexico, *in* Prince, K.R. and Leake, S.A., eds, U.S. Geological Survey Subsidence Interest Group Conference, Proceedings of the Technical Meeting, Las Vegas, Nevada, February 14–16, 1995: U.S. Geological Survey Open-File Report 97–47, p. 21–26.

_____1998, Piezometric-extensometric estimations of specific storage in the Albuquerque Basin, New Mexico, *in* Borchers, J.W., ed., Land subsidence; case histories and current research—Proceedings of the Dr. Joseph F. Poland Symposium on Land Subsidence: Association of Engineering Geologists Special Publication 8, p. 435–440.

Heywood, C.E., Galloway, D.L., and Stork, S.V., 2002, Ground displacements caused by aquifer-system water-level variations observed using interferometric synthetic aperature radar near Albuquerque, New Mexico: U.S. Geological Survey Water-Resources Investigations Report 02–4235, 18 p.

Hill, M.C., 1992, A computer program (MODFLOWP) for estimating parameters of a transient, three-dimensional, ground-water flow model using nonlinear regression: U.S. Geological Survey Open-File Report 91–484, 358 p.

_____1998, Methods and guidelines for effective model calibration: U.S. Geological Survey Water-Resources Investigations Report 98–4005, 90 p.

Hoffmann, Jörn, Galloway, D.L., and Zebker, H.A., 2003, Inverse modeling of interbed storage parameters using land subsidence observations, Antelope Valley, California: Water Resources Research, v. 39, no. 2.

Hoffmann, Jörn, Leake, S.A., Galloway, D.L., and Wilson, A.M., in press, MODFLOW–2000 ground-water model—User guide to the subsidence and aquifer-system compaction (SUB) package: U.S. Geological Survey Open-File Report 03–233.

Hoffmann, Jörn, Zebker, H.A., Galloway, D.L., and Amelung, Falk, 2001, Seasonal subsidence and rebound in Las Vegas Valley, Nevada, observed by synthetic aperture radar interferometry: Water Resources Research, v. 37, no. 6, p. 1,551–1,566.

Holdahl, S.R., and Morrison, N.L., 1974, Regional investigations of vertical crustal movements in the U.S. using precise relevelings and mareograph data: Tectonophysics, v. 23, p. 373–390.

Holzer, T.L., 1984, Ground failure induced by ground-water withdrawal from unconsolidated sediment, *in* Holzer, T.L., ed., Man-induced land subsidence: Geological Society of America Reviews in Engineering Geology, v. 6, p. 67–105.

Holzer, T.L., Davis, S.N., and Lofgren, B.E., 1979, Faulting caused by groundwater extraction in south-central Arizona: Journal of Geophysical Research, v. 84, no. B2, p. 603–612.

Hopkins, H.T., Bower, R.F., Aba, J.M., and Harsh, J.F., 1981, Potentiometric-surface map for the Cretaceous aquifer, Virginia Coastal Plain, 1978: U.S. Geological Survey Water-Resources Investigations/Open-File Report 80–965, 1 sheet.

Howell, J.V., 1960, Glossary of geology and related sciences (2d ed.): Washington, D.C., American Geological Institute, 200 p.

Hsieh, P.A., 1996, Deformation induced changes in hydraulic head during ground-water withdrawal: Ground Water, v. 34, no. 6, p. 1,082–1,089.

Hudson, M.R., Minor, S.A., Grauch, V.J.S., and Personius, S.F., 1999, Preliminary characterization of faults in the middle Rio Grande Basin, *in* Bartolino, J.R., ed., U.S. Geological Survey middle Rio Grande Basin study—Proceedings of the Third Annual Workshop, Albuquerque, New Mexico, February 24–25, 1999: U.S. Geological Survey Open-File Report 99–203, p. 40–41.

HydroSOLVE, Inc., 2003, AQTESOLV for Windows version 3.5: Reston, Va., HydroSolve, Inc.

Ikehara, M.E., Galloway, D.L., Fielding, E., Bürgmann, R., Lewis, A.S., and Ahmadi, B., 1998, InSAR imagery reveals seasonal and longer-term land-surface elevation changes influenced by ground-water levels and fault alignment in Santa Clara Valley, California [abs.]: Eos (supplement) Transactions, American Geophysical Union, no. 45, p. F37.

Ikehara, M.E., and Phillips, S.P., 1994, Determination of land subsidence related to ground-water-level declines using global positioning system and leveling surveys in Antelope Valley, Los Angeles and Kern Counties, California, 1992: U.S. Geological Survey Water-Resources Investigations Report 94–4184, 102 p.

Intergovernmental Panel on Climate Change, Working Group II, 1996, Climate change 1995, impacts, adaptations, and mitigation of climate change—Scientific-technical analyses: New York, Cambridge University Press, 872 p.

_____2001, Changes in sea level, *in* Climate change 2001, impacts, adaptations, and vulnerability—Contribution of Working Group II to the Third Assessment Report of the Intergovernmental Panel on Climate Change: New York, Cambridge University Press, p. 639–681.

Ireland, R.L., Poland, J.F., and Riley, F.S., 1984, Land subsidence in the San Joaquin Valley, California, as of 1980: U.S. Geological Survey Professional Paper 437–I, 93 p.

Jackson, D.D., Aki, Keiitti, Cornell, C.A., Dieterich, J.H., Henyey, T.L., Mahdyiar, Mehrdad, Schwartz, David, and Ward, S.N., 1995, Seismic hazards in southern California—Probable earthquakes, 1994 to 2024: Bulletin of the Seismological Society of America, v. 85, no. 2, p. 379–439.

Jacob, C.E., 1940, On the flow of water in an elastic artesian aquifer: Transactions American Geophysical Union, v. 2, p. 574–586.

_____1946, Radial flow in a leaky artesian aquifer: Transactions American Geophysical Union, v. 27, no. 2, p. 198–205.

Jones, P.H., 1975, Geothermal and hydrodynamic regimes in the Northern Gulf of Mexico Basin, *in* Proceedings of the Second U.S. Symposium on the Development and Use of Geothermal Resources: Baton Rouge, La., Louisiana State University, Office of Research, p. 15–89.

Kasmarek, M.C., Coplin, L.S., and Santos, H.X., 1996, Water-level altitudes 1996, water-level changes 1977–96 and 1995–96, and compaction 1973–95 in the Chicot and Evangeline aquifers, Houston-Galveston region, Texas: U.S. Geological Survey Open-File Report 96–163, 8 sheets.

Kasmarek, M.C., and Strom, E.W., 2002, Hydrogeology and simulation of ground-water flow and land-surface subsidence in the Chicot and Evangeline aquifers, Houston area, Texas: U.S. Geological Survey Water-Resources Investigations Report 02–4022, 61 p.

Kazmann, R.G., 1988, Modern hydrology: Dublin, Ohio, National Water Well Association, 426 p.

Kelly, V.C., 1977, Geology of the Albuquerque Basin, New Mexico: Socorro, New Mexico Bureau of Mines and Mineral Resources Memoir 33, 60 p.

Laney, R.L., Raymond, R.H., and Winikka, C.C., 1978, Maps showing water-level declines, land subsidence, and earth fissures in south-central Arizona: U.S. Geological Survey Water-Resources Investigations Report 78–83, 2 sheets, scale 1:125,000.

Las Vegas Valley Water District, 1998, Las Vegas Valley Water District Artificial Recharge Project 1998, year end report: Variously paged.

Leake, S.A., 1990, Interbed storage changes and compaction in models of regional ground-water flow: Water Resources Research, v. 26, no. 9, p. 1,939–1,950.

Leake, S.A., and Lilly, M.R., 1997, Documentation of a computer program (FHB1) for assignment of transient specified-flow and specified-head boundaries in applications of the modular finite-difference ground-water flow model (MODFLOW): U.S. Geological Survey Open-File Report 97–571, 50 p.

Leake, S.A., and Prudic, D.E., 1991, Documentation of a computer program to simulate aquifer-system compaction using the modular finite-difference ground-water flow model: U.S. Geological Survey Techniques of Water-Resources Investigations book 6, chap. A2, 68 p.

Leighton, D.A., and Phillips, S.P., 2003, Simulation of ground-water flow and land subsidence in the Antelope Valley ground-water basin, California: U.S. Geological Survey Water-Resources Investigations Report 03–4016, 107 p

Lord, A.E., Koerner, R.M., and Curran, J.W., 1977, Fundamental studies of acoustic emissions in soils, *in* Hardy, H.R., Jr., and Leighton, F.W., eds., Proceedings, first conference on acoustic emission/microseismic activity in geologic structures and materials: Clausthal, Germany, Trans Tech Publications, p. 135–148.

Lu, Zhong, and Danskin, W.R., 2001, InSAR analysis of natural recharge to define structure of a ground-water basin, San Bernardino, California: Geophysical Research Letters, v. 28, no. 13, p. 2,661–2,664.

Malmberg, G.T., 1964, Land subsidence in Las Vegas Valley, Nevada, 1935–1963: Nevada Department of Conservation and Natural Resources, Water Resources Information Series Report 5, 10 p.

_____1965, Available water supply of the Las Vegas ground-water basin, Nevada: U.S. Geological Survey Water-Supply Paper 1780, 116 p., 13 pls.

Massonnet, D., and Feigl, K.L., 1998, Radar interferometry and its application to changes in the earth's surface: Reviews of Geophysics, v. 36, no. 4, p. 441–500.

Massonnet, D., Feigl, K.L., Rossi, M., and Adragna, F., 1994, Radar interferometric mapping of deformation in the year after the Landers earthquake: Nature, v. 369, p. 227–230.

Massonnet, Didier, Rossi, Marc, Carmona, Cesar, Adragna, Frederic, Peltzer, Gilles, Feigl, Kurt, and Rabaute, Thierry, 1993, The displacement field of the Landers earthquake mapped by radar interferometry: Nature, v. 364, p. 138–142.

Maxey, G.B., and Jameson, C.H., 1948, Geology and water resources of Las Vegas, Pahrump, and Indian Springs Valleys, Clark and Nye Counties, Nevada: Nevada State Engineer, Water Resources Bulletin 5, 121 p., 7 pls.; appendix 1, 128 p., 1 pl; appendix 2, 43 p.

McDonald, M.G., and Harbaugh, A.W., 1988, A modular three-dimensional finite-difference ground-water flow model: U.S. Geological Survey Techniques of Water-Resources Investigations, book 6, chap. A1, 586 p.

McFarland, E.R., 1999, Hydrogeologic framework and ground-water flow in the fall zone of Virginia: U.S. Geological Survey Water-Resources Investigations Report 99–4093, 83 p.

Meade, R.H., 1995, Setting—Geology, hydrology, sediments, and engineering of the Mississippi River, *in* Meade, R.H., ed., Contaminants in the Mississippi River, 1987–92: U.S. Geological Survey Circular 1133, p. 13–29.

Meinzer, O.E., 1928, Compressibility and elasticity of artesian aquifers: Economic Geology, v. 23, no. 3, p. 263–291.

Meinzer, O.E., and Hard, H.A., 1925, The artesian-water supply of the Dakota Sandstone in North Dakota with special reference to the Edgeley quadrangle: U.S. Geological Survey Water-Supply Paper 520–E, p. 73–95.

Meng, A.A., III, and Harsh, J.F., 1988, Hydrogeologic framework of the Virginia Coastal Plain: U.S. Geological Survey Professional Paper 1404–C, 82 p.

Metzger, L.F., Ikehara, M.E., and Howle, J.F., 2002, Vertical-deformation, water-level, microgravity, geodetic, water-chemistry, and flow-rate data collected during injection, storage, and recovery tests at Lancaster, Antelope Valley, California, September 1995 through September 1998: U.S. Geological Survey Open-File Report 01–414, 85 p.

Meyer, W.R., and Carr, J.E., 1979, A digital model for simulation of ground-water hydrology in the Houston area, Texas: Texas Department of Water Resources Report LP–103, 133 p.

Mills, William, Kennedy, John, Miller, Craig, Leslie, Greg, Herndon, Roy, Sovich, Tim, Rigby, Marty, Bradford, Susan, Tru, L., Coughran, Thom, Leung, E., Renna, Jeffrey, Bell, Richard, Seckel, Karl, and Everest, Bill, 1999, Orange County Water District, master plan report: Orange County Water District.

Mimura, N., and Harasawa, H., 2000, Data book of sea-level rise: Tsukuba, Japan, Center for Global Environmental Research, National Institute for Environmental Studies, Environment Agency of Japan, 128 p.

Mindling, A.L., 1971, A summary of data relating to land subsidence in Las Vegas Valley: Reno, Center for Water Resources Research, Desert Research Institute, University of Nevada, 55 p.

Morgan, D.S., and Dettinger, M.D., 1996, Ground-water conditions in Las Vegas Valley, Clark County, Nevada—Part 2, Hydrogeology and simulation of ground-water flow: U.S. Geological Survey Water-Supply Paper 2320–B, 124 p., 2 pls.

National Oceanic and Atmospheric Administration, 2002, The Saffir-Simpson Hurricane Scale: Accessed July 26, 2002, at URL http://www.nhc.noaa.gov/aboutsshs.html.

Nelson, G.L., 1982, Vertical movement of ground water under the Merrill Field landfill, Anchorage, Alaska: U.S. Geological Survey Open-File Report 82–1016, 24 p.

Neuman, S.P., and Witherspoon, P.A., 1969, Theory of flow in a confined two-aquifer system: Water Resources Research, v. 5, p. 803–816.

_____1969, Applicability of current theories of flow in leaky aquifers: Water Resources Research, v. 5, p. 817–829.

_____1972, Field determination of the hydraulic properties of leaky multiple-aquifer systems: Water Resources Research, v. 8, p. 1,284–1,298.

Neuzil, C.E., 1986, Groundwater flow in low-permeability environments: Water Resources Research, v. 22, no. 8, p. 1,163–1,195.

Nieto, A.S., and Young, R.A., 1998, Retsof Salt Mine collapse and aquifer dewatering, Genesee Valley, Livingston County, New York, *in* Borchers, J.W., ed., Land subsidence; case histories and current research—Proceedings of the Dr. Joseph F. Poland Symposium on Land Subsidence: Association of Engineering Geologists Special Publication no. 8, p. 309–325.

Nishikawa, Tracy, Rewis, D.L., and Martin, Peter, 2001, Numerical simulation of ground-water flow and land subsidence at Edwards Air Force Base, Antelope Valley, California: U.S. Geological Survey Water-Resources Investigations Report 01–4038, 111 p.

Noble, J.E., Bush, P.W., Kasmarek, M.C., and Barbie, D.L., 1996, Estimated depth to the water table and estimated rate of recharge in outcrops of the Chicot and Evangeline aquifers near Houston, Texas: U.S. Geological Survey Water-Resources Investigations Report 96–4018, 19 p.

Paillet, F.L., and Crowder, R.E., 1996, A generalized approach for the interpretation of geophysical well logs in ground-water studies—Theory and application: Ground Water, v. 34, no. 5, p. 883–898.

Pavelko, M.T., 2000, Ground-water and aquifer-system-compaction data from the Lorenzi site, Las Vegas, Nevada, 1994–99: U.S. Geological Survey Open-File Report 00–362, 26 p.

Peltzer, Gilles, Crampé, F., Hensley, Scott, and Rosen, P.A., 2001, Transient strain accumulation and fault interaction in the eastern California shear zone: Geology, v. 29, no. 11, p. 975–978.

Peltzer, Gilles, Crampé, F., and King, G., 1999, Evidence of nonlinear elasticity of the crust from the M_w 7.6 Manyi (Tibet) earthquake: Science, v. 286, p. 272–276.

Peltzer, Gilles, Crampé, F., and Rosen, P.A., 2001, The M_w 7.1, Hector Mine, California earthquake—Surface rupture, surface displacement field, and fault slip solution from ERS SAR data: Earth and Planetary Sciences, v. 333, p. 545–555.

Peltzer, Gilles, and Rosen, Paul, 1995, Surface displacement of the 17 May 1993 Eureka Valley, California earthquake observed by SAR interferometry: Science, v. 268, p. 1,333–1,336.

Peltzer, Gilles, Rosen, Paul, Rogez, Francois, and Hudnut, Ken, 1996 Postseismic rebound in fault step-overs caused by pore fluid flow: Science, v. 273, p. 1,202–1,204.

Plume, R.W., 1989, Ground-water conditions in Las Vegas Valley, Clark County, Nevada—Part I, Hydrogeologic framework: U.S. Geological Survey Water-Supply Paper 2320–A, 15 p., 5 pls.

Plummer, L.N., Bexfield, L.M., Anderholm, S.K., Sanford, W.E., and Busenberg, Eurybiades, 2001, Geochemical characterization of ground-water flow in parts of the Santa Fe Group aquifer system, middle Rio Grande Basin, New Mexico, *in* Cole, J.C., ed., U.S. Geological Survey middle Rio Grande Basin study—Proceedings of the Fourth Annual Workshop, Albuquerque, New Mexico, February 15–16, 2000: U.S. Geological Survey Open-File Report 00–488, p. 7–10.

Poeter, E.P., and Hill, M.C., 1998, Documentation of UCODE, a computer code for universal inverse modeling: U.S. Geological Survey Water-Resources Investigations Report 98–4080, 116 p.

Poland, J.F., ed, 1984, Guidebook to studies of land subsidence due to ground-water withdrawal: Paris, United Nations Education, Scientific and Cultural Organization, Studies and Reports in Hydrology 40, 305 p.

Poland, J.F., and Davis, G.H., 1969, Land subsidence due to withdrawals of fluids, *in* Varnes, D.J., and Kiersch, G., eds., Reviews in engineering geology—Volume 2: Geological Society of America, p. 187–269.

Poland, J.F., and Ireland, R.L., 1988, Land subsidence in the Santa Clara Valley, California, as of 1982: U.S. Geological Survey Professional Paper 497–F, 61 p.

Poland, J.F., Lofgren, B.E., Ireland, R.L., and Pugh, R.G., 1975, Land subsidence in the San Joaquin Valley, California, as of 1972: U.S. Geological Survey Professional Paper 437–H, 78 p.

Poland, J.F., and Piper, A.M., 1956, Ground-water geology of the coastal zone, Long Beach-Santa Ana area, California: U. S. Geological Survey Water-Supply Paper 1109, 162 p.

Powars, D.S., 2000, The effects of the Chesapeake Bay impact crater on the geologic framework and the

correlation of hydrogeologic units of southeastern Virginia, south of the James River: U.S. Geological Survey Professional Paper 1622, 53 p., 1 pl.

Pratt, W.E., and Johnson, D.W., 1926, Local subsidence of the Goose Creek oil field: Journal of Geology, v. 34, no. 7, p. 577–590.

Prescott, W.H., 1996, Satellites and earthquakes—A new continuous GPS array for Los Angeles, Yes, it will radically improve seismic risk assessment for Los Angeles: EOS, Transactions, American Geophysical Union, v. 77, p. 417.

Riley, F.S., 1969, Analysis of borehole extensometer data from central California, *in* Tison, L.J., ed., Land subsidence, volume 2: International Association of Hydrological Sciences Publication 89, p. 423–431.

_____1986, Developments in borehole extensometry, *in* Johnson, I.A., Carbognin, Laura, and Ubertini, L., eds., Land subsidence—Proceedings of the Third International Symposium on Land Subsidence, Venice, Italy, March 19–25, 1984: International Association of Hydrological Sciences Publication 151, p. 169–186.

_____1998, Mechanics of aquifer systems—The scientific legacy of Joseph F. Poland, *in* Borchers, J.W., ed., Land subsidence; case histories and current research—Proceedings of the Dr. Joseph F. Poland Symposium on Land Subsidence: Association of Engineering Geologists Special Publication no. 8, p. 13–27.

Rosen, P.A., Hensley, Scott, Joughin, Ian, Li, F., Madsen, S., Rodriguez, Ernesto, and Goldstein, R.M., 2000, Synthetic aperture radar interferometry, *in* International Geoscience and Remote Sensing Symposium, Proceedings: Institute of Electrical and Electronics Engineers, v. 88, no. 3, p. 333–382.

Rucker, M.L., and Keaton, J.R., 1998, Tracing an earth fissure using seismic-refraction methods with physical verification, *in* Borchers, J.W., ed., Land subsidence; case histories and current research—Proceedings of the Dr. Joseph F. Poland Symposium on Land Subsidence: Association of Engineering Geologists Special Publication no. 8, p. 207–216.

Sandwell, David, and Price, E., 1998, Phase gradient approach to stacking interferograms: Journal of Geophysical Research, v. 103, no. B12, p. 30,183–30,204.

Sandwell, David, and Sichoix, L., 2000, Topographic phase recovery from stacked ERS interferometry and a low-resolution digital elevation model: Journal of Geophysical Research, v. 105, no. B12, p. 28,211–28,222.

Sandwell, David, Sichoix, L., Agnew, D., Bock, Y., and Minster, J.B., 2000, Near real-time radar interferometry of the M_w 7.1 Hector Mine earthquake: Geophysical Research Letters, v. 27, no. 19, p. 3,101–3,105.

Schenewerk, Mark, Dillinger, William, and Hilla, Steve, 1999, Program for adjustment of GPS ephemerides (PAGES): Accessed September 25, 2002, at URL http://www.ngs.noaa.gov/GRD/GPS/DOC/pages/pages.html

Schumann, H.H., and Poland, J.F., 1970, Land subsidence, earth fissures, and groundwater withdrawal in south-central Arizona, U.S.A.: International Association of Scientific Hydrology Publication 88, p. 295–302.

Sewerage and Water Board of New Orleans, 2001, Drainage archives: Accessed August 23, 2001, at URL http://www.swbnola.org/drainage_info.html.

Shaw, J.H., and Shearer, P.M., 1999, An elusive blind-thrust fault beneath metropolitan Los Angeles: Science, v. 283, no. 5407, p. 1,516–1,518.

Shaw, J.H., and Suppe, John, 1996, Earthquake hazards of active blind-thrust faults under the central Los Angeles Basin, California: Journal of Geophysical Research, v. 101 B4, p. 8,623–8,642.

Shindle, M., 1999, ESCHER—An algorithm for unwrapping an interferogram phase file using the branch-cut method: Fairbanks, Alaska, SAR Facility.

Sneed, Michelle, and Galloway, D.L., 2000, Aquifer-system compaction and land subsidence—Measurements, analyses, and simulations, the Holly site, Edwards Air Force Base, Antelope Valley, California: U.S. Geological Survey Water-Resources Investigations Report 00–4015, 65 p.

Sneed, Michelle, Ikehara, M.E., Galloway, D.L., and Amelung, Falk, 2001, Detection and measurement of land subsidence using global positioning system and interferometric synthetic aperture radar, Coachella Valley, California, 1996–98: U.S. Geological Survey Water-Resources Investigation Report 01–4193, 26 p.

Snowden, J.O., Ward, W.C., and Studlick, J.R.J., 1980, Geology of greater New Orleans—Its relationship to land subsidence and flooding: New Orleans, La., New Orleans Geological Society, Inc., 34 p.

Stork, S.V., and Sneed, M., 2002, Houston-Galveston Bay area, Texas, from space—A new tool for mapping land subsidence: U.S. Geological Survey Fact Sheet 110–02, 6 p.

Terzaghi, Karl, 1925, Erdbaumechanik auf bodenphysikalisher Grundlage: Wien, Austria, Deuticke, 399 p.

Tiedeman, C.R., Kernodle, J.M., and McAda, D.P., 1998, Application of nonlinear-regression methods to a ground-water flow model of the Albuquerque Basin, New Mexico: U.S. Geological Survey Water-Resources Investigations Report 98–4172, 90 p.

Theis, C.V., 1935, The relation between the lowering of the piezometric surface and the rate and duration of discharge of a well using ground-water storage: Transactions American Geophysical Union, v. 16, p. 519–524.

Tolman, C.F., and Poland, J.F., 1940, Ground-water infiltration, and ground-surface recession in Santa Clara Valley, Santa Clara County, California: Transactions American Geophysical Union, v. 21, p. 23–24.

Trahan, L.J., 1989, Soil survey of Orleans Parish, Louisiana: U.S. Department of Agriculture, Soil Conservation Service [published in cooperation with the Louisiana Agricultural Experiment Station and the Louisiana Soil and Water Conservation Committee].

U.S. Army Corps of Engineers, 1970, Hurricane Camille 14–22 August 1969: Mobile, Ala., U.S. Army Corps of Engineers Mobile District, 80 p.

Wagner, H.M., 1975, Principals of operations research: Englewood Cliffs, N.J., Prentice-Hall, Inc., 1,039 p.

Waichler, S.R., and Cochran, G.F., 1993, Modeling and prediction of land subsidence in Las Vegas Valley, Nevada, *in* Bell, J.W. and Price, J.G., Subsidence in Las Vegas Valley, 1980–91—Final project report: Nevada Bureau of Mines and Geology Open-File Report 93–4 [variously paged], 9 pl.

Walls, Christian, Rockwell, T.K., Mueller, K., Block, Y., Williams, S., Pfanner, J., Dolan, J.F., and Fang, P., 1998, Escape tectonics in the Los Angeles metropolitan region and implications for seismic risk: Nature, v. 394, no. 6691, p. 356–360.

Williams, T.A., and Williamson, A.K., 1989, Estimating water-table altitudes for regional ground-water flow modeling, U.S. Gulf Coast: Ground Water, v. 27, no. 3, p. 333–340.

Williamson, A.K., Prudic, D.E., and Swain, L.A., 1989, Ground-water flow in the Central Valley, California: U.S. Geological Survey Professional Paper 1401–D, 127 p.

Winston, W.L., 1987, Operations research, applications, and algorithms: Boston, Mass., Duxbury Press, 1,025 p.

Wrege, B.M., Hasbrouck, W.P., and Schumann, H.H., 1985, Seismic surface-wave attenuation across earth fissures in the alluvium, south-central Arizona, *in* Graves, B., Lehr, J.H., and Butcher, K., eds., Surface and borehole geophysical methods in ground water investigations, Second National Conference and Exposition, Fort Worth, Texas, February 12–14, 1985: Dublin, Ohio, National Water Well Association, p. 121–131.

Yager, R.M., and Fountain, J.C., 2001, Effect of natural gas exsolution on specific storage in a confined aquifer undergoing water level decline: Ground Water, v. 39, no. 4, p. 517–525.

Yager, R.M., Miller, T.S., and Kappel, W.M., 2001, Simulated effects of salt-mine collapse on ground-water flow and land subsidence in a glacial aquifer system, Livingston County, New York: U.S. Geological Survey Professional Paper 1611, 83 p.

Zebker, H.A., Rosen, P.A., Goldstein, R.M., Gabriel, A., and Werner, C.L., 1994, On the derivation of coseismic displacement fields using differential radar interferometry—The Landers earthquake: Journal of Geophysical Research, v. 99, no. B10, p. 19,617–19,634.

Zhang, Jie, Bock, Yehuda, Johnson, H.O., Fang, Peng, Williams, Simon, Genrich, Joachim, Wdowinski, Shimon, and Behr, Jeff, 1997, Southern California permanent GPS geodetic array—Error analysis of daily position estimates and site velocities: Journal of Geophysical Research, v. 102, no. B8, p. 18,035–18,055.

Zilkoski, D.B., and Reese, S.M., 1986, Subsidence in the vicinity of New Orleans as indicated by analysis of geodetic leveling data: U.S. Department of Commerce, National Oceanic and Atmospheric Administration, Technical Report NOS 120 NGS 38, 111 p.